



Synchrophasor-based Overhead Line Impedance Monitoring

Deborah Ritzmann

Thesis submitted in partial fulfilment of the requirements for the degree of
Doctor of Philosophy

School of the Built Environment

April 2017

Abstract

Thermal limits of overhead transmission lines create network constraints that can result in curtailment of renewable energy generation. Thermal limits are conventionally static and based on worst-case, non-cooling ambient weather conditions, leading to under-utilization of overhead lines. Utilization can be increased and network constraints reduced by rating overhead lines dynamically, based on actual conductor temperature. Installation and maintenance of temperature and weather sensors along an overhead line is expensive and laborious. A more cost-effective solution is to derive average conductor temperature from overhead line impedance parameters, which can be calculated from measurements of electrical signals at each line end. Synchronized phasor measurement technology is becoming increasingly available in substations to capture voltage and current signals with high accuracy and reporting rates. It is known that the substation instrumentation channel can introduce significant systematic errors to the phasor measurements, which in turn cause inaccurate line impedance parameter and temperature values.

This thesis presents novel methods for accurate, real-time monitoring of overhead line impedance parameters using synchronized phasor measurements that have systematic errors. In contrast to previous research, the time-variance and temperature dependence of line resistance as well as compensation of systematic errors is taken into account in the system model to increase parameter estimation accuracy. In addition, an algorithm for the selection of the best parameter estimates from different measurement sets is given.

The effectiveness of the novel methods is demonstrated in several case studies on measurement data from simulations and an actual overhead line. The results show that the identified correction factors compensate systematic measurement errors, leading to a reduction in impedance parameter estimation errors of at least one order of magnitude compared to existing methods. Furthermore, the accuracy of real-time estimation of average conductor temperature was increased by at least one order of magnitude relative to previously proposed methods.

Declaration

I confirm that this is my own work and the use of all material from other sources has been properly and fully acknowledged.

Deborah Ritzmann

Acknowledgements

I would like to thank Dr Ben Potter and Prof William Holderbaum for their excellent academic supervision throughout my doctoral training, especially for their ready availability to discuss problems and thoughtful feedback on my writing.

My thanks also go to Dr Paul Wright whose support and experience have been invaluable inputs to conducting my research, and who has always made me feel welcome at NPL. Further, I would like to thank his colleagues at NPL, Peter, Pravin and Adrian, for their technical support.

I would like to express my gratitude to Prof Johan Rens and his colleagues at North-West University, South Africa, for their collaboration and for hosting me at their institution.

Thanks are also due to the Climate-KIC of the European Institute of Innovation and Technology for funding my PhD and for enriching my experience through their summer schools and wider community.

I am indebted to all my colleagues in and associated with the Energy Research Lab, especially to Laura whose advice has always been extremely useful before and during the PhD, to Timur for sharing his wealth of experience gathered as a research student and assistant at Reading University, to Max for teaching me about high throughput computing and other technical matters and to Ana for many lunchtime discussions and reminding me not to get too stressed.

I would like to thank my family and friends for their continued support, especially my mother Doris who encouraged me to embark on the adventurous journey of doctoral training as well as my friend Anna for helping me to get through the most difficult stages of writing this thesis.

Table of Contents

Table of Contents	xii
List of Tables	xvi
List of Figures	xx
List of Acronyms	xxi
1 Introduction	1
1.1 Background and motivation	1
1.2 Problem statement	4
1.3 Contributions	5
1.4 Publications	6
1.5 Thesis structure	7
2 Literature review	9
2.1 Introduction	9
2.2 Background	10
2.2.1 Transmission line theory	12
2.2.2 Synchronized phasor measurements	24
2.2.3 Estimation theory	27
2.3 Review of overhead line impedance parameter identification	34
2.3.1 Power system state and parameter estimation	34
2.3.2 Estimation methods based on transient signal measurements	35
2.3.3 Steady-state estimation methods for transposed lines	37
2.3.4 Steady-state estimation methods for untransposed lines	45
2.3.5 Summary	47
2.4 Discussion and conclusion	50

3	Comparison of existing synchrophasor-based impedance parameter estimation methods	51
3.1	Introduction	51
3.2	Overview of methods under consideration	52
3.2.1	Single-phase methods	53
3.2.2	Three-phase methods	58
3.3	Assessment criteria for parameter estimation results	67
3.4	Application of methods to field data	69
3.4.1	Properties of the line and the data	69
3.4.2	Analysis of parameter estimation results	75
3.4.3	Summary and discussion of results	86
3.5	Application of methods to data from a transmission line simulation	88
3.5.1	Properties of the simulation	88
3.5.2	Simulated scenarios	90
3.5.3	Analysis of parameter estimation results	91
3.5.4	Summary and discussion of results	99
3.6	Conclusion	100
4	A new method for reducing variability in impedance parameter values estimated from measurements with systematic errors	101
4.1	Introduction	101
4.2	A new method for accurate impedance parameter estimation from synchrophasor measurements with systematic errors	103
4.2.1	A modified parameter estimation problem for short lines	103
4.2.2	Propagation of systematic measurement errors	105
4.2.3	Explanation of the new method for short lines	106
4.3	Case study 1: short transmission lines	110
4.3.1	Experimental set-up and operation	110
4.3.2	Analysis of parameter estimation results	113
4.3.3	Discussion of results	118
4.4	Extension of the method to the pi-model for longer lines	119
4.4.1	Modification of the pi-circuit model	119
4.4.2	Explanation of the new method for the pi-circuit model	120
4.5	Case study 2: medium-length and long lines	124
4.5.1	Properties of the simulation	124
4.5.2	Metrics for evaluation of method performance	126
4.5.3	Analysis of parameter estimation results	127
4.5.4	Discussion of results	133

4.6	Conclusion	135
5	An innovative approach to increasing the accuracy of real-time impedance parameter monitoring	137
5.1	Introduction	137
5.2	Methods	139
5.2.1	A different parameter estimation problem	139
5.2.2	Estimation of correction factors and resistance-temperature parameters	141
5.2.3	Selection of optimal parameter estimates	146
5.3	Case study 1: physical simulation of three-phase measurements . . .	148
5.3.1	Laboratory-based measurements	148
5.3.2	Analysis of parameter estimation results	149
5.3.3	Discussion of results	157
5.4	Case study 2: field measurements	158
5.4.1	Analysis of parameter estimation results	161
5.4.2	Discussion of results	172
5.5	Conclusion	173
6	Conclusion	175
6.1	Summary and discussion of contributions to knowledge	175
6.2	Future work	179
	References	183
	Appendices	197
A	Chapter 3	199
A.1	Sensitivity of series inductance and shunt capacitance to conductor temperature	199
A.1.1	Series inductance	199
A.1.2	Shunt capacitance	201
A.2	Preservation of positive sequence through the delta-star conversion .	203
A.3	Calculation of average conductor temperature	205
A.4	Field measurement results	210
A.5	Simulation measurement results	210

B Chapter 4	213
B.1 Estimating the uncertainty in the calculated impedance of a copper coil	213
B.2 Derivation of net error	215
B.2.1 Partial derivatives of Z and Y	216
B.2.2 Net error approximation	216
C Chapter 5	219
C.1 Selection of measurement subsets	219
C.2 Case study 1 results	220
C.2.1 Individual case	220
C.3 Case study 2 results	224
C.3.1 Day 8	224
C.3.2 Cross validation	230

List of Tables

2.1	Overview of steady-state methods for overhead line impedance parameter identification	48
3.1	Selection of parameter estimation methods, grouped by transmission line model	53
3.2	Assessment criteria for acceptable parameter estimates	68
3.3	Equivalent pi-circuit positive sequence transmission line parameter values at $T_c = 20^\circ\text{C}$	72
3.4	Numerical limits for acceptable parameter estimates	74
3.5	Selection of parameter estimation methods, grouped by transmission line model	75
3.6	Acceptability of resistance estimates - field measurements, numerical values are given in Table A.2	78
3.7	Acceptability of reactance estimates - field measurements, numerical values are given in Table A.2	81
3.8	Acceptability of conductance estimates - field measurements, numerical values are given in Table A.2	83
3.9	Acceptability of susceptance estimates - field measurements, numerical values are given in Table A.2	84
3.10	Acceptability of all parameter estimates - field measurements, numerical values are given in Table A.2	86
3.11	Description of simulated scenarios	90
3.12	Systematic errors in the Systematic Error Scenario	91
3.13	Acceptability of estimates in the Ideal Scenario, numerical values are given in Table A.3	92
3.14	Acceptability of estimates in the Delta-star Scenario, numerical values are given in Table A.4	93
3.15	Acceptability of estimates in the Variation Scenario, numerical values are given in Table A.5	94

3.16	Acceptability of estimates in the Uncertainty Scenario, numerical values are given in Table A.6	95
3.17	Acceptability of estimates in the Systematic Error Scenario, numerical values are given in Table A.7	96
3.18	Acceptability of estimates in the Realistic Scenario, numerical values are given in Table A.8	98
3.19	Summary of acceptability scores	99
4.1	Sum of squared residuals S_R and S_X with and without correction constants	115
4.2	Systematic errors in the synchrophasor measurements - individual case	128
4.3	Parameter errors for one individual case	131
4.4	Errors in resistance R for 10^5 cases	131
4.5	Errors in reactance X for 10^5 cases	132
4.6	Errors in conductance G for 10^5 cases	132
4.7	Errors in susceptance B for 10^5 cases	132
5.1	Systematic errors and corrections for one individual case	150
5.2	Rms of parameter errors for one individual case	152
5.3	Standard deviation of parameter errors for one individual case . . .	153
5.4	95th percentiles of the rms of parameter errors for 100 cases, 95 % confidence bounds are given in brackets	154
5.5	95th percentiles of the standard deviation of parameter errors for 100 cases, 95 % confidence bounds are given in brackets	156
5.6	Limits for acceptable parameter estimates	161
5.7	Values of identified correction factors for Day 8	161
5.8	Acceptability of estimated impedance and admittance parameters for Day 8, numerical values are given in Table C.1	166
5.9	Rms error $E_{\Delta T_c}$ and standard deviation of errors $\Sigma_{\Delta T_c}$ in estimated temperature for Day 8	166
5.10	Estimation day 8 - number of days with acceptable estimated values of Median (M) and Interdecile Range (IDR) of each parameter, and the total number of acceptable values over ten days, numerical values are given in Table C.2.	167

5.11	Estimation day 8 - rms error $E_{\Delta T_c}$ and standard deviation of error $\Sigma_{\Delta T_c}$ of estimated temperature values, numerical values are given in Tables C.3 and C.4	168
5.12	Number of days with acceptable estimated values of Median (M) and Interdecile Range (IDR), when correction factors and resistance-temperature parameters are estimated from Days 1 to 10 by NMLT, numerical values are given in Table C.5	169
5.13	Number of days with acceptable estimated values of Median (M) and Interdecile Range (IDR), when correction factors and resistance-temperature parameters are estimated from Days 1 to 10 by NMNL, numerical values are given in Table C.6	170
5.14	Cross validation of NMLT - each column gives the rms error $E_{\Delta T_c}$ and standard deviation of errors $\Sigma_{\Delta T_c}$ in calculated temperature, numerical values are given in Tables C.7 and C.8	171
5.15	NMNL - each column gives the rms and standard deviation of errors in calculated temperature, numerical values are given in Tables C.9 and C.10	171
A.1	List of fixed input quantity values	208
A.2	Results for field measurements, 22-hour period, as presented in Tables 3.6, 3.7, 3.8, 3.9 and 3.10	210
A.3	Results for the Ideal Scenario, as presented in Table 3.13	210
A.4	Results for the Delta-star Scenario, as presented in Table 3.14	211
A.5	Results for the Variation Scenario, as presented in Table 3.15	211
A.6	Results for the Uncertainty Scenario, as presented in Table 3.16	211
A.7	Results for the Systematic Error Scenario, as presented in Table 3.17	212
A.8	Results for the Realistic Scenario, as presented in Table 3.18	212
B.1	Components of uncertainty calculation for resistance	214
C.1	Values of Median (M) and Interdecile Range (IDR) for impedance and admittance parameters for Day 8, as presented in Table 5.8	228
C.2	Estimation day 8 - number of days with acceptable estimated values of Median (M) and Interdecile Range (IDR) of each parameter, and the total number of acceptable values over ten days, as presented in Table 5.10	228
C.3	Estimation day 8 - rms error $E_{\Delta T_c}$ of estimated temperature values in °C, as presented in Table 5.11	229

C.4	Estimation day 8 - standard deviation of error $\Sigma_{\Delta T_c}$ of estimated temperature values in °C, as presented in Table 5.11	229
C.5	Number of days with acceptable estimated values of Median (M) and Interdecile Range (IDR), when correction factors and resistance-temperature parameters are estimated from Days 1 to 10 by NMLT as presented in Table 5.12	230
C.6	Number of days with acceptable estimated values of Median (M) and Interdecile Range (IDR), when correction factors and resistance-temperature parameters are estimated from Days 1 to 10 by NMNL, as presented in Table 5.13	230
C.7	Cross validation of NMLT - rms error $E_{\Delta T_c}$ of estimated temperature values in °C, as presented in Table 5.14	231
C.8	NMLT - standard deviation of error $\Sigma_{\Delta T_c}$ of estimated temperature values in °C, as presented in Table 5.14	231
C.9	Cross validation of NMNL - rms error $E_{\Delta T_c}$ of estimated temperature values in °C, as presented in Table 5.15	232
C.10	Cross validation of NMNL - standard deviation of error $\Sigma_{\Delta T_c}$ of estimated temperature values in °C, as presented in Table 5.15 . . .	232

List of Figures

1.1	World net electricity generation by energy source, 2010-40 [1]	2
1.2	Illustration of the problem addressed in this thesis	4
2.1	Examples of transmission line towers	10
2.2	Small transmission line section	13
2.3	Bergeron model equivalent circuit	14
2.4	Diagram of a two-port network	16
2.5	Transmission line equivalent circuits	17
2.6	Example of a line transposition pattern	19
2.7	Schematic diagram of the geometrical configuration of two actual conductors and their images [48]	21
2.8	Main hardware components of the synchrophasor measurement pro- cess [54]	24
2.9	Sinusoidal waveform and its phasor representation in the complex plane [57]	25
3.1	Diagram of a pi-circuit	53
3.2	Diagram of a two-port network	56
3.3	Diagram of a three-phase equivalent pi-circuit	58
3.4	Positive sequence line-to-line voltage amplitude	70
3.5	Positive sequence voltage phase angle	70
3.6	Positive sequence current amplitude	71
3.7	Positive sequence active power	72
3.8	Calculated conductor temperature and resistance as well as mean ambient temperature during the chosen 24-hour period	73
3.9	Positive sequence resistance estimates for the first six hours of the 24-hour period	76
3.10	Positive sequence reactance estimates for the first six hours of the 24-hour period	76

3.11	Voltage phase angle and negative current magnitude over the 24-hour period	77
3.12	Resistance estimates from field measurements, single-phase methods	79
3.13	Resistance estimates from field measurements, three-phase methods	79
3.14	Resistance estimates from field measurements against active power, single-phase methods	80
3.15	Condition number of the design matrix for linear estimation methods, and of the final Jacobian matrix for the non-linear methods . .	81
3.16	Reactance estimates from field measurements, single-phase methods	82
3.17	Reactance estimates from field measurements, three-phase methods	82
3.18	Conductance estimates from field measurements, single-phase methods	83
3.19	Conductance estimates from field measurements, three-phase methods	84
3.20	Susceptance estimates from field measurements, single-phase methods	85
3.21	Susceptance estimates from field measurements, three-phase methods	85
3.22	Schematic diagram of the simulation circuit	88
3.23	Measured and simulated current amplitude, SE refers to Sending end and RE to Receiving end	89
3.24	Positive sequence resistance, three-phase methods - Ideal Scenario .	92
3.25	Positive sequence resistance, single-phase methods - Variation Scenario	94
3.26	Positive sequence resistance, three-phase methods - Variation Scenario	95
3.27	Positive sequence resistance, single-phase methods - Systematic Error Scenario	97
3.28	Positive sequence resistance against active power, single-phase methods - Systematic Error Scenario	97
4.1	Diagram of a circuit for a short transmission line	103
4.2	Phasor diagram of sending end voltage, rotation and scaling due to systematic errors are shown	104
4.3	Schematic diagram illustrating the steps of the new method. Initially, the calculated parameter values have step changes over time due to systematic measurement errors. A linear function of time is fitted and the residuals are calculated. Over the iterations of the optimization process, correction factors are identified such that the residuals are reduced. At the end of the optimization process, residuals are minimized and calculated parameter values follow a constant time model.	109

4.4	Schematic diagram showing the set-up of the overhead line model and measurement circuit	110
4.5	Amplitude of the voltages at each line end over the test period . . .	111
4.6	Amplitude of the line current over the test period	112
4.7	Active power at each line end over the test period, values are overlapping	112
4.8	Measured reference resistance values	114
4.9	Average surface temperature of copper coil over the test period . . .	114
4.10	Measured reference reactance values	115
4.11	Resistance values calculated without correction constants	116
4.12	Resistance values calculated with correction constants	117
4.13	Calculated reactance values over the test period	117
4.14	Diagram of a pi-circuit	119
4.15	Flow chart that summarizes the steps of the proposed method for the pi-circuit model	123
4.16	Schematic diagram of the simulation circuit	124
4.17	Amplitude of the sending and receiving end voltages over the period of the simulation	125
4.18	Amplitude of the sending and receiving end currents over the period of the simulation, their difference is very small compared to the individual values	125
4.19	Values of the identified correction constants over time for the individual simulation case	128
4.20	Nominal and estimated values of resistance R over time for the individual simulation case	129
4.21	Nominal and estimated values of reactance X over time for the individual simulation case	129
4.22	Nominal and estimated values of conductance G over time for the individual simulation case	130
4.23	Nominal and estimated values of susceptance B over time for the individual simulation case	130
5.1	Diagram of a pi-circuit	139
5.2	Experimental setup for laboratory-based synchrophasor measurements	148
5.3	Nominal and estimated values of resistance R over time for the individual case	151
5.4	Mean values of sending and receiving end active power for ten 22-hour periods	159

5.5	Calculated average conductor temperature for ten 22-hour periods	160
5.6	Estimated values of resistance R over time for Day 8, by the new methods and existing single-phase methods	163
5.7	Estimated values of conductor temperature T_c over time for Day 8, by the new methods and existing single-phase methods	165
6.1	Illustration of the problem addressed in this thesis	176
A.1	Schematic diagram of the geometrical configuration of two actual conductors and their images	200
A.2	Phasor diagram of star and delta voltages	203
A.3	Heat transfer rates as calculated from the heat balance equation	209
C.1	Nominal and estimated values of reactance X over time for the individual case	221
C.2	Nominal and estimated values of conductance G over time for the individual case	222
C.3	Nominal and estimated values of susceptance B over time for the individual case	223
C.4	Estimated values of reactance X over time for Day 8, by the new methods and existing single-phase methods	225
C.5	Estimated values of conductance G over time for Day 8, by the new methods and existing single-phase methods	226
C.6	Estimated values of susceptance B over time for Day 8, by the new methods and existing single-phase methods	227

List of Acronyms

AAAC	All Aluminium Alloy Conductor
AAC	All Aluminium Conductor
AC	Alternating Current
ACAR	Aluminium Conductor Alloy Reinforced
ACSR	Aluminium Conductor Steel Reinforced
DC	Direct Current
DFT	Discrete Fourier Transform
EKF	Extended Kalman filter
GLS	Generalized least-squares
GPS	Global Positioning System
IDR	Interdecile Range
LLS3	Linear Least-squares
LMS	Least mean squares
M	Median
MLE	Maximum likelihood estimator
MLEs	Maximum likelihood estimators
NLCO3	Non-linear Constraint Optimization
NLLC3	Non-linear Least-squares with Calibration Factors
NLOE1	Non-linear Optimal Estimator
NMLT	New Method - Linear Time
NMNL	New Method - Non-linear Least-squares
OLS	Ordinary least-squares
PM	Proposed Method
PMUs	Phasor Measurement Units
RLS	Recursive least-squares
rms	root-mean-square
SCADA	Supervisory Control And Data Acquisition
SM1	Single Measurement
TLS	Total least-squares

TLS1	Total Least-squares
TPLL1	Two-port Linear Least-squares - Single-phase
TPLL3	Two-port Linear Least-squares - Three-phase
TVE	Total Vector Error
UK	United Kingdom
USA	United States of America
UTC	Coordinated Universal Time
WAMPAC	Wide Area Monitoring, Protection And Control
WAMS	Wide Area Monitoring System
WLS	Weighted least-squares

Chapter 1

Introduction

This chapter provides an introduction to this thesis. First of all, Section 1.1 discusses background and motivation; a problem statement is given in Section 1.2; the contributions made in this thesis are outlined in Section 1.3, followed by a list of publications in Section 1.4 and details of the thesis structure in Section 1.5.

1.1 Background and motivation

Individuals and organizations across the world rely on availability of electricity to carry out essential daily activities. Global electricity generation is set to increase by 69 % by 2040 while commitments to reduce greenhouse gas emissions are predicted to lead to 3 % average annual growth in electricity generation from renewable resources, as illustrated in Figure 1.1 [1]. These developments are transforming transmission and distribution of electric power.

System operators have to manage generation that is less controllable and more decentralized, but must still provide security and economy of supply. To meet these deliverables, system operators rely on effective monitoring, protection and control of the power system. Accurate knowledge of the system state is crucial for recognising, preventing and isolating catastrophic failures that can compromise safety and lead to financial losses.

Over the past three decades a new generation of power system measurement technology has evolved, which is revolutionizing system operation. Through synchronized phasor measurement technology it has become possible to simultaneously measure magnitude, phase angle and frequency of voltage and current signals across a power system spanning hundreds of kilometres [2]. Worldwide, Wide Area Monitoring, Protection And Control (WAMPAC) systems are being developed and deployed on the basis of synchrophasor measurement capabilities [3–5].

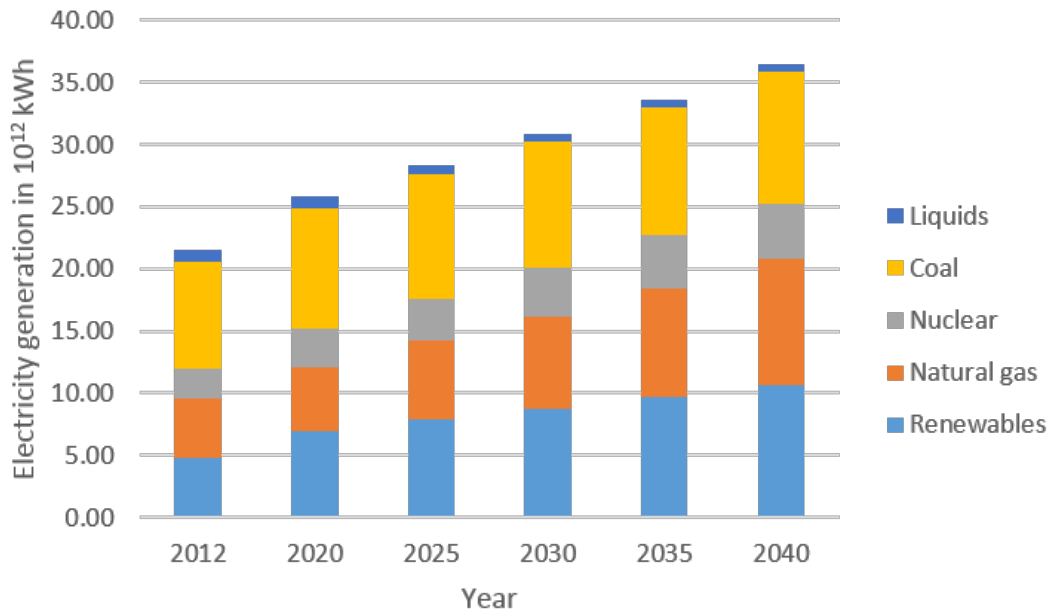


Figure 1.1: World net electricity generation by energy source, 2010-40 [1]

A WAMPAC includes communications infrastructure that allows system-wide synchrophasor measurement data to be collected at a central point, where the data is fed into numerous applications that ensure system reliability through increased situational awareness. Key application areas are real-time system visualization, prevention as well as post-event analysis of faults, validation of system models, advanced state estimation, real-time congestion management, real-time angular, voltage, and frequency stability, improved damping of inter-area oscillations, design of adaptive protection and control systems [6].

Validation of system model parameters is a synchrophasor measurement application that stands out since power system models underpin fundamental operational activities including contingency analysis, state estimation, protection and fault location [7–9]. An important set of network data that feed into the system model are impedance parameters of overhead lines. Measurement accuracies of 0.1% or better, synchronization to Coordinated Universal Time (UTC) within 1 μ s and reporting rates of up to 50 per second [10] make synchrophasor measurements suitable candidates for overhead line impedance determination. High accuracy measurements are required because the impedance derives from differences that are often at least one order of magnitude smaller than the absolute quantities. Moreover, impedance parameters can be linked to the thermal state of overhead line conductors and thus used to obtain dynamic line ratings, which in turn have the potential to increase system security and reduce operational costs [11].

By utilizing synchrophasor measurements to determine overhead line impedance parameters, a more accurate model representation of power systems can be achieved as well as real-time awareness of asset health. For these reasons, synchrophasor-based overhead line impedance monitoring is considered to be of significant value to increased system reliability; hence, in this thesis novel contributions are made to advance the methodology that is required to realize this powerful application.

1.2 Problem statement

The central problem of this thesis is the identification of overhead line impedance parameters from synchronized measurements of voltage and current such that average conductor temperature can be tracked. An overall framework is needed, which takes synchrophasor measurements as inputs and returns values of conductor temperature as outputs. To establish such a framework, the physical processes and relationships that are relevant to link voltage and current, line impedance parameters and temperature with sufficient accuracy must be identified; notably, the synchrophasor measurement process, transmission line theory and conductor-temperature relationship. It must be resolved which parameters can be drawn from *a priori* knowledge and which are unknown. To complete the framework, effective estimation methods are required to identify values of unknown parameters. The problem is illustrated in Figure 1.2.

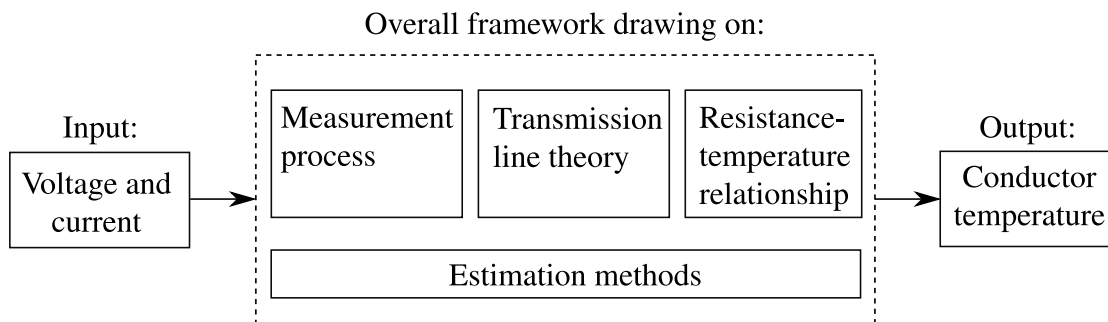


Figure 1.2: Illustration of the problem addressed in this thesis

Existing methods for overhead line impedance parameter identification assume that series resistance is constant. To track changing parameter values, only voltage and current measurements from a short moving time window can be used for parameter estimation. The lack of variation in system state can cause underdetermination and ill-conditioning of the parameter estimation problem, which leads to numerical inaccuracy of estimated values; this problem intensifies if other parameters must be determined in addition to overhead line impedance, such as measurement calibration factors. These aspects will be outlined in detail in Chapter 2, which reviews previous research on this problem.

1.3 Contributions

In light of the problem statement given in Section 1.2, this thesis makes the following contributions:

Comparative assessment of existing methods for synchrophasor-based impedance parameter identification. It is shown that there is at least one actual overhead line system, for which different types of existing methods cannot track impedance parameters with an accuracy suitable for temperature monitoring. Various strengths and weaknesses of the methods in terms of robustness to real-world, non-ideal conditions are revealed; in particular, systematic errors in the phasor measurements as well as poor conditioning of the parameter estimation problems are identified as practical obstacles.

Novel methods for accurate monitoring of overhead line impedance parameters and average conductor temperature. New methods are presented, which treat series resistance as a time-variant parameter. It is recognized that more system information in addition to synchrophasor measurements of voltage and current is needed to identify all relevant parameters. The first novel development is to incorporate knowledge of variation of impedance parameters over time to identify correction factors for systematic measurement errors. A further innovation is the utilization of conductor temperature measurements such that correction factors and resistance-temperature parameters can be estimated for the system using synchrophasor measurements from an unlimited time span; in addition, an algorithm for selecting the best parameter values from different time spans is given. The key strengths of the novel methodology are increased numerical accuracy and consistency of estimated parameters through better conditioned estimation problems as well as increased reliability of estimated temperature values.

1.4 Publications

The work that will be presented in this thesis has been disseminated through the following publications:

- D. Ritzmann, J. Rens, P. S. Wright, W. Holderbaum and B. Potter, “A novel approach to noninvasive measurement of overhead line impedance parameters,” *IEEE Transactions on Instrumentation and Measurement*, vol. 66, no. 6, pp. 1155–1163, Jun. 2017
- D. Ritzmann, P. S. Wright, W. Holderbaum and B. Potter, “A method for accurate transmission line impedance parameter estimation,” *IEEE Transactions on Instrumentation and Measurement*, vol. 65, no. 10, pp. 2204–2213, Oct. 2016
- D. Ritzmann, W. Holderbaum, B. Potter and P. Wright, “Improving the accuracy of synchrophasor-based overhead line impedance measurement,” in *2015 IEEE International Workshop on Applied Measurements for Power Systems (AMPS)*, IEEE, Sep. 2015, pp. 132–137
- D. Ritzmann, P. S. Wright, W. Holderbaum and B. Potter, “Application and analysis of synchrophasor-based online impedance measurement methods,” in *23rd International Conference on Electricity Distribution (CIRED)*, Lyon, 2015

1.5 Thesis structure

This section gives an overview of the structure of this thesis.

Chapter 2 is a literature review that provides a theoretical foundation and justification for the research in this thesis. The fields of transmission line theory, synchrophasor measurement and estimation theory are first considered on an individual basis. Subsequently, previous research that has combined concepts from these three fields to produce methods for synchrophasor-based overhead line impedance parameter identification will be examined carefully. The need for further research is outlined at the end of the chapter.

Chapter 3 presents two comparative studies. In the first study, the results of implementation of different types of existing methods for impedance parameter identification from synchrophasor measurements on an actual overhead line are presented. The effectiveness of the methods is assessed and compared according to a set of criteria defined in the chapter. Since none of the selected methods gives results with acceptable accuracy, the second study uses a software simulation of the overhead line to understand the limits of the selected existing methods. Impedance parameters are estimated in different scenarios under ideal and non-ideal measurement conditions. The results reveal systematic measurement errors as a cause for unacceptable field measurement results.

Chapter 4 proposes a method for real-time monitoring of overhead line impedance parameters from synchrophasor measurements with systematic errors. The novelty of the method is distinguished by its utilization of information about the dynamic behaviour of overhead line impedance and admittance; specifically, time-variance of series resistance and time-invariance of series reactance and shunt parameters. The effectiveness of the innovative method is demonstrated in two case studies. The first case study is on measurements from a laboratory-based short transmission line model; the second case study tests the method on different cases of systematic measurement errors taken from a software simulation of an overhead line. While the shift in fundamental assumptions elevates the method with respect to existing work, its limits are recognised.

Chapter 5 builds on the findings of the previous chapters to introduce robust methodology for accurate real-time monitoring of overhead line impedance. A new parameter estimation problem is defined, which seeks to find values of not only measurement correction factors but also parameters of the linear resistance-temperature relationship. Two methods are presented for estimation of the unknowns from voltage, current and conductor temperature measured over an arbitrary time span.

The first method is an extension of the work from Chapter 4, while the second method is developed from existing work. In addition, an algorithm for selection of the best parameter estimates from various measurement sets is given. The novel methods are first verified in a case study on a laboratory-based emulation of a transmission line and then in a second case study on field data from the same overhead line investigated in Chapter 3.

Chapter 6 concludes the thesis by summarizing the contributions to knowledge and outlining areas for future work.

Chapter 2

Literature review

2.1 Introduction

Knowledge of accurate overhead line impedance parameters is important for various power system operational activities, including state estimation, fault location, line protection and conductor temperature monitoring. Therefore, overhead line impedance parameter identification has been the subject of a wealth of previous research. To determine overhead line impedance in real-time, technological and theoretical concepts behind synchrophasor measurements must be combined with transmission line theory and modelling as well as system parameter identification.

This chapter provides a foundation that supports the research in this thesis and reviews strengths and weaknesses of previous research. Section 2.2 gives background knowledge on topics that underpin synchrophasor-based overhead line impedance monitoring including transmission line theory, synchrophasor measurements and estimation theory; Section 2.3 reviews recently proposed impedance estimation methods and identifies gaps that need to be addressed to advance synchrophasor-based overhead line impedance monitoring. Section 2.4 concludes this chapter.

2.2 Background

The purpose of electric power systems is to generate and deliver electrical energy to customers for industrial or domestic consumption. Since the places of generation are often far from the load centres, bulk transfer of electrical power over hundreds of kilometres is necessary and achieved through transmission along overhead power lines. To minimize resistive losses, power is transmitted at high voltage levels; for instance, at 400 kV and 275 kV in the United Kingdom (UK) and at 765 kV, 500 kV and 345 kV in the United States of America (USA) [16].

Overhead power lines consist of bare metal conductors that are suspended from supporting towers via insulators. Modern power systems normally have three phases, and each phase of an overhead line consists of one conductor or several in a bundle. The arrangement of the conductors depends on the structure of the supporting towers, examples of which are shown in Figure 2.1; many structures are designed to support multiple three-phase circuits, the tower in Figure 2.1b supports a double-circuit line.



(a) 380 kV transmission line tower 7610-74 in Wittighausen, Baden-Württemberg, Germany¹



(b) 400 kV L6 D transmission line tower with quad conductor bundles near Aust, Gloucestershire, England²

Figure 2.1: Examples of transmission line towers

The actual conducting cables consist of layered strands of aluminium in composition with other materials. Common conductor types are Aluminium Conductor Steel Reinforced (ACSR), Aluminium Conductor Alloy Reinforced (ACAR), All Aluminium Conductor (AAC) and All Aluminium Alloy Conductor (AAAC) [17, 18]. The selection of conductor type and size must be such that various limiting factors satisfy the requirements for the transmission line, including maximum allowable conductor current, line power and voltage loss, required spans and sags as well as resilience to environmental conditions [18].

The material properties and physical arrangement of the conductors determine the electrical properties of the transmission line, which are series resistance and inductance as well as shunt conductance and capacitance. These electrical parameters in turn influence the drops in voltage and current across the line. Relationships between line voltage and current and electrical parameters are given by transmission line theory, which will be discussed next.

¹Photo credit: Zonk43 (own work) via Wikimedia Commons, https://commons.wikimedia.org/wiki/File:Anlage7610_Mast74_22072016_1.JPG, accessed on 11/02/2017, reproduced without modification under the Creative Commons Attribution-Share Alike 3.0 Unported licence, <https://creativecommons.org/licenses/by-sa/3.0/deed.en>

²Photo credit: Yummifruitbat (own work) via Wikimedia Commons, https://commons.wikimedia.org/wiki/File:Pylon_ds.jpg, accessed on 11/02/2017, reproduced without modification under the Creative Commons Attribution-Share Alike 2.5 Generic licence, <https://creativecommons.org/licenses/by-sa/2.5/deed.en>

2.2.1 Transmission line theory

The theory of transmission lines evolved in the 19th century through significant contributions from Lord Kelvin and Oliver Heaviside [19, 20], in the wake of the invention of the telegraph and installation of the first transatlantic communication cables. Transmission line theory gives mathematical relationships that describe the propagation of electrical signals along conductors with respect to distance and time. The speed of propagation, attenuation and phase shift of the signals along the line depend on the electrical properties of the conductors and surrounding medium. The following aspects of transmission line theory will be discussed:

- Single-phase telegraph equations
 - Time domain solutions
 - Frequency domain solutions
- Three-phase telegraph equations
- Other overhead line modelling aspects
 - Non-uniformity
 - Untransposed overhead lines
 - Thermal and mechanical coupling
- Calculation of line parameters from handbook formulae

2.2.1.1 Single-phase telegraph equations

Overhead line conductors are normally assumed to be uniform, i.e. to have constant circular cross-section and to be parallel to each other and the earth at all points along the line. The surrounding air is assumed to be a homogeneous medium, which means that the permittivity and permeability are constant through time and space. Overhead transmission lines are lossy since they have series resistance and shunt conductance. Under these assumptions, the relationship between voltage and current at any given time and distance along the line is given by the telegraph equations [20], which can be derived from Maxwell's equations for transverse electromagnetic fields, or by applying Kirchhoff's laws to an infinitely small line section modelled by the circuit in Figure 2.2.

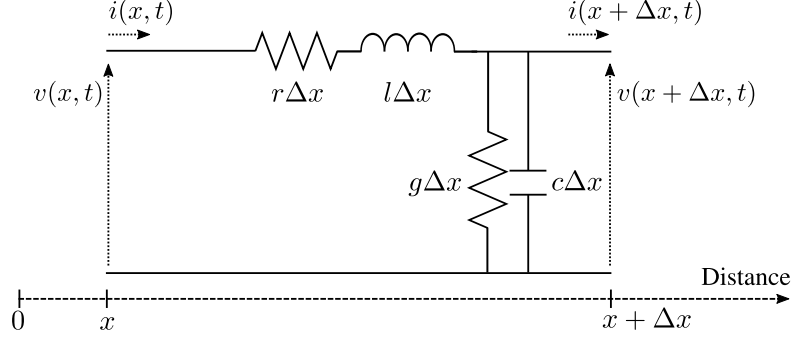


Figure 2.2: Small transmission line section

Define $v(x, t), i(x, t) \in \mathbb{R}$ as line voltage and current signals at time $t \in \mathbb{R}_{\geq 0}$ and distance $x \in \mathbb{R}_{\geq 0}$ along the line; $r, l, g, c \in \mathbb{R}_{\geq 0}$ are the per-unit-length resistance, inductance, conductance and capacitance, respectively. The telegraph equations for a single-phase line are

$$\frac{\partial v(x, t)}{\partial x} = -ri(x, t) - l\frac{\partial i(x, t)}{\partial t} \quad (2.1)$$

$$\frac{\partial i(x, t)}{\partial x} = -gv(x, t) - c\frac{\partial v(x, t)}{\partial t}. \quad (2.2)$$

Equations (2.1) and (2.2) are coupled, first-order differential equations in the time domain. In the following paragraphs, solutions of these time domain equations are discussed.

A. Time domain solutions

The advantage of analysing the time domain telegraph equations is that voltage $v(x, t)$ and current $i(x, t)$ can be arbitrary functions of time and thus describe any non-steady state transient signal. For a lossless line ($r = g = 0$), d'Alembert's formula can be used to obtain a general solution consisting of forward travelling waves $i_+, v_+ : \mathbb{R}^2 \rightarrow \mathbb{R}$ and backward travelling waves $i_-, v_- : \mathbb{R}^2 \rightarrow \mathbb{R}$ [21]:

$$v(x, t) = v_+(x - \nu t) + v_-(x + \nu t) \quad (2.3)$$

$$i(x, t) = i_+(x - \nu t) + i_-(x + \nu t), \quad (2.4)$$

where $\nu = 1/\sqrt{lc}$ is the velocity of propagation. The method of characteristics, also known as Bergeron's method [22], can be used to obtain a full solution using the terminal conditions at $x = 0$ and $x = x_l$ for a line of length $x_l \in \mathbb{R}_{\geq 0}$:

$$i(0, t) = \frac{v(0, t)}{z_c} - \frac{v(x_l, t - \tau)}{z_c} - i(x_l, t - \tau) \quad (2.5)$$

$$i(x_l, t) = \frac{v(x_l, t)}{z_c} - \frac{v(0, t - \tau)}{z_c} - i(0, t - \tau), \quad (2.6)$$

where $\tau = x_l/\nu$ is the time it takes to travel along the line at the propagation velocity and $z_c = \sqrt{l/c}$ is the line's characteristic impedance. Equations (2.5) and (2.6) correspond to the equivalent circuit shown in Figure 2.3, known as the Bergeron model, whereby the current sources are defined as $i_0(t - \tau) = -\frac{v(x_l, t - \tau)}{z_c} - i(x_l, t - \tau)$, $i_{x_l}(t - \tau) = -\frac{v(0, t - \tau)}{z_c} - i(0, t - \tau)$ [23].

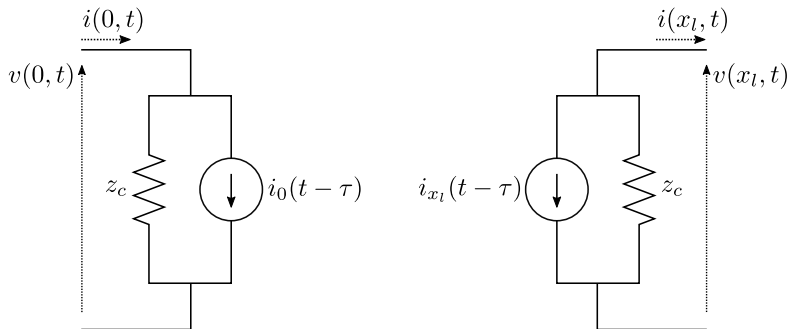


Figure 2.3: Bergeron model equivalent circuit

For lossy lines ($r, g \neq 0$), there is no general analytical solution to the telegraph equations [24, 25]. The Bergeron model can be extended to approximate lines with resistive losses [23]. Define the total line resistance $R = rx_l$; $Z = z_c + R/4$; $h = (z_c - R/4)/Z$. In Figure 2.3, z_c must be replaced with Z to incorporate the resistive losses. The equations for a lossy line with $g = 0$ are

$$i(0, t) = \frac{1+h}{2} \left(\frac{1+h}{Z} v(x_l, t) - hi(x_l, t - \tau) \right) + \frac{1-h}{2} \left(\frac{1+h}{Z} v(0, t - \tau) - hi(0, t - \tau) \right) \quad (2.7)$$

$$i(x_l, t) = \frac{1+h}{2} \left(\frac{1+h}{Z} v(0, t) - hi(0, t - \tau) \right) + \frac{1-h}{2} \left(\frac{1+h}{Z} v(x_l, t - \tau) - hi(x_l, t - \tau) \right). \quad (2.8)$$

The Bergeron model does not represent frequency-dependent line parameters. As an alternative, the telegraph equations can be solved in the frequency domain and transformed back to the time domain to obtain a solution, but the inverse Fourier transform results in convolution integrals that are not directly integrable [25]. The convolution integrals must be evaluated numerically, for instance by the Finite Difference Time Domain method [25, 26]. It is far easier to model frequency-dependent line parameters in the frequency domain, which will be discussed next.

B. Frequency domain solutions

The frequency domain telegraph equations and general solution will be given first, thereafter, transmission line models based on a particular solution are discussed. In the frequency domain, voltage and current signals are decomposed into different frequency components by a Fourier transform. The time domain signals can be recovered through inverse transformation. For each frequency, the telegraph equations can be analysed individually. Define voltage and current phasors $V(x), I(x) \in \mathbb{C}$ as signal components at angular frequency $\omega \in \mathbb{R}_{\geq 0}$. The telegraph equations in $V(x), I(x)$ are

$$\frac{dV(x)}{dx} = -rI(x) - j\omega lI(x) \quad (2.9)$$

$$\frac{dI(x)}{dx} = -gV(x) - j\omega cV(x). \quad (2.10)$$

Define line impedance $z \in \mathbb{C}$ and admittance $y \in \mathbb{C}$ as $z = r + j\omega l$, $y = g + j\omega c$, where r, l, g, c are per-unit-length resistance, inductance, conductance and capacitance at frequency ω . Then (2.9) and (2.10) become

$$\frac{dV(x)}{dx} = -zI(x) \quad (2.11)$$

$$\frac{dI(x)}{dx} = -yV(x). \quad (2.12)$$

By differentiating with respect to x and substitution, equations (2.11) and (2.12) become wave equations:

$$\frac{d^2V(x)}{dx^2} = zyV(x) \quad (2.13)$$

$$\frac{d^2I(x)}{dx^2} = yzI(x). \quad (2.14)$$

The general solutions are

$$V(x) = a_1 \exp(\sqrt{zy}x) + a_2 \exp(-\sqrt{zy}x) \quad (2.15)$$

$$I(x) = b_1 \exp(\sqrt{zy}x) + b_2 \exp(-\sqrt{zy}x), \quad (2.16)$$

where $a_1, a_2, b_1, b_2 \in \mathbb{C}$ are general constants. Define $\gamma = \sqrt{zy}$ as the propagation constant. Particular solutions are found using boundary conditions of voltage and current. In the following paragraphs, different line models are discussed that arise when boundary conditions $V(0) = V_s, V(x_l) = V_r, I(0) = I_s, I(x_l) = I_r$ are used to determine constants a_1, a_2, b_1, b_2 .

Line model 1: Distributed line

Given boundary conditions $V(0) = V_s, V(x_l) = V_r, I(0) = I_s, I(x_l) = I_r$ for a line of length $x_l \in \mathbb{R}_{\geq 0}$, solutions (2.15) and (2.16) become

$$V_s = \cosh(\gamma x_l) V_r + Z_c \sinh(\gamma x_l) I_r \quad (2.17)$$

$$I_s = \frac{1}{Z_c} \sinh(\gamma x_l) V_r + \cosh(\gamma x_l) I_r, \quad (2.18)$$

where $Z_c = \sqrt{z/y}$ is the characteristic impedance. Equations (2.17) and (2.18) are known as the distributed line model, relating sending and receiving end currents and voltages to per-unit-length line parameters [27].

Line model 2: Two-port network equivalent

As a general equivalent circuit, a transmission line can be replaced by a two-port network as shown in Figure 2.4 [28].

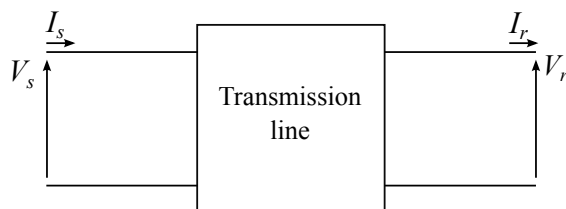


Figure 2.4: Diagram of a two-port network

The two-port network model consists of two linear equations that relate the terminal voltages and currents. Depending on the choice of independent terminal quantities, the network parameters are classified into impedance parameters, hybrid parameters and chain parameters as well as their corresponding inverses [29]. In the case of a transmission line, the voltage and current at one line end are considered to be independent, while those at the other end are dependent; hence, V_s, I_s, V_r, I_r are related by the chain parameters $A, B, C, D \in \mathbb{C}$:

$$\begin{bmatrix} V_s \\ I_s \end{bmatrix} = \begin{bmatrix} A & B \\ C & D \end{bmatrix} = \begin{bmatrix} V_r \\ I_r \end{bmatrix}. \quad (2.19)$$

By comparing equations (2.17,2.18) with (2.19), it can be observed that the two-port network becomes equivalent to the distributed line model if $A = D = \cosh(\gamma x_l)$, $B = Z_c \sinh(\gamma x_l)$ and $C = 1/Z_c \sinh(\gamma x_l)$. The equivalent two-port network is symmetric since $A = D$ and reciprocal since $AD - BC = 1$; therefore the network can consist only of passive, linear components, without dependent sources.

Line model 3: Equivalent and nominal circuits

In principle, the equivalent two-port network can be resolved into any symmetric circuit consisting of linear elements. However, there are only two equivalent circuits that consist of the minimum number of three elements; the T-circuit and the pi-circuit are the simplest equivalent circuit models to represent a transmission line [30]. Both configurations are shown in Figure 2.5.

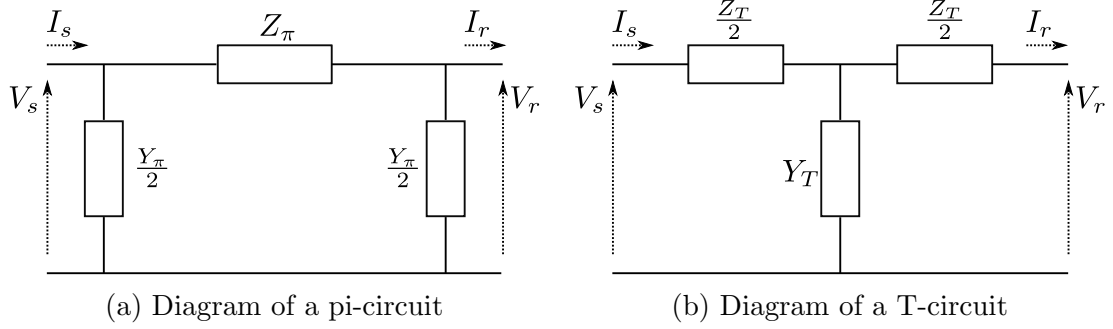


Figure 2.5: Transmission line equivalent circuits

The pi-circuit equations are

$$V_s - V_r = (I_s - V_r Y_\pi / 2) Z_\pi \quad (2.20)$$

$$I_s - I_r = 2(V_s + V_r) Y_\pi, \quad (2.21)$$

where $Z_\pi = Z_c \sinh(\gamma x_l)$ is referred to as series impedance and $Y_\pi = 2/Z_c \tanh(\gamma x_l / 2)$ as shunt admittance of a line of length x_l . For lines that are sufficiently short relative to the signal wavelength, pi-circuit parameters can be approximated as $Z_\pi = z x_l$, $Y_\pi = y x_l$; the circuit is then an approximate representation of the distributed line model, referred to as the nominal pi-circuit. The T-circuit equations are

$$V_s - V_r = (I_s + I_r) Z_T / 2 \quad (2.22)$$

$$I_s - I_r = (V_s - I_s Z_T / 2) Y_T, \quad (2.23)$$

where $Y_T = 1/Z_c \sinh(\gamma x_l)$ and $Z_T = 2Z_c \tanh(\gamma x_l / 2)$ for an equivalent representation of the distributed line model and $Y_T = y x_l$, $Z_T = z x_l$ for a nominal T-circuit.

2.2.1.2 Three-phase telegraph equations

The models discussed in the preceding paragraphs are for single-phase transmission lines. For a three-phase line, the voltages and currents are summarized by the vectors $\mathbf{v}(x, t), \mathbf{i}(x, t) \in \mathbb{R}^3$ and the electrical properties by the matrices $\mathbf{r}, \mathbf{l}, \mathbf{g}, \mathbf{c} \in \mathbb{R}^{3 \times 3}$, such that the time domain telegraph equations become

$$\frac{\partial \mathbf{v}(x, t)}{\partial x} = -\mathbf{r}\mathbf{i}(x, t) - \mathbf{l} \frac{\partial \mathbf{i}(x, t)}{\partial t} \quad (2.24)$$

$$\frac{\partial \mathbf{i}(x, t)}{\partial x} = -\mathbf{g}\mathbf{v}(x, t) - \mathbf{c} \frac{\partial \mathbf{v}(x, t)}{\partial t}. \quad (2.25)$$

Suppose voltage and current signals $\mathbf{v}(x, t), \mathbf{i}(x, t)$ are transformed to the frequency domain by a Discrete Fourier Transform (DFT). Let $\mathbf{V}(x), \mathbf{I}(x) \in \mathbb{C}^3$ be vectors of voltage and current phasors, and $\mathbf{z}, \mathbf{y} \in \mathbb{C}^{3 \times 3}$ per-unit-length impedance and admittance matrices for angular frequency $\omega \in \mathbb{R}_{\geq 0}$. Then the second order frequency domain telegraph equations are

$$\frac{d^2 \mathbf{V}(x)}{dx^2} = -\mathbf{z}\mathbf{y}\mathbf{V}(x) \quad (2.26)$$

$$\frac{d^2 \mathbf{I}(x)}{dx^2} = -\mathbf{y}\mathbf{z}\mathbf{I}(x). \quad (2.27)$$

The parameter matrices $\mathbf{r}, \mathbf{l}, \mathbf{g}, \mathbf{c}, \mathbf{z}, \mathbf{y}$ are non-diagonal, thus, voltage and current are coupled between the three phases both in the time and in the frequency domain, which means there is no general, closed-form solution to the differential equations. However, decoupling can be achieved through a similarity transformation of the three-phase voltage and current vectors. The decoupling process is the same for the time and frequency domain, but for simplicity a brief overview will be given in the frequency domain only. Define modal voltage and current vectors $\mathbf{V}_m, \mathbf{I}_m \in \mathbb{C}^3$ and constant transformation matrices $\mathbf{T}_v, \mathbf{T}_i \in \mathbb{C}^{3 \times 3}$, then

$$\mathbf{V}(x) = \mathbf{T}_v \mathbf{V}_m(x) \quad (2.28)$$

$$\mathbf{I}(x) = \mathbf{T}_i \mathbf{I}_m(x). \quad (2.29)$$

Substitution into (2.26) and (2.27) gives

$$\frac{d^2 \mathbf{V}_m(x)}{dx^2} = -\mathbf{T}_v^{-1} \mathbf{z}\mathbf{y}\mathbf{T}_v \mathbf{V}_m(x) = -\boldsymbol{\gamma}_v^2 \mathbf{V}_m(x) \quad (2.30)$$

$$\frac{d^2 \mathbf{I}_m(x)}{dx^2} = -\mathbf{T}_i^{-1} \mathbf{y}\mathbf{z}\mathbf{T}_i \mathbf{I}_m(x) = -\boldsymbol{\gamma}_i^2 \mathbf{I}_m(x). \quad (2.31)$$

In order for (2.30) and (2.31) to decouple, $\boldsymbol{\gamma}_v^2$ and $\boldsymbol{\gamma}_i^2$ must be diagonal matrices, which implies that their diagonal elements are eigenvalues of $\mathbf{z}\mathbf{y}$ and $\mathbf{y}\mathbf{z}$,

respectively, while the column vectors of \mathbf{T}_v and \mathbf{T}_i are the corresponding eigenvectors [31]. Since \mathbf{z} and \mathbf{y} are symmetric matrices, $\mathbf{zy} = [\mathbf{yz}]^T$, which implies that \mathbf{zy} and \mathbf{yz} have the same eigenvalues, hence, $\gamma_v^2 = \gamma_i^2 = \gamma^2$ [32]. Once $\mathbf{T}_v, \mathbf{T}_i$ are chosen such that the modal wave equations decouple, each mode can be treated as a single-phase system using the solution methods and equivalent models discussed previously.

In general, knowledge of the impedance and admittance matrices is required to select decoupling transformation matrices. However, if the self and mutual parameters are equal for all three phases, i.e. if the diagonal elements of the impedance (and admittance) matrix are equal and all off-diagonal elements are equal, decoupling transformation matrices can be chosen without knowledge of the parameter values. This assumption holds if the three overhead line phase conductors are transposed, as illustrated in Figure 2.6.

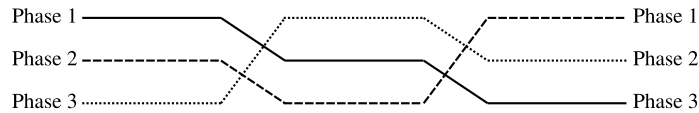


Figure 2.6: Example of a line transposition pattern

There are two general transformations that are commonly used in power systems analysis: the symmetrical component transformation into zero, positive and negative sequence components, and the Clarke transformation into alpha, beta and gamma components [33, 34].

2.2.1.3 Other overhead line modelling aspects

In the previous paragraphs, transmission line equations and models for uniform, transposed lines have been considered, describing only the relationship between electrical signals and parameters. In the following paragraphs, modelling approaches for non-uniform and untransposed lines are discussed, as well as modelling of mechanical and thermal line properties.

A. Non-uniformity

In practice, overhead transmission lines are not uniform; the line parameters are functions of distance along the line due to sagging of the conductors and temperature gradients. Representation of non-uniformity in transmission line models has been studied extensively, with one dominant approach being the segmentation of the line into uniform sections with different parameters [35–37]. Common applications of non-uniform line models are analysis of waves travelling on transmission

line towers, overhead lines that pass through mountainous regions, across rivers or different climatic zones [36, 37].

B. Untransposed overhead lines

For overhead lines that are untransposed and do not have a vertically symmetrical conductor arrangement, the Clarke and symmetrical component transformations do not result in decoupled modes. Assuming that the per-unit-length line parameters are known, individual transformation matrices for untransposed lines can be computed numerically in the frequency domain. The computation is more complicated in the time domain due to frequency dependence [38, 39], and not possible if line impedance and admittance parameters are not known *a priori*. An alternative approach is the use of approximate transformation matrices or to avoid modal transformation by working with phase-domain models [40, 41].

C. Thermal and mechanical coupling

Transmission line theory is first and foremost concerned with the electrical states and parameters, but in practical overhead power line operation, modelling of thermal and mechanical properties is also of interest. The thermal state of the conductors is defined by their temperature, which is a result of internal Joule heating and external warming and cooling effects [42, 43]. Conductor temperature is coupled to the electrical line model via the series resistance; define $R_0 \in \mathbb{R}_{\geq 0}$ as the conductor resistance at a reference temperature $T_0 \in \mathbb{R}$, $R : \mathbb{R} \rightarrow \mathbb{R}_{\geq 0}$ as the conductor resistance at temperature $T \in \mathbb{R}$ and $\alpha \in [-1, 1]$ as the resistance-temperature coefficient. Then the linear resistance-temperature relationship is

$$R(T_c) = R_0(1 + \alpha(T - T_0)). \quad (2.32)$$

In equation (2.32), R_0 and $R(T_c)$ are per-unit-length DC values; however, the relationship can also be defined for AC values [43]. The coefficient α is then based on two reference points $(R_0, T_0), (R_1, T_1)$:

$$\alpha = \frac{1}{R_0} \frac{R_1 - R_0}{T_1 - T_0}. \quad (2.33)$$

Temperature is related to the conductor length via thermal expansion, which determines the height above ground via the mechanical sag-tension model [44, 45]. Conductor height in turn influences line inductance and capacitance as will be discussed next, hence, the electrical properties are also coupled to the mechanical model.

2.2.1.4 Calculation of line parameters from handbook formulae

A. Series impedance matrix

In the 1920s, John Carson developed formulae for the calculation of self and mutual impedance of bare overhead conductors with ground return [46]. These formulae are based on the solution of Maxwell's equations for transverse electromagnetic waves propagating along straight, uniform, parallel conductors and are functions of conductor resistance, spacing and earth resistivity. To the present day, Carson's equations form the basis for impedance calculations in handbooks and computer programs [47, 48]. The formulae are based on the method of images, whereby a reflection of the conductors below the ground is considered as shown in Figure 2.7.

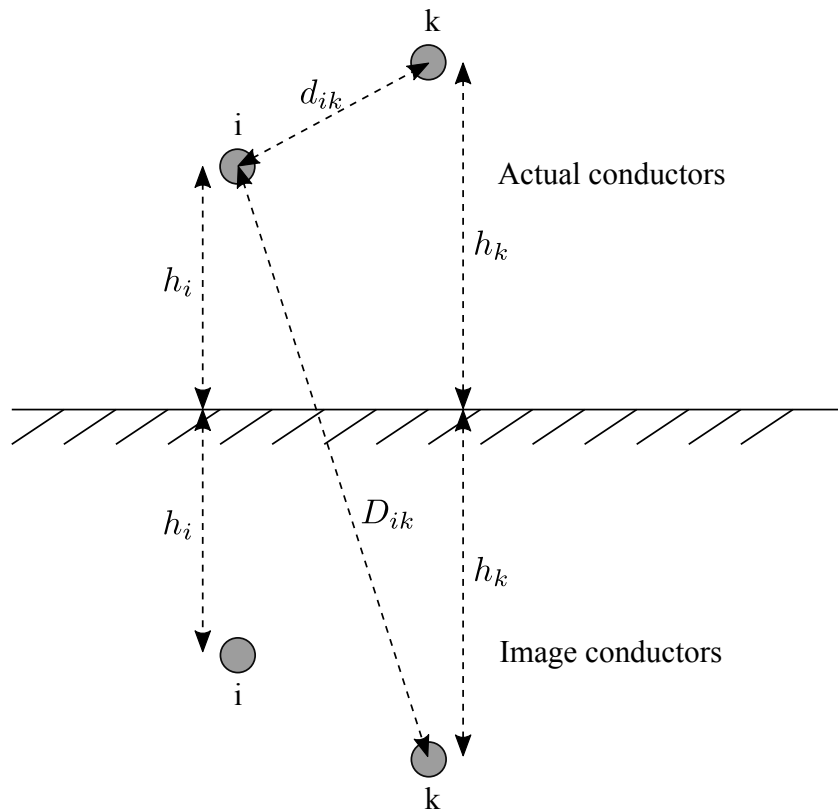


Figure 2.7: Schematic diagram of the geometrical configuration of two actual conductors and their images [48]

Define the following variables:

$z_{s_i} \in \mathbb{C}$	per-unit-length self impedance of the i th conductor with ground return
$z_{m_{ik}} \in \mathbb{C}$	per-unit-length mutual impedance between the i th and k th conductors with ground return
$g_i \in \mathbb{R}_{\geq 0}$	geometric mean radius of i th conductor
$h_i \in \mathbb{R}_{\geq 0}$	height of i th conductor
$r_i \in \mathbb{R}_{\geq 0}$	AC resistance of i th conductor
$d_{ik} \in \mathbb{R}_{\geq 0}$	distance between the i th and k th conductors
$D_{ik} \in \mathbb{R}_{\geq 0}$	distance between the i th conductor and image of k th conductors
$f \in \mathbb{R}_{\geq 0}$	frequency, $\omega = 2\pi f$ - angular frequency
$\mu \in \mathbb{R}_{\geq 0}$	permeability of the conductor
$I_g \in \mathbb{C}$	infinite integral that models the effect of earth resistivity

Then

$$z_{s_i} = r_i + j \frac{\omega \mu}{2\pi} \ln(h_i/g_i) + 4\omega I_g \quad (2.34)$$

$$z_{m_{ik}} = j \frac{\omega \mu}{2\pi} \ln(D_{ik}/d_{ik}) + 4\omega I_g. \quad (2.35)$$

Calculated values of z_{s_i} and $z_{m_{ik}}$ are used to construct impedance matrices with dimension $n \times n$, where n is the total number of conductors including ground wires. Equations (2.34) and (2.35) show that the earth's resistivity introduces mutual resistance into the overhead line model. However, when positive sequence impedance is computed for a transposed three-phase line as

$$z_{s_i} - z_{m_{ik}} = r_i + j \frac{\omega \mu}{2\pi} \ln\left(\frac{h_i d_{ik}}{g_i D_{ik}}\right), \quad (2.36)$$

the term $4\omega I_g$ vanishes such that positive sequence resistance equals AC resistance.

B. Shunt admittance matrix

Shunt admittance is calculated by considering the potential of a conductor due to its own charge and that of other transmission line conductors; since shunt conductance is normally several orders of magnitude smaller than susceptance, it is often neglected in admittance calculations [34, 49]. Define

n	number of conductors above ground
$q_i \in \mathbb{C}$	charge per-unit-length of i th conductor, $i = 1, 2, 3, \dots, n$
$d_{ii} \in \mathbb{R}_{\geq 0}$	radius of i th conductor
$d_{ik} \in \mathbb{R}_{\geq 0}$	distance between the i th and k th conductor, $i \neq k$
$D_{ii} \in \mathbb{R}_{\geq 0}$	distance between the i th conductor and its image

$D_{ik} \in \mathbb{R}_{\geq 0}$ distance between the i th conductor and image of k th conductors, $i \neq k$
 $\epsilon \in \mathbb{R}_{\geq 0}$ permittivity of the medium
 $V_i \in \mathbb{C}$ voltage of i th conductor to ground

By derivation from Gauss's law for electric fields, V_i is given by [34]:

$$V_i = \frac{1}{2\pi\epsilon} \sum_{m=1}^n q_m \ln \left(\frac{D_{im}}{d_{im}} \right) \quad (2.37)$$

Define the following matrices:

$\mathbf{P} \in \mathbb{C}^{n \times n}$ - potential coefficient matrix with elements

$$p_{ij} = \frac{1}{2\pi\epsilon} \ln \left(\frac{D_{ii}}{d_{ij}} \right). \quad (2.38)$$

$\mathbf{V} \in \mathbb{C}^n$ - voltage vector, $\mathbf{V} = [V_1 \ V_2 \ V_3 \ \dots \ V_n]^T$,

$\mathbf{Q} \in \mathbb{C}^n$ - charge vector, $\mathbf{Q} = [q_1 \ q_2 \ q_3 \ \dots \ q_n]^T$

Based on (2.37), the voltages for n conductors can be summarized by the matrix equation

$$\mathbf{V} = \mathbf{P}\mathbf{Q}. \quad (2.39)$$

Capacitance is defined as the ratio of charge to voltage, $C = q/V$. Given matrices \mathbf{Q} and \mathbf{V} , let \mathbf{C} be the matrix of capacitance coefficients (also known as Maxwell's coefficients [34]), where

$$\mathbf{C} = \mathbf{Q}\mathbf{V}^{-1} = \mathbf{P}^{-1}. \quad (2.40)$$

The shunt admittance matrix is thus given by

$$\mathbf{Y} = j\omega\mathbf{C}. \quad (2.41)$$

By making use of conditions relating to bundling of conductors into three phases and assuming ground wires are at zero potential, the dimension of the impedance and admittance matrices \mathbf{Z} and \mathbf{Y} can be reduced to 3×3 for use with three-phase models [47, 50, 51].

In terms of power network modelling, Carson's formulae provide a static estimate of overhead line impedance and admittance matrices that depends on the chosen input values. To obtain a real-time estimate, the resistance must be adjusted for the actual conductor temperature, and inductance and capacitance values for the actual conductor height and spacing. Alternatively, the transmission line models discussed earlier in this section can be used to calculate impedance and admittance values if voltage and current measurements are available.

2.2.2 Synchronized phasor measurements

Synchronized phasor (synchrophasor) measurement is the estimation of the amplitude and phase angle of the fundamental frequency component of waveforms with respect to a common time reference. The concept became technologically feasible in the 1980s with the widespread availability of the Global Positioning System (GPS) as a synchronization source. Since then, synchronized measurement devices have been installed in many power networks, often spanning large geographical areas; they are collectively referred to as a Wide Area Monitoring System (WAMS) [52]. In this section, an overview will be given of the hardware behind the synchrophasor measurement process, phasor estimation algorithms and measurement accuracy.

2.2.2.1 Synchrophasor measurement technology

The earliest instruments with synchrophasor measurement capability were specially designed Phasor Measurement Units (PMUs); a prototype was built at Virginia Polytechnic Institute in 1988 [53]. Figure 2.8 shows the main hardware components required for the synchrophasor measurement process.

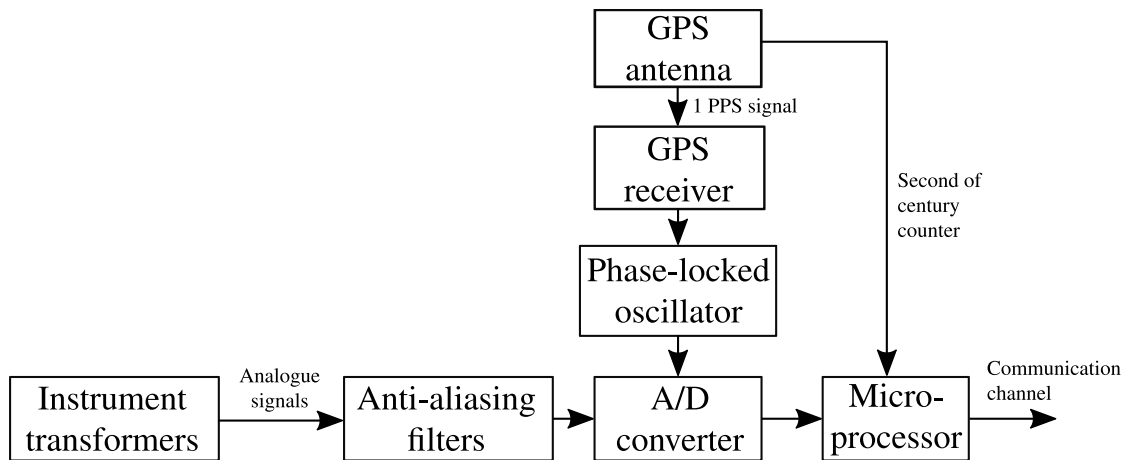


Figure 2.8: Main hardware components of the synchrophasor measurement process [54]

The analogue signals first pass through an anti-aliasing filter and are then sampled by an analogue-to-digital (A/D) converter, whose sampling clock is phase-locked to the 1 PPS (Pulse Per Second) signal provided by a GPS receiver. The microprocessor estimates phasors from the sampled signals as well as frequency and its rate of change, adds a UTC time tag and produces an output data file that can be communicated to a phasor data concentrator for system wide monitoring. Since the 1990s, a number of manufacturers around the world have developed

commercially available instruments. In recent years, there has been a move away from single-purpose PMUs towards integrating synchrophasor measurement into other substation instruments such as fault recorders, power quality analysers or multi-functional intelligent electronic devices [55].

To support interoperability of instruments from different manufacturers, the IEEE has produced a Standard for Synchrophasor Measurements for Power Systems that defines the phasor and frequency measurement as well as accuracy and synchronization requirements under static and dynamic conditions [56].

2.2.2.2 Phasor estimation

A phasor is a frequency domain representation of a sinusoidal waveform in the time domain. Given the waveform $x(t) = X_0 \cos(\omega t + \phi)$ with amplitude $X_0 \in \mathbb{R}$ and phase angle $\phi \in [-\pi, \pi]$ at angular frequency $\omega \in \mathbb{R}_{\geq 0}$, the phasor representation is $X = X_0/\sqrt{2}(\cos(\phi) + j \sin(\phi))$; the concept is illustrated by the waveform and phasor diagram in Figure 2.9.

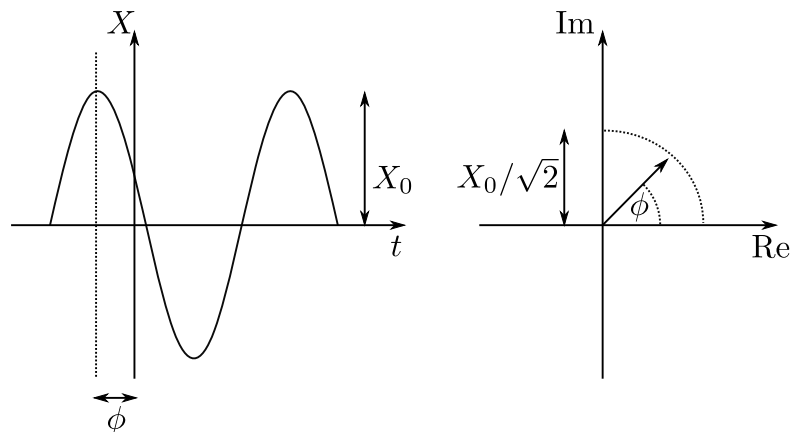


Figure 2.9: Sinusoidal waveform and its phasor representation in the complex plane [57]

The Discrete Fourier Transform (DFT) is the classical method of extracting the amplitude and phase angle of the fundamental frequency component from one cycle of sampled voltage and current signals. The phasor X describes a signal with constant amplitude and phase angle. Actual waveforms in power systems vary over time, therefore the phasor estimates are continuously updated using a sliding one-cycle window. The computational cost of the DFT can be reduced through recursive evaluation [58]. In addition to amplitude and phase angle modulation, power system voltage and current waveforms are subject to off-nominal frequencies and harmonic distortion, which can introduce errors in the phasor estimates. To maximize the accuracy of phasor estimation under off-nominal frequency and dynamic

conditions, a wide range of algorithms have been proposed. Examples include modifications of the classical, one-cycle DFT such as the Smart DFT [59], Shifting Window Average Method [60], Short Time Fourier Transform [61] or Fourier Transform with Taylor series derivatives [62]; other approaches are estimation by Kalman filter [63], Newton’s method [64] and Prony’s method [65]. Comparative analysis of phasor estimation algorithms has shown that the conventional one-cycle DFT satisfies standard requirements when the input signals are in steady-state close to nominal frequency (± 1 Hz), but other algorithms must be used to maintain accuracy at off-nominal frequencies and under dynamic conditions [66].

2.2.2.3 Synchrophasor measurement accuracy

The accuracy of synchrophasor measurement devices depends on the technical specifications of the instruments such as the resolution and sampling rate of the A/D converter, the synchronization and stability of the internal clock and the phasor estimation algorithm. The IEEE Standard for Synchrophasor Measurements for Power Systems sets the minimum accuracy level for synchrophasor measurements to 1 % Total Vector Error (TVE) [56], a metric that combines errors in magnitude and phase angle. However, instruments that are currently on the market can achieve 0.1 % or better [10, 67] and synchronization to within 1 μ s of UTC.

Before the voltage and current signals are processed for synchrophasor measurement, they must pass through the substation instrumentation channel, which consists of instrument transformers, burdens and cables [52]. These components can alter the signal magnitude and phase angle and thus the overall accuracy of the phasor measurements can be an order of magnitude worse than that of the synchrophasor measurement device [68]. Physical, on-site calibration of substation instrumentation channels is rare since it is time-consuming and expensive. One alternative is to calculate calibration factors through modelling and simulation of the entire instrumentation channel [69], which requires detailed knowledge of the properties of all components. Another approach are state estimation techniques, based on synchronized phasor measurements at various network nodes and accurate knowledge of the system model, including transmission line impedance parameters [70–73].

2.2.3 Estimation theory

The central topic of this thesis is the determination of the parameters of a mathematical overhead line model using synchrophasor data, thus, a system identification problem. According to Ljung, the system identification procedure consists of three basic entities [74]. The first entity is the data, which in this case arises from the synchrophasor measurements at the line ends during normal operation. The second entity are the set of candidate models. For overhead lines, parametrized model structures can be drawn from transmission line theory as reviewed in Section 2.2.1; the selected set are then classed as grey box models since transmission line theory derives from physical laws and the model parameters have a physical interpretation. Given a parametrized model structure, the task of system identification is to estimate parameter values such that the model satisfies an equivalence criterion, which is “a rule by which candidate models can be assessed using the data” and forms the third entity [74]. Different parameter estimation methods and their assessment criteria are discussed in the rest of this section, including:

- Bayes’ estimator
- Maximum likelihood estimator
- Least-squares estimators for linear models
- Recursive methods
- Non-linear parameter estimation

2.2.3.1 Bayes’ estimator

A Bayes’ estimator assumes that the probability density function of the measured system variables, probability density function of parameter values and cost function that is minimized when the parameter estimate equals the actual parameter values of the system are known *a priori*. Once the system measurements have been made, the *a posteriori* conditional probability density function of the parameters can be computed using Bayes’ theorem [75]. The risk of choosing a parameter estimate given the available measurements is defined as the expected value of the cost function. A Bayes’ estimator yields the parameter values that minimize this risk [75].

A commonly chosen cost function is the mean square error, defined as the expectation of the errors between estimated and true parameter values. The best parameter estimate gives the minimum mean square error.

2.2.3.2 Maximum likelihood estimator (MLE)

MLEs, as introduced by Fisher in 1912 [76], assume less *a priori* knowledge than Bayes' estimators; only the probability density function of the measured system variables is assumed to be known. The model parameters are assumed to be constant values, i.e. uniformly distributed, instead of random variables. The *a posteriori* probability density function of observing the measured values given certain parameter values is said to be the likelihood function [75]. The MLE gives the parameter values that maximize this likelihood function.

2.2.3.3 Least-squares estimators for linear models

Define a matrix of input variables $\mathbf{X} \in \mathbb{R}^{n \times m}$, a vector of output variables $\mathbf{Y} \in \mathbb{R}^n$, a parameter vector $\boldsymbol{\theta} \in \mathbb{R}^m$ and vector of errors $\boldsymbol{\epsilon} \in \mathbb{R}^n$ related by a linear model

$$\mathbf{Y} = \mathbf{X}\boldsymbol{\theta} + \boldsymbol{\epsilon}. \quad (2.42)$$

There are various estimators with closed-form solutions that yield best parameter estimates under different assumptions about the error terms $\boldsymbol{\epsilon}$. Four prominent methods are discussed in the following paragraphs.

A. Generalized least-squares (GLS) estimator

The GLS method assumes knowledge of the variances and correlations of the errors in measured system variables [77]. The expected value of the errors is assumed to be zero, $E(\boldsymbol{\epsilon}) = 0$, and their conditional variance is given by a known symmetric matrix $\boldsymbol{\Omega} \in \mathbb{R}^{n \times n}$, $\text{Var}(\boldsymbol{\epsilon}) = \boldsymbol{\Omega}$. Define a cost function $C : \mathbb{R}^m \rightarrow \mathbb{R}$. By solving the optimization problem

$$\underset{\boldsymbol{\theta}}{\text{minimize}} \quad C(\boldsymbol{\theta}) = (\mathbf{Y} - \mathbf{X}\boldsymbol{\theta})^T \boldsymbol{\Omega}^{-1} (\mathbf{Y} - \mathbf{X}\boldsymbol{\theta}), \quad (2.43)$$

the GLS estimator gives a parameter estimate

$$\hat{\boldsymbol{\theta}} = (\mathbf{X}\boldsymbol{\Omega}^{-1}\mathbf{X})^{-1} \mathbf{X}^T \boldsymbol{\Omega}^{-1} \mathbf{Y}. \quad (2.44)$$

The Gauss-Markov theorem applies to the GLS estimator, thus it is the best linear unbiased estimator (BLUE) for the parameters $\boldsymbol{\theta}$.

A.1 Weighted least-squares (WLS) estimator

The WLS estimator is a special case of the GLS estimator in that the off-diagonal elements of the conditional variance matrix $\boldsymbol{\Omega}$ are zero, i.e. the errors are not

correlated. The diagonal elements of $\mathbf{\Omega}$ are the variances of the system variables. By minimizing the sum of squared errors weighted by the reciprocals of these variances, a parameter estimate is found.

C. Ordinary least-squares (OLS) estimator

The OLS estimator can be applied if it can be assumed that the error terms are uncorrelated and all measurements have the same variance. The best parameter estimate is then given by

$$\hat{\boldsymbol{\theta}} = (\mathbf{X}^T \mathbf{X})^{-1} \mathbf{X}^T \mathbf{Y}. \quad (2.45)$$

The product $(\mathbf{X}^T \mathbf{X})^{-1} \mathbf{X}^T$ is the pseudo-inverse of \mathbf{X} , which implies that \mathbf{X} must have full rank. Application of the OLS method dates back to Gauss and Legendre [78] and is probably one of the most commonly used estimation methods.

D. Total least-squares (TLS) estimator

The linear model given by (2.42) assumes that measurements of output variables \mathbf{Y} have errors modelled by $\boldsymbol{\epsilon}$. In addition, it can be assumed that input variables \mathbf{X} are also subject to errors $\mathbf{E} \in \mathbb{R}^n$:

$$\mathbf{Y} = (\mathbf{X} + \mathbf{E})\boldsymbol{\theta} + \boldsymbol{\epsilon}. \quad (2.46)$$

The TLS estimator seeks to minimize the Frobenius norm $\|\mathbf{\Omega}(\mathbf{E}|\boldsymbol{\epsilon})\mathbf{\Lambda}\|_F$, where $\mathbf{\Omega}, \mathbf{\Lambda} \in \mathbb{R}^{n \times n}$ are weighting matrices for measurements in \mathbf{Y} and \mathbf{X} , respectively. The best parameter estimate is computed using the singular value decomposition of $\mathbf{\Omega}(\mathbf{X}|\mathbf{Y})\mathbf{\Lambda}$ [79].

2.2.3.4 Recursive methods

Recursive estimation methods, also referred to as adaptive filters, update estimated parameter values as new measurements become available, without having to include all previously available measurements in the calculation. Such methods can have the benefit of computational efficiency while tracking changes in parameter values over time (real-time identification).

Define $Y_i \in \mathbb{R}$ as measured system output values and $\mathbf{X}_i \in \mathbb{R}^k$ as a vector of k system input values at time $t_i \in \mathbb{R}_{\geq 0}, i = 1, 2, 3, \dots$ related linearly by a vector $\boldsymbol{\theta}_i \in \mathbb{R}^k$ of k parameters, i.e. $Y_i = \mathbf{X}_i^T \boldsymbol{\theta}_i$. Furthermore, define $\hat{Y}_i \in \mathbb{R}$ as the calculated output for a parameter estimate $\hat{\boldsymbol{\theta}}_i$, i.e. $\hat{Y}_i = \mathbf{X}_i^T \hat{\boldsymbol{\theta}}_i$.

Recursive parameter estimates are computed as [75]:

$$\hat{\boldsymbol{\theta}}_{i+1} = \hat{\boldsymbol{\theta}}_i + \mathbf{G}_i e_i, \quad (2.47)$$

where $\mathbf{G}_i \in \mathbb{R}^k$ is a gain matrix and e_i is an error term given by

$$e_i = Y_i - \hat{Y}_i. \quad (2.48)$$

There are two types of adaptive filters, those based on a statistical framework (stochastic) and those based on a deterministic framework. Three commonly used recursive estimation methods are discussed in the following paragraphs.

A. Recursive least-squares (RLS) estimator

The RLS estimator is based on a deterministic framework. RLS can also be traced back to Gauss' work in the 19th century, however, it was mostly unused until a rediscovery by Plackett in 1950 [80]. Suppose that N consecutive measurements are available; a parameter estimate $\hat{\boldsymbol{\theta}}_N$ is obtained by minimizing the weighted sum of squares

$$\sum_{i=1}^N w_i e_i^2, \quad (2.49)$$

where e_i is as defined by (2.48), w_i are weighting factors, conventionally chosen as $w_i = \lambda^{N-i}$, $\lambda \in (0, 1)$. λ is referred to as a forgetting factor since $\lambda < 1$ reduces the weight of older error terms. The RLS estimator computes $\hat{\boldsymbol{\theta}}_N$ as

$$e_N = Y_N - \mathbf{X}_N^T \hat{\boldsymbol{\theta}}_{N-1} \quad (2.50)$$

$$\boldsymbol{\Psi}_N = \lambda \boldsymbol{\Psi}_{N-1} + \mathbf{X}_N \mathbf{X}_N^T \quad (2.51)$$

$$\mathbf{G}_N = \boldsymbol{\Psi}_N^{-1} \mathbf{X}_N^T \quad (2.52)$$

$$\hat{\boldsymbol{\theta}}_N = \hat{\boldsymbol{\theta}}_{N-1} + \mathbf{G}_N e_N. \quad (2.53)$$

Conventionally, the RLS algorithm is initialized with $\hat{\boldsymbol{\theta}}_1 = 0$ and $\boldsymbol{\Psi}_1 = \delta \mathbf{I}$, where δ is a small positive value and $\mathbf{I} \in \mathbb{R}^{k \times k}$ is the identity matrix. The RLS estimator converges faster than stochastic algorithms, but has higher computational complexity [81].

B. Least mean squares (LMS) estimator

The LMS estimator is a stochastic estimator developed by Widrow and Hoff [82]; parameter estimates are found recursively by minimizing the expected value of the squared error, $E(e_i^2)$, which gives the following expression

$$\hat{\boldsymbol{\theta}}_{i+1} = \hat{\boldsymbol{\theta}}_i + \mu \nabla e_i^2 = \hat{\boldsymbol{\theta}}_i + 2\mu e_i \mathbf{X}_i, \quad (2.54)$$

where e_i is as defined by (2.48), $\mu \in \mathbb{R}$ is the step size and $\nabla = [\frac{\partial}{\partial \theta_1}, \frac{\partial}{\partial \theta_2}, \frac{\partial}{\partial \theta_3}, \dots, \frac{\partial}{\partial \theta_k}]$. The LMS estimator is a very popular adaptive filter due to its simplicity and associated computational efficiency.

C. Kalman filter

The Kalman filter is a stochastic recursive estimator for linear dynamic systems described by a state-space model [83, 84]. Define $\mathbf{Y}_i \in \mathbb{R}^n$ as system output measurements and $\boldsymbol{\theta}_i \in \mathbb{R}^k$ as a state vector at time $t_i \in \mathbb{R}_{\geq 0}$, let $\mathbf{X}_i \in \mathbb{R}^{n \times k}$ be a matrix that relates the system state vector and measurements, $\mathbf{A}_i \in \mathbb{R}^{k \times k}$ a matrix that relates consecutive state vectors and $\mathbf{e}_i, \mathbf{u}_i \in \mathbb{R}^k$ be vectors that model white noise. Then the state-space model is given by

$$\boldsymbol{\theta}_i = \mathbf{A}_i \boldsymbol{\theta}_{i-1} + \mathbf{e}_i \quad (2.55)$$

$$\mathbf{Y}_i = \mathbf{X}_i \boldsymbol{\theta}_i + \mathbf{u}_i, \quad (2.56)$$

where (2.56) and (2.55) are commonly called the process model and measurement model, respectively. The recursive computation of the state vector estimate $\hat{\boldsymbol{\theta}}_i$ at time t_i can be divided into two steps. The first step is a prediction:

$$\hat{\boldsymbol{\theta}}_{i|i-1} = \mathbf{A}_i \hat{\boldsymbol{\theta}}_{i-1|i-1} \quad (2.57)$$

$$\mathbf{P}_{i|i-1} = \mathbf{A}_i \mathbf{P}_{i-1} \mathbf{A}_i^T + \mathbf{Q}_i, \quad (2.58)$$

where \mathbf{P}_i and $\mathbf{Q}_i \in \mathbb{R}^{k \times k}$ are covariance matrices of $\hat{\boldsymbol{\theta}}_{i|i}$ and \mathbf{e}_i , respectively. The second step is an update:

$$\mathbf{r}_i = \mathbf{Y}_i - \mathbf{X}_i \hat{\boldsymbol{\theta}}_{i|i-1} \quad (2.59)$$

$$\mathbf{S}_i = \mathbf{X}_i \mathbf{P}_{i|i-1} \mathbf{X}_i^T + \mathbf{R}_i \quad (2.60)$$

$$\mathbf{K}_i = \mathbf{P}_{i|i-1} \mathbf{X}_i^T \mathbf{S}_i^{-1} \quad (2.61)$$

$$\hat{\boldsymbol{\theta}}_{i|i} = \hat{\boldsymbol{\theta}}_{i|i-1} + \mathbf{K}_i \mathbf{r}_i \quad (2.62)$$

$$\mathbf{P}_{i|i} = (\mathbf{I} - \mathbf{K}_i \mathbf{X}_i) \mathbf{P}_{i|i-1}, \quad (2.63)$$

where \mathbf{r}_i is a vector of measurement residuals, \mathbf{S}_i is the residual covariance matrix, $\mathbf{R}_i \in \mathbb{R}^{k \times k}$ is the covariance matrix of the measurement noise \mathbf{u}_i , \mathbf{K}_i is the Kalman gain, $\hat{\boldsymbol{\theta}}_{i|i}$ is the updated state estimate and $\mathbf{P}_{i|i}$ is the updated covariance of the estimate. The Kalman filter is suitable if the dynamic and stochastic model of the state vector are known *a priori*.

2.2.3.5 Non-linear parameter estimation

The parameter estimation problem is more difficult for a non-linear model. Suppose the system output measurement $Y \in \mathbb{R}$ is a function of system inputs $\mathbf{X} \in \mathbb{R}^m$ and parameters $\boldsymbol{\theta} \in \mathbb{R}^k$, then a non-linear model is given by

$$Y = f(\mathbf{X}, \boldsymbol{\theta}) + \epsilon, \quad (2.64)$$

where $f : \mathbb{R}^{m+k} \rightarrow \mathbb{R}$ is a non-linear function and $\epsilon \in \mathbb{R}$ is an error term. Some common algorithms for finding a parameter estimate for non-linear systems are discussed in the following paragraphs.

A. Non-linear least-squares estimation

The least-squares criterion can be applied to non-linear models in the same way as for linear models. Given the model (2.64), the best parameter estimate is found by minimizing the sum of squares of the error terms,

$$\sum_{i=1}^n e_i^2 = \sum_{i=1}^n (Y_i - f(\mathbf{X}_i, \boldsymbol{\theta}))^2, \quad (2.65)$$

where the subscript $i = 1, 2, 3, \dots, n$ labels errors from n measurements. In contrast to the linear least-squares problem, there is no closed-form solution to this optimization problem. Instead, an iterative numerical algorithm is normally used to find an approximate local minimum for a given initial estimate. Gradient methods require evaluation of the derivatives of the objective function, examples are the Gauss-Newton, steepest descent and Levenberg-Marquardt methods [75]. If the derivatives cannot be calculated, pattern or direct search methods can be used such as Nelder and Mead's simplex algorithm.

B. Extended Kalman filter (EKF)

The EKF extends the Kalman filter to non-linear estimation problems. Define $\boldsymbol{\theta}_i \in \mathbb{R}^k$ as a state vector, $\mathbf{X}_i \in \mathbb{R}^m$ as system input measurements and $Y_i \in \mathbb{R}$ as system output measurements at time $t_i \in \mathbb{R}_{\geq 0}$;

furthermore, let $u_i \in \mathbb{R}$ and $\mathbf{e}_i \in \mathbb{R}^k$ be white noise terms and $f : \mathbb{R}^{k+m} \rightarrow \mathbb{R}$, $h : \mathbb{R}^k \rightarrow \mathbb{R}^k$ be non-linear, differentiable functions. The state-space model can then be expressed as

$$\boldsymbol{\theta}_i = f(\boldsymbol{\theta}_{i-1}) + \mathbf{e}_{i-1}, \quad (2.66)$$

$$Y_i = h(\mathbf{X}_i, \boldsymbol{\theta}_i) + u_i. \quad (2.67)$$

Define $\mathbf{J}_{f_i}, \mathbf{J}_{h_i} \in \mathbb{R}^k$ as the Jacobians of f and h , i.e.

$$\mathbf{J}_{f_i} = \frac{\partial f}{\partial \boldsymbol{\theta}_i} \quad (2.68)$$

$$\mathbf{J}_{h_i} = \frac{\partial h}{\partial \boldsymbol{\theta}_{i-1}}. \quad (2.69)$$

The prediction step of the EKF is given by:

$$\hat{\boldsymbol{\theta}}_{i|i-1} = f(\hat{\boldsymbol{\theta}}_{i-1|i-1}) \quad (2.70)$$

$$\mathbf{P}_{i|i-1} = \mathbf{J}_{f_{i-1}} \mathbf{P}_{i-1} \mathbf{J}_{f_{i-1}}^T + \mathbf{Q}_{1_i}, \quad (2.71)$$

where \mathbf{P}_i and $\mathbf{Q}_{1_i} \in \mathbf{R}^{k \times k}$ are covariance matrices of $\hat{\boldsymbol{\theta}}_{i|i}$ and \mathbf{e}_i , respectively. The update is as follows:

$$\mathbf{r}_i = \mathbf{Y}_i - h(\mathbf{X}_i, \hat{\boldsymbol{\theta}}_{i|i-1}) \quad (2.72)$$

$$\mathbf{S}_i = \mathbf{J}_{h_i} \mathbf{P}_{i|i-1} \mathbf{J}_{h_i}^T + \mathbf{Q}_{2_i} \quad (2.73)$$

$$\mathbf{K}_i = \mathbf{P}_{i|i-1} \mathbf{J}_{h_i}^T \mathbf{S}_i^{-1} \quad (2.74)$$

$$\hat{\boldsymbol{\theta}}_{i|i} = \hat{\boldsymbol{\theta}}_{i|i-1} + \mathbf{K}_i \mathbf{r}_i \quad (2.75)$$

$$\mathbf{P}_{i|i} = (\mathbf{I} - \mathbf{K}_i \mathbf{J}_{h_i}) \mathbf{P}_{i|i-1}, \quad (2.76)$$

where \mathbf{r}_i is a vector of measurement residuals, \mathbf{S}_i is the residual covariance matrix, \mathbf{K}_i is the Kalman gain, $\hat{\boldsymbol{\theta}}_{i|i}$ is the updated state estimate and $\mathbf{P}_{i|i}$ is the updated covariance of the estimate. The EKF is effectively a Kalman filter applied to a linearisation of the model around the current state vector estimate.

2.2.3.6 Summary

An overview has been given of parameter estimation algorithms for linear and non-linear models. The algorithms differ in their assumptions about *a priori* knowledge of parameter values, system state variables and noise, optimization criteria, computational complexity and between batch and recursive computation. In the next section, previous research that uses estimation theory to solve the parameter identification problem for overhead transmission lines will be reviewed.

2.3 Review of overhead line impedance parameter identification

In Section 2.2, background was given on transmission line theory, synchrophasor measurements and parameter estimation methods - the major theoretical and practical building blocks that underpin the task of synchrophasor-based overhead line impedance monitoring. In this section, previous research that pulls these building blocks together will be assessed. Firstly, power system parameter estimation, which has evolved from power system state estimation will be considered; then, identification methods for individual lines are discussed, including those that utilize data from transient events, Supervisory Control And Data Acquisition (SCADA) and synchrophasor measurements. At the end of this section, the need for further research on synchrophasor-based overhead line impedance monitoring will be outlined.

2.3.1 Power system state and parameter estimation

Power system state estimation was developed in the late 1960s [85–87] and is the process of estimating voltage phasors for all nodes of the system using a network model as well as measurements of voltage, current and power taken at some of the nodes. The network model consists of transmission lines, shunt capacitors or reactors and transformers [7]. Classically, the state vector of voltage phasors is estimated using WLS, which has been discussed in Section 2.2.3.3. The errors in the system measurements are assumed to be independent and to have a Gaussian distribution, in this case WLS is a maximum likelihood estimator. An integral part of ensuring accuracy of the state estimation process is the detection and identification of bad data, which are measurements with errors that are not due to uncertainty. A common bad data detection method is Chi-square testing of the measurement residuals; if bad data is detected, largest normalized residual or hypothesis testing can be used to identify and discard the erroneous measurement [7].

Soon after the inception of power system state estimation, it was realized that errors in line impedance parameters assumed in the system model can significantly deteriorate the accuracy of the estimated state vector [88, 89]. Therefore, state estimators have been adapted and extended to detect and correct parameter errors. Zarco and Exposito have grouped existing state and parameter estimation methods into two main categories; the first category are methods based on residual sensitivity analysis and the second category are methods that augment the state vector [90]. Methods belonging to the first category use a calculated residual sen-

sitivity matrix to estimate the parameter error [91], while methods in the second category estimate system states and parameters simultaneously. The simultaneous state and parameter estimation problem can be solved using a batch method such as WLS [92, 93] or using recursive algorithms based on Kalman filter theory [89, 94, 95]. Other proposals include application of genetic algorithms [96], innovation graph methods [97] and particle filtering [98].

The parameter estimation methods that have been developed to improve the accuracy of power system state estimation are designed to optimize the system model by utilizing measurements from different points in the network to estimate the parameters of one or more transmission lines. These methods take a top-down approach that is not primarily concerned with the physical interpretation and validation of the parameter values. Alternatively, the line parameter estimation problem can be approached from a bottom-up perspective, whereby the sub-problem of identifying the impedance parameters that cause differences in voltage and current values across an individual line is considered. Previous research on solving this sub-problem will be reviewed in the rest of this section.

2.3.2 Estimation methods based on transient signal measurements

The first applications of synchronized voltage and current measurements to overhead line impedance estimation were reported in the mid-1990s. Philippot and Maun used digital fault recorders to sample three-phase voltages and currents at both ends of a 44.3 km, 380 kV overhead line [99]. The signals were post-synchronized with respect to UTC as provided by GPS receivers and phasors were estimated using a DFT-based algorithm. Measurements were taken during different system conditions including light and heavy line loading, while all phases were open at one end, and during single-pole tripping and auto-reclosing at one and both ends. Before impedance parameter estimation, the phase quantities were transformed into Clarke components. The distributed line model was assumed. The configuration of the line conductors had horizontal symmetry without transposition, meaning that the modal equations did not decouple fully. The non-linear least-squares problem was solved using Nelder and Mead's simplex algorithm. Once a parameter estimate was obtained, the Chi-square test was applied to check for gross measurement errors and the covariance matrix of the parameters was estimated to compute confidence intervals. Based on the confidence intervals and comparison with parameter calculation by Carson's formulae, the parameter accuracy was stated to be 1% to 3%.

Koglin and Schmidt presented a similar study [100]. However, measurements reported by digital relays instead of digital fault recorders were used to estimate line parameters. The relays were triggered by external transient events, thereby building a fault data record. Furthermore, the line was assumed to be transposed and the symmetrical component transformation was applied to obtain decoupled positive, negative and zero sequence modes. For each mode, a weighted least-squares problem was solved to obtain estimates of the short-circuit input impedance and open-circuit output admittance of a symmetric, reciprocal two-port network. Results from a case study on a 22 km, 400 kV transmission line were reported; specifically, zero and positive sequence reactance values estimated from 19 external phase-to-ground faults. The estimated values were within 10% of handbook calculations.

The argument for including recordings of transient events in impedance parameter estimation is that they provide excitation of zero sequence components [101, 102]. This excitation is particularly relevant for untransposed lines whose modal equations are coupled, which implies that the positive sequence parameters cannot be determined independently from the zero sequence. Schulze and Schegner have proposed a method specifically for untransposed, unsymmetrical lines, assuming a phase domain, lumped parameter model and using synchronized measurements from protective relays [101]. To describe the transient signals more accurately, voltage and current phasors are assumed to be time-varying and their derivatives are included in the estimation model; parameters are estimated using the linear least-squares method. Application to a laboratory-based dynamic network model resulted in estimated impedance parameters within $\pm 6\%$ of reference values. In a later contribution Schulze *et al.* decreased parameter errors to below 1% by using Prony's method instead of a DFT to decompose the transient voltage and current signals [9]; this approach assumes that the current contains damped transients and that the correct signal model order is known *a priori*.

Hu and Chen also proposed a time-domain method to estimate self and mutual parameters using the time domain first-order differential equations for parallel transmission lines and synchronized transient signal samples [103]; first-order derivatives are estimated as the gradient between consecutive samples. Zero and positive sequence parameters are calculated from the estimated phase domain values. Results of field application of the proposed method to two 30 km, 220 kV parallel transmission lines were within 2.5% of independently measured reference values.

Voltage and current measurements of transient events provide a range of excitation states of the overhead line system for comprehensive impedance parameter identification. One of the main objectives of the methods discussed in the previous paragraphs is to estimate zero sequence parameters, which are used in setting protective relays. With respect to real-time monitoring of line impedance parameters, it must be remembered that transient signals are only available occasionally as the power system is usually in steady-state. In the rest of this section, methods that utilize steady-state measurements only are discussed.

2.3.3 Steady-state estimation methods for transposed lines

For transposed lines, the self and mutual impedance parameters are assumed to be equal for all three phases. In Section 2.2.1, it was explained that through the symmetrical component or Clarke transformation the three-phase transmission line equations of transposed lines can be decomposed into three decoupled modes. Each mode is then equivalent to a single-phase system. In the following paragraphs, existing methods for identification of positive sequence parameters will be discussed. The methods are equally applicable to determine zero sequence parameters, but in steady-state operation, voltage and current do normally not contain zero sequence components.

2.3.3.1 Estimation methods using SCADA data

SCADA systems have been in use since the 1960s to support power system monitoring and operation. Remote terminal units installed in substations report measurements of voltage and current magnitude as well as active and reactive power as part of SCADA. Such SCADA measurements typically have lower accuracy and reporting rates compared to synchrophasor measurements [104]. To maximize the accuracy of estimated line impedance parameters, synchrophasor measurements are the preferable choice over conventional SCADA measurements. However, as opposed to SCADA measurements, synchrophasor measurement facilities are not widely available across all power networks. For this reason, Wang *et al.* have presented an algorithm for tracking line parameters using SCADA data only. The algorithm uses measurements of voltage magnitude as well as active and reactive power at each line end; the measurements are assumed to be average values across three phases. A single-phase nominal pi-circuit models the transmission line. The non-linear model equations are solved in a least-squares sense using the Levenberg-Marquardt method [106, 107] with theoretically calculated param-

eter values as starting points. If the propagation speed along the overhead line is assumed to be known, one measurement of sending and receiving end quantities suffices; otherwise, line parameters are estimated using multiple measurements of different levels of power flow. The line resistance is assumed to be constant over 30 min intervals, from which multiple measurements are chosen. The parameter estimation process is repeated for different combinations of measurements and the sum of squared residuals is evaluated; the final parameter estimate is the mean of the best 5% of results. The proposed SCADA data method was implemented to estimate line parameters of two 240 kV transmission lines. For each line, tracked values over one summer and one winter 24-hour period were reported, as well as average values for each 24-hour period. The estimated average values are consistent with theoretically calculated line parameters; resistance was higher in the summer than in the winter, while reactance and susceptance did not differ significantly. However, from the reported results it cannot be concluded whether the variation of the resistance values during the 24-hour periods was consistent with changes in conductor temperature.

If synchrophasor measurements are available at one line end, but only conventional SCADA measurements are available at the other line end, the hybrid approach proposed by Mousavi-Seyedi *et al.* is suitable [108]. It is assumed that the SCADA data provides magnitudes of voltage and current; hence, the phase angles are eliminated from the positive sequence equivalent pi-circuit model equations. Line impedance parameters are estimated by non-linear WLS using multiple measurements of different line loading conditions and assuming line parameters remain constant. The proposed method has been extended to three-terminal transmission lines. The parameter estimation results from a study on a laboratory network simulator were within 3% of reference values.

A different hybrid approach has been proposed by Sivanagaraju *et al.* [109]; the phase angles of voltage and current signals at the end of the transmission line that has only SCADA measurements are estimated using the available voltage and current magnitude and power, synchrophasor measurements from the other line end and assuming that the line's shunt conductance is zero. Once the phase angles are estimated, voltage and current phasors from both line ends are available and methods that use only synchrophasors can be used to estimate line parameters. The reported parameter error was lower than 0.5%, however, the uncertainty in the parameter values reached up to 70%.

SCADA-based methods have a practical advantage in that they are not dependent on availability of synchrophasor measurement technology, which has not

yet become standard substation equipment. Moreover, if synchrophasor measurements are available at one or two line ends, the methods are still applicable since synchrophasors contain conventional SCADA quantities. On the other hand, the magnitude accuracy of synchrophasor measurements is one order of magnitude better than conventional SCADA measurements, and synchronization to within $1\ \mu\text{s}$ of UTC allows for a more accurate measurement of the instantaneous difference in phase angles across the line. Hence, the overall achievable parameter estimation accuracy is higher when synchrophasor measurements are used [109].

2.3.3.2 Estimation methods assuming a distributed line model

The frequency-domain distributed parameter model as described by (2.17) and (2.18) in Section 2.2.1.1 relates voltages and currents at the two ends of an overhead line through hyperbolic functions; the line's electrical properties are represented by the characteristic impedance and propagation constant, which are defined in terms of per-unit-length impedance and admittance. Methods that estimate the parameters of the distributed line model using synchrophasor measurements are discussed in the following paragraphs.

A. Single measurement method

The distributed parameter transmission line model consists of two equations, which can be solved simultaneously for the two unknowns. The characteristic impedance and propagation constant can be calculated by substituting a single synchrophasor measurement of voltage and current [110]. This algorithm is very simple, however, it does not attempt to filter measurement errors.

B. Non-linear least-squares estimation

To estimate accurate per-unit-length impedance parameters from noisy synchrophasor measurements, Du and Liao have proposed to use a weighted non-linear least-squares estimator [111]. In addition to the impedance parameters, voltage and current variables are included in the vector of unknowns, imitating augmented state estimation. Moreover, the distributed line model is extended by a synchronization angle. After a first round of iterative parameter estimation, the Chi-square test is applied to the residuals to detect measurements with gross errors, including unsynchronized measurements; parameter estimation is repeated without such 'bad' measurements to obtain a more accurate result. Adaptations of the method to lines with series compensation, double-circuit lines and lines sharing

one bus have also been presented. The method has been tested in a simulation study on a 320 km, 500 kV transmission line; synchrophasor measurements were contaminated with Gaussian noise [112]. In each parameter estimation, three measurements of different line loading conditions were used. Gross errors such as a synchronization error of 10° or 20 % magnitude error in a single voltage or current measurement were detected successfully. Per-unit-length resistance was estimated to within 10 %, while errors in reactance and susceptance were less than 1 %.

2.3.3.3 Estimation methods assuming a two-port network model

As discussed in Section 2.2.1.1, a transmission line can be represented by a symmetric and reciprocal two-port network with chain parameters.

A. Double measurement method

Wilson *et al.* proposed to obtain a closed-form solution for the chain parameters using Cramer’s rule with two synchrophasor measurements [113]. The two measurements must be from different power flow conditions to ensure linear independence. The method was verified with actual synchrophasor measurements of a 530 km, 525 kV transmission line. One pair of measurements was used to calculate chain parameter values, which were then used to compute active and reactive power at one line end for six other measurements; finally, the difference between parameter-based, predicted power values and actual measurements was calculated. It was found that the synchrophasor-based chain parameter values gave better power predictions than parameter values obtained by theoretical calculation or software simulation.

Wilson *et al.*’s study demonstrated that synchrophasor measurements can be used to improve the accuracy of a two-port network representation of a transmission line compared to theoretical parameter identification methods. However, the authors also recognized that the reported values are not absolute measurements since the substation instrument transformers were not calibrated. Therefore, the chain parameter values do not necessarily reflect the actual electrical conductor properties.

B. Linear least-squares estimation

Shi *et al.* used the double measurement method to compute chain parameter values and from these pi-circuit series impedance and shunt admittance were computed. The parameter estimates were robust to bias errors in the synchrophasor measure-

ments, however, measurements with 1 % Gaussian noise caused parameter errors in excess of 200 %. To reduce sensitivity to Gaussian noise, it was proposed to compute the chain parameters by ordinary least-squares estimation using more than two measurements. This approach decreased errors in reactance and susceptance estimates to below 10 % and errors in resistance remained above 20 %. While the error level was reduced by a factor of ten, errors in resistance values in excess of 20 % are unacceptable as they would correspond to an error in conductor temperature of 50 °C.

2.3.3.4 Estimation methods assuming a pi-circuit model

The per-unit-length line parameters can be calculated from pi-circuit impedance and admittance parameters. The equivalent pi-circuit model as described by (2.20) and (2.21) in Section 2.2.1.1 is one of the most commonly used transmission line models and various proposals for estimation of series impedance and shunt admittance from synchrophasor measurements at the transmission line ends exist.

A. Single measurement method

The single measurement method is the simplest way to obtain an estimate of the pi-circuit parameters. The two pi-circuit equations are solved for the unknown series impedance and shunt admittance through algebraic manipulation, giving a closed-form solution [114, 115]. Only one synchrophasor measurement of voltage and current at both line ends is required to compute parameter values, which makes the method ideal for real-time impedance parameter calculation. However, the disadvantage of using only one measurement is that random errors due to uncertainty are not filtered. A simulation study on a 19 km, 230 kV line by Shi *et al.* has shown that the method can give very accurate parameter values (less than 0.1 % error) when synchrophasor measurements have no errors. When synchrophasors have random or systematic errors of magnitude 1 %, the errors in parameter estimates increased to over 100 %, demonstrating high error sensitivity of the single measurement method [114].

B. Non-linear least-squares estimation

Like any measurement, reported synchrophasors are subject to random noise due to uncertainty. One approach to filter random measurement errors is to estimate parameters in a least-squares sense from multiple measurements. Since the pi-circuit equations are non-linear in impedance and admittance parameters, a non-linear

least-squares estimation problem must be solved using an iterative algorithm. Shi *et al.* presented this approach and the results of their simulation study showed that non-linear least-squares parameter estimates are more robust to systematic measurement errors than the single measurement method [114]; given random measurement errors, reactance estimates had a higher accuracy while shunt susceptance was less accurate than single measurement method results. It was also found that the parameter error decreased as the number of measurements of different loading conditions increased. The common iterative algorithms require an initial parameter estimate to search for an optimal value; hence, the final estimate depends on *a priori* knowledge.

C. Linear least-squares estimation

Through a change of variable, the pi-circuit model equations become linear in the unknown parameters. Therefore, parameter values can be estimated from multiple measurements by the method of linear least-squares, as proposed by Bi *et al.* [116]. The voltage measurements are taken as input quantities, while the currents form the output measurement vector. Similarly to non-linear least-squares estimation, the parameter estimation accuracy has been found to increase with the number of utilized measurements [116, 117]. One advantage of the linear least-squares problem is that it has a closed-form solution and no initial parameter guess is required, as opposed to non-linear least-squares estimation.

D. Total least-squares estimation

Ding *et al.* proposed application of the TLS estimator to obtain pi-circuit parameter values [118]. In contrast to the ordinary least-squares estimator, random errors are assumed in the current measurement vector *and* voltage input measurements. In addition to Kirchhoff's laws, the power flow equations for the pi-circuit are included in the estimation model. Line impedance parameters are estimated continuously through time from a moving window of measurements. To assess the credibility of parameter estimates, probability density curves are estimated to obtain confidence intervals. In a simulation study of a 500 kV transmission line, voltage and current measurements were contaminated with Gaussian and uniform random noise to compare the TLS estimator with the single measurement method. Both methods gave the same mean parameter values for a given time period, but the TLS estimator resulted in much lower fluctuation; for instance, the standard deviation of resistance estimates from measurements with 0.2% Gaussian noise was 20% of the mean value by the single measurement method, while the TLS

estimator resulted in only 7%. TLS parameter estimates from field data were also reported with low fluctuation, but only for a time span of 60 s.

Dasgupta and Soman made a similar proposal to employ a TLS estimator for computing impedance parameters of the equivalent pi-circuit, but without the use of power flow equations [119]. The importance of selecting measurements from different operating conditions was emphasized by suggesting a selection criterion based on the difference in voltage measurements. To increase the robustness of the parameter estimation process, the Durbin-Watson test is used to check for serial correlation in the measurement residuals after parameter estimation. The argument is that such correlation can be caused by a bias error introduced by a faulty voltage transformer. The proposed TLS estimator was compared to the OLS estimator in a simulation study on a 220 km, 230 kV transmission line; 1% Gaussian noise was added to the phasor measurements. Both estimation methods gave root-mean-square (rms) errors of the parameter values below 5%, and in particular the accuracy of the series impedance was significantly higher for the TLS estimator. When one of the capacitive voltage transformers was simulated to have a 20% drift in the capacitor, the Durbin-Watson test successfully indicated bad data and thus unreliable parameter estimation results.

E. Extended Kalman filter

Hering and Janecek's method uses the extended Kalman filter to recursively estimate line impedance parameters as well as conductor temperature [120]. For the temperature, a dynamic model based on the heat-balance equation for bare overhead line conductors is assumed. In contrast to other methods, the series resistance at a reference temperature is estimated instead of the actual line resistance. Hence, all line impedance parameters are assumed constant. Furthermore, it is assumed that the synchrophasor measurements of the currents can have a systematic error, which is included in the pi-circuit model equations and unknown parameter vector. At each time step, the line impedance parameters are updated in accordance with the latest synchrophasor measurements and the estimated conductor temperature is updated based on the latest measurements of ambient temperature, wind speed and direction. Estimation results based on field measurements of two 110 kV overhead lines over several months were presented. Series reactance values and reference resistance converged to constant values after approximately two months. Estimated conductor temperature was also reported and within normal operating range, however, there was no independent temperature measurement available for validation. Inclusion of the current calibration factor improved the

parameter estimation results significantly. Hering *et al.* have made an innovative proposal by focussing on a constant resistance parameter at a given reference temperature, since this approach allows estimation from synchrophasor measurements taken over an unlimited time period. The previously discussed linear and non-linear least-squares estimators assume that the actual line resistance is constant over the measurement period, which limits the number of available measurements from different line loading conditions and thus the achievable parameter estimation accuracy. On the other hand, Hering *et al.*'s approach requires ambient weather data, which is not necessarily available for all overhead lines.

F. Non-linear constrained optimization

Dan and Raisz have defined a constrained non-linear optimization problem to find accurate pi-circuit parameter values [122]. The objective function is the rms error between synchrophasor measurements from one line end and voltage and current phasors calculated from possible parameter values and synchrophasor measurements from the other line end. The initial parameter estimate is obtained by theoretical calculation. A non-linear constraint is introduced based on the fact that the propagation speed must not exceed the speed of light. Possible parameter values were subject to feasible upper and lower bounds based on expected variations in line sag and earth resistivity. Additionally, magnitude and phase angle correction factors for all voltage and current variables were included in the estimation model to take account of constant, systematic errors introduced by instrument transformers. The proposed optimization problem was solved for a 14 km, 400 kV overhead line using field measurements collected over one week to find a parameter estimate that reduces the objective function compared to the theoretical estimate. This method can be used to obtain a more accurate model description of the overhead line. However, it cannot be known to what extent the parameter estimate describes the physical properties of the line. By including correction factors for all measurements, the number of unknowns to be estimated increased from 6 to 30, which means that more measurements of different operating conditions are necessary to achieve numerical accuracy. Impedance parameters were assumed to be constant over the measurement period, hence, the method is not suitable for real-time monitoring.

2.3.4 Steady-state estimation methods for untransposed lines

For overhead lines that are not transposed, the symmetrical component and Clarke transformations do not result in decoupled modes. The system can be treated in the same way as a transposed line by ignoring the coupling and estimating individual modal parameters as described in the previous paragraphs. This approach was taken by Asti *et al.* [123]; simulation study results showed that errors in resistance can be as high as 10% while errors in reactance reached above 20%.

To avoid parameter estimation errors arising from an approximate decoupling assumption for untransposed lines, several researchers have proposed to estimate self and mutual parameters using a coupled three-phase model without any modal transformation.

2.3.4.1 Estimation methods assuming a pi-circuit model

The conventional representation of three-phase transmission lines is a lumped element, pi-circuit model consisting of six equations that contain twelve unknown parameters. Thus, the system of equations is under-determined and does not have a single measurement, closed-form solution.

A. Kalman filter

Mishra *et al.* suggested to estimate self and mutual impedance parameters recursively using a Kalman filter [124]. The parameters are assumed to be constant over time and the synchrophasor measurements are assumed to have zero mean Gaussian noise. In a simulation study, the proposed method was shown to give more accurate parameter estimates than a WLS estimator; all parameter errors were below 1%.

B. Non-linear least-squares estimation

Wu *et al.* proposed to estimate impedance parameters simultaneously with calibration factors for instrument transformers at one line end [125]. The non-linear estimation problem is solved in a least-squares sense using the Newton-Raphson method. It is argued that if synchrophasor measurements are pre-calibrated at one bus of a network, the method can be used to estimate calibration factors for all other network buses. A simulation study of a 500 kV, 30-bus network consisting of 36 transmission lines was presented. It was assumed that synchrophasor measurements are available from all buses and pre-calibrated at one bus. Ten snapshots

of network measurements taken over a 24-hour variable load profile were used to estimate impedance parameters of all lines and calibration factors for 29 buses. The calibration errors were up to 10% in magnitude and 5° in phase angle, no random noise was added to the measurements. The proposed method estimated line impedance parameters to within 0.1%, voltage magnitude was calibrated to within 0.03%, current magnitude to 1% and voltage and current phase angles to within 0.1° and 1°, respectively.

While Wu *et al.* recognize the importance of taking account of instrumentation channel errors in the impedance parameter estimation process, they do not consider problems of ill-conditioning and numerical instability that can arise by increasing the number of unknowns in the estimation problem; furthermore, impedance parameters were assumed to be constant over a 24-hour period, such that measurements from different line loading conditions became available. To monitor changes in impedance parameters, measurements snapshots taken over one hour or less must suffice to estimate parameters.

C. Non-linear constrained optimization

Zhou *et al.* formulated a non-linear constrained optimization problem [126]. The objective function is the euclidean norm of measurement residuals based on the three-phase pi-model equations. The parameter search space is limited by upper and lower bounds around theoretically calculated parameter values. In addition, inequality constraints are set based on the relative size of impedance parameters, i.e. resistance must be smaller than reactance. One synchrophasor measurement of voltage and current at both line ends is used to solve the optimization problem and obtain a parameter estimate. Using all parameter estimates from a five-second interval, a re-sampling technique is used to obtain an estimate of the parameter variance, which is used to judge the credibility of the parameter mean. Estimation results from field data over a one-hour period were reported, series impedance and shunt admittance differed from theoretical values by 8%.

D. Linear least-squares estimation

In the same manner as the single-phase pi-model, the three-phase model equations can be made linear in the unknown impedance parameters. Shi *et al.* proposed to use ordinary least-squares estimation to compute a parameter estimate [127]. A simulation study on a 230 kV transmission line was presented to demonstrate the effectiveness of the method compared to assuming a transposed line model and using the single and double measurement methods. An unbalanced load with

14% negative sequence current was assumed as well as zero-mean, 1% Gaussian measurement noise. Assuming a line length over 150 km, the single and double measurement methods gave errors in resistance and reactance of at least 10%, while the linear least-squares estimator achieved 1%. For shorter lines, errors rose above 10%, but remained below the single and double measurement methods, which reached over 30%.

In contrast to non-linear estimation approaches, the linear least-squares estimator gives a closed-form solution and does not rely on initial parameter estimates as inputs, which means that the final estimate is not distorted by inaccurate *a priori* knowledge or theoretical calculations. On the other hand, systematic measurement errors have not been considered explicitly.

2.3.4.2 Estimation methods assuming a two-port network model

A three-phase transmission line can also be represented by three coupled two-port networks characterized by four chain parameter matrices, which are identified by ordinary least-square estimation as proposed by Lowe [128]. From the chain parameters, pi-circuit impedance and admittance parameters can be calculated. In a simulation study of a 150 kV line, the proposed method was compared with Shi *et al.*'s linear least-squares estimator for the pi-circuit [127]; the error in estimated parameters for measurements with $\pm 1\%$ systematic errors and zero-mean, 1% Gaussian noise was reported. Series resistance and reactance estimates by Lowe's method had less than 5% error even if the synchrophasor measurements had systematic errors, while Shi *et al.*'s method resulted in errors over 10%. The relative performance of the two methods was the opposite for shunt susceptance estimates. In a similar manner, resistance and reactance estimated by Lowe's method were more robust to random measurement errors, while susceptance was more accurately estimated by Shi *et al.*'s method.

2.3.5 Summary

In this section, a detailed review of past research on overhead line impedance parameter identification has been presented. Initially, parameter estimation methods that were developed to increase the accuracy of network models used in power system state estimation were discussed. The focus then shifted to research that investigated the fundamental problem at the heart of network parameter estimation: how to accurately determine the impedance parameters of an individual overhead line from signal measurements at both line ends.

Table 2.1: Overview of steady-state methods for overhead line impedance parameter identification

	Pi-circuit		Distributed line	Two-port network
Transposed	Single measurement methods:	Non-linear least-squares estimation:	Single measurement methods:	Double measurement methods:
	<ul style="list-style-type: none"> • Shengfang <i>et al.</i> [115] • Shi <i>et al.</i> [114] 	<ul style="list-style-type: none"> • Shi <i>et al.</i> [114] • Borda <i>et al.</i> [129] 	<ul style="list-style-type: none"> • Jiang <i>et al.</i> [110] 	<ul style="list-style-type: none"> • Wilson <i>et al.</i> [113]
	Linear least-squares estimation:	<ul style="list-style-type: none"> • Dan and Raisz [122]¹ • Mousavi-Seyedi <i>et al.</i> [108]² • Wang <i>et al.</i> [105]² 	Non-linear least-squares estimation:	Linear least-squares estimation:
	<ul style="list-style-type: none"> • Bi <i>et al.</i> [116] • Rubesa <i>et al.</i> [117] 	Extended Kalman filter:	<ul style="list-style-type: none"> • Liao and Kezunovic [112]¹; Du and Liao [111]¹ 	<ul style="list-style-type: none"> • Shi <i>et al.</i> [114]
Total least-squares estimation:	<ul style="list-style-type: none"> • Ding <i>et al.</i> [118] • Dasgupta and Soman [119] 	<ul style="list-style-type: none"> • Hering and Janecek [120]¹ 		
Untransposed	Linear least-squares estimation:	Non-linear least-squares estimation:	Single measurement methods:	Linear least-squares estimation:
	<ul style="list-style-type: none"> • Shi <i>et al.</i> [127] 	<ul style="list-style-type: none"> • Wu <i>et al.</i> [125]¹ 	<ul style="list-style-type: none"> • Asti <i>et al.</i> [123] 	<ul style="list-style-type: none"> • Lowe [128]
	Kalman filter:	Non-linear constrained optimization:		
	<ul style="list-style-type: none"> • Mishra <i>et al.</i> [124] 	<ul style="list-style-type: none"> • Zhou <i>et al.</i> [126] 		

¹ Inclusion of one or more calibration factors

² Use of classical SCADA measurements

A distinction has been made between methods that rely on transient signal measurements (Section 2.3.2) and those that utilize only steady-state measurements. Methods in the latter category are of interest for real-time monitoring applications, and have been grouped into those for transposed lines (Section 2.3.3) and those for untransposed lines (Section 2.3.4). Table 2.1 provides a structured overview of both transposed and untransposed line methods, which differ in their choice of model (distributed line, pi-circuit, two-port network), estimation method (single measurement, double measurement, linear and non-linear estimators) as well as assumptions about measurement errors and parameter time-variance. The combination of these choices and assumptions determines the parameter estimation accuracy and whether a given method is suitable for real-time line impedance monitoring.

The single measurement method [114, 115] is the simplest algorithm for overhead line impedance parameter identification due to its ease of implementation and low computational cost; furthermore, the method is ideal for real-time monitoring since impedance parameters can be updated with every new measurement that becomes available. However, the single measurement method has been shown to be sensitive to random and systematic measurement errors.

Linear [114, 116, 118] and non-linear [111, 129] least-squares estimators can reduce sensitivity to random noise by filtering from multiple measurements taken under different line loading conditions; simultaneous estimation of line impedance parameters and measurement calibration factors has been suggested to compensate for systematic errors [122, 125]. These estimators assume that resistance is a constant parameter; changes in resistance can still be tracked by estimating from a sliding time window of measurements [118]. But it is not known if the parameter estimation accuracy remains acceptable if there is no change in line loading during a time window.

Recursive estimation by a Kalman filter is an alternative approach to track changes in impedance parameters while filtering random measurement noise and estimating calibration factors [121]; yet, this method requires weather data from the vicinity of the overhead line in addition to voltage and current measurements.

2.4 Discussion and conclusion

In this chapter, a literature review of previous research relating to the real-time monitoring of overhead line impedance parameters has been presented. Relevant concepts in transmission line theory, synchrophasor measurement and estimation theory have been discussed. The previous section has focussed on how these fields overlap in past research on overhead line impedance parameter identification.

It is desirable to maximize the accuracy of estimated impedance parameter values to obtain the most accurate system representation. The minimum accuracy requirements depend on the specific practical application and the discretion of power system operators. For conductor temperature monitoring, the error level should be at least one order of magnitude smaller than the operating temperatures, which can reach up to 150 °C [43]. Hence, errors in resistance estimates should not exceed 4%, which corresponds to 10 °C given a temperature coefficient of 0.004 °C⁻¹.

To the best of the author's knowledge, there is no existing method capable of monitoring overhead line impedance parameters in real-time such that average conductor temperature can be tracked using synchrophasor measurements that are subject to random and systematic measurement errors. This conclusion is supported by recent field studies, which have demonstrated difficulties in achieving consistently accurate overhead line impedance parameter tracking [4, 130]. This gap will be addressed by the work presented in this thesis. In order to build upon the existing methods, their relative strengths and weaknesses must first be understood.

Previous comparative studies have been limited since they have compared a maximum of four methods at a time, in some cases using only simulated phasor measurements [114, 127]. The parameter estimation accuracies reported from different studies cannot be compared directly since they are based on different types of error quantities and on data sets from a range of overhead line systems with varying types and levels of measurement noise; furthermore, some studies report accuracies only for average parameter estimates rather than real-time monitoring.

In the next chapter, eight different existing methods are compared under the same conditions, using field data as well as a simulation study. Chapters 4 and 5 will build on strengths such as the simplicity of the single measurement method and compensation of systematic errors with correction factors, to develop novel methods that can track overhead line impedance parameters with acceptable accuracy.

Chapter 3

Comparison of existing synchrophasor-based impedance parameter estimation methods

3.1 Introduction

In Chapter 2, existing research relating to synchrophasor-based impedance parameter estimation of transmission lines was reviewed; in particular, an overview was given of assumptions about line models, phasor measurements and estimation methods. The choice of assumptions and estimation method is crucial, since it determines the achievable accuracy of the determined impedance parameter values.

Existing approaches assume either a single-phase model, which can be used as an equivalent of a transposed three-phase line, or a full three-phase model, which is more complex but reflects the asymmetry of untransposed lines. In terms of system dynamics, impedance parameters are often assumed to be constant over time. On the one hand, there is an incentive to keep the assumed line model as simple as possible, with the minimum number of unknown variables, as this reduces the complexity and improves the conditioning of the parameter estimation problem. On the other hand, it is vital for the model to reflect the system with sufficient detail, such that the relevant electrical properties can be extracted with the required accuracy.

With regards to the phasor measurements, most approaches assume that they are subject to random noise with a Gaussian distribution. Based on this assumption, several previous works propose least-squares estimation from an overdetermined set to obtain parameter values; in addition, they may use statistical tests to detect and remove outliers. If the assumptions about line models and measure-

ments hold for the system under consideration, the existing approaches produce parameter estimates with good accuracy, as has been demonstrated in many case studies. But transmission line systems and field measurement conditions vary widely, which means that these assumptions can be too general and rigid, and the methods will fail to be effective in all cases. In order to monitor thermal changes in resistance, parameter values need to be reported in real-time, based on a limited set of measurements. In addition to random errors, phasor measurements can be subject to systematic errors that can distort impedance parameter estimates if not reflected in the system model.

In this chapter, it will be shown that there is at least one overhead line system for which a range of existing impedance parameter estimation methods is not effective for real-time monitoring, and that systematic measurement errors are a key barrier to achieving acceptable parameter estimation accuracy. A minimum acceptable level of parameter estimation accuracy is a 4% error, corresponding to 10°C given a resistance-temperature coefficient of 0.004 °C⁻¹. The content of this chapter is structured as follows: firstly, a representative selection of existing parameter estimation methods is given and assessment criteria are defined; the third section gives results of application of the methods to field data, revealing their limitations; the fourth section gives results of application to simulated phasor measurement with the aim of reproducing failures observed in field data results; the final section concludes the chapter.

3.2 Overview of methods under consideration

In Chapter 2, a wide range of existing approaches for line impedance parameter estimation have been identified, consisting of different combinations of possible transmission line models and calculation or estimation methods. It is not feasible to consider each of the identified approaches individually in this chapter. However, many approaches are similar in their assumptions and thus a sample of eight methods has been selected. Table 3.1 lists the selected estimation methods, grouped by the assumed transmission line model. The sample includes methods assuming transposed and untransposed lines, pi-circuit and two-port network models, linear and non-linear estimation as well as methods with and without calibration factors. Sections 3.2.1 and 3.2.2 will give details on how each selected method works.

Table 3.1: Selection of parameter estimation methods, grouped by transmission line model

Model:	Pi-circuit	Two-port network
Transposed	Single Measurement (SM1) Total Least-squares (TLS1) Non-linear Optimal Estimator (NLOE1)	Two-port Linear Least-squares - Single-phase (TPLL1)
Untransposed	Linear Least-squares (LLS3) Non-linear Constraint Optimization (NLCO3) Non-linear Least-squares with Calibration Factors (NLLC3)	Two-port Linear Least-squares - Three-phase (TPLL3)

3.2.1 Single-phase methods

In this thesis, the term 'single-phase methods' refers to methods that identify positive sequence impedance and admittance parameters for transposed transmission lines. The positive sequence is modelled as a single-phase pi-circuit as shown in Figure 3.1. There are two unknowns: the positive sequence impedance Z and positive sequence admittance Y to be determined from synchronized phasor measurements of voltage and current; let V_s, I_s, V_r, I_r be the positive sequence quantities, subscripts r and s denote sending and receiving ends, respectively.

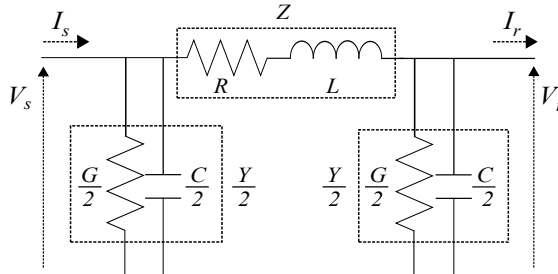


Figure 3.1: Diagram of a pi-circuit

By Kirchhoff's Current and Voltage Laws,

$$V_s = (I_s - \frac{Y}{2}V_s)Z + V_r \quad (3.1)$$

$$I_s = (V_s + V_r)\frac{Y}{2} + I_r, \quad (3.2)$$

where $V_s, I_s, V_r, I_r, Z, Y \in \mathbb{C}$, $Z = R + jX$, $X = 2\pi fL$, $Y = G + jB$, $B = 2\pi fC$ and $R, X, G, B, L, C, f \in \mathbb{R}_{\geq 0}$. R is the resistance, X is the inductive reactance, G is the conductance and B is the capacitive susceptance. It is assumed that sets of measurements V_s, I_s, V_r, I_r are reported at regular time intervals.

3.2.1.1 Single Measurement (SM1)

The SM1 method calculates positive sequence impedance Z and admittance Y from a single set of measurements V_s, I_s, V_r, I_r measured at the same time instant [115]. The two measurement equations (3.1) and (3.2) form a fully determined set, hence, they can be rearranged to give formulae for Z and Y :

$$Z = \frac{V_s^2 - V_r^2}{V_s I_r + V_r I_s} \quad (3.3)$$

$$Y = 2 \frac{I_s - I_r}{V_s + V_r}. \quad (3.4)$$

Equations (3.3) and (3.4) are used to calculate parameter estimates in real time for every available set of measurements V_s, I_s, V_r, I_r .

3.2.1.2 Total Least-squares (TLS1)

The TLS1 method is based on a similar principle as ordinary least-squares, with the difference that random errors are not only assumed to occur in the measurement vector, but also in the design matrix [118, 119]. The existing total least-squares approaches assume that shunt conductance G is zero. Based on (3.1) and (3.2), the following model equations are used:

$$I_s = (V_s - V_r)Y_Z + V_s \frac{Y}{2} \quad (3.5)$$

$$I_r = (V_s - V_r)Y_Z - V_r \frac{Y}{2}, \quad (3.6)$$

where $Y_Z = 1/Z = G_Z + jB_Z, Y = jB$. These equations can be expanded and written in matrix form by taking real and imaginary parts. Suppose $n \in \mathbb{N}$ measurement sets from consecutive time instants are available. Let $\Delta V = V_s - V_r = \text{Re}(\Delta V) + j \text{Im}(\Delta V)$ and define matrices $\mathbf{H} \in \mathbb{R}^{4n \times 3}, \mathbf{x} \in \mathbb{R}^3$ and $\mathbf{M} \in \mathbb{R}^{4n}$, where

$$\mathbf{M} = \begin{bmatrix} \text{Re}(I_s) \\ \text{Im}(I_s) \\ \text{Re}(I_r) \\ \text{Im}(I_r) \end{bmatrix}, \mathbf{H} = \begin{bmatrix} \text{Re}(\Delta V) & -\text{Im}(\Delta V) & -\text{Im}(V_s) \\ \text{Im}(\Delta V) & \text{Re}(\Delta V) & \text{Re}(V_s) \\ \text{Re}(\Delta V) & -\text{Im}(\Delta V) & -\text{Im}(V_r) \\ \text{Im}(\Delta V) & \text{Re}(\Delta V) & \text{Re}(V_r) \end{bmatrix}, \mathbf{x} = \begin{bmatrix} G_Z \\ B_Z \\ B/2 \end{bmatrix}. \quad (3.7)$$

Then (3.5) and (3.6) are summarized by the matrix equation

$$\mathbf{M} = \mathbf{H}\mathbf{x}. \quad (3.8)$$

To model random measurement noise, equation (3.8) is extended by two matrices $\mathbf{E} \in \mathbb{R}^{4n \times 3}$, $\boldsymbol{\varepsilon} \in \mathbb{R}^{4n}$:

$$\mathbf{M} + \boldsymbol{\varepsilon} = (\mathbf{H} + \mathbf{E})\mathbf{x}, \quad (3.9)$$

which can be rewritten using augmented matrices:

$$([\mathbf{H} \ \mathbf{M}] + [\mathbf{E} \ \boldsymbol{\varepsilon}]) \begin{bmatrix} \mathbf{x} \\ -1 \end{bmatrix} = 0. \quad (3.10)$$

The best estimate of parameter vector \mathbf{x} minimizes the sum of squares of the elements of matrix $[\mathbf{E} \ \boldsymbol{\varepsilon}]$ and is found from the singular value decomposition of matrix $[\mathbf{H} \ \mathbf{M}]$ [119].

3.2.1.3 Non-linear Optimal Estimator (NLOE1)

The NLOE1 uses only one of the pi-circuit model equations, equation (3.1), with an additional unknown variable, synchronization angle $\alpha \in \mathbb{R}$ [111]. Impedance parameter estimates are found from $n \in \mathbb{N}$ sets of phasor measurements by minimizing a cost function that is based on the model equation (3.1) and estimates of the measured quantities and synchronization angle. Rewrite (3.1) as

$$V_s - I_s Z + V_s Z \frac{Y}{2} - V_r \exp(j\alpha) = 0. \quad (3.11)$$

Define a vector of variables to be estimated, $\mathbf{P} \in \mathbb{R}^{5+6n}$,

$$\mathbf{P} = [R, X, G, B, v_{s_k}, w_{s_k}, v_{r_k}, \theta_{s_k}, \rho_{s_k}, \theta_{r_k}, \alpha], k = 1, 2, 3, \dots, n,$$

where v and w are voltage and current magnitude, respectively, and $\theta, \rho \in [-\pi, \pi]$ are voltage and current phase angle, respectively. Let $\mathbf{F}(\mathbf{P}) \in \mathbb{R}^{8n+1}$, $\mathbf{F}(\mathbf{P}) = [f_{1_k}, f_{2_k}, g_{1_k}, g_{2_k}, g_{3_k}, g_{4_k}, g_{5_k}, g_{6_k}, h]^T$ be the vector of measurement functions, where $f_{p_k} : \mathbb{R}^{10} \rightarrow \mathbb{R}$, $p = 1, 2$, $g_{q_k}, h : \mathbb{R} \rightarrow \mathbb{R}$, $q = 1, 2, 3, \dots, 6$, and

$$\begin{aligned} f_{1_k} &= \text{Re}(V_{s_k} - I_{s_k} Z + V_{s_k} ZY/2 - V_{r_k} \exp(j\alpha)), \\ f_{2_k} &= \text{Im}(V_{s_k} - I_{s_k} Z + V_{s_k} ZY/2 - V_{r_k} \exp(j\alpha)) \end{aligned} \quad (3.12)$$

$$\begin{aligned} g_{1_k} &= v_{s_k}, g_{2_k} = w_{s_k}, g_{3_k} = v_{r_k}, \\ g_{4_k} &= \theta_{s_k}, g_{5_k} = \rho_{s_k}, g_{6_k} = \theta_{r_k}, h = \alpha. \end{aligned} \quad (3.13)$$

The voltage and current magnitudes v, w and phase angles θ, ρ as well as synchronization angle α are included in the vector of unknowns \mathbf{P} and vector of measurement functions $\mathbf{F}(\mathbf{P})$ such that the residuals between estimated values and measured or assumed values can be used to detect individual measurements

with errors larger than the measurement uncertainty; these can be caused by transient failure of the measurement instrumentation. Hence, define the measurement vector $\mathbf{M} \in \mathbb{R}^{8n+1}$ such that

$$\mathbf{M} = [M_i, \tilde{v}_{s_k}, \tilde{w}_{s_k}, \tilde{v}_{r_k}, \tilde{\theta}_{s_k}, \tilde{\rho}_{s_k}, \tilde{\theta}_{r_k}, 0]^T, M_i = 0, i = 1, \dots, 2n, k = 1, 2, 3, \dots, n,$$

where the tilde denotes measured values of current and voltage magnitude and phase angle. The first $2n$ entries of \mathbf{M} are set to zero since for exact measurements and parameter values, $f_{1_k}, f_{2_k} = 0$ according to the model equation (3.11). The estimation model can then be expressed as

$$\mathbf{M} = \mathbf{F}(\mathbf{P}) + \boldsymbol{\varepsilon}, \quad (3.14)$$

where $\boldsymbol{\varepsilon} \in \mathbb{R}^{8n+1}$ models measurement uncertainty. Define $J \in \mathbb{R}$:

$$J = [\mathbf{M} - \mathbf{F}(\mathbf{P})]^T [\mathbf{M} - \mathbf{F}(\mathbf{P})]. \quad (3.15)$$

The best estimate of parameter vector \mathbf{P} is computed iteratively such that J is minimized. The Chi-square test is applied to detect any bad measurements, which can then be removed and to obtain a new, more accurate parameter estimate from the remaining measurements.

3.2.1.4 Two-port Linear Least-squares - Single-phase (TPLL1)

Figure 3.2 shows a two-port network that models a transmission line.

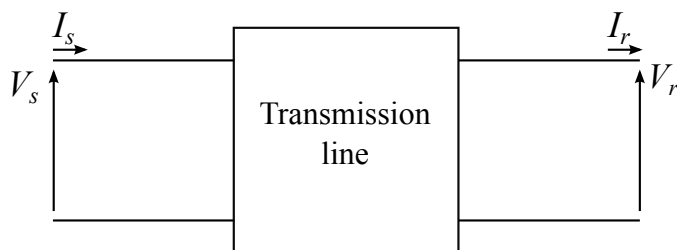


Figure 3.2: Diagram of a two-port network

The sending end signals can be expressed in terms of the receiving end signals:

$$V_s = AV_r + BI_r \quad (3.16)$$

$$I_s = CV_r + DI_r. \quad (3.17)$$

$A, B, C, D \in \mathbb{C}$ are constant parameter values. In general, these two equations decouple the sending end voltage and current. Constants A, B can be used to calculate V_s from V_r, I_r and independently, C, D can be used to calculate I_s .

In order to infer values of transmission line impedance and admittance, assumptions must be made about the internal structure of the two-port network. If a symmetrical pi-circuit is assumed, the following relationships hold:

$$A = 1 + ZY/2 \quad (3.18)$$

$$B = Z \quad (3.19)$$

$$C = Y + ZY^2/4 \quad (3.20)$$

$$D = 1 + ZY/2. \quad (3.21)$$

Thus it suffices to find constants A and B in order to calculate values for Z and Y . Given $n, n \geq 2$, sets of phasor measurements, the linear least-squares estimates of A and B are computed as follows [114]. Firstly, equation (3.16) is split into real and imaginary parts:

$$\operatorname{Re}(V_s) = \operatorname{Re}(V_r) \operatorname{Re}(A) - \operatorname{Im}(V_r) \operatorname{Im}(A) + \operatorname{Re}(I_r) \operatorname{Re}(B) - \operatorname{Im}(I_r) \operatorname{Im}(B) \quad (3.22)$$

$$\operatorname{Im}(V_s) = \operatorname{Im}(V_r) \operatorname{Re}(A) + \operatorname{Re}(V_r) \operatorname{Im}(A) + \operatorname{Im}(I_r) \operatorname{Re}(B) + \operatorname{Re}(I_r) \operatorname{Im}(B) \quad (3.23)$$

Define matrices $\mathbf{M} \in \mathbb{R}^{2n}$, $\mathbf{H} \in \mathbb{R}^{2n \times 4}$, $\boldsymbol{\theta} \in \mathbb{R}^4$, where

$$\mathbf{H} = \begin{bmatrix} \operatorname{Re}(V_{r_k}) & -\operatorname{Im}(V_{r_k}) & \operatorname{Re}(I_{r_k}) & -\operatorname{Im}(I_{r_k}) \\ \operatorname{Im}(V_{r_k}) & \operatorname{Re}(V_{r_k}) & \operatorname{Im}(I_{r_k}) & \operatorname{Re}(I_{r_k}) \end{bmatrix}, \quad \mathbf{M} = \begin{bmatrix} \operatorname{Re}(V_{s_k}) \\ \operatorname{Im}(V_{s_k}) \end{bmatrix},$$

$$\boldsymbol{\theta} = \begin{bmatrix} \operatorname{Re}(A) & \operatorname{Im}(A) & \operatorname{Re}(B) & \operatorname{Im}(B) \end{bmatrix}$$

with $k = 1, 2, 3, \dots, n$. Then (3.22) and (3.23) can be summarized by the matrix equation

$$\mathbf{M} = \mathbf{H}\boldsymbol{\theta} + \boldsymbol{\epsilon}, \quad (3.24)$$

where $\boldsymbol{\epsilon} \in \mathbb{R}^{2n}$ is an error term. The linear least-squares estimate of $\boldsymbol{\theta}$ is computed using

$$\hat{\boldsymbol{\theta}} = (\mathbf{H}^T \mathbf{H})^{-1} \mathbf{H}^T \mathbf{M}. \quad (3.25)$$

From $\boldsymbol{\theta} = [\hat{\theta}_1, \hat{\theta}_2, \hat{\theta}_3, \hat{\theta}_4]$, estimates of A and B are obtained:

$$\hat{A} = \hat{\theta}_1 + j\hat{\theta}_2, \quad \hat{B} = \hat{\theta}_3 + j\hat{\theta}_4.$$

Estimates of impedance parameters Z and Y are then calculated as follows, using (3.18) and (3.19):

$$\hat{Z} = \hat{B} \quad (3.26)$$

$$\hat{Y} = 2(\hat{A} - 1)/\hat{Z}. \quad (3.27)$$

Parameters are estimated at regular time intervals from a moving window consisting of the last n measurement sets.

3.2.2 Three-phase methods

The methods that identify impedance and admittance matrices for the general three-phase transmission line model are referred to as 'three-phase methods' in this thesis. This section first gives an overview of the general three-phase line model. Figure 3.3 shows a diagram of a three-phase pi-circuit.

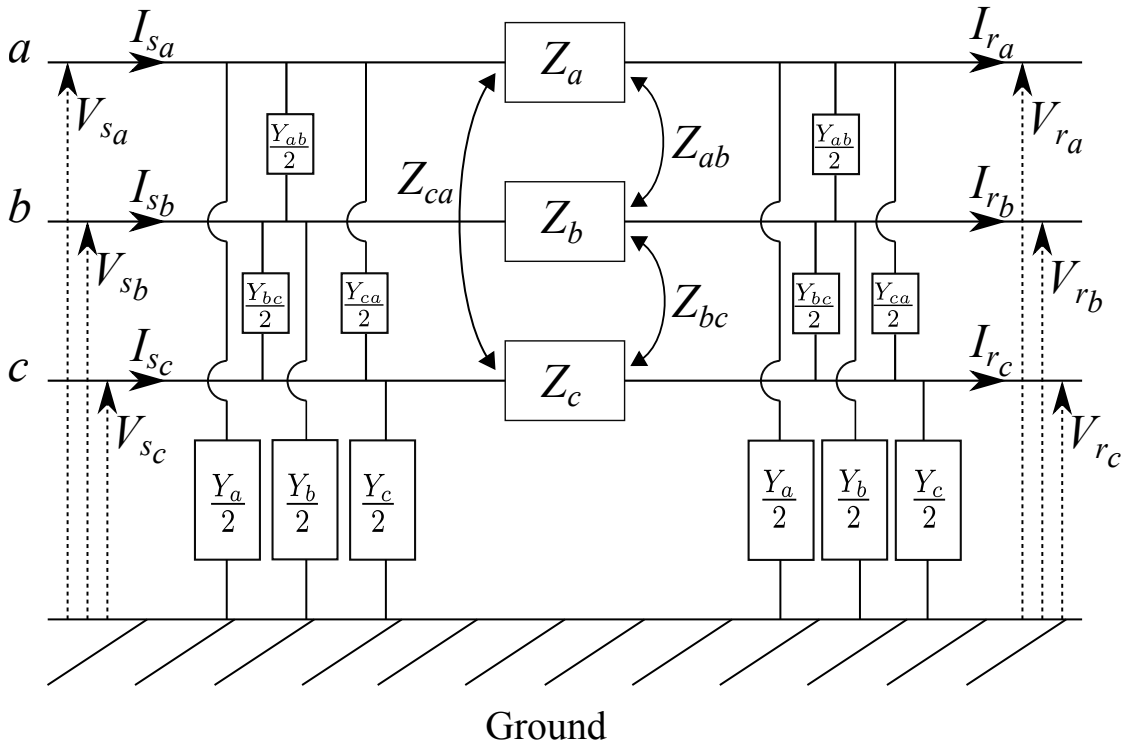


Figure 3.3: Diagram of a three-phase equivalent pi-circuit

Each of the phases, labelled a, b and c , has a series component $Z_a, Z_b, Z_c \in \mathbb{C}$, which represents the self impedance, and a shunt component $Y_a, Y_b, Y_c \in \mathbb{C}$, which represents the self admittance to ground. There is mutual impedance between each pair of phases, modelled by $Z_{ab}, Z_{bc}, Z_{ca} \in \mathbb{C}$, as well as mutual admittance, $Y_{ab}, Y_{bc}, Y_{ca} \in \mathbb{C}$. Measurements of voltage and current are modelled by $V_{s_a}, V_{s_b}, V_{s_c}, V_{r_a}, V_{r_b}, V_{r_c} \in \mathbb{C}$ and $I_{s_a}, I_{s_b}, I_{s_c}, I_{r_a}, I_{r_b}, I_{r_c} \in \mathbb{C}$, respectively, and sets of these are assumed to be reported at regular time intervals.

For ease of manipulation, the three-phase measurements are summarized as vectors $\mathbf{V}_s, \mathbf{I}_s, \mathbf{V}_r, \mathbf{I}_r \in \mathbb{C}^3$, where

$$\mathbf{V}_s = \begin{bmatrix} V_{s_a} & V_{s_b} & V_{s_c} \end{bmatrix}^T, \quad \mathbf{V}_r = \begin{bmatrix} V_{r_a} & V_{r_b} & V_{r_c} \end{bmatrix}^T, \\ \mathbf{I}_s = \begin{bmatrix} I_{s_a} & I_{s_b} & I_{s_c} \end{bmatrix}^T, \quad \mathbf{I}_r = \begin{bmatrix} I_{r_a} & I_{r_b} & I_{r_c} \end{bmatrix}^T.$$

Self and mutual impedance and admittance are summarized as matrices $\mathbf{Z}, \mathbf{Y} \in \mathbb{C}^{3 \times 3}$, where

$$\mathbf{Z} = \begin{bmatrix} Z_a & Z_{ab} & Z_{ac} \\ Z_{ab} & Z_b & Z_{bc} \\ Z_{ac} & Z_{bc} & Z_c \end{bmatrix} = \begin{bmatrix} R_a + jX_a & R_{ab} + jX_{ab} & R_{ac} + jX_{ac} \\ R_{ab} + jX_{ab} & R_b + jX_b & R_{bc} + jX_{bc} \\ R_{ac} + jX_{ac} & R_{bc} + jX_{bc} & R_c + jX_c \end{bmatrix}, \\ \mathbf{Y} = \begin{bmatrix} Y_a & Y_{ab} & Y_{ac} \\ Y_{ab} & Y_b & Y_{bc} \\ Y_{ac} & Y_{bc} & Y_c \end{bmatrix} = \begin{bmatrix} G_a + jB_a & G_{ab} + jB_{ab} & G_{ac} + jB_{ac} \\ G_{ab} + jB_{ab} & G_b + jB_b & G_{bc} + jB_{bc} \\ G_{ac} + jB_{ac} & G_{bc} + jB_{bc} & G_c + jB_c \end{bmatrix}.$$

$R_a, R_b, R_c, R_{ab}, R_{bc}, R_{ac}, X_a, X_b, X_c, X_{ab}, X_{bc}, X_{ac}, G_a, G_b, G_c, G_{ab}, G_{bc}, G_{ac}, B_a, B_b, B_c, B_{ab}, B_{bc}, B_{ac} \in \mathbb{R}_{\geq 0}$ are the self and mutual resistance, reactance, conductance and susceptance values. The voltages, currents, impedance and admittance components are related by the following matrix equations:

$$\mathbf{V}_s - \mathbf{V}_r = \mathbf{Z}(\mathbf{I}_s - \mathbf{Y}\mathbf{V}_s/2) \quad (3.28)$$

$$\mathbf{I}_s - \mathbf{I}_r = \mathbf{Y}(\mathbf{V}_s + \mathbf{V}_r)/2. \quad (3.29)$$

Four methods that are designed to estimate values of \mathbf{Z} and \mathbf{Y} from sets of measurements $\mathbf{V}_s, \mathbf{I}_s, \mathbf{V}_r, \mathbf{I}_r$ have been selected for comparison in this chapter; each method is explained in the following paragraphs.

3.2.2.1 Linear Least-squares (LLS3)

The impedance and admittance matrices \mathbf{Z} and \mathbf{Y} of a three-phase transmission line can be estimated using linear least-squares estimation [127]. Shunt conductance is assumed to be zero, hence, $\mathbf{Y} = j\mathbf{B}$. Define matrices $\Delta\mathbf{V} = \mathbf{V}_s - \mathbf{V}_r$, $\Delta\mathbf{I} = \mathbf{I}_s - \mathbf{I}_r \in \mathbb{C}^3$. The model equations (3.28) and (3.29) are rewritten as

$$\Delta\mathbf{V} = \mathbf{Z}(\mathbf{I}_s - \mathbf{Y}\mathbf{V}_s/2) \quad (3.30)$$

$$\Delta\mathbf{I} = \mathbf{Y}(\mathbf{V}_s + \mathbf{V}_r)/2. \quad (3.31)$$

Equation (3.30) can be made linear in unknown matrices by multiplying with $\mathbf{y} = \mathbf{g} + j\mathbf{b} = \mathbf{Z}^{-1}$:

$$\mathbf{I}_s = \mathbf{Y}\mathbf{V}_s/2 + \mathbf{y}\Delta\mathbf{V} \quad (3.32)$$

Equations (3.31) and (3.32) each contain three scalar equations; if real and imaginary parts are taken, the system is described by twelve real, scalar equations. To summarize these into one matrix equation, let $\Sigma\mathbf{V} = \mathbf{V}_s + \mathbf{V}_r$ and define vectors $\mathbf{M} \in \mathbb{R}^{12}$, $\boldsymbol{\theta} \in \mathbb{R}^{18}$ and matrix $\mathbf{H} \in \mathbb{R}^{12 \times 18}$, where

$$\mathbf{M} = [\text{Re}(\mathbf{I}_s), \text{Im}(\mathbf{I}_s), \text{Re}(\Delta\mathbf{I}), \text{Im}(\Delta\mathbf{I})]^T, \boldsymbol{\theta} = [\mathbf{g}, \mathbf{b}, \mathbf{B}]^T,$$

with

$$\mathbf{g} = [g_a, g_{ab}, g_{ac}, g_b, g_{bc}, g_c], \mathbf{b} = [b_a, b_{ab}, b_{ac}, b_b, b_{bc}, b_c],$$

$$\mathbf{B} = [B_a, B_{ab}, B_{ac}, B_b, B_{bc}, B_c],$$

and

$$\mathbf{H} = \begin{bmatrix} -V_{s_a}^{Im} & 0 & 0 & V_{s_a}^{Re} & 0 & 0 & -\Sigma V_{s_a}^{Im} & 0 & 0 & \Sigma V_{s_a}^{Re} & 0 & 0 \\ -V_{s_b}^{Im} & -V_{s_a}^{Im} & 0 & V_{s_b}^{Re} & V_{s_a}^{Re} & 0 & -\Sigma V_{s_b}^{Im} & -\Sigma V_a^{Im} & 0 & \Sigma V_{s_b}^{Re} & \Sigma V_a^{Re} & 0 \\ -V_{s_c}^{Im} & 0 & -V_{s_a}^{Im} & V_{s_c}^{Re} & 0 & V_{s_a}^{Re} & -\Sigma V_{s_c}^{Im} & 0 & -\Sigma V_{s_a}^{Im} & \Sigma V_{s_c}^{Re} & 0 & \Sigma V_{s_a}^{Re} \\ 0 & -V_{s_b}^{Im} & 0 & 0 & V_{s_b}^{Re} & 0 & 0 & -\Sigma V_{s_b}^{Im} & 0 & 0 & \Sigma V_{s_b}^{Re} & 0 \\ 0 & -V_{s_c}^{Im} & -V_{s_b}^{Im} & 0 & V_{s_c}^{Re} & V_{s_b}^{Re} & 0 & -\Sigma V_{s_c}^{Im} & -\Sigma V_{s_b}^{Im} & 0 & \Sigma V_{s_c}^{Re} & \Sigma V_{s_b}^{Re} \\ 0 & 0 & -V_{s_c}^{Im} & 0 & 0 & V_{s_c}^{Re} & 0 & 0 & -\Sigma V_{s_c}^{Im} & 0 & 0 & \Sigma V_{s_c}^{Re} \\ \Delta V_a^{Re} & 0 & 0 & \Delta V_a^{Im} & 0 & 0 & 0 & 0 & 0 & 0 & 0 & 0 \\ \Delta V_b^{Re} & \Delta V_a^{Re} & 0 & \Delta V_b^{Im} & \Delta V_a^{Im} & 0 & 0 & 0 & 0 & 0 & 0 & 0 \\ \Delta V_c^{Re} & 0 & \Delta V_a^{Re} & \Delta V_c^{Im} & 0 & \Delta V_a^{Im} & 0 & 0 & 0 & 0 & 0 & 0 \\ 0 & \Delta V_b^{Re} & 0 & 0 & \Delta V_b^{Im} & 0 & 0 & 0 & 0 & 0 & 0 & 0 \\ 0 & \Delta V_c^{Re} & \Delta V_b^{Re} & 0 & \Delta V_c^{Im} & \Delta V_b^{Im} & 0 & 0 & 0 & 0 & 0 & 0 \\ 0 & 0 & \Delta V_c^{Re} & 0 & 0 & \Delta V_c^{Im} & 0 & 0 & 0 & 0 & 0 & 0 \\ -\Delta V_a^{Im} & 0 & 0 & \Delta V_a^{Re} & 0 & 0 & 0 & 0 & 0 & 0 & 0 & 0 \\ -\Delta V_b^{Im} & -\Delta V_a^{Im} & 0 & \Delta V_b^{Re} & \Delta V_a^{Re} & 0 & 0 & 0 & 0 & 0 & 0 & 0 \\ -\Delta V_c^{Im} & 0 & -\Delta V_a^{Im} & \Delta V_c^{Re} & 0 & \Delta V_a^{Re} & 0 & 0 & 0 & 0 & 0 & 0 \\ 0 & -\Delta V_b^{Im} & 0 & 0 & \Delta V_b^{Im} & 0 & 0 & 0 & 0 & 0 & 0 & 0 \\ 0 & -\Delta V_c^{Im} & -\Delta V_b^{Im} & 0 & \Delta V_c^{Im} & \Delta V_b^{Re} & 0 & 0 & 0 & 0 & 0 & 0 \\ 0 & 0 & -\Delta V_c^{Im} & 0 & 0 & \Delta V_c^{Re} & 0 & 0 & 0 & 0 & 0 & 0 \end{bmatrix}^T.$$

Superscripts *Re* and *Im* refer to real and imaginary parts. The matrix equation that summarizes the twelve real equations is

$$\mathbf{M} = \mathbf{H}\boldsymbol{\theta}. \quad (3.33)$$

Given $n, n \geq 2$ sets of phasor measurements, matrices \mathbf{M} and \mathbf{H} are expanded to give $\mathbf{M} \in \mathbb{R}^{12n}$, $\mathbf{H} \in \mathbb{R}^{12n \times 18}$. Linear least-squares estimates of \mathbf{g} , \mathbf{b} and \mathbf{B} are obtained using

$$\hat{\boldsymbol{\theta}} = [\hat{\mathbf{g}}, \hat{\mathbf{b}}, \hat{\mathbf{B}}] = (\mathbf{H}^T\mathbf{H})^{-1}\mathbf{H}^T\mathbf{M}. \quad (3.34)$$

Estimates of impedance \mathbf{Z} and admittance \mathbf{Y} are given by

$$\hat{\mathbf{Z}} = (\hat{\mathbf{g}} + j\hat{\mathbf{b}})^{-1} \quad (3.35)$$

$$\hat{\mathbf{Y}} = j\hat{\mathbf{B}}. \quad (3.36)$$

Estimates $\hat{\mathbf{Z}}$ and $\hat{\mathbf{Y}}$ are computed at regular time intervals from the most recent n measurement sets.

3.2.2.2 Non-linear Least-squares with Calibration Factors (NLLC3)

The calibration factors of instrument transformers that are part of the phasor measurement chain are often unknown. To increase the accuracy of estimated impedance parameter values, the NLLC3 method assumes that instrument transformers at one line end have been calibrated and calibration factors for the other line end are estimated simultaneously with the parameter values [125].

Let $\mathbf{K}_V, \mathbf{K}_I \in \mathbb{C}^{3 \times 3}$ be diagonal matrices of calibration factors for the voltage and current measurements $\mathbf{V}_r, \mathbf{I}_r$ at the receiving line end. The three-phase model equations are then

$$\mathbf{V}_s = \mathbf{K}_V \mathbf{V}_r + \mathbf{Z}(\mathbf{I}_s - \mathbf{Y}\mathbf{V}_s/2) \quad (3.37)$$

$$\mathbf{V}_s = \mathbf{K}_V \mathbf{V}_r + \mathbf{Z}(\mathbf{K}_I \mathbf{I}_r + \mathbf{Y}\mathbf{K}_V \mathbf{V}_r/2). \quad (3.38)$$

Let

$$\mathbf{X}_1 = (\mathbf{I} + \mathbf{Z}\mathbf{Y})\mathbf{K}_V, \mathbf{X}_2 = (\mathbf{I} + \mathbf{Z}\mathbf{Y})^2, \mathbf{X}_3 = (\mathbf{I} + \mathbf{Z}\mathbf{Y})\mathbf{Z}, \mathbf{X}_4 = \mathbf{Z}\mathbf{K}_I,$$

where $\mathbf{I} \in \mathbb{R}^{3 \times 3}$ is the three-dimensional identity matrix. Then (3.37) and (3.38) can be rewritten as

$$0 = \mathbf{X}_2 \mathbf{V}_s - \mathbf{X}_1 \mathbf{V}_r - \mathbf{X}_3 \mathbf{I}_s \quad (3.39)$$

$$0 = -\mathbf{V}_s + \mathbf{X}_1 \mathbf{V}_r + \mathbf{X}_4 \mathbf{I}_r. \quad (3.40)$$

The diagonal elements $K_{V_a}, K_{V_b}, K_{V_c} \in \mathbb{R}$ of \mathbf{K}_V can be expressed as

$$0 = K_{V_a} - \sqrt{\frac{X_{1a}}{(\mathbf{X}_1^{-1} \mathbf{X}_2)_a}}, \quad 0 = K_{V_b} - \sqrt{\frac{X_{1b}}{(\mathbf{X}_1^{-1} \mathbf{X}_2)_b}}, \quad 0 = K_{V_c} - \sqrt{\frac{X_{1c}}{(\mathbf{X}_1^{-1} \mathbf{X}_2)_c}}, \quad (3.41)$$

where subscripts a, b, c refer to the three diagonal elements of the respective matrices. Notice that the negative square root is ignored as the calibration factors

must have a positive real part. Further, define $\mathbf{X}_5 \in \mathbb{C}^{3 \times 3}$, where

$$0 = \mathbf{X}_5 - \mathbf{X}_1 \mathbf{K}_V. \quad (3.42)$$

Then

$$0 = \mathbf{Z} - \mathbf{X}_5^{-1} \mathbf{X}_3 \quad (3.43)$$

$$0 = \mathbf{Y} - \mathbf{Z}^{-1} (\mathbf{X}_5^{-1} - \mathbf{I}) \quad (3.44)$$

$$0 = K_{I_a} - \frac{X_{4a}}{Z_a}, \quad 0 = K_{I_b} - \frac{X_{4b}}{Z_b}, \quad 0 = K_{I_c} - \frac{X_{4c}}{Z_c}. \quad (3.45)$$

Equations (3.39) to (3.45) are used to define a vector of objective functions $\mathbf{F} \in \mathbb{C}^{39}$ to be minimised to obtain an optimal estimate $\hat{\boldsymbol{\theta}}$ of $\boldsymbol{\theta} \in \mathbb{C}^{63}$, the vector of unknowns that consists of the non-zero elements of matrices $\mathbf{X}_1, \mathbf{X}_2, \mathbf{X}_3, \mathbf{X}_4, \mathbf{X}_5, \mathbf{K}_V, \mathbf{K}_I, \mathbf{Z}, \mathbf{Y}$. Multiple measurement sets $\mathbf{V}_s, \mathbf{I}_s, \mathbf{V}_r, \mathbf{I}_r$ are required to compute a value for $\hat{\boldsymbol{\theta}}$; given $n \in \mathbb{N}$ measurement sets, the function vector expands to $\mathbf{F} \in \mathbb{C}^{6n+33}$. At each time instant, parameter vector $\hat{\boldsymbol{\theta}}$ is computed by a non-linear least-squares estimator such as the Newton-Raphson method, using the most recent n measurement sets.

3.2.2.3 Non-linear Constraint Optimization (NLCO3)

The parameter estimation problem for the untransposed line model can also be formulated as a non-linear constrained optimization problem [126]. Firstly, a variable $\mathbf{D} \in \mathbb{C}^{3 \times 3}$, $\mathbf{D} = \mathbf{Z}\mathbf{Y}$, is introduced, and let

$$\mathbf{D} = \begin{bmatrix} D_a & D_{ab} & D_{ac} \\ D_{ab} & D_b & D_{bc} \\ D_{ac} & D_{bc} & D_c \end{bmatrix} = \begin{bmatrix} S_a + jT_a & S_{ab} + jT_{ab} & S_{ac} + jT_{ac} \\ S_{ab} + jT_{ab} & S_b + jT_b & S_{bc} + jT_{bc} \\ S_{ac} + jT_{ac} & S_{bc} + jT_{bc} & S_c + jT_c \end{bmatrix},$$

$D_a, D_b, D_c, D_{ab}, D_{bc}, D_{ac} \in \mathbb{C}$, $S_a, S_b, S_c, S_{ab}, S_{bc}, S_{ac}, T_a, T_b, T_c, T_{ab}, T_{bc}, T_{ac} \in \mathbb{R}$.

The model equations become

$$\Delta \mathbf{V} = \mathbf{Z}\mathbf{I}_s - \mathbf{D}\mathbf{V}_s/2 \quad (3.46)$$

$$\Delta \mathbf{I} = \mathbf{Y}(\mathbf{V}_s + \mathbf{V}_r)/2. \quad (3.47)$$

Matrix equations (3.46) and (3.47) can be expanded into six scalar equations that are used to formulate objective functions $f_1, f_2, f_3 : \mathbb{C}^6 \rightarrow \mathbb{C}, f_4, f_5, f_6 : \mathbb{C}^3 \rightarrow \mathbb{C}$:

$$f_1 = Z_a I_{s_a} + Z_{ab} I_{s_b} + Z_{ac} I_{s_c} - (D_a V_{s_a} + D_{ab} V_{s_b} + D_{ac} V_{s_c})/2 \quad (3.48)$$

$$f_2 = Z_{ab} I_{s_a} + Z_b I_{s_b} + Z_{bc} I_{s_c} - (D_{ab} V_{s_a} + D_b V_{s_b} + D_{bc} V_{s_c})/2 \quad (3.49)$$

$$f_3 = Z_{ac} I_{s_a} + Z_{bc} I_{s_b} + Z_c I_{s_c} - (D_{ac} V_{s_a} + D_{bc} V_{s_b} + D_c V_{s_c})/2 \quad (3.50)$$

$$f_4 = (Y_a(V_{s_a} + V_{r_a}) + Y_{ab}(V_{s_b} + V_{r_b}) + Y_{ac}(V_{s_c} + V_{r_c}))/2 \quad (3.51)$$

$$f_5 = (Y_{ab}(V_{s_a} + V_{r_a}) + Y_b(V_{s_b} + V_{r_b}) + Y_{bc}(V_{s_c} + V_{r_c}))/2 \quad (3.52)$$

$$f_6 = (Y_{ac}(V_{s_a} + V_{r_a}) + Y_{bc}(V_{s_b} + V_{r_b}) + Y_c(V_{s_c} + V_{r_c}))/2 \quad (3.53)$$

Define the parameter vector $\boldsymbol{\theta} \in \mathbb{R}^{30}$,

$$\begin{aligned} \boldsymbol{\theta} = [& R_a, R_b, R_c, R_{ab}, R_{bc}, R_{ac}, X_a, X_b, X_c, X_{ab}, X_{bc}, X_{ac}, \\ & S_a, S_b, S_c, S_{ab}, S_{bc}, S_{ac}, T_a, T_b, T_c, T_{ab}, T_{bc}, T_{ac}, \\ & B_a, B_b, B_c, B_{ab}, B_{bc}, B_{ac}] \end{aligned}$$

and let $\mathbf{F}(\boldsymbol{\theta}) \in \mathbb{R}^{12}$ be the vector of objective functions,

$$\mathbf{F}(\boldsymbol{\theta}) = [f_1^{Re}, f_2^{Re}, f_3^{Re}, f_1^{Im}, f_2^{Im}, f_3^{Im}, f_4^{Re}, f_5^{Re}, f_6^{Re}, f_4^{Im}, f_5^{Im}, f_6^{Im}]^T.$$

From the relation $\mathbf{D} = \mathbf{Z}\mathbf{Y}$, six non-linear functions $g_1, g_2, g_3, g_4, g_5, g_6 : \mathbb{C}^6 \rightarrow \mathbb{C}$ are formulated:

$$g_1 = Z_a Y_a + Z_{ab} Y_{ab} + Z_{ac} Y_{ac} \quad (3.54)$$

$$g_2 = Z_{ab} Y_{ab} + Z_b Y_b + Z_{bc} Y_{bc} \quad (3.55)$$

$$g_3 = Z_{ac} Y_{ac} + Z_{bc} Y_{bc} + Z_c Y_c \quad (3.56)$$

$$g_4 = Z_a Y_{ab} + Z_{ab} Y_b + Z_{ac} Y_{bc} \quad (3.57)$$

$$g_5 = Z_a Y_{ac} + Z_{ab} Y_{bc} + Z_{ac} Y_c \quad (3.58)$$

$$g_6 = Z_{ab} Y_{ac} + Z_b Y_{bc} + Z_{bc} Y_c, \quad (3.59)$$

which can be expanded into real and imaginary parts to define twelve equality constraints:

$$\text{Re}(g_1) = S_a \quad \text{Re}(g_2) = S_b \quad \text{Re}(g_3) = S_c \quad (3.60)$$

$$\text{Im}(g_1) = T_a \quad \text{Im}(g_2) = T_b \quad \text{Im}(g_3) = T_c \quad (3.61)$$

$$\text{Re}(g_4) = S_{ab} \quad \text{Re}(g_5) = S_{ac} \quad \text{Re}(g_6) = S_{bc} \quad (3.62)$$

$$\text{Im}(g_4) = T_{ab} \quad \text{Im}(g_5) = T_{ac} \quad \text{Im}(g_6) = T_{bc}. \quad (3.63)$$

Additionally, inequality constraints can be defined based on the fact that line series resistance is normally smaller than series reactance,

$$R_a \leq X_a \qquad R_b \leq X_b \qquad R_c \leq X_c \qquad (3.64)$$

$$R_{ab} \leq X_{ab} \qquad R_{bc} \leq X_{bc} \qquad R_{ac} \leq X_{ac}. \qquad (3.65)$$

Define the measurement vector $\mathbf{M} \in \mathbb{R}^{12}$ as $\mathbf{M} = [\Delta\mathbf{V}^T, \Delta\mathbf{I}^T]^T$. An optimal parameter estimate is found by solving the following non-linear constrained optimization problem:

$$\begin{aligned} & \underset{\boldsymbol{\theta}}{\text{minimize}} && |\mathbf{F}(\boldsymbol{\theta}) - \mathbf{M}|^2 \\ & \text{subject to} && (3.60) \text{ to } (3.65), \\ & && \theta_i - 0.1|\theta_i| \leq \theta_i \leq \theta_i + 0.1|\theta_i|. \end{aligned} \qquad (3.66)$$

$\theta_i, i = 1, \dots, 30$, are the starting points for the optimization and equal to theoretically calculated parameter values. Lower and upper bounds are set to $\theta_i \pm 10\%$. Given n measurement sets, the dimensions of vectors \mathbf{F} and \mathbf{M} increase to $\mathbf{F}, \mathbf{M} \in \mathbb{R}^{12n}$. At each time instant, a window of the most recent n measurements is used to obtain an estimate $\hat{\boldsymbol{\theta}}$, from which estimated impedance and admittance matrices $\hat{\mathbf{Z}}$ and $\hat{\mathbf{Y}}$ are obtained.

3.2.2.4 Two-port Linear Least-squares - Three-phase (TPLL3)

As was explained in Section 3.2.1.4, a single-phase transmission line can be modelled by a two-port network whereby the sending and receiving end signals are related by the chain parameters A, B, C, D as in (3.16) and (3.17). This representation can be extended to the three-phase case [128]. Firstly, rearrange the three-phase model equations such that $\mathbf{V}_s, \mathbf{I}_s$ are expressed in terms of $\mathbf{V}_r, \mathbf{I}_r, \mathbf{Z}, \mathbf{Y}$:

$$\mathbf{V}_s = (\mathbf{I} + \mathbf{Z}\mathbf{Y})\mathbf{V}_r/2 + \mathbf{Z}\mathbf{I}_r \qquad (3.67)$$

$$\mathbf{I}_s = (\mathbf{Y} + \mathbf{Y}\mathbf{Z}\mathbf{Y})\mathbf{V}_r/4 + \mathbf{Y}\mathbf{Z}\mathbf{I}_r/2. \qquad (3.68)$$

Then, define matrices $\mathbf{A}, \mathbf{B}, \mathbf{C}, \mathbf{D} \in \mathbb{C}^{3 \times 3}$, where

$$\mathbf{A} = \mathbf{I} + \mathbf{Z}\mathbf{Y}/2, \mathbf{B} = \mathbf{Z}, \mathbf{C} = \mathbf{Y}\mathbf{Z}\mathbf{Y}/4 + \mathbf{Y}, \mathbf{D} = \mathbf{I} + \mathbf{Y}\mathbf{Z}/2, \qquad (3.69)$$

and $\mathbf{I} \in \mathbb{R}^{3 \times 3}$ is the identity matrix.

Substitute (3.69) into (3.67) and (3.68) to get

$$\mathbf{V}_s = \mathbf{A}\mathbf{V}_r + \mathbf{B}\mathbf{I}_r \quad (3.70)$$

$$\mathbf{I}_s = \mathbf{C}\mathbf{V}_r + \mathbf{D}\mathbf{I}_r. \quad (3.71)$$

As for the single-phase case, it suffices to consider (3.70) and to find values for \mathbf{A} and \mathbf{B} , from which estimates of \mathbf{Z} and \mathbf{Y} are derived. Define $\boldsymbol{\theta} \in \mathbb{C}^{18}$ as the vector of unknown elements of \mathbf{A} and \mathbf{B} ,

$$\boldsymbol{\theta} = [A_{11}, A_{12}, \dots, A_{ij}, B_{11}, B_{12}, \dots, B_{ij}]^T,$$

where $i, j = 1, 2, 3$ refer to the rows columns of \mathbf{A} and \mathbf{B} . In addition, define $\mathbf{H} \in \mathbb{C}^{3 \times 18}$, $\mathbf{H} = [\mathbf{H}_V \ \mathbf{H}_I]$, $\mathbf{H}_V, \mathbf{H}_I \in \mathbb{C}^{3 \times 9}$, where

$$\mathbf{H}_V = \begin{bmatrix} \mathbf{V}_r^T & 0 & 0 \\ 0 & \mathbf{V}_r^T & 0 \\ 0 & 0 & \mathbf{V}_r^T \end{bmatrix}, \quad \mathbf{H}_I = \begin{bmatrix} \mathbf{I}_r^T & 0 & 0 \\ 0 & \mathbf{I}_r^T & 0 \\ 0 & 0 & \mathbf{I}_r^T \end{bmatrix}.$$

Then (3.70) can be expressed as the matrix equation

$$\mathbf{V}_s = \mathbf{H}\boldsymbol{\theta}. \quad (3.72)$$

For n sets of measurements, the dimensions of \mathbf{V}_s and \mathbf{H} become $\mathbf{V}_s \in \mathbb{C}^{3n}$, $\mathbf{H} \in \mathbb{C}^{3n \times 18}$. The linear least-squares estimate of $\boldsymbol{\theta}$ is calculated using

$$\hat{\boldsymbol{\theta}} = (\mathbf{H}^* \mathbf{H})^{-1} \mathbf{H}^* \mathbf{V}_s, \quad (3.73)$$

where the superscript $*$ denotes the conjugate transpose of a matrix. $\hat{\boldsymbol{\theta}}$ gives estimates of the elements of \mathbf{A} and \mathbf{B} , $\hat{\boldsymbol{\theta}} = [\hat{A}_{11}, \hat{A}_{12}, \dots, \hat{A}_{ij}, \hat{B}_{11}, \hat{B}_{12}, \dots, \hat{B}_{ij}]^T$, such that

$$\hat{\mathbf{A}} = \begin{bmatrix} \hat{A}_{11} & \hat{A}_{12} & \hat{A}_{13} \\ \hat{A}_{21} & \hat{A}_{22} & \hat{A}_{23} \\ \hat{A}_{31} & \hat{A}_{32} & \hat{A}_{33} \end{bmatrix}, \quad \hat{\mathbf{B}} = \begin{bmatrix} \hat{B}_{11} & \hat{B}_{12} & \hat{B}_{13} \\ \hat{B}_{21} & \hat{B}_{22} & \hat{B}_{23} \\ \hat{B}_{31} & \hat{B}_{32} & \hat{B}_{33} \end{bmatrix}.$$

Hence, estimates of the impedance and admittance matrices \mathbf{Z} and \mathbf{Y} are calculated:

$$\hat{\mathbf{Z}} = \hat{\mathbf{B}} \quad (3.74)$$

$$\hat{\mathbf{Y}} = 2(\hat{\mathbf{A}} - \mathbf{I})\hat{\mathbf{Z}}^{-1}. \quad (3.75)$$

$\hat{\mathbf{Z}}$ and $\hat{\mathbf{Y}}$ are computed at regular time steps from the last n sets of measurements.

3.2.2.5 Computation of positive sequence parameters for three-phase methods

To compare estimated impedance parameters from single-phase and three-phase methods, positive sequence components are obtained from the impedance and admittance matrices $\hat{\mathbf{Z}}$ and $\hat{\mathbf{Y}}$ through the sequence transformation:

$$\begin{bmatrix} \hat{Z}_0 & \hat{Z}_{01} & \hat{Z}_{02} \\ \hat{Z}_{10} & \hat{Z}_1 & \hat{Z}_{12} \\ \hat{Z}_{20} & \hat{Z}_{21} & \hat{Z}_2 \end{bmatrix} = \frac{1}{3} \begin{bmatrix} 1 & 1 & 1 \\ 1 & a^2 & a \\ 1 & a & a^2 \end{bmatrix} \begin{bmatrix} \hat{Z}_a & \hat{Z}_{ab} & \hat{Z}_{ac} \\ \hat{Z}_{ab} & \hat{Z}_b & \hat{Z}_{bc} \\ \hat{Z}_{ac} & \hat{Z}_{bc} & \hat{Z}_c \end{bmatrix} \begin{bmatrix} 1 & 1 & 1 \\ 1 & a & a^2 \\ 1 & a^2 & a \end{bmatrix} \quad (3.76)$$

where $a \in \mathbb{C}$, $a = \exp(j\frac{2\pi}{3})$, $\hat{Z}_0, \hat{Z}_1, \hat{Z}_2 \in \mathbb{C}$ are the zero, positive and negative sequence self impedances, respectively, and $\hat{Z}_{01}, \hat{Z}_{10}, \hat{Z}_{02}, \hat{Z}_{20}, \hat{Z}_{12}, \hat{Z}_{21} \in \mathbb{C}$ are mutual sequence impedances, which are zero for lines with perfect phase symmetry. \hat{Z}_1 is computed as follows:

$$\hat{Z}_1 = \frac{1}{3}(\hat{Z}_a + \hat{Z}_b + \hat{Z}_c - (\hat{Z}_{ab} + \hat{Z}_{bc} + \hat{Z}_{ac})). \quad (3.77)$$

Thus, the positive sequence impedance is the difference between the average self impedance and average mutual impedance of the three phases. \hat{Z}_1 is the quantity that is compared to the estimated positive sequence impedance from the single-phase methods. \hat{Y}_1 is calculated in the same manner.

3.3 Assessment criteria for parameter estimation results

A set of criteria must be defined to assess and compare the effectiveness of the eight selected impedance parameter estimation methods. An ideal numerical criterion is the error between synchrophasor-based parameter estimates and independently measured reference values. In practice, such reference values are rarely available. But theoretical reference values can be calculated using knowledge of geometrical and electrical properties of the overhead line [46]. Furthermore, measurements of conductor temperature or ambient weather conditions can be used to calculate thermal variation of the impedance parameter values over time [43].

Table 3.2 lists two assessment criteria for the synchrophasor-based estimated values of positive sequence impedance and admittance, defined with respect to theoretically calculated values. The first criterion is based on the median parameter estimates for a given time period and assesses whether the estimates are physically possible and consistent with electromagnetic theory. Negative parameter values, for instance, are unphysical and therefore unacceptable. A generous acceptability margin of $\pm 50\%$ is set as the impedance of the actual overhead line system can differ from the theoretical reference values due to incorrect assumptions in the theoretical calculation; for instance, the line properties can change through ageing or alterations by the network operator. For conductance, the limit of the first criterion is defined such that an acceptable estimated value accounts for a difference in current across the line of less than 10% of minimum current. The reason for this choice is that a conductance estimate can be further than $\pm 50\%$ from the theoretical value, yet cause a difference in current that is negligible compared to the measurement uncertainty (up to 1% according to TVE limits [56]), and thus the estimate is still acceptable.

The second criterion, the Interdecile Range (IDR) of the estimated parameter values, assesses the level of variation over time. Resistance-temperature coefficients of common overhead line conductors are of the order of $0.004\text{ }^{\circ}\text{C}^{-1}$; therefore resistance can change by several percent of the reference value at $20\text{ }^{\circ}\text{C}$, depending on the conductor temperature during the given time period. If the theoretically predicted range is below 0.4% of the reference value (less than 1° change in conductor temperature), interdecile ranges of the synchrophasor-based resistance estimates of up to 0.8% are acceptable to allow for measurement uncertainty; otherwise, the measured IDR is deemed acceptable if it does not exceed theoretical predictions by more than 50%.

Table 3.2: Assessment criteria for acceptable parameter estimates

	Median of estimated parameter values over a given time period	Interdecile Range (IDR) of estimated parameter values over a given time period
Resistance	within $\pm 50\%$ of the theoretical value	less than maximum of $\{0.8\%$ of theoretical reference value, 150% of theoretical range $\}$
Reactance		less than 5% of the theoretical parameter value
Susceptance		
Conductance	within $\pm 10\%$ of (minimum line current/nominal phase voltage)	less than 10% of (minimum line current/nominal phase voltage)

The self and mutual inductive reactance and capacitive susceptance are related to conductor height above ground and can thus change due to thermal expansion of the overhead line. But the changes in the positive sequence quantities are negligible as discussed in Appendix A.1, hence, series reactance and shunt susceptance are assumed constant in this instance. The limit of 5% for IDR has been chosen since repeated estimations of reactance and susceptance will not yield exactly the same value due to random measurement uncertainty; a 5% limit means that a measurement uncertainty of 1% , which corresponds to an expanded uncertainty of $\pm 2\%$, is acceptable. Conductance can change with the level of humidity and the estimates have uncertainty; therefore variation within the limits of associated current difference of up to 10% of minimum current is acceptable. This set of criteria forms the basis for the comparison of synchrophasor-based parameter estimation results that will be presented in Sections 3.4 and 3.5.

3.4 Application of methods to field data

All of the methods introduced in Section 3.2 have been applied to field measurements to estimate impedance parameters for an actual transmission line. In the first part of this section, details are given of the known properties of the transmission line system and the synchrophasor measurements; in the second part, the results of the parameter estimation are presented, followed by a comparative discussion of the methods.

3.4.1 Properties of the line and the data

The transmission line under consideration is a fully transposed three-phase overhead line of length 521 km located in Namibia. The nominal voltage and frequency are 330 kV and 50 Hz, respectively, and the line supplies electricity generated at a hydroelectric power plant in the north of the country to load centres in the south.

3.4.1.1 Field measurements

During a field measurement campaign, GPS-synchronized power quality instruments recorded rms amplitudes and phase angles of the fundamental frequency components of voltage and current signals at 0.1 s intervals with an accuracy of 0.1 %. The rms values and phase angles were combined into complex phasors and averaged over one-minute intervals (600 measurements), giving 1440 sets of sending and receiving end voltage and current phasors for each 24-hour period that were used for parameter estimation. By taking averages of the measurements, random uncertainty was reduced by a factor of $\sqrt{600} = 24.5$. The interval length of one minute was chosen such that thermal variation in impedance can be tracked; typical thermal time constants are between 5 min and 20 min [43].

For the purpose of comparing the parameter estimates given by the methods explained in Section 3.2, measurements from one 24-hour period with a variable load profile have been chosen for presentation in this chapter such that the methods can be tested under a range of conditions. There are differences between daily load profiles, but the chosen period is not atypical for the overhead line.

The magnitude of the positive sequence line-to-line voltage phasors at each line end is shown in Figure 3.4; the sending end voltage is less variable and closer to the nominal voltage level than the receiving end values as expected for the voltage near a large generation plant.

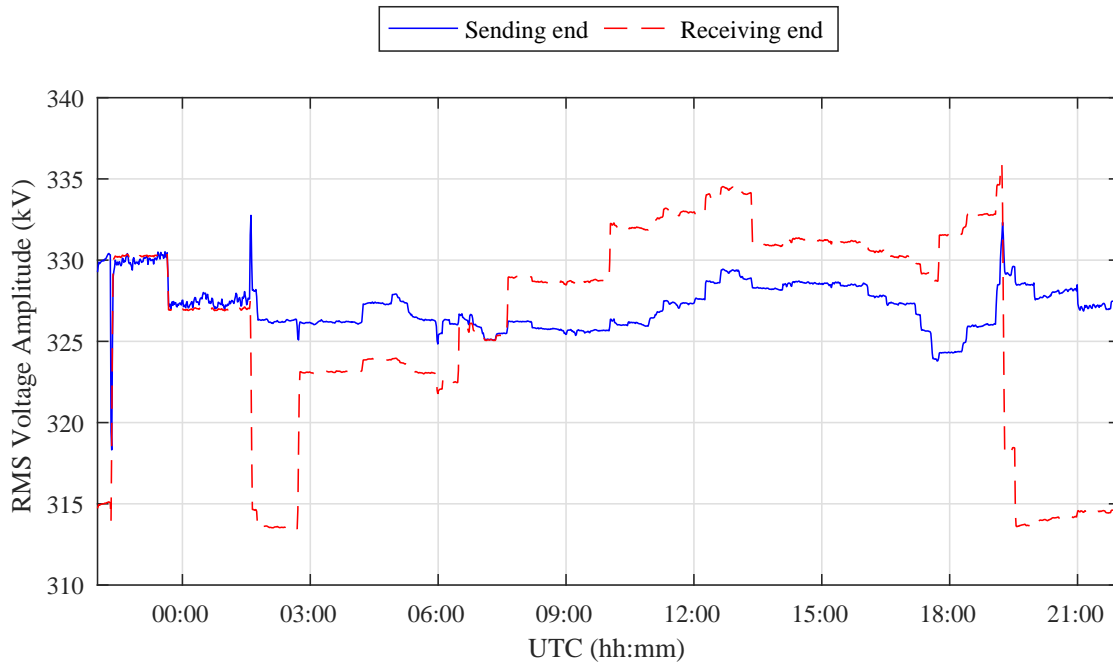


Figure 3.4: Positive sequence line-to-line voltage amplitude

In Figure 3.5, it can be observed that the receiving end voltage lags the sending end for the majority of the period, except in the initial hours, between 22:30 and 01:30.

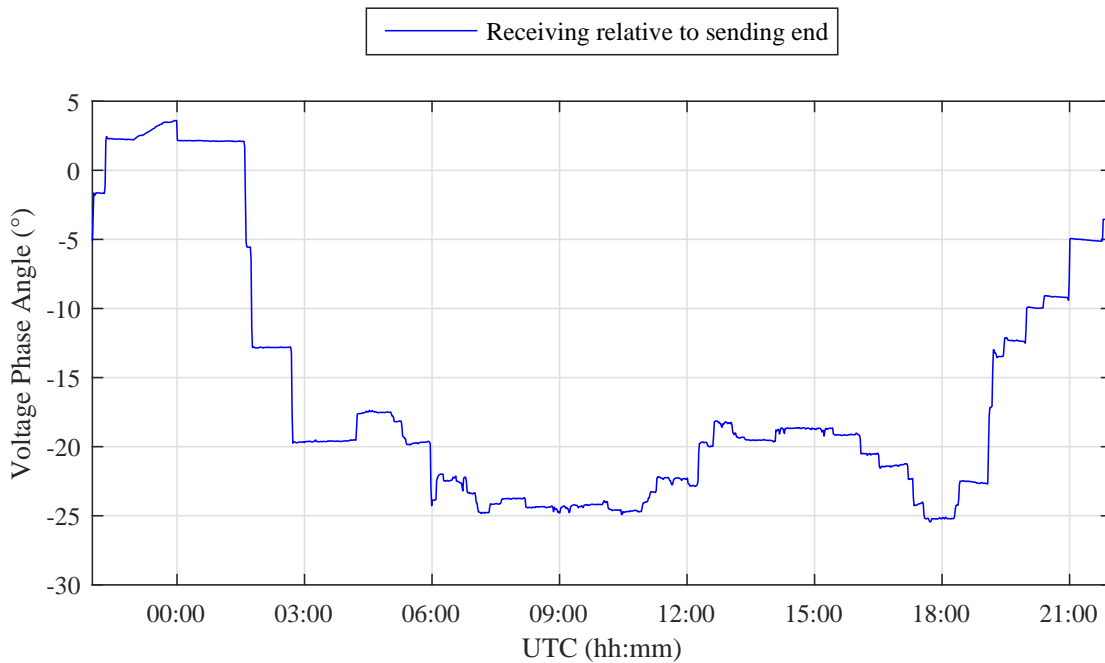


Figure 3.5: Positive sequence voltage phase angle

The voltage measurements were taken line-to-line (in delta configuration) because no neutral or direct ground connection was available in the substations. Zero sequence components are lost if voltages are measured in delta configuration, but the positive sequence is fully preserved as shown in Appendix A.2. Since the selected algorithms for impedance parameter estimation require line-to-neutral or line-to-ground (star configuration) voltages, the following delta-star conversion has been applied:

$$\mathbf{V}_{\text{star}} = \frac{1}{\sqrt{3}} \mathbf{V}_{\text{delta}} \exp(-j\pi/6), \quad (3.78)$$

where $\mathbf{V}_{\text{delta}} \in \mathbb{C}^3$ is substituted by the three-phase measurements from each line end.

Figure 3.6 shows that the current magnitude is lowest in the hours around midnight and peaks at 600 A at 18:00; in general, the sending end current is larger than the receiving end, which points to significant capacitive leakage along the line.

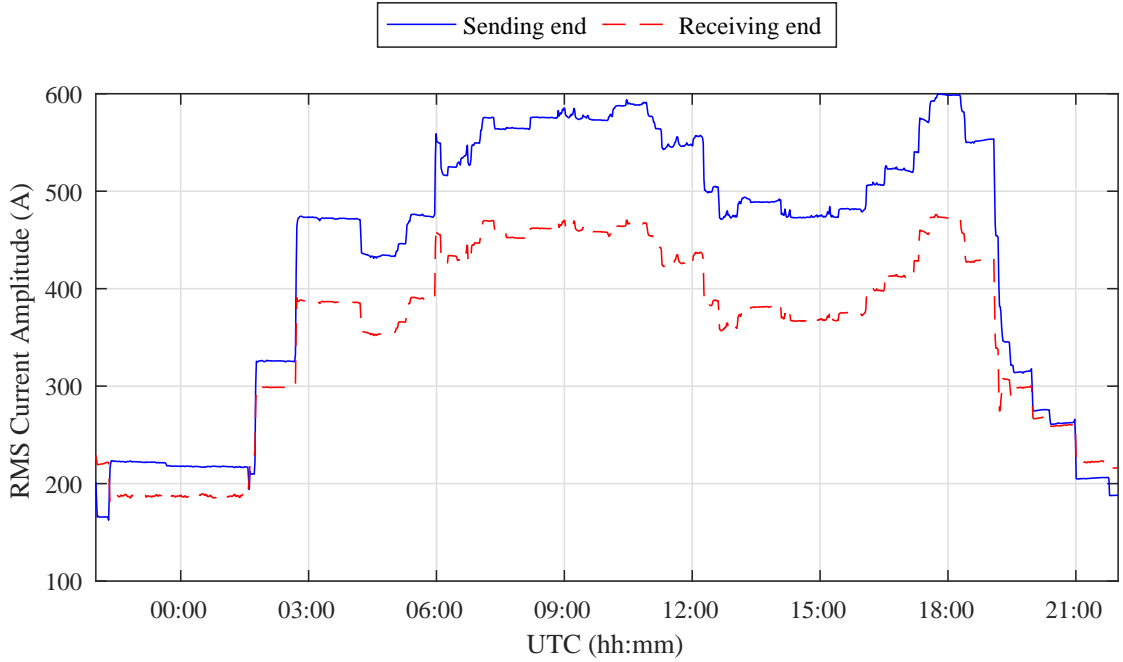


Figure 3.6: Positive sequence current amplitude

The level of active power is shown in Figure 3.7; more power is transferred in the daytime, especially during the morning and early evening hours. Around midnight, when demand is below 20 MW, active power is actually negative, which implies a reversal of the direction of power flow; this observation corresponds to the time when the receiving end voltage phase angle leads the sending end.

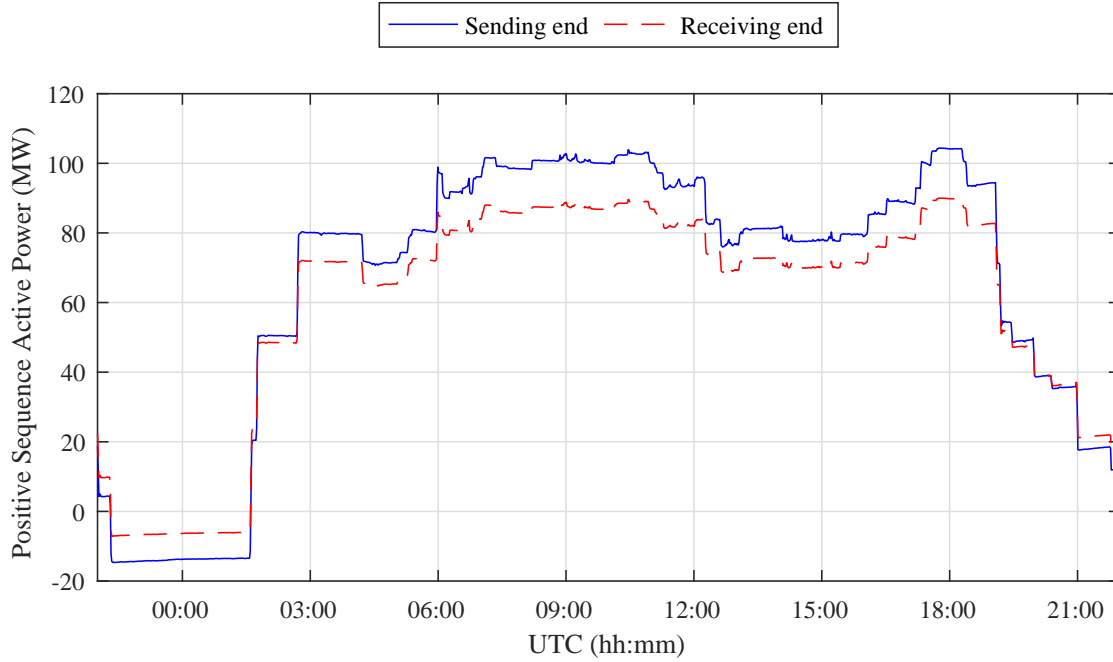


Figure 3.7: Positive sequence active power

3.4.1.2 Theoretical impedance parameter calculation

The MATLAB[®] Simscape[™] Power Systems[™] program *power_lineparam* was used to calculate per unit length values of resistance, inductance and capacitance. The inputs to the program are number and types of conductors as well as tower geometry and ground resistivity; formulae derived from electromagnetic theory are used to compute per unit length positive sequence parameters [48]. Pi-circuit equivalent parameter values are shown in Table 3.3. The parameter values obtained in this manner are likely to differ from actual values since conductor properties change over time due to ageing and exposition to the elements; however, this calculation method is a standard procedure and provides the best estimates in the absence of independent line impedance measurements.

Table 3.3: Equivalent pi-circuit positive sequence transmission line parameter values at $T_c = 20^\circ\text{C}$

Resistance R	16.2 Ω
Inductance L	600 mH
Reactance X at $f = 50$ Hz	189 Ω
Conductance G	3.74 μS
Capacitance C	5.00 μF
Susceptance B at $f = 50$ Hz	1.57 mS

The conductor temperature was estimated from the current magnitude and

ambient weather conditions including air temperature, wind speed and direction and solar radiation using the heat balance equation [43]. Details of the iterative calculation for the line under consideration are given in Appendix A.3, the estimated temperature and resulting resistance values are shown in Figure 3.8.

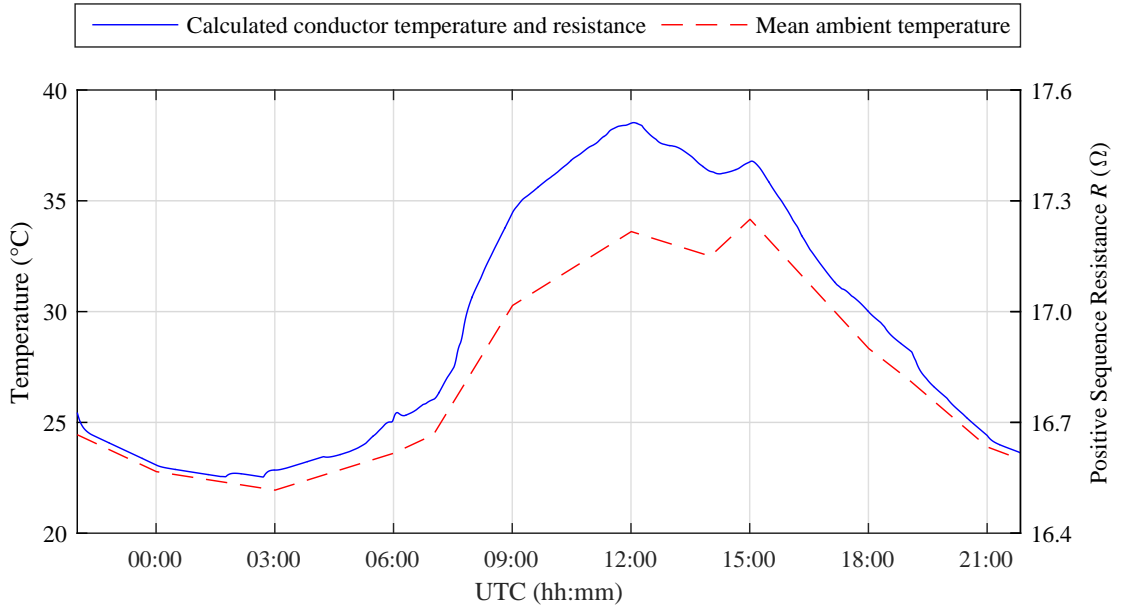


Figure 3.8: Calculated conductor temperature and resistance as well as mean ambient temperature during the chosen 24-hour period

The range of estimated conductor temperature is 16°C , which leads to an interval of resistance values of $[16.5, 17.5] \Omega$. In order to obtain accurate temperature estimates ($\pm 5^{\circ}\text{C}$), data from various weather stations installed in the vicinity and spread along the length of the line is required [131, 132]. Since it was only possible to obtain historical hourly weather data from two stations 200 km from each line end, the estimated conductor temperature may deviate from the actual value. However, the estimate provides an indication of a realistic level of daily variation in line temperature, given the location of the overhead line. Based on the theoretical parameter calculation, numerical values can be assigned to the acceptability limits introduced in Section 3.3. The values are given in Table 3.4.

Table 3.4: Numerical limits for acceptable parameter estimates

	Median of estimated parameter values over a given time period	Interdecile range of estimated parameter values over a given time period
Resistance	$\pm 50\%$ of $16.2\ \Omega$ gives $[8.1, 24.3]\ \Omega$	less than maximum of $\{0.8\%$ of $16.2\ \Omega = 0.13\ \Omega, 150\%$ of $17.5 - 16.5 = 1\ \Omega\}$ gives $< 1.5\ \Omega$
Reactance	$\pm 50\%$ of $189\ \Omega$ gives $[95, 284]\ \Omega$	less than 5% of $189\ \Omega$ gives $< 9.45\ \Omega$
Susceptance	$\pm 50\%$ of $1.57\ \text{mS}$ gives $[0.79, 2.36]\ \text{mS}$	less than 5% of $1.57\ \text{mS}$ gives $< 0.079\ \text{mS}$
Conductance	within $\pm 10\%$ of (minimum line current/nominal phase voltage) gives $\pm 0.1 \frac{190}{330e3\sqrt{3}} = \pm 0.06\ \text{mS}$	less than 10% of (minimum line current/nominal phase voltage) gives $< 0.06\ \text{mS}$

3.4.2 Analysis of parameter estimation results

The names and acronyms of the methods that have been implemented to estimate line parameters are summarized in Table 3.5.

Table 3.5: Selection of parameter estimation methods, grouped by transmission line model

Model:	Pi-circuit	Two-port network
Transposed	Single Measurement (SM1) Total Least-squares (TLS1) Non-linear Optimal Estimator (NLOE1)	Two-port Linear Least-squares - Single-phase (TPLL1)
Untransposed	Linear Least-squares (LLS3) Non-linear Constraint Optimization (NLCO3) Non-linear Least-squares with Calibration Factors (NLLC3)	Two-port Linear Least-squares - Three-phase (TPLL3)

By the SM1 method, parameter estimates for positive sequence resistance R , reactance X , conductance G and susceptance B have been calculated from each available set of phasor measurements $V_{s_i}, I_{s_i}, V_{r_i}, I_{r_i}$ from time t_i . In this instance, one set of measurements $V_{s_i}, I_{s_i}, V_{r_i}, I_{r_i}$ was available every minute. Hence, this method uses only the system state captured by the most recent measurement. In contrast, the other methods require multiple measurement sets that reflect different system states such that their problem formulation becomes fully or overdetermined and well-conditioned. To get an estimate as close as possible to the current average line temperature, the moving window must be as short as possible. However, it was found that for the chosen data set of the line under consideration, the consistency of the parameter estimates with theoretical predictions decreased with the length of the time window. With the aim of balancing these two opposing factors, 60 measurement sets from a moving window of one hour were used in each estimation.

3.4.2.1 Exclusion of measurements from impedance parameter estimation

Initially, measurements from the entire 24-hour period were used for parameter estimation. But it was found that three of the selected methods produced extreme parameter estimation results between 23:00 and 01:00. This phenomenon can be observed in Figures 3.9 and 3.10.

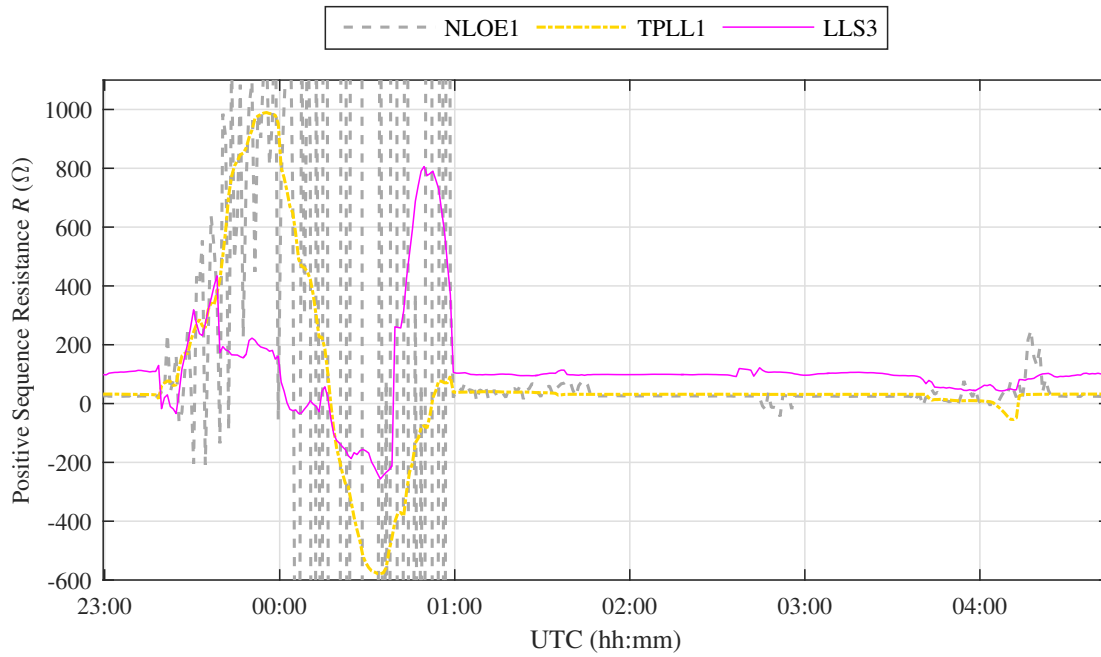


Figure 3.9: Positive sequence resistance estimates for the first six hours of the 24-hour period

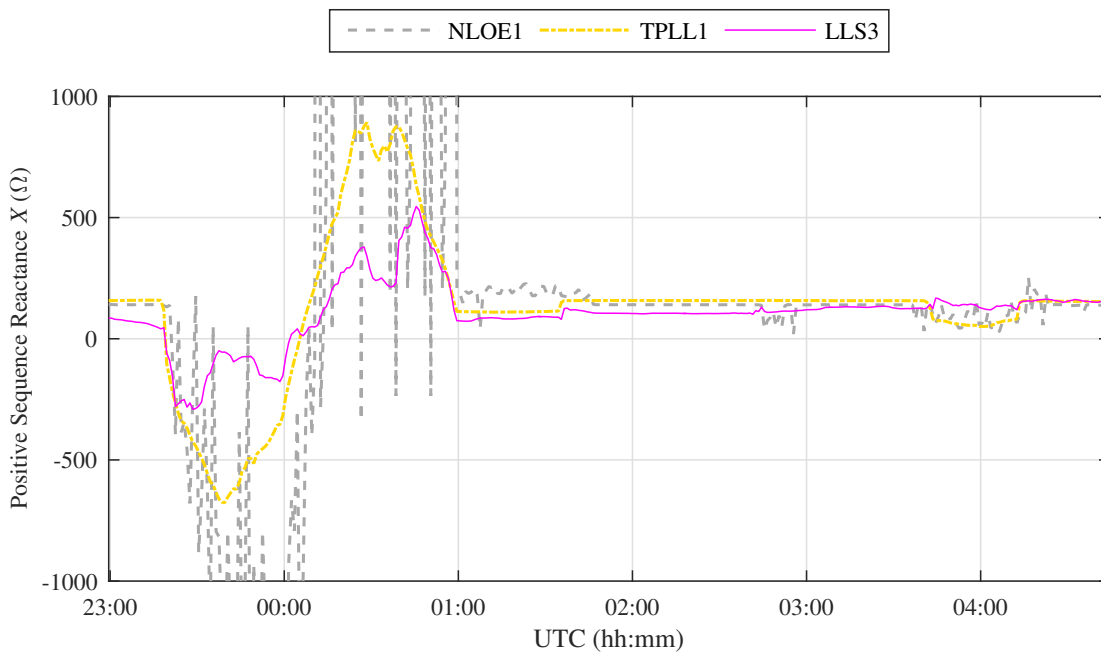


Figure 3.10: Positive sequence reactance estimates for the first six hours of the 24-hour period

During the two-hour period, the NLOE1, TPLL1 and LLS3 methods yield estimates of resistance whose magnitudes are greater than ten times the theoretical reference value of $16.2\ \Omega$ and some estimates are negative.

Similarly, negative reactance values have been estimated for this time period and estimates with magnitudes exceeding $500\ \Omega$, more than double the theoretical reference value of $189\ \Omega$. It is not physically possible for the overhead line to have impedance parameters that are negative and/or of this magnitude.

These extreme impedance parameter estimates can be explained by unusual synchrophasor measurements between 23:00 and 00:00, which form part of the 60-minute moving windows used to calculate estimates by the NLOE1, TPLL1 and LLS3 methods until 01:00. In Figure 3.11, the black rectangle highlights the fact that the phase angle between sending and receiving end voltages increases continuously between 23:00 and 00:00, while there is no response in the current magnitude. But during the rest of the 24-hour period the current magnitude is responsive to changes in the magnitude of the voltage phase angle across the line. This phenomenon has also occurred in the hour to midnight on other days. Because these measurements are untypical and resulting in unphysical parameter estimates, measurements before 00:00 will not be considered from this point onwards.

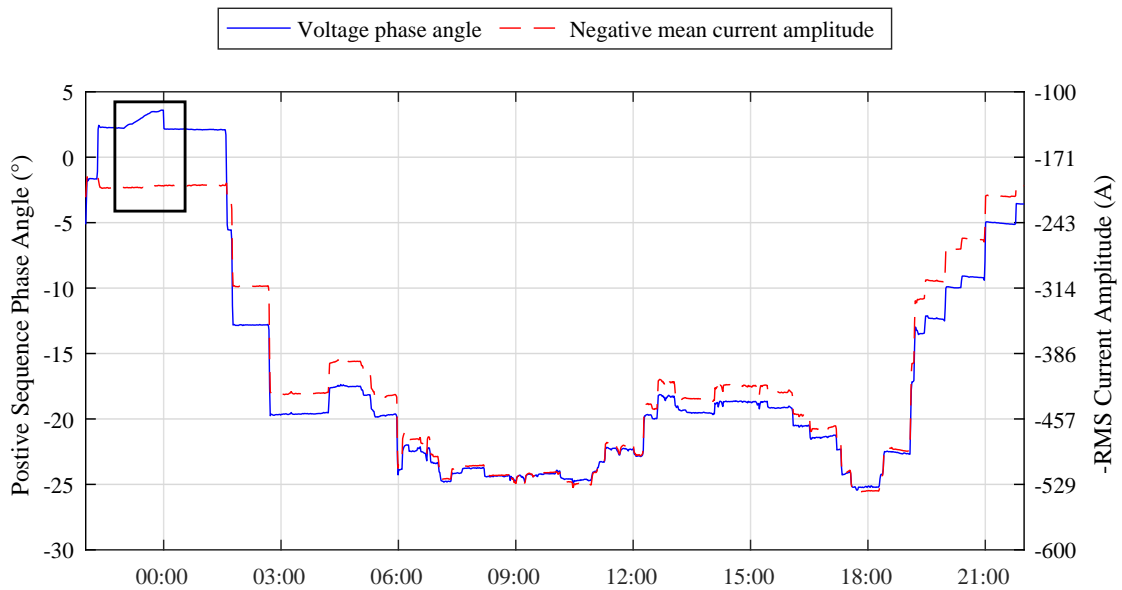


Figure 3.11: Voltage phase angle and negative current magnitude over the 24-hour period

In the following paragraphs, the acceptability of parameter estimation results from field measurements will be assessed with respect to the criteria defined in Table 3.4. Values of the median and interdecile range for all parameters are given in Appendix A.4.

3.4.2.2 Resistance

Table 3.6 gives an evaluation of the resistance estimates for the chosen 22-hour period for the eight selected methods against the criteria in Table 3.4. A check mark (✓) indicates an acceptable value, while a cross (✗) indicates an unacceptable value. The median parameter estimate is only acceptable for the NLCO3 method, and none of the selected methods gives resistance estimates with an acceptable interdecile range.

Table 3.6: Acceptability of resistance estimates - field measurements, numerical values are given in Table A.2

	Single-phase		Three-phase	
	Median	Interdecile range	Median	Interdecile range
SM1	✗	✗	LLS3	✗
TLS1	✗	✗	NLLC3	✗
NLOE1	✗	✗	NLCO3	✓
TPLL1	✗	✗	TPLL3	✗

Figures 3.12 and 3.13 show the estimated resistance values for the selected eight methods over the 22-hour period. It can be seen that for the majority of the time, the single-phase methods give resistance values between $20\ \Omega$ and $40\ \Omega$. In contrast, resistance estimates by the three-phase methods occupy a greater range: estimates by the TPLL3 method oscillate between $40\ \Omega$ and $140\ \Omega$, while the LLS3 gives values ranging from $-20\ \Omega$ to $80\ \Omega$ and results for the NLLC3 method have a median value of $0.3\ \Omega$ and IDR of $40.6\ \Omega$. The NLCO3 method's estimates are between $10\ \Omega$ and $30\ \Omega$ and are thus closest to the theoretically calculated positive sequence resistance of $16.2\ \Omega$; furthermore, the values are lower at the beginning and end of the time period, which is consistent with predicted thermal variation.

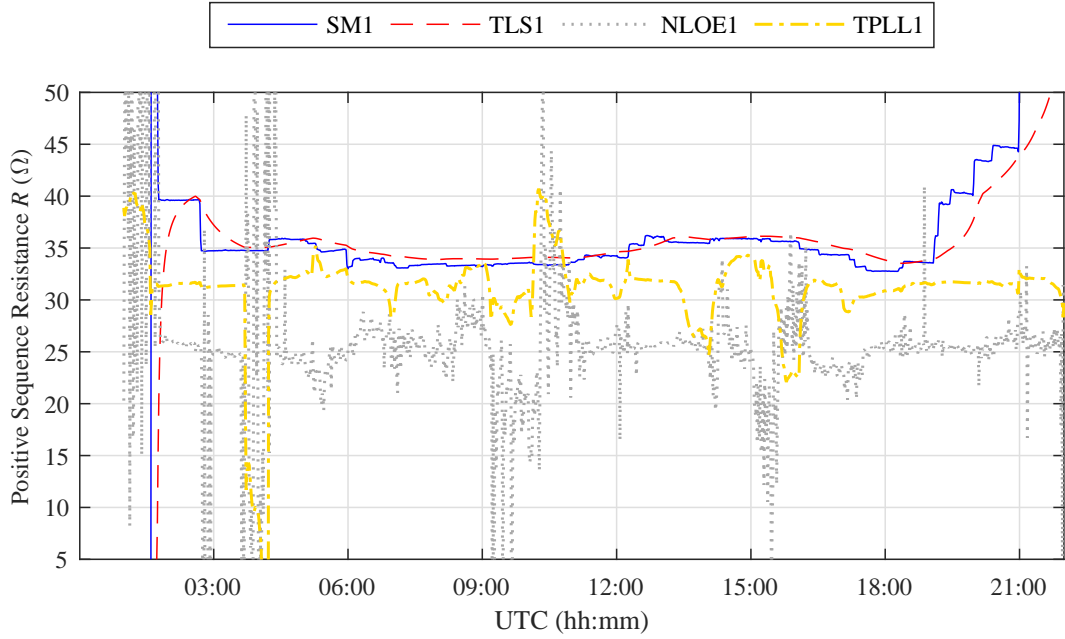


Figure 3.12: Resistance estimates from field measurements, single-phase methods

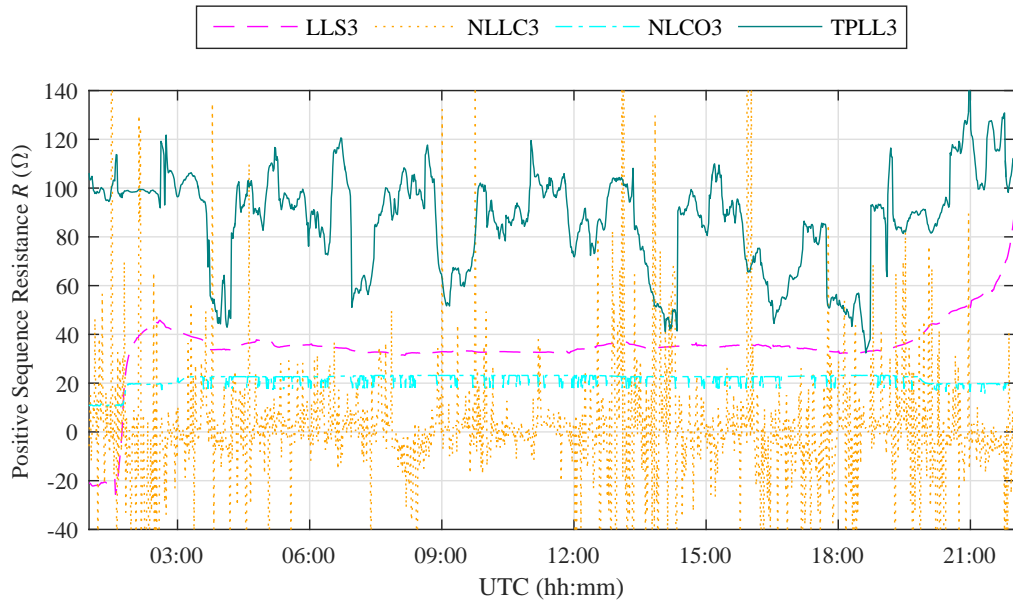


Figure 3.13: Resistance estimates from field measurements, three-phase methods

Figures 3.12 and 3.13 also show that for the SM1, TLS1 and LLS3 methods, resistance values are diverging at the beginning and end of the time period, when power flow is lowest. The other methods produce non-systematic variation over time, which is not linked to the system state. Figure 3.14 shows a scatter plot of resistance values against active power for the single-phase methods; the distribution of points for the SM1 method suggests an inverse relationship, which points to a systematic error in the phasor measurements.

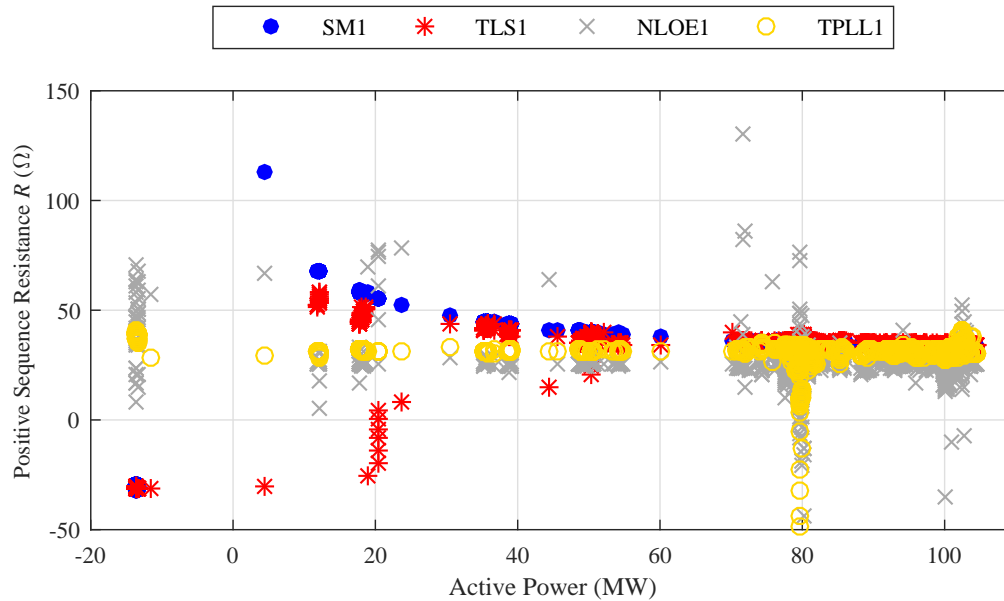


Figure 3.14: Resistance estimates from field measurements against active power, single-phase methods

Figure 3.15 shows the condition numbers of the design matrices for the TLS1, TPLL1, LLS3 and TPLL3 methods, and of the final Jacobian matrices for the NLOE1 and NLLC3 methods. The condition number gives a worst case upper bound for the sensitivity of parameter estimates to errors in the input measurements. For the three-phase methods, the condition numbers are above 10^5 , which implies that deviations in phasor measurements of 0.1% can cause parameter errors of 10^4 % and is a possible explanation for the wider range of estimated values given by the three-phase methods. The poor conditioning relative to single-phase methods is due to the fact that the three-phase methods attempt to estimate up to three times the number of unknown parameters; besides, the phase voltages are approximate and have lost their zero sequence component due to the line-to-line measurement.

The single-phase methods have condition numbers below 10^5 ; the TLS1 method has the lowest condition numbers over the time period and hence its problem formulation is better conditioned and has lower sensitivity to measurement errors in this particular case.

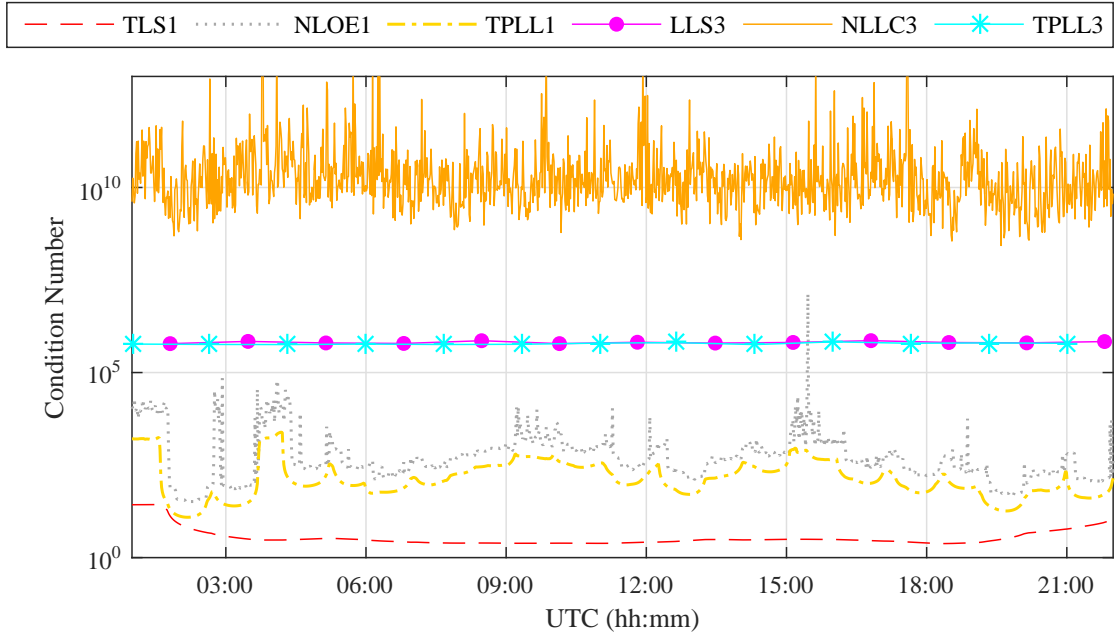


Figure 3.15: Condition number of the design matrix for linear estimation methods, and of the final Jacobian matrix for the non-linear methods

3.4.2.3 Reactance

Both the median and interdecile range of reactance estimates are acceptable for the SM1, TLS1 and LLS3 methods, while neither value is acceptable for the NLLC3 method, as Table 3.7 shows. The other non-linear estimators (NLOE1, NLLC3) and two-port methods (TPLL1, TPLL3) have acceptable median values, but their interdecile range of reactance estimates is inconsistent with the theoretical prediction.

Table 3.7: Acceptability of reactance estimates - field measurements, numerical values are given in Table A.2

	Single-phase		Three-phase		
	Median	Interdecile range	Median	Interdecile range	
SM1	✓	✓	LLS3	✓	✓
TLS1	✓	✓	NLLC3	✗	✗
NLOE1	✓	✗	NLLC3	✓	✗
TPLL1	✓	✗	TPLL3	✓	✗

Figures 3.16 and 3.17 show that for the methods with acceptable median and interdecile range (SM1, TLS1 and LLS3), the reactance estimates are between $140\ \Omega$ and $150\ \Omega$ for the majority of the 22-hour period (03:00 to 18:00). The NLOE1, TPLL1 and TPLL3 methods on the other hand, give estimates that occupy a wider range, mainly $100\ \Omega$ to $160\ \Omega$.

Results from the NLLC3 method are oscillating around zero, concentrating between $\pm 50 \Omega$, which makes them unacceptable.

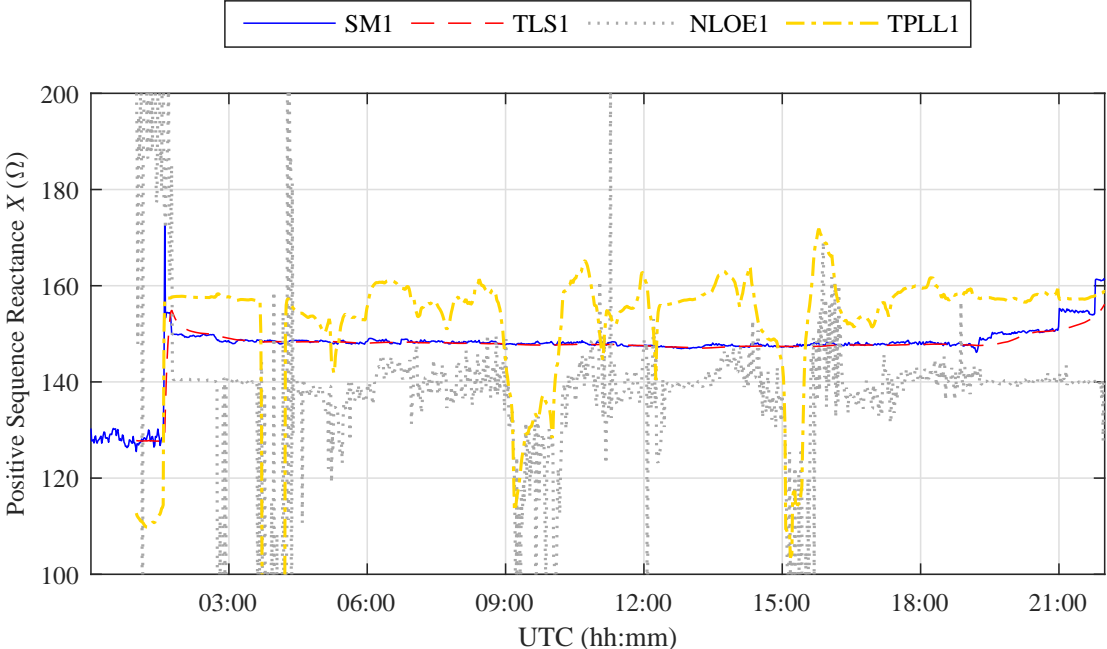


Figure 3.16: Reactance estimates from field measurements, single-phase methods

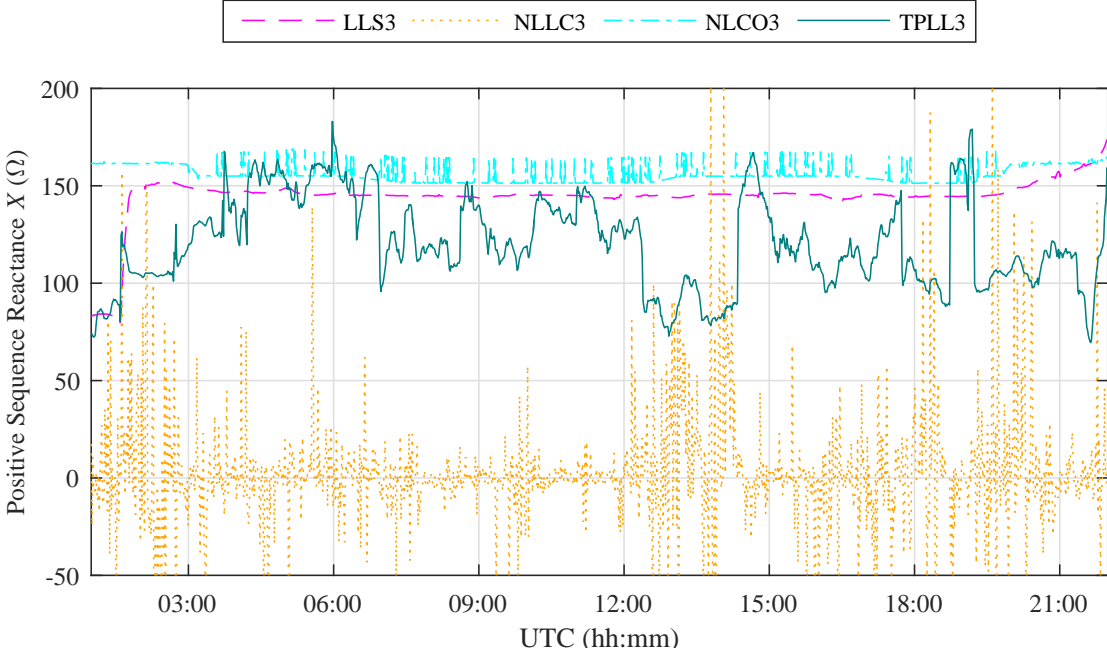


Figure 3.17: Reactance estimates from field measurements, three-phase methods

3.4.2.4 Conductance

For shunt conductance, the TLS1, LLS3 and NLCO3 methods assume a zero value and thus give acceptable values for median and interdecile range. Out of the remaining five methods, only the SM1 method gives an acceptable median as can be seen in Table 3.8.

Table 3.8: Acceptability of conductance estimates - field measurements, numerical values are given in Table A.2

	Single-phase		Three-phase	
	Median	Interdecile range	Median	Interdecile range
SM1	✓	✗	LLS3	✓
TLS1	✓	✓	NLLC3	✗
NLOE1	✗	✗	NLCO3	✓
TPLL1	✗	✗	TPLL3	✗

Figures 3.18 and 3.19 show the conductance estimates over the 22-hour period. The SM1 method gives the narrowest range of non-zero estimates, within ± 0.5 mS and negative at the start and end of the period. The NLOE1 method gives mostly negative conductance values, some of which fall below -1 mS, while the TPLL1 method has three peaks that rise above 1 mS.

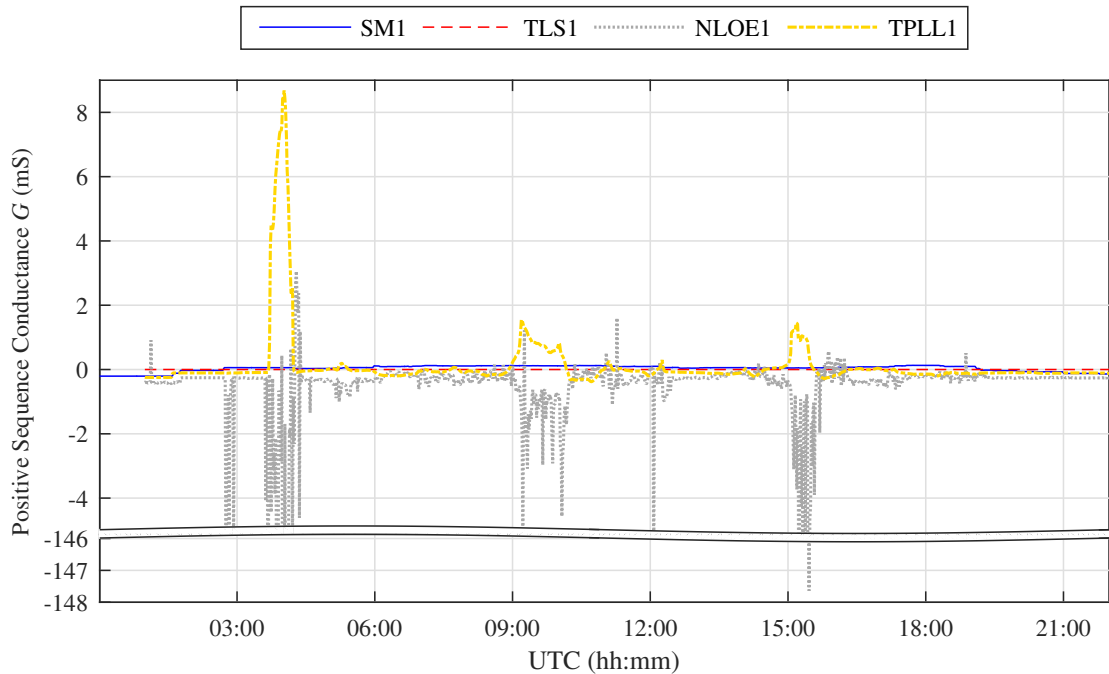


Figure 3.18: Conductance estimates from field measurements, single-phase methods

Out of the three-phase methods, the NLLC3 and TPLL3 methods give unacceptable results, including estimates outside ± 10 mS, as can be observed in Figure 3.19.

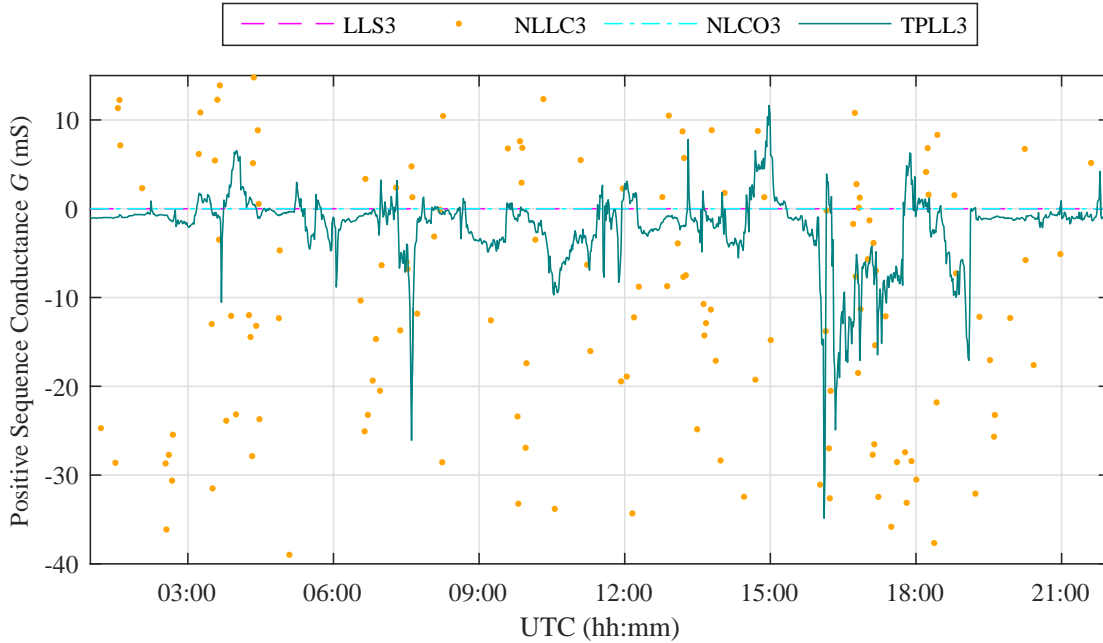


Figure 3.19: Conductance estimates from field measurements, three-phase methods

3.4.2.5 Susceptance

As for reactance, the SM1, TLS1 and LLS3 methods give acceptable values for median and interquartile range of susceptance estimates over the 22-hour period. The acceptability for all selected methods is given in Table 3.9.

Table 3.9: Acceptability of susceptance estimates - field measurements, numerical values are given in Table A.2

	Single-phase		Three-phase	
	Median	Interdecile range	Median	Interdecile range
SM1	✓	✓	LLS3	✓
TLS1	✓	✓	NLLC3	✗
NLOE1	✓	✗	NLCO3	✗
TPLL1	✓	✗	TPLL3	✗

Figure 3.20 shows the stability of susceptance estimates from the SM1 and TLS1 methods over time, with all values lying between 2 mS and 2.2 mS. The NLOE1 and TPLL1 methods give values that are mostly between 1.6 mS and 2.4 mS and hence have acceptable median values, but at approximately 04:00,

10:00 and 15:00, both methods yield extreme values, which cause the interdecile range to become unacceptable.

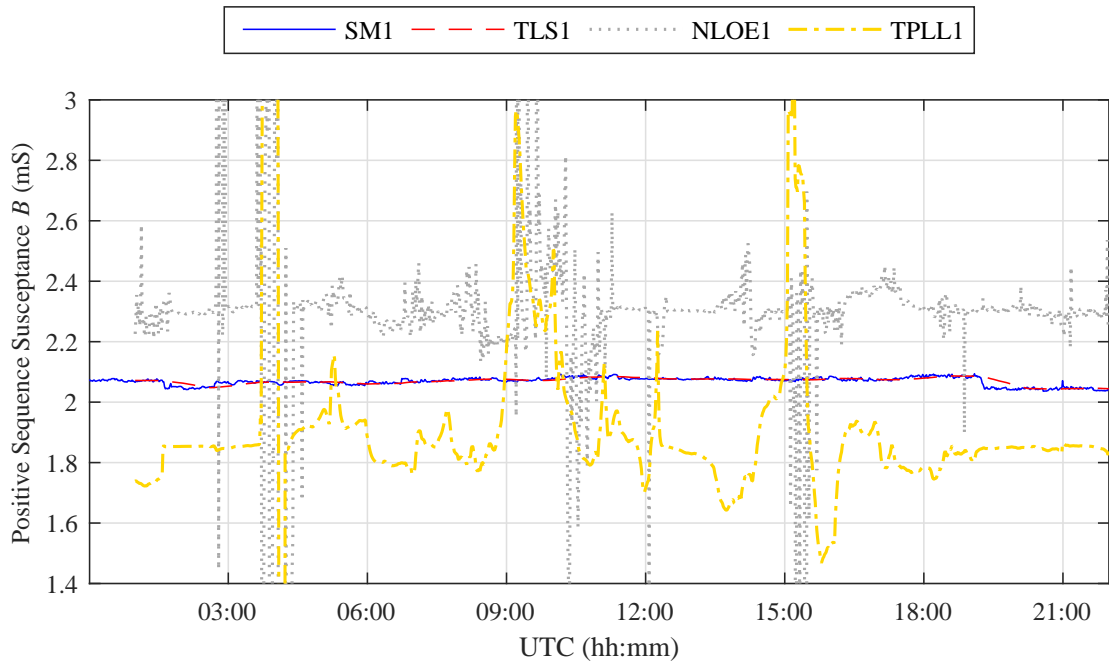


Figure 3.20: Susceptance estimates from field measurements, single-phase methods

As for conductance, the NLLC3 and TPLL3 methods give unacceptable results, including estimates outside ± 10 mS, as shown in Figure 3.21.

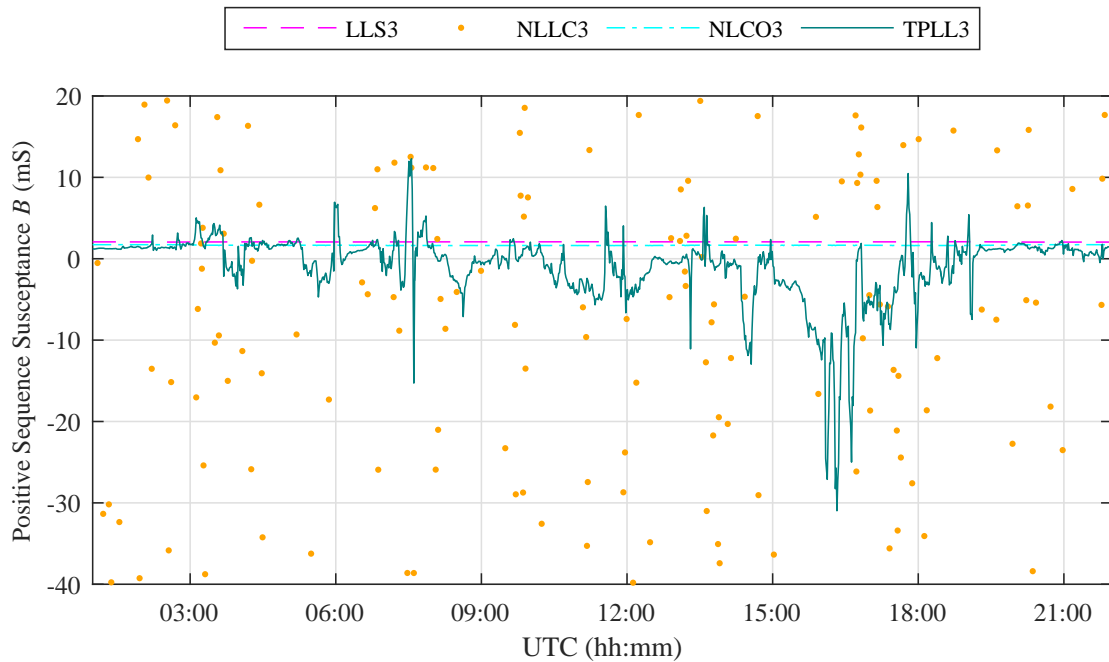


Figure 3.21: Susceptance estimates from field measurements, three-phase methods

3.4.3 Summary and discussion of results

Table 3.10 summarizes the acceptability of the parameter values estimated by the eight selected methods for the chosen 22-hour period. The resistance estimates have the lowest acceptability, while reactance and susceptance estimates agreed more closely with theoretical reference values.

Table 3.10: Acceptability of all parameter estimates - field measurements, numerical values are given in Table A.2

	Resistance		Reactance		Conductance		Susceptance		Score ³
	M ¹	IDR ²	M	IDR	M	IDR	M	IDR	
SM1	✗	✗	✓	✓	✓	✗	✓	✓	5
TLS1	✗	✗	✓	✓	✓	✓	✓	✓	6
NLOE1	✗	✗	✓	✗	✗	✗	✓	✗	2
TPLL1	✗	✗	✓	✗	✗	✗	✓	✗	2
LLS3	✗	✗	✓	✓	✓	✓	✓	✓	6
NLLC3	✗	✗	✗	✗	✗	✗	✗	✗	0
NLCO3	✓	✗	✓	✗	✓	✓	✓	✗	5
TPLL3	✗	✗	✓	✗	✗	✗	✗	✗	1

¹ Median

² Interdecile Range

³ Number of acceptable values, i.e. number of check marks in each row (maximum 8)

The Total Least-squares (TLS1) and Linear Least-squares (LLS3) methods have performed best as they have produced acceptable values for three out of four impedance parameters, whereas Non-linear Least-squares with Calibration Factors (NLLC3) is the worst method with no acceptable results. The methods assuming two-port networks (TPLL1 and TPLL3) have also scored poorly, achieving no more than two acceptable values. The Non-linear Constraint Optimization (NLCO3) method has scored highly and is the only method with an acceptable median resistance estimate. The reason is that this method uses the theoretically calculated values as starting points in the optimization algorithm, combined with upper and lower bounds of $\pm 10\%$ around these starting points. Thus the results from this method do not serve as independent, experimental validation of the theoretical predictions.

The three-phase method LLS3 achieved the same number of acceptable parameter values as a single-phase method TLS1, given that the phase voltages used in the estimation were approximated from delta measurements without zero sequence components.

The other two three-phase methods NLLC3 and TPLL3 scored particularly poorly, giving rise to the question whether whether some three-phase methods require zero sequence components.

Overall, none of the selected methods has given acceptable results for all four parameters. The results are least accurate for resistance, the parameter with the highest temperature sensitivity, which means tracking of changes in average conductor temperature is not possible with the selected methods.

In this comparative study, synchrophasor measurements from only one transmission line were utilized. The observed performance of the methods cannot be generalized to all overhead line systems as they differ in their locations, lengths, geometries, operational states and other properties. However, the results demonstrate that there is at least one type of system, for which a variety of existing methods has limitations.

In order to accurately monitor impedance parameters of lines such as that considered in this section, the mechanisms behind the failure of existing methods must be understood. Then, specific problems can be defined and put at the centre of the development of new, more effective parameter estimation algorithms. In the next section, a software simulation of the line will be used to reproduce the failures of the selected methods that were observed in the practical application to field data.

3.5 Application of methods to data from a transmission line simulation

Section 3.4 has shown that the existing methods have limitations with regards to accurately identifying transmission line impedance and admittance parameters in real-time. In order to extend and develop methods that overcome these problems, it must first be understood how the methods are failing. In this section, possible mechanisms will be investigated using a transmission line simulation, whereby line parameter values and measurement accuracy can be controlled. Details of the simulation set-up will be given as well as the results of impedance parameter estimation from simulated measurements in various scenarios.

3.5.1 Properties of the simulation

The simulation of the transmission line whose parameters were estimated in Section 3.4, was implemented using MATLAB[®] Simscape[™] Power Systems[™] software. Figure 3.22 shows a block diagram of the components: three voltage sources at each line end as network equivalents, a distributed transmission line and signal measurement blocks.

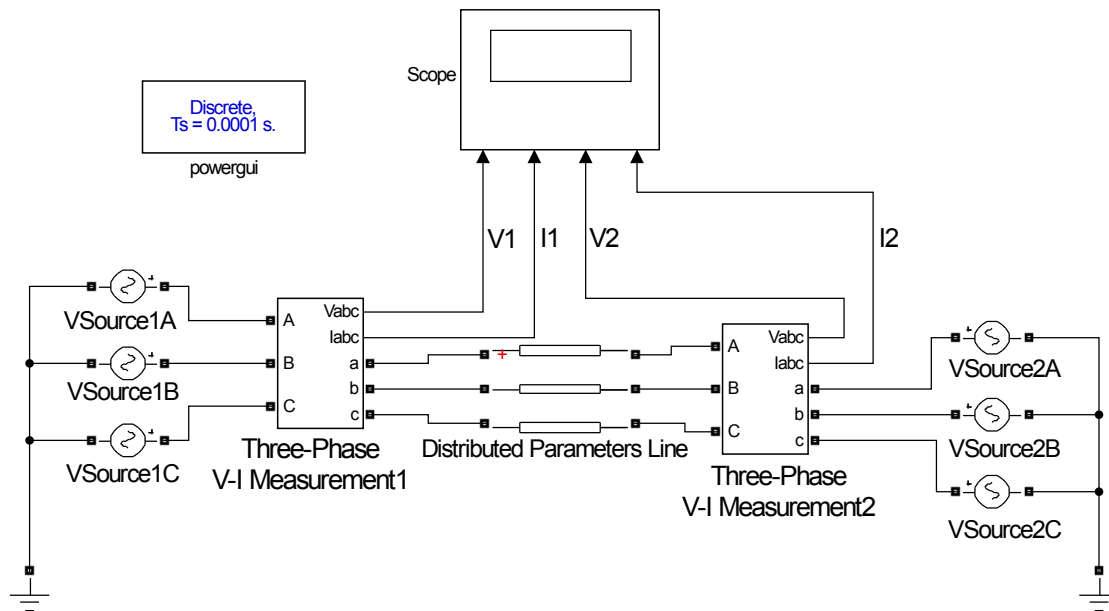


Figure 3.22: Schematic diagram of the simulation circuit

The values of measured line-to-line voltage phasors (see Figures 3.4 and 3.5) were converted to star voltages as inputs to the simulation. Specifically, 1440 60-second mean values from the chosen 24-hour period were used, such that 1440 individual states were simulated. The frequency was set to 50 Hz. The properties of the transmission line were set to the theoretically calculated values as given in Table 3.3. Measurements of line-to-ground voltage and current waveforms at the line ends were taken and a Discrete Fourier Transform was applied to calculate rms amplitude and phase angles [57]. Figure 3.23 shows the resulting positive sequence current measurements as well as field measurement values; the magnitude of the simulated values is lower compared to the field values for both sending and receiving end and the difference between the line ends is smaller.

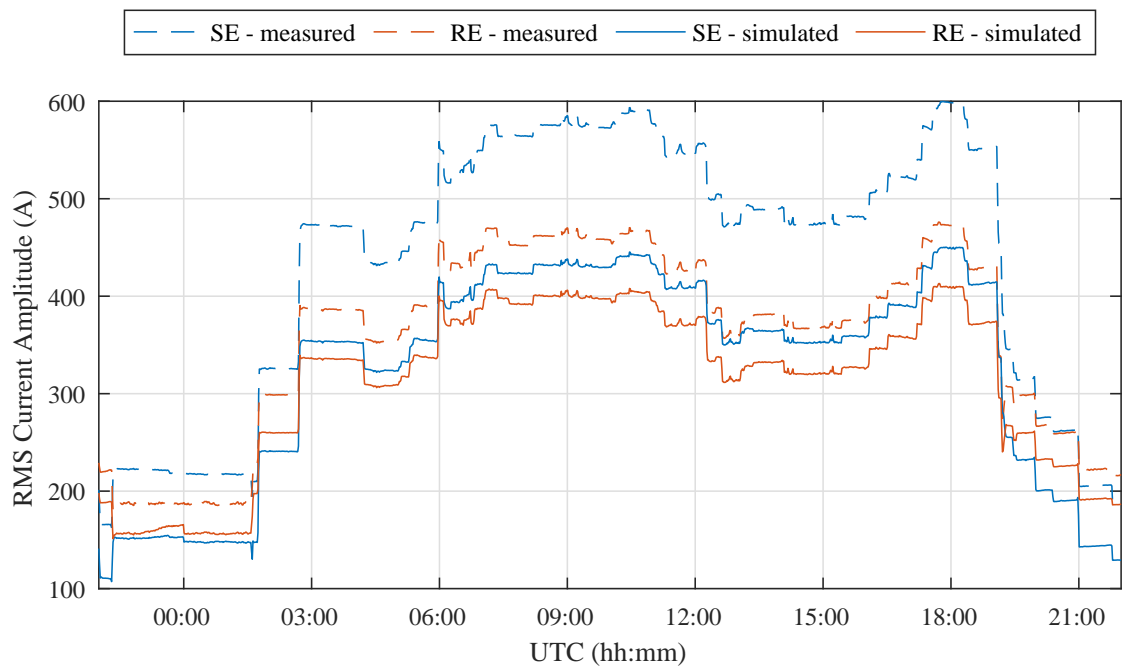


Figure 3.23: Measured and simulated current amplitude, SE refers to Sending end and RE to Receiving end

3.5.2 Simulated scenarios

Six different scenarios have been created to reproduce the failures of existing parameter estimation algorithms as demonstrated in Section 3.4. Table 3.11 describes each scenario.

Table 3.11: Description of simulated scenarios

1	Ideal Scenario Line impedance parameters are kept constant throughout. The voltage and current phasors are used directly in the parameter estimation algorithms.
2	Delta-star Scenario Line impedance parameters are kept constant throughout. Voltages are measured in delta configuration and converted to star voltages before parameter estimation, as explained in Section 3.4.1.1.
3	Variation Scenario For every simulated state, the line resistance values are updated in accordance with the calculated average conductor temperature given in Section 3.8.
4	Uncertainty Scenario Line impedance parameters are kept constant throughout. Magnitude and phase angles of voltage and current are contaminated with Gaussian noise before impedance parameter estimation.
5	Systematic Error Scenario Line impedance parameters are kept constant throughout. Constant proportional errors in magnitudes and additive errors in phase angles are added to simulated voltage phasors before parameter estimation.
6	Realistic Scenario Scenarios 2 to 5 are combined: voltage measurements are converted from delta to star, resistance is varied over time, Gaussian noise and systematic errors are added to the measurements.

In the Uncertainty Scenario, random errors from a normal distribution with standard deviations of 0.05 % in magnitude and 0.5 mrad in phase angle were added to the measurements. These standard deviations correspond to expanded uncertainties of 0.1 % and 1 mrad, respectively, with a coverage probability of 95 % and are chosen in line with the accuracy of the power quality instruments that were used in the field measurement campaign [67]. For each of the 1440 simulated states, the measurement set of voltage and current phasors was duplicated 600 times to represent measurements taken at 0.1-second intervals; random errors were added and the measurements were then averaged to return to 1440 sets.

Table 3.12 lists the systematic errors that were applied to all measurements before parameter estimation in the Systematic Error Scenario. The errors were chosen as a possible set based on previous characterization of instrumentation channels and existing accuracy classes of instrument transformers [68]. Standard

Table 3.12: Systematic errors in the Systematic Error Scenario

	V_s	V_r	I_s	I_r
Magnitude (%)	1	-2	2	3
Phase angle (mrad)	-0.01	0.03	-0.02	0.01

accuracy classes for voltage transformers range from 0.1 to 3 [133], hence, the chosen errors in the voltages are at the high end of the spectrum. Standard accuracy classes for current transformers range from 0.1 to 5 [134], which places the errors in the Systematic Error Scenario midway between best and worst case accuracies.

3.5.3 Analysis of parameter estimation results

In the following paragraphs, the acceptability of parameter estimation results from each scenario will be assessed with respect to the criteria defined in Table 3.4. Values of the Median (M) and Interdecile Range (IDR) for all parameters and scenarios are given in Appendix A.5.

3.5.3.1 Ideal Scenario

Table 3.13 lists the acceptability of the Median (M) and IDR of parameter estimates from the eight selected methods in the Ideal Scenario. Six of the methods achieve a score of eight, which means the median and IDR are acceptable for all four parameters. The remaining two three-phase methods, LLS3 and NLCO3, have unacceptable values for the IDR of the resistance. These two methods assume a constant value of zero for conductance, which causes variation in the best estimates of resistance between the different system states that occurred over the time period. This variation can be observed in Figure 3.24: the IDR is increased due to the estimated values at the beginning and end of the period, when power flow is lowest.

Table 3.13: Acceptability of estimates in the Ideal Scenario, numerical values are given in Table A.3

	Resistance		Reactance		Conductance		Susceptance		Score ¹
	M	IDR	M	IDR	M	IDR	M	IDR	
SM1	✓	✓	✓	✓	✓	✓	✓	✓	8
TLS1	✓	✓	✓	✓	✓	✓	✓	✓	8
NLOE1	✓	✓	✓	✓	✓	✓	✓	✓	8
TPLL1	✓	✓	✓	✓	✓	✓	✓	✓	8
LLS3	✓	✗	✓	✓	✓	✓	✓	✓	7
NLLC3	✓	✓	✓	✓	✓	✓	✓	✓	8
NLCO3	✓	✗	✓	✓	✓	✓	✓	✓	7
TPLL3	✓	✓	✓	✓	✓	✓	✓	✓	8

¹ Number of acceptable values, i.e. number of check marks in each row (maximum 8)

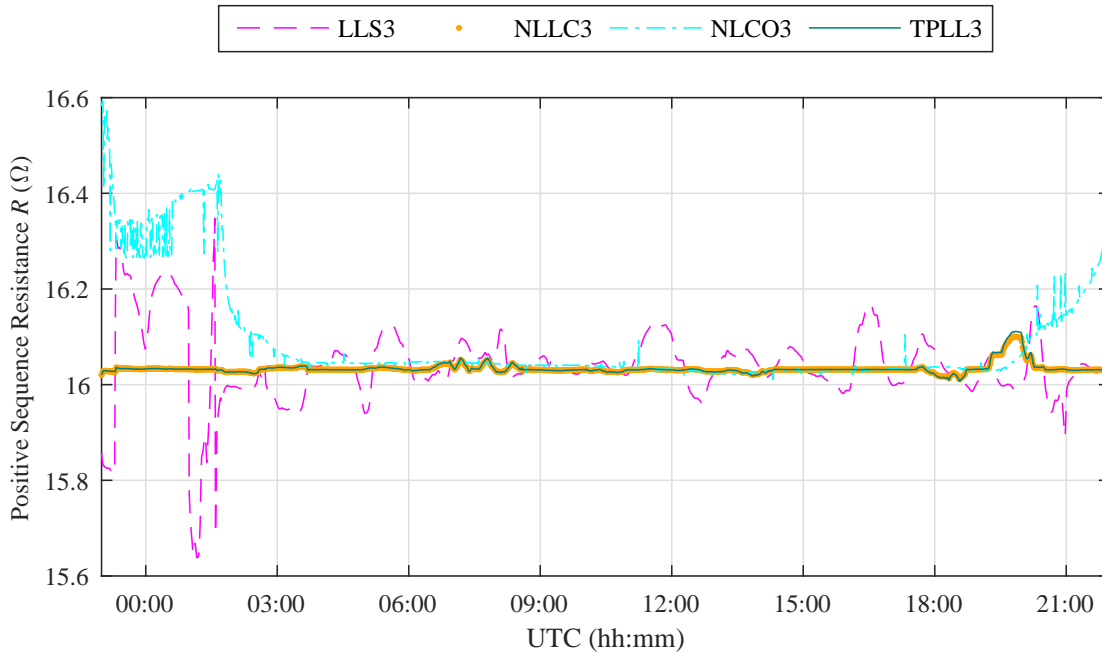


Figure 3.24: Positive sequence resistance, three-phase methods - Ideal Scenario

The results for the Ideal Scenario show that six of the selected methods estimate impedance parameters effectively given perfect measurements without zero sequence components from the line under consideration. Furthermore, it has been established that negligence of conductance can reduce the accuracy of estimated resistance to an unacceptable level. In field applications, measurements are made under non-ideal conditions. The remaining scenarios will demonstrate how these conditions can affect the acceptability of parameter values estimated by the selected methods.

3.5.3.2 Delta-star Scenario

Table 3.14 summarizes the acceptability of the parameter estimates for the eight selected methods in the Delta-star Scenario.

Table 3.14: Acceptability of estimates in the Delta-star Scenario, numerical values are given in Table A.4

	Resistance		Reactance		Conductance		Susceptance		Score ¹
	M	IDR	M	IDR	M	IDR	M	IDR	
SM1	✓	✓	✓	✓	✓	✓	✓	✓	8
TLS1	✓	✓	✓	✓	✓	✓	✓	✓	8
NLOE1	✓	✓	✓	✓	✓	✓	✓	✓	8
TPLL1	✓	✓	✓	✓	✓	✓	✓	✓	8
LLS3	✓	✗	✓	✓	✓	✓	✓	✓	7
NLLC3	✗	✗	✗	✗	✗	✗	✗	✗	0
NLCO3	✓	✗	✓	✓	✓	✓	✓	✓	7
TPLL3	✗	✓	✓	✓	✗	✓	✓	✓	6

¹ Number of acceptable values, i.e. number of check marks in each row (maximum 8)

All of the single-phase methods give fully acceptable values, which is as expected since the positive sequence is preserved through the delta-star transformation as explained in Appendix A.2. In the same manner as in the Ideal Scenario, the LLS3 and NLLC3 methods score seven because of an unacceptable IDR of resistance estimates, but are otherwise unaffected. The NLCO3 method, on the other hand, has produced no acceptable values in this scenario; the approximation of phase voltages caused by the delta-star transformation have made the method completely ineffective. The three-phase two-port network method, TPLL3, gives acceptable values for reactance and susceptance as well as for the IDR of resistance and conductance. However, the delta-star conversion of the voltage measurements causes the median of resistance and conductance to lie outside of the acceptable range.

3.5.3.3 Variation Scenario

Acceptability of parameter estimates in the Variation Scenario are shown in Table 3.15. Half of the methods (SM1, TLS1, LLS3, NLCO3) achieved the maximum score by giving acceptable values for resistance, reactance, conductance and susceptance. The NLOE1, TPLL1 and TPLL3 methods follow closely with a score of seven; all three methods have unacceptable values for the IDR of estimated resistance over the time period.

Table 3.15: Acceptability of estimates in the Variation Scenario, numerical values are given in Table A.5

	Resistance		Reactance		Conductance		Susceptance		Score ¹
	M	IDR	M	IDR	M	IDR	M	IDR	
SM1	✓	✓	✓	✓	✓	✓	✓	✓	8
TLS1	✓	✓	✓	✓	✓	✓	✓	✓	8
NLOE1	✓	✗	✓	✓	✓	✓	✓	✓	7
TPLL1	✓	✗	✓	✓	✓	✓	✓	✓	7
LIS3	✓	✓	✓	✓	✓	✓	✓	✓	8
NLLC3	✓	✗	✓	✗	✓	✗	✓	✗	4
NLCO3	✓	✓	✓	✓	✓	✓	✓	✓	8
TPLL3	✓	✗	✓	✓	✓	✓	✓	✓	7

¹ Number of acceptable values, i.e. number of check marks in each row (maximum 8)

The NLLC3 method lags behind with a score of four; only the median values are acceptable. To illustrate the extent to which the methods track changing parameter values, plots of estimated resistance over time are shown in Figures 3.25 and 3.26.

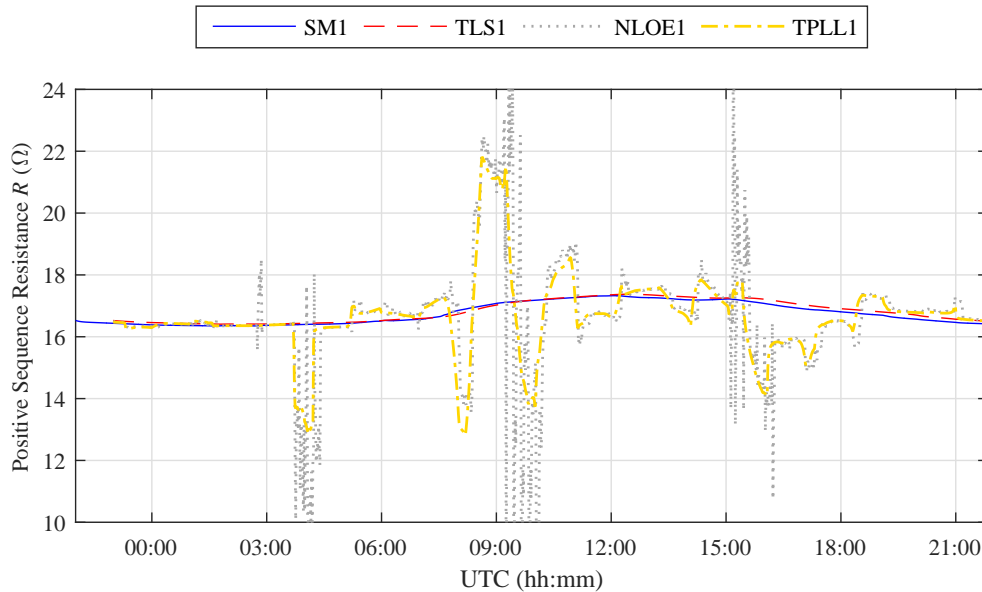


Figure 3.25: Positive sequence resistance, single-phase methods - Variation Scenario

It can be observed that the SM1, TLS1 and NLCO3 methods give estimates that form a smooth curve over time with a crest during the day when conductor temperature is increased (c.f. Figure 3.8). In contrast, the other five methods have several peaks and troughs that lie outside the nominal range of $[16.5, 17.5]$ Ω .

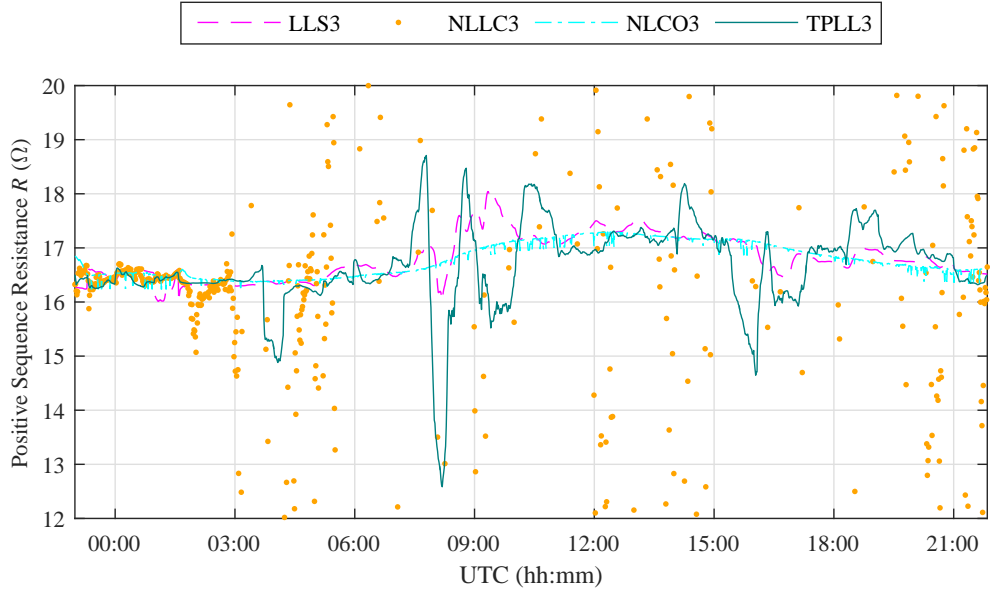


Figure 3.26: Positive sequence resistance, three-phase methods - Variation Scenario

3.5.3.4 Uncertainty Scenario

From Table 3.16 it can be seen that the SM1 and TLS1 methods are robust to the level of Gaussian noise introduced in the measurements, as the median and IDR are acceptable for all parameters.

Table 3.16: Acceptability of estimates in the Uncertainty Scenario, numerical values are given in Table A.6

	Resistance		Reactance		Conductance		Susceptance		Score ¹
	M	IDR	M	IDR	M	IDR	M	IDR	
SM1	✓	✓	✓	✓	✓	✓	✓	✓	8
TLS1	✓	✓	✓	✓	✓	✓	✓	✓	8
NLOE1	✓	✗	✓	✓	✓	✓	✓	✓	7
TPLL1	✓	✗	✓	✓	✓	✓	✓	✓	7
LLS3	✓	✗	✓	✓	✓	✓	✓	✓	7
NLLC3	✓	✗	✓	✗	✗	✗	✓	✗	3
NLCO3	✗	✗	✗	✗	✓	✓	✓	✓	4
TPLL3	✓	✗	✓	✗	✓	✗	✓	✗	4

¹ Number of acceptable values, i.e. number of check marks in each row (maximum 8)

All methods give acceptable median values of susceptance estimates in this scenario and all but the NLCO3 method give acceptable median values of resistance and reactance. The added measurement noise causes increased variation of the parameter estimates for several methods, as can be seen from the number of unacceptable values of the IDR across all four parameters.

3.5.3.5 Systematic Error Scenario

Table 3.17 shows the impact of systematic measurement errors on the acceptability of impedance and admittance parameter estimates.

Table 3.17: Acceptability of estimates in the Systematic Error Scenario, numerical values are given in Table A.7

	Resistance		Reactance		Conductance		Susceptance		Score ¹
	M ¹	IDR	M	IDR	M	IDR	M	IDR	
SM1	✗	✗	✓	✗	✓	✓	✓	✗	4
TLS1	✗	✗	✓	✗	✓	✓	✓	✗	4
NLOE1	✗	✓	✓	✓	✗	✓	✓	✓	6
TPLL1	✓	✓	✓	✓	✗	✓	✓	✓	7
LLS3	✓	✗	✓	✗	✓	✓	✓	✗	5
NLLC3	✓	✓	✓	✓	✓	✓	✓	✓	8
NLCO3	✗	✗	✓	✗	✓	✓	✓	✓	5
TPLL3	✓	✓	✓	✓	✗	✓	✓	✓	7

³ Number of acceptable values, i.e. number of check marks in each row (maximum 8)

In contrast to the other scenarios, the SM1 and TLS1 score poorly with only four acceptable values. On the other hand, the NLLC3 method gave acceptable values for median and IDR for all parameters and is thus robust to the systematic measurement errors. The two-port network methods (TPLL1 and TPLL3) follow closely with seven acceptable values. All methods give acceptable estimates of the median values of reactance and susceptance. In this scenario, the number of acceptable values is lowest for resistance.

Figure 3.27 illustrates the effect of systematic errors in the synchrophasor measurements on the resistance values estimated by the single-phase methods. The NLOE1 and TPLL1 methods both give constant estimates over time, with errors of 61 % and 20 % relative to the nominal value, respectively. The resistance values estimated by the SM1 and TLS1 methods follow a sinusoidal pattern between 06:00 and 18:00, but diverge before and after this time interval, when power flow is lowest.

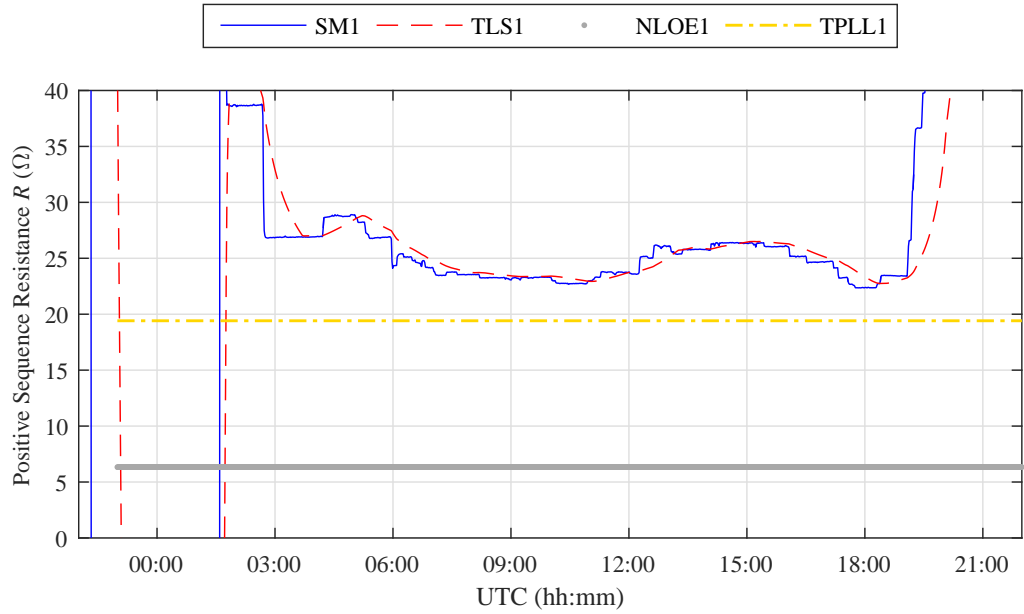


Figure 3.27: Positive sequence resistance, single-phase methods - Systematic Error Scenario

The characteristic variation of resistance values estimated by the SM1 method can be understood by considering the scatter plot in Figure 3.28, which shows an inverse relationship between the SM1 resistance values and the level of active power in the line.

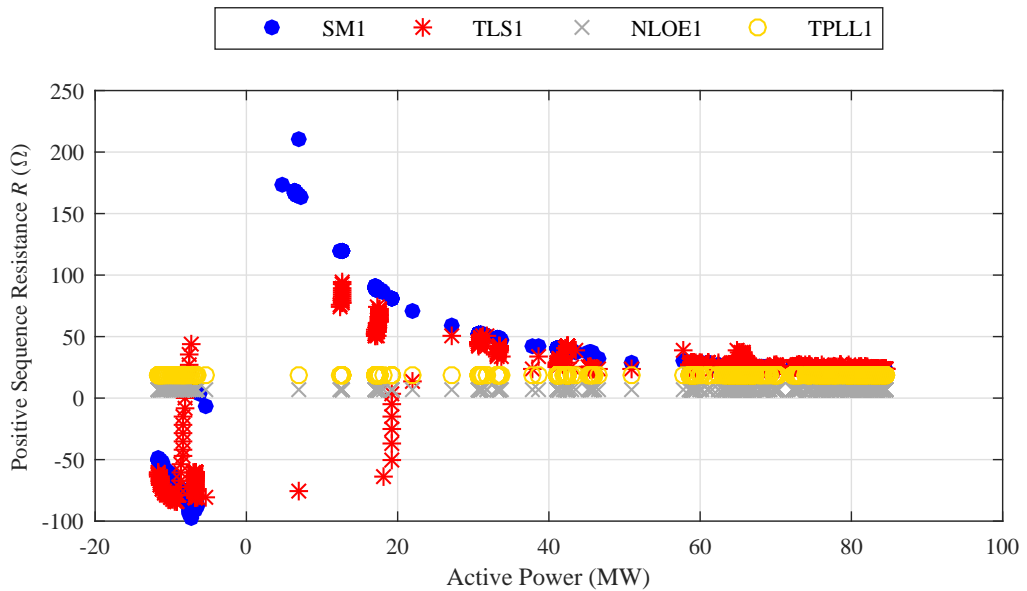


Figure 3.28: Positive sequence resistance against active power, single-phase methods - Systematic Error Scenario

The same observation was made for the resistance values estimated from field data in Section 3.4.2.2, Figure 3.14.

3.5.3.6 Realistic Scenario

In the Realistic Scenario, voltages were converted from delta to star, resistance values were varied over time according to changes in average conductor temperature, and Gaussian noise as well as systematic errors were added to the phasor measurements. The aim of this combination is to imitate the field measurement case. Table 3.18 lists the acceptability of parameter estimates in this scenario.

Table 3.18: Acceptability of estimates in the Realistic Scenario, numerical values are given in Table A.8

	Resistance		Reactance		Conductance		Susceptance		Score ¹
	M	IDR	M	IDR	M	IDR	M	IDR	
SM1	✗	✗	✓	✗	✓	✓	✓	✗	4
TLS1	✗	✗	✓	✗	✓	✓	✓	✗	4
NLOE1	✗	✗	✓	✓	✗	✓	✓	✓	5
TPLL1	✓	✗	✓	✓	✗	✓	✓	✓	6
LLS3	✓	✗	✓	✗	✓	✓	✓	✗	5
NLLC3	✗	✗	✓	✗	✗	✗	✗	✗	1
NLCO3	✓	✗	✓	✗	✓	✓	✓	✗	5
TPLL3	✗	✗	✓	✗	✗	✗	✓	✗	2

¹ Number of acceptable values, i.e. number of check marks in each row (maximum 8)

The TPLL1 method is most effective with six acceptable values, followed by the NLOE1 and LLS3 methods with a score of five. The NLLC3 and TPLL3 methods perform worst, with scores of one and two, respectively. None of the methods gives an acceptable IDR for resistance. The accuracy of estimated variation in reactance and susceptance is unacceptable for six of the methods. Yet, all methods give acceptable median values for reactance estimates.

3.5.4 Summary and discussion of results

The parameter estimation results presented in Section 3.5.3 have revealed a variety of strengths and weaknesses of the eight selected methods in estimating impedance parameters for the line under consideration. Table 3.19 lists the scores achieved by the selected methods in the six simulated scenarios. In addition, the cumulative score across the scenarios is given as well as the scores from field measurement application presented in Section 3.4.3, Table 3.10.

Table 3.19: Summary of acceptability scores

	Field measurements	Scenario						Total (out of 48) ¹
		1	2	3	4	5	6	
SM1	5	8	8	8	8	4	4	40
TLS1	6	8	8	8	8	4	4	40
NLOE1	2	8	8	7	7	6	5	41
TPLL1	2	8	8	7	7	7	6	43
LLS3	6	7	7	8	7	5	5	39
NLLC3	0	8	0	4	3	8	1	24
NLCO3	5	7	7	8	4	5	5	36
TPLL3	1	8	6	7	4	7	2	34

¹ Sum of scores for scenarios 1 to 6 in each row, the maximum score per scenario is 8, hence the maximum total score is 48

The TPLL1 and NLOE1 methods score highest in the Realistic Scenario and cumulatively across all scenarios and are thus the strongest of the eight selected methods in this comparison. However, in field measurement application, TPLL1 and NLOE1 are in joint fifth place. This difference in ranking implies that the failure of TPLL1 and NLOE1 in estimating impedance parameters with acceptable accuracy from field measurements has not been explained by the simulation study.

Nevertheless, the results from the simulation scenarios give insights into the failure of the SM1 and TLS1 methods, which are among the methods with the highest acceptability of parameter estimates from field measurements. In the simulated scenarios, these two methods have demonstrated robustness to delta-star conversion of voltage measurements, variation of line resistance and random measurement noise. But the Systematic Error and Realistic Scenarios have exposed the weaknesses of the SM1 and TLS1 methods in response to phasor measurements that have constant, systematic errors. The analysis of the resistance estimates in the Systematic Error Scenario suggests that systematic errors are the cause of the unacceptable values given by the SM1 when field measurements are used.

Hence, a specific problem can be defined: how to calculate line impedance parameters with acceptable accuracy given synchronized phasor measurements that are subject to systematic errors. The NLLC3 method is designed to tackle this problem by introducing calibration factors to the system model. Indeed, this method gives fully acceptable values in the Systematic Error Scenario, but it is not robust to other non-ideal conditions as shown by its low score of one in the Realistic Scenario.

The identified advantages and limitations of the selected methods are based on their performance for a specific data set from one transmission line and cannot be generalized for all overhead line systems. However, the occurrence of non-ideal measurement conditions is not limited to the line under consideration. Therefore, solutions to the identified specific problem can be extended to other systems.

3.6 Conclusion

The main finding of this chapter is the fact that there is at least one overhead line system, for which a variety of existing methods is not effective at real-time monitoring of impedance parameters.

An overview was given of a representative selection of eight methods that were used to obtain parameter estimates from actual synchrophasor data from a long transmission line as well as from simulated phasor measurements. Acceptability criteria were defined for the assessment of the effectiveness of the methods. Against these criteria, none of the selected methods gave fully acceptable parameter estimation results from field measurements; acceptability was particularly low for resistance estimates.

The results from six simulation scenarios that imitated ideal and non-ideal measurement conditions revealed individual strengths and weaknesses of the methods under consideration. Systematic measurement errors were identified as a specific obstacle to acceptable impedance parameter estimation accuracy. Hence, there is a practical need to develop new methodology that is robust to this type of error and able to track changes in impedance parameters in real-time. Chapter 4 will analyse in detail how systematic measurement errors propagate to the parameter estimates and propose a new method to reduce their negative impact on parameter estimation accuracy.

Chapter 4

A new method for reducing variability in impedance parameter values estimated from measurements with systematic errors

4.1 Introduction

In Chapter 3, a selection of eight existing methods was used to estimate impedance parameters from field measurements for an actual overhead line. It was found that none of these methods produced results with acceptable accuracy; for seven of the methods the median estimated value for resistance had an error greater than 50 % and for all eight methods the interdecile range of resistance values exceeded the reference value by at least 50 %. A software simulation of the overhead line showed that certain non-ideal measurement conditions cause the selected methods to give unacceptable parameter estimation results for the line under consideration. In particular, systematic errors in the phasor measurements have been identified as an obstacle to sufficient parameter estimation accuracy. Systematic errors refer to errors in magnitude and phase angle that are constant through time. The presence of such errors is a known problem and various proposals for calibration exist [70–73, 125]. To the best of the author’s knowledge, the existing approaches assume *a priori* knowledge of line impedance parameter values. Often, these values are only based on theoretical calculations instead of system measurements. Therefore the problem of measurement calibration and impedance parameter estimation should

be tackled jointly. The Non-linear Least-squares with Calibration Factors (NLLC3) method attempts to find an optimal solution to this combined problem [125], and in Section 3.5, the method proved to be effective with simulated phasor measurements that were contaminated with systematic errors. However, the NLLC3 method gave unacceptable parameter estimation results under other simulated non-ideal measurement conditions: when voltage measurements were converted from delta to star, when resistance was changing over time and when the measurements were contaminated with Gaussian noise. For this reason, there is a need to develop methods by which overhead line impedance parameters can be estimated with acceptable accuracy, in real-time and under non-ideal measurement conditions.

In this chapter, an innovative method for identifying both impedance parameters and calibration constants will be presented. Initially, single-phase short transmission lines are considered due to the simplicity of the circuit model. A modified impedance parameter estimation problem that includes calibration constants will be introduced in the next section; thereafter, the new method will be explained, followed by a case study on measurements from a laboratory-based line model. The novel method is then extended to medium-length lines and its effectiveness is demonstrated in a second case study that involves software simulation of 10^5 different cases of systematic errors.

4.2 A new method for accurate impedance parameter estimation from synchrophasor measurements with systematic errors

In this chapter, impedance parameter estimation is restricted to single-phase transmission lines as the model is simpler with fewer equations and unknowns than the general three-phase model (see Section 3.2). However, the proposed method will also be applicable to obtain positive sequence impedance parameters of transposed three-phase lines.

4.2.1 A modified parameter estimation problem for short lines

Firstly, the short line model is modified to include systematic measurement errors; Figure 4.1 shows the relevant circuit diagram [135].

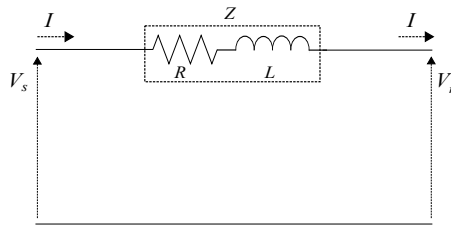


Figure 4.1: Diagram of a circuit for a short transmission line

For lines shorter than 80 km, the capacitive leakage current is negligible; therefore the line is assumed to have no shunt admittance and the current to be uniform along its length [136]. Series impedance $Z \in \mathbb{C}$ is to be estimated from synchronized phasor measurements of sending and receiving end voltages $V_s, V_r \in \mathbb{C}$ and current $I \in \mathbb{C}$. The circuit equation is

$$V_s - V_r = ZI, \quad (4.1)$$

where $Z = R + jX$. $R \in \mathbb{R}_{\geq 0}$ and $X \in \mathbb{R}_{\geq 0}$ are the series resistance and reactance, respectively, with $X = 2\pi fL$, where $f \in \mathbb{R}_{\geq 0}$ is the frequency and $L \in \mathbb{R}_{\geq 0}$ is the inductance. Z is calculated using

$$Z = \frac{V_s - V_r}{I}. \quad (4.2)$$

This model equation needs to be adapted to reflect systematic errors in the phasor measurements.

The adaptation consists of multiplicative and additive constants that model deviations in the magnitude and phase angle of voltage and current [70–73, 125]. Define $\tilde{V}_s, \tilde{V}_r, \tilde{I} \in \mathbb{C}$ as synchronized phasor measurements that have systematic errors $-a_s, -a_r, -b \in \mathbb{R}$ in magnitude and $-\phi_s, -\phi_r, -\theta \in [-\pi, \pi]$ in phase angle, respectively. Then the corrected phasors are given by

$$V_s = (1 + a_s)\tilde{V}_s \exp(j\phi_s) \quad (4.3)$$

$$V_r = (1 + a_r)\tilde{V}_r \exp(j\phi_r) \quad (4.4)$$

$$I = (1 + b)\tilde{I} \exp(j\theta). \quad (4.5)$$

Figure 4.2 shows a schematic diagram of V_s and \tilde{V}_s in the complex plane. It can be observed that the error $-\phi_s$ in phase angle causes a rotation, while $-a_s$ scales the magnitude of V_s . Equivalent diagrams of V_r, \tilde{V}_r and I, \tilde{I} can be drawn.

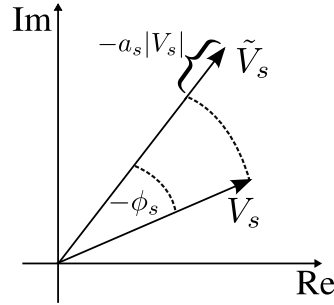


Figure 4.2: Phasor diagram of sending end voltage, rotation and scaling due to systematic errors are shown

The model equation (4.2) is modified to include systematic errors by substituting V_s, V_r and I with expressions (4.3) to (4.5):

$$Z = \frac{(1 + a_s)\tilde{V}_s \exp(j\phi_s) - (1 + a_r)\tilde{V}_r \exp(j\phi_r)}{(1 + b)\tilde{I} \exp(j\theta)}. \quad (4.6)$$

The new parameter estimation problem is as follows: given measurements $\tilde{V}_s, \tilde{V}_r, \tilde{I}$, determine values for $a_s, \phi_s, a_r, \phi_r, b, \theta$ such that Z can be calculated. Next, this problem is analysed by considering the effect of errors $-a_s, -\phi_s, -a_r, -\phi_r, -b, -\theta$ on calculated impedance Z .

4.2.2 Propagation of systematic measurement errors

The propagation of the systematic errors to impedance Z is considered before the new method is explained. Define $\Delta Z \in \mathbb{C}$ as the error in impedance due to $a_s, \phi_s, a_r, \phi_r, b, \theta$:

$$\Delta Z = \frac{\tilde{V}_s - \tilde{V}_r}{\tilde{I}} - \frac{V_s - V_r}{I} \quad (4.7)$$

$$= \frac{1}{I} \left(\frac{V_s(1+b)}{1+a_s} \exp(j(\theta - \phi_s)) - \frac{V_r(1+b)}{1+a_r} \exp(j(\theta - \phi_r)) - V_s + V_r \right). \quad (4.8)$$

To simplify this expression, the following first order approximations are made:

$$(1 + a_{s,r})^{-1} \approx 1 - a_{s,r} \quad (4.9)$$

$$\exp(-j\phi_{s,r}) \approx 1 - j\phi_{s,r} \quad (4.10)$$

$$\exp(j\theta) \approx 1 + j\theta, \quad (4.11)$$

since $a_{s,r}, \phi_{s,r}, \theta \ll 1$. Then

$$\Delta Z \approx \frac{1}{I} [(1+b)(1+j\theta) [(1-a_s)(1-j\phi_s)V_s - (1-a_r)(1-j\phi_r)V_r] - V_s + V_r] \quad (4.12)$$

$$= \frac{1}{I} [(1+b+j\theta+jb\theta) [(1-a_s-j\phi_s+ja_s\phi_s)V_s - (1-a_r-j\phi_r+ja_r\phi_r)V_r] - V_s + V_r] \quad (4.13)$$

$$\approx \frac{(b+j\theta-a_s-j\phi_s)V_s - (b+j\theta-a_r-j\phi_r)V_r}{I} \quad (4.14)$$

$$= (b+j\theta)Z + \frac{(a_r+j\phi_r)V_r - (a_s+j\phi_s)V_s}{I}, \quad (4.15)$$

where the terms in $ja_s\phi_s, ja_r\phi_r, jb\theta, ba_s, ba_r, jb\phi_s, jb\phi_r, ja_s\theta, ja_r\theta, \theta\phi_s, \theta\phi_r$ have been ignored to obtain (4.14). Let

$$\Delta Z_1 = (b+j\theta)Z, \quad \Delta Z_2 = \frac{(a_r+j\phi_r)V_r - (a_s+j\phi_s)V_s}{I}. \quad (4.16)$$

The following observations are made:

1. ΔZ_1 gives the error in Z caused by errors $-b, -\theta$ in current I . The term is a constant proportion of the impedance value that is independent of the system state V_s, V_r, I . The correct value of impedance Z acts as the sensitivity coefficient.
2. ΔZ_2 gives the error in Z caused by errors $-a_{s,r}, -\phi_{s,r}$ in voltages V_s, V_r . The response of ΔZ to different system states V_s, V_r, I depends on the values of

$a_{s,r}, \phi_{s,r}$. If, for instance, $a_s + j\phi_s = a_r + j\phi_r$,

$$\Delta Z = (b + j\theta)Z + (a_r + j\phi_r)\frac{V_r - V_s}{I} = (b + j\theta - a_r - j\phi_r)Z. \quad (4.17)$$

In this case, ΔZ is a fixed proportion of Z , regardless of the measured system state. On the other hand, if $a_s + j\phi_s = -(a_r + j\phi_r)$, i.e. the errors in the sending and receiving end voltages are equal and opposite,

$$\Delta Z = (b + j\theta)Z + (a_s + j\phi_s)\frac{V_r + V_s}{I}. \quad (4.18)$$

In this case, the second term in the expression for ΔZ is proportional to $V_s + V_r$ and inversely proportional to the current I . Hence, the sensitivity of ΔZ to the system state V_s, V_r, I depends on the 'net error' $\varepsilon_{net} = a_s + j\phi_s - (a_r + j\phi_r) = a_s - a_r + j(\phi_s - \phi_r)$.

The second observation implies that if $\varepsilon_{net} \neq 0$, the errors in calculated series impedance Z vary over time in response to changes in line loading. This increased variability in estimated impedance parameter values due to systematic measurement errors will be exploited by the new method.

4.2.3 Explanation of the new method for short lines

The new method identifies correction factors for the synchrophasor measurements by minimizing the variability of calculated impedance parameters over time. To simplify the problem initially, a correction factor is only included for the receiving end voltage. The problem is formally stated as follows:

Given $n \in \mathbb{N}$ sets of phasor measurements $\tilde{V}_{s_i}, \tilde{V}_{r_i}, \tilde{I}_i$, each taken at time instants $t_i \in \mathbb{R}_{\geq 0}, i = 1, 2, 3, \dots, n$ over the time period $t_n - t_1$, identify optimal values of correction constants a, ϕ such that impedance Z_i can be calculated accurately.

$\tilde{V}_{s_i}, \tilde{V}_{r_i}, \tilde{I}_i, a, \phi$ are related by

$$Z_i = \frac{\tilde{V}_{s_i} - (1 + a)\tilde{V}_{r_i} \exp(j\phi)}{\tilde{I}_i}, \quad (4.19)$$

where resistance is given by $R_i = \text{Re}(Z_i)$ and reactance by $X_i = \text{Im}(Z_i)$.

Note that for a given set of measurements, the resistance and reactance can be defined as functions of the correction factors, $R_i, X_i : \mathbb{R}^2 \rightarrow \mathbb{R}$. a and ϕ will be found by making the variation of $R_i(a, \phi), X_i(a, \phi)$ with respect to t_i consistent with physical expectations.

To quantify increased variation in the calculated parameter values, assumptions are made about the actual behaviour of line resistance and reactance over time. Since the resistance can vary significantly with conductor temperature, it is assumed to change linearly between t_1 and t_n [43]. Reactance is assumed to be constant as it has very low temperature sensitivity (see Appendix A.1). Based on these assumptions, the measure of variation is the sum of the residuals between R_i and a fitted linear model and between X_i and a constant value. Hence, define two model functions $f_R, f_X : \mathbb{R}_{\geq 0} \rightarrow \mathbb{R}$,

$$f_R(t_i) = q_r t_i + r_R \quad (4.20)$$

$$f_X(t_i) = r_X, \quad (4.21)$$

where $q_r, r_R, r_X \in \mathbb{R}$ are constants. Values for q_r, r_R are obtained by linear least-squares estimation from calculated values R_i . Define matrices $\mathbf{R} \in \mathbb{R}^n, \mathbf{H} \in \mathbb{R}^{n \times 2}, \mathbf{Q} \in \mathbb{R}^2$, where

$$\mathbf{R} = [R_1 \dots R_n]^T, \mathbf{H} = \begin{bmatrix} t_1 & \dots & t_n \\ 1 & 1 & 1 \end{bmatrix}^T, \mathbf{Q} = [q_r \ r_r]^T.$$

Based on (4.20), define the n -dimensional model

$$\mathbf{R} = \mathbf{H}\mathbf{Q} + \boldsymbol{\varepsilon}, \quad (4.22)$$

where $\boldsymbol{\varepsilon} \in \mathbb{R}^n, \boldsymbol{\varepsilon} = [\varepsilon_1 \dots \varepsilon_n]^T$ are error terms. The least-squares estimate of \mathbf{Q} is computed using

$$\hat{\mathbf{Q}} = (\mathbf{H}^T \mathbf{H})^{-1} \mathbf{H}^T \mathbf{R}. \quad (4.23)$$

Constant r_X is calculated as the mean value of X_i :

$$r_X = \frac{1}{n} \sum_{i=1}^n X_i. \quad (4.24)$$

The sums of the squared residuals $S_R, S_X \in \mathbb{R}_{\geq 0}$ between the calculated parameter values R_i, X_i and fitted linear functions f_R, f_X are given by

$$S_R = \sum_{i=1}^n (R_i(a, \phi) - f_R(t_i))^2 \quad (4.25)$$

$$S_X = \sum_{i=1}^n (X_i(a, \phi) - f_X(t_i))^2. \quad (4.26)$$

Now an optimization problem can be formulated:

$$\begin{aligned} & \underset{a, \phi}{\text{minimize}} && g(a, \phi) = S_R + S_X \\ & \text{subject to} && |a| < l_a, |\phi| < l_\phi, \end{aligned} \tag{4.27}$$

where $l_a, l_\phi \in (0, 1)$ are bounding values that are chosen as the maximum expected systematic error values. Equation (4.27) is a non-linear, constrained optimization problem. The objective function $g : \mathbb{R}^2 \rightarrow \mathbb{R}_{\geq 0}$ is convex since it is the sum of independent variables $S_R, S_X \in \mathbb{R}_{\geq 0}$; therefore, any local minimum of $g(a, \phi)$ is a global minimum. Various algorithms are available that can efficiently identify local minima for non-linear, constrained optimization problems. In this instance, the interior-point method is used [137]. Figure 4.3 shows a schematic diagram that illustrates the optimization process of the new method.

The identified correction constants a, ϕ are used to calculate impedance Z_i from measurements $V_{s_i}, \tilde{V}_{r_i}, I_i$ at time t_i using (4.19). As only the most recent set of measurements is used, parameters are calculated in real-time such that changes can be monitored.

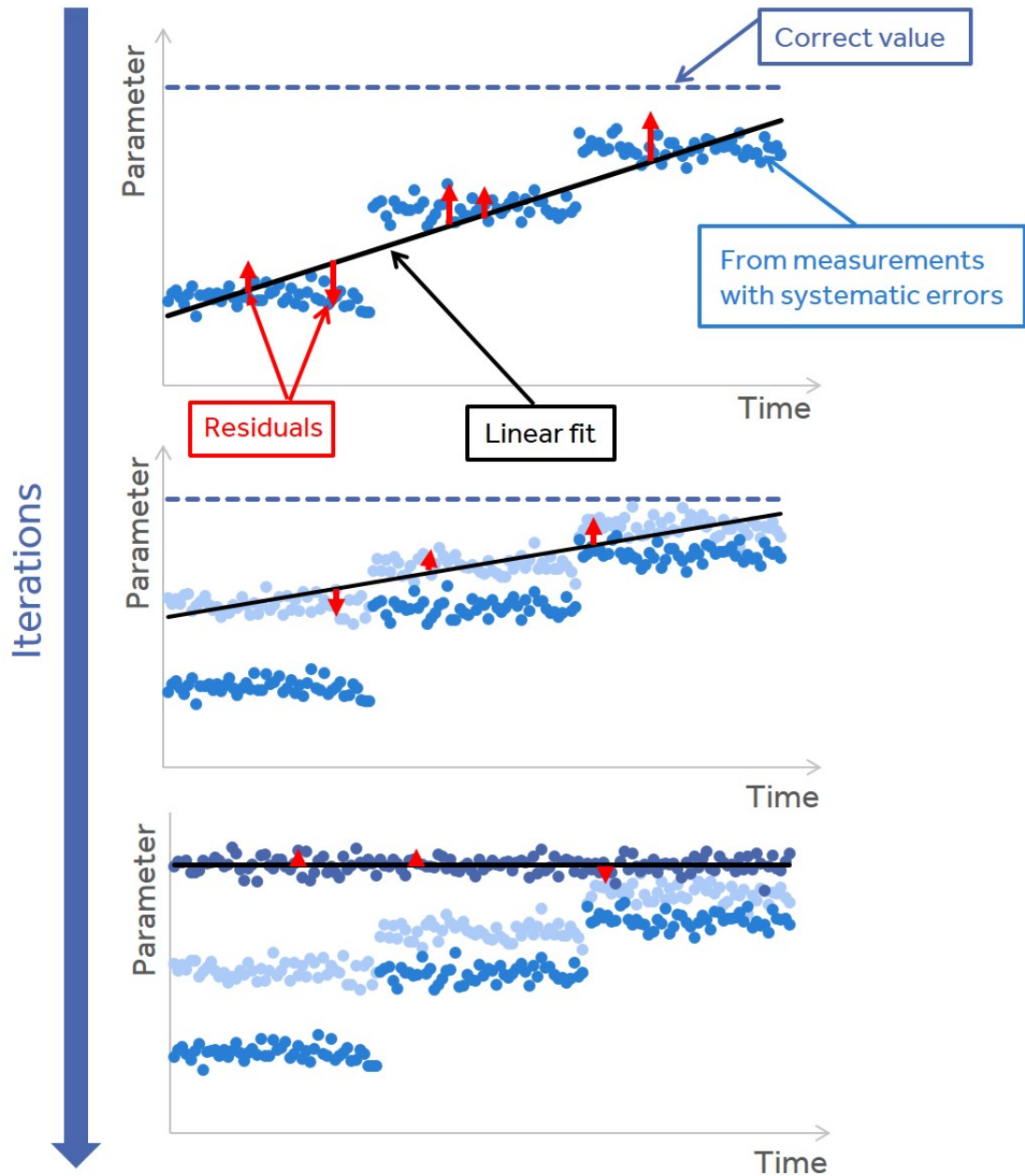


Figure 4.3: Schematic diagram illustrating the steps of the new method. Initially, the calculated parameter values have step changes over time due to systematic measurement errors. A linear function of time is fitted and the residuals are calculated. Over the iterations of the optimization process, correction factors are identified such that the residuals are reduced. At the end of the optimization process, residuals are minimized and calculated parameter values follow a constant time model.

4.3 Case study 1: short transmission lines

The novel method that was presented in the previous section was implemented to estimate the series impedance of a laboratory-based, single-phase, short transmission line model from synchronized phasor measurements. Firstly, a description of the set-up and operation of the physical overhead line model is given, thereafter the results are presented and discussed.

4.3.1 Experimental set-up and operation

4.3.1.1 Overhead line equivalent circuit

The laboratory-based overhead line model consisted of an equivalent short line circuit. Figure 4.4 shows a schematic diagram of the arrangement.

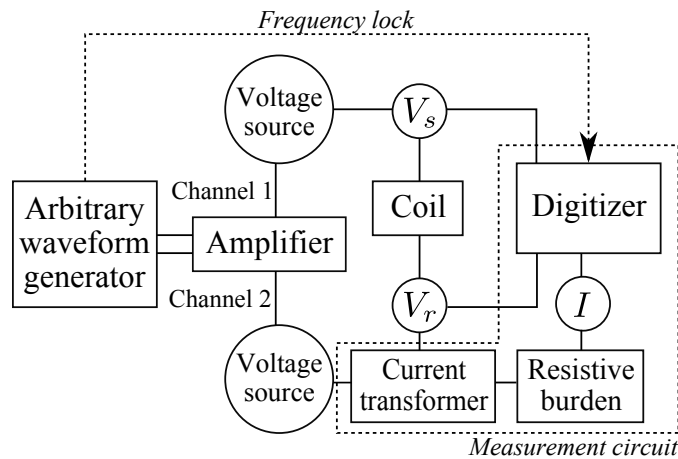


Figure 4.4: Schematic diagram showing the set-up of the overhead line model and measurement circuit

Two Alternating Current (AC) voltage sources were used to model the network at either end of the line. The voltage signals were produced with a fixed phase relationship at a frequency of 50 Hz by two channels of a multi-channel arbitrary waveform generator and then amplified to the required magnitude (using two channels of a three-phase amplifier). The lumped impedance was provided by an inductor coil with internal resistance.

4.3.1.2 Measurement circuit

A calibrated digitizer instrument was used to synchronously sample voltage and current [138]. The inductor coil was fitted with voltage outputs, which were connected directly to the two 230 V input channels of the instrument.

The current was stepped down by a calibrated current transformer connected in series with the inductor. The secondary circuit consisted of a calibrated, resistive burden (nominal value of $10\ \Omega$); the voltage across the burden was fed into the instrument's 1 V channel. The sampling frequency of 20.48 kHz was locked to the nominal power system frequency of 50 Hz, which was generated by the arbitrary waveform generator. Voltage and current phasors were estimated using a DFT from signal samples at 0.1 s intervals. This window length was chosen as it is the minimum period to match an integer number of samples (2048) at 20.48 kHz with an integer number of sinusoidal cycles (five) at a signal frequency of 50 Hz, thereby increasing the accuracy of estimated phasors.

4.3.1.3 Operating conditions

Each automated test was configured to last 15 minutes (900 s), during which the current was varied to produce a range of line loading conditions. The current was controlled by varying the amplitude of the two voltage sources to produce a potential difference as shown in Figure 4.5; the resulting current magnitude was in the interval $[0,3]$ A as shown in Figure 4.6. The direction of power flow was reversed three times during the test, which can be seen in Figure 4.7, where the active power value changes sign at times 280 s, 550 s and 830 s.

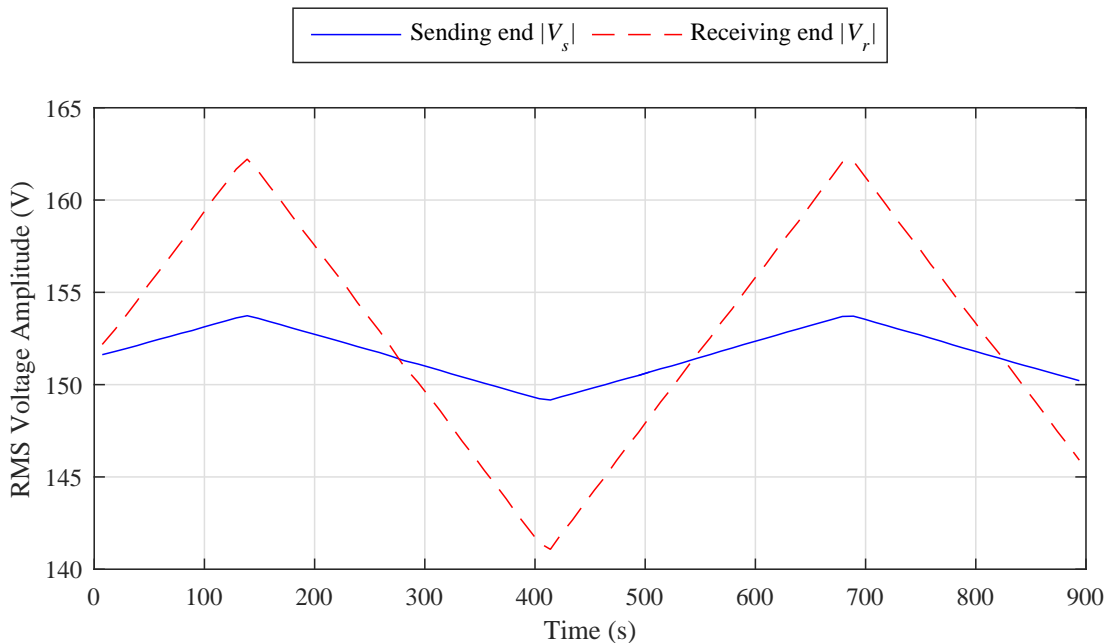


Figure 4.5: Amplitude of the voltages at each line end over the test period

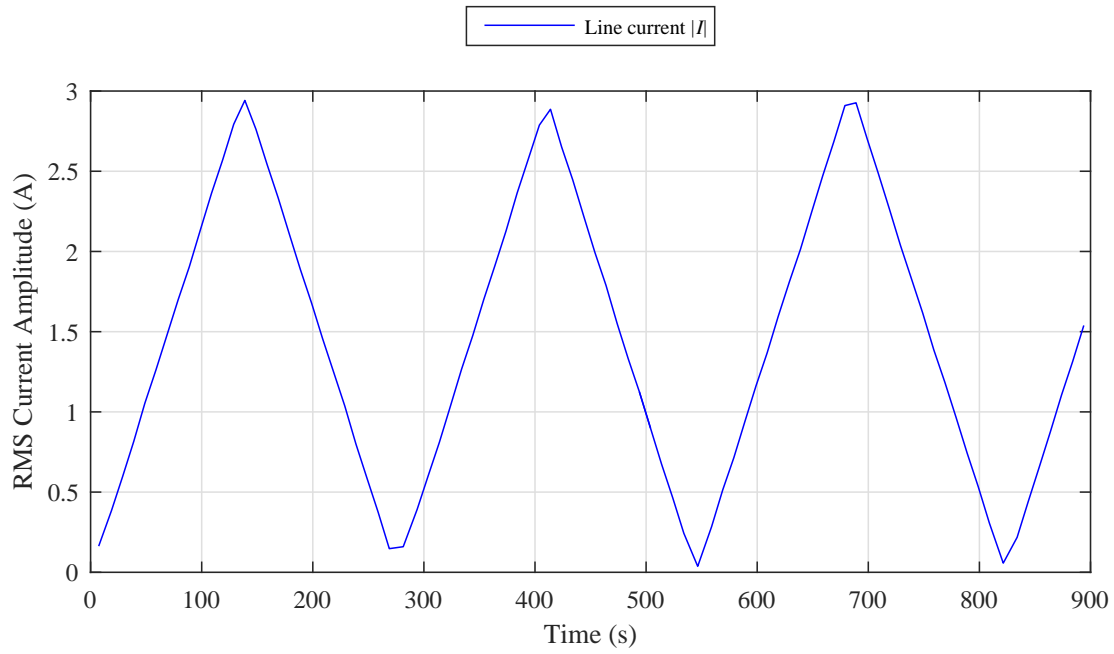


Figure 4.6: Amplitude of the line current over the test period

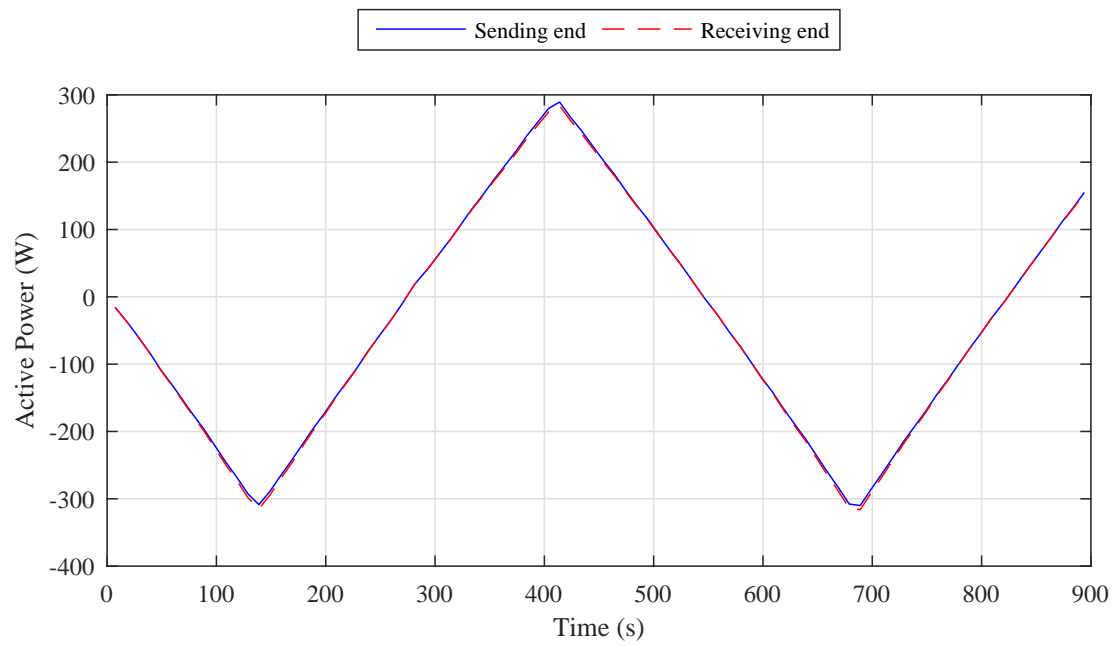


Figure 4.7: Active power at each line end over the test period, values are overlapping

4.3.2 Analysis of parameter estimation results

An impedance estimate was calculated from each set of voltage and current phasors V_{s_i}, V_{r_i}, I_i . The impedance values were further averaged over 10 s intervals. A longer interval can be chosen to achieve greater reduction in random measurement uncertainty; however, the resolution of observed changes in impedance decreases at the same time. The appropriate interval length must be selected in line with the thermal time constant of the system and specific application requirements.

4.3.2.1 Reference values of impedance

Initially, phasor measurements V_{s_i}, V_{r_i}, I_i were utilized to determine reference values for the impedance parameters R and X using (4.2); the results are shown in Figures 4.8 and 4.10. The shaded area shows the expanded uncertainties, which have a coverage probability of 95%. The uncertainties were estimated in accordance with the Guide to the Expression of Uncertainty in Measurements [139], details are referred to Appendix B.1.

It can be observed in Figure 4.8 that there is a 0.3% increase in resistance over the test period, of approximately $2 \text{ m}\Omega$, which is attributed to Joule heating of the copper coil. Given that the resistance-temperature coefficient for copper is $0.004 \text{ }^\circ\text{C}^{-1}$, the change in resistance corresponds to an increase in the coil temperature of $0.7 \text{ }^\circ\text{C}$, according to the linear resistance-temperature relationship (2.32). Figure 4.9 shows the average measured surface temperature of the coil, indicating an increase of approximately $0.6 \text{ }^\circ\text{C}$. There is a lack of reliability in this measurement because of the uncertainty of $\pm 0.16 \text{ }^\circ\text{C}$ of the temperature sensors (27% of the measured change); nevertheless the change in coil temperature is tracked to within $0.1 \text{ }^\circ\text{C}$ by the calculated resistance.

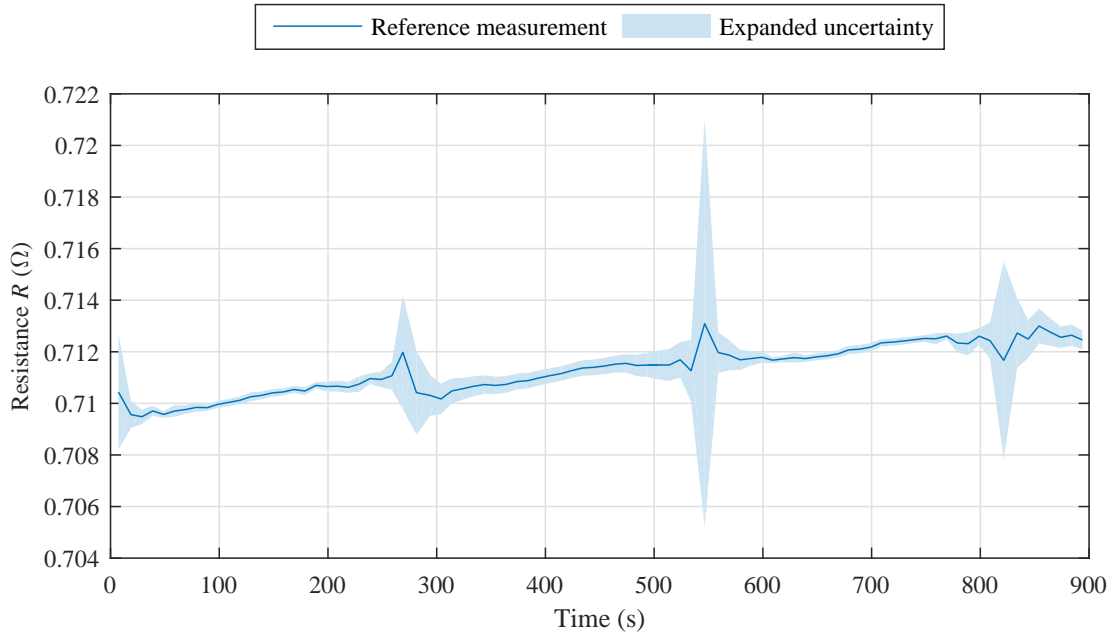


Figure 4.8: Measured reference resistance values

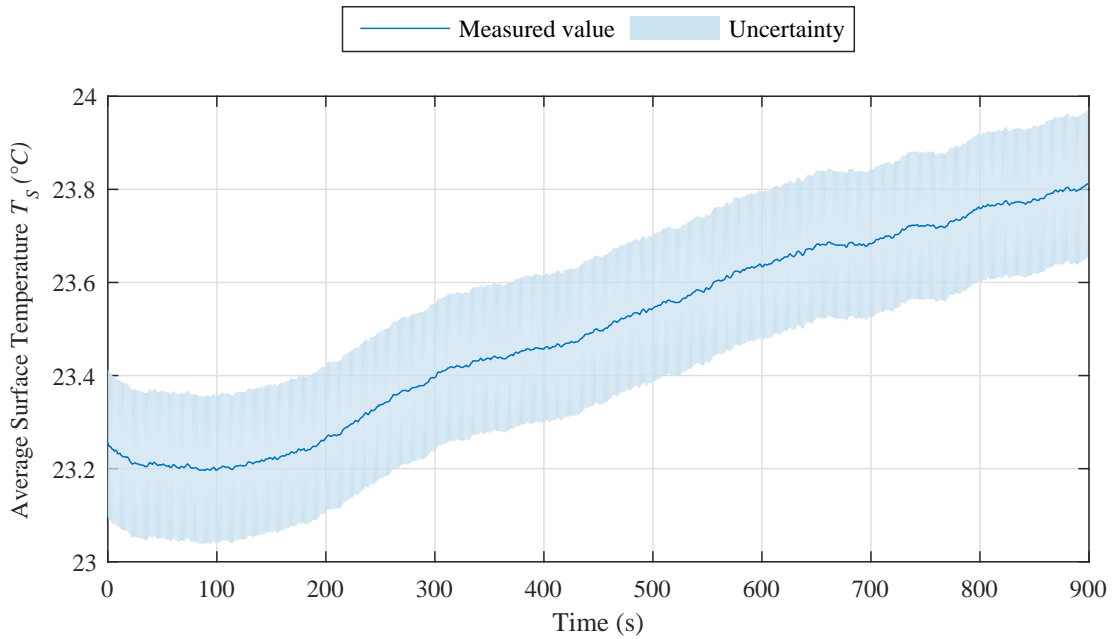


Figure 4.9: Average surface temperature of copper coil over the test period

As there is no significant change in the geometry such as thermal expansion of the copper coil, the reactance values in Figure 4.10 do not have variation that is linked to temperature; instead, the values oscillate about a mean value of $3.209\ \Omega$.

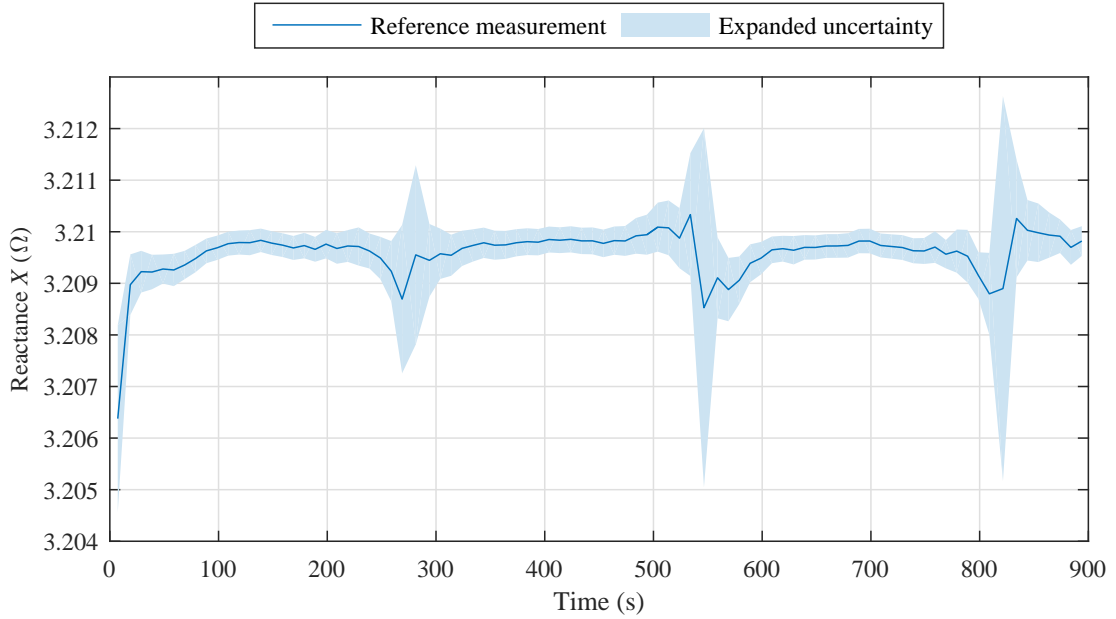


Figure 4.10: Measured reference reactance values

4.3.2.2 Systematic errors

A systematic error was added to the receiving end voltage measurement as modelled in (4.19), with $a = -5.00 \times 10^{-4}$, $\phi = 100 \mu\text{rad}$. These correspond to a TVE of 0.05 %, which is well below the 1 % limit suggested in the standard for synchrophasor measurements [56]. In practice, such errors are present if the instrument calibration is unknown or outdated.

Since the resistance only changes by 0.3 % and approximately linearly over the test period (correlation coefficient of 0.94), all measurement sets $V_{s_i}, V_{r_i}, I_i, t_1 = 10 \text{ s}, t_n = 900 \text{ s}$ were used to solve optimization problem (4.27) with $l_a = l_\phi = 0.01$; the following values were identified for the correction constants: $a = -4.99 \times 10^{-4}$, $\phi = 99.1 \mu\text{rad}$. In Table 4.1 it can be seen that the correction constants reduce the sums of the squared residuals S_R, S_X (given by (4.25) and (4.26)), thus the calculated parameter values are closer to physically consistent, linear behaviour over time.

Table 4.1: Sum of squared residuals S_R and S_X with and without correction constants

	S_R	S_X
No correction constants (Ω^2)	1.17	0.84
With correction constants (Ω^2)	6.46×10^{-6}	7.19×10^{-6}

Figures 4.11 to 4.13 show the resistance and reactance values calculated from measurements with systematic errors using (4.19), both including and excluding the correction constants a, ϕ that were identified using the newly proposed method. The percentage error E was calculated relative to the reference parameter values R_{0_i}, X_0 :

$$E_{R_i} = 100(R_i - R_{0_i})/R_{0_i} \quad (4.28)$$

$$E_{X_i} = 100(X_i - X_0)/X_0, \quad (4.29)$$

where subscript i refers to calculations for time instant t_i . R_{0_i} is the calculated reference resistance at each t_i , while X_0 is the mean value of the calculated reference values over the time period.

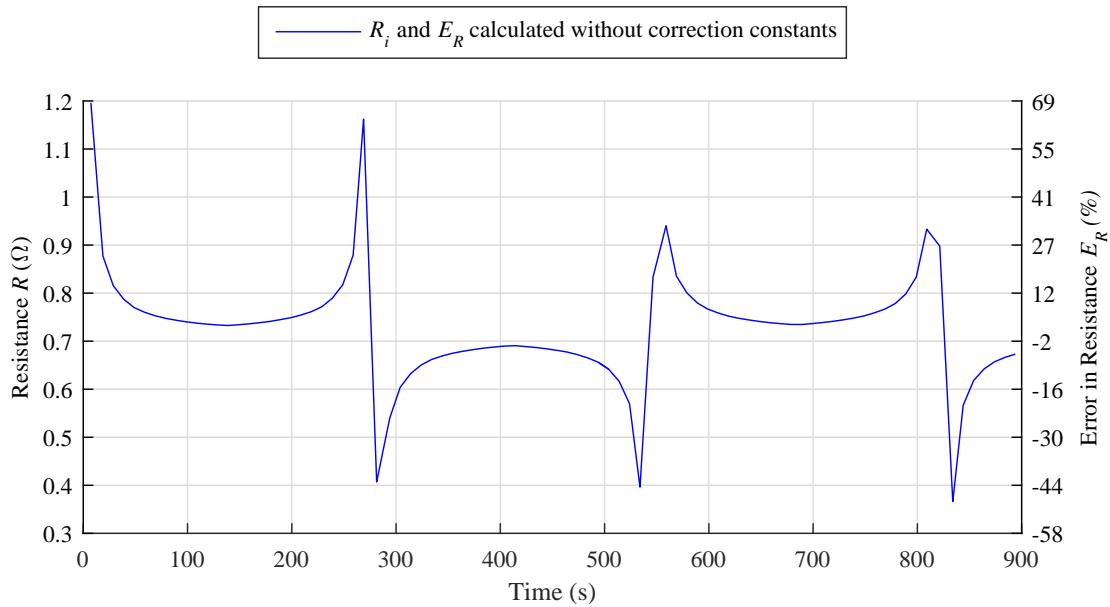


Figure 4.11: Resistance values calculated without correction constants

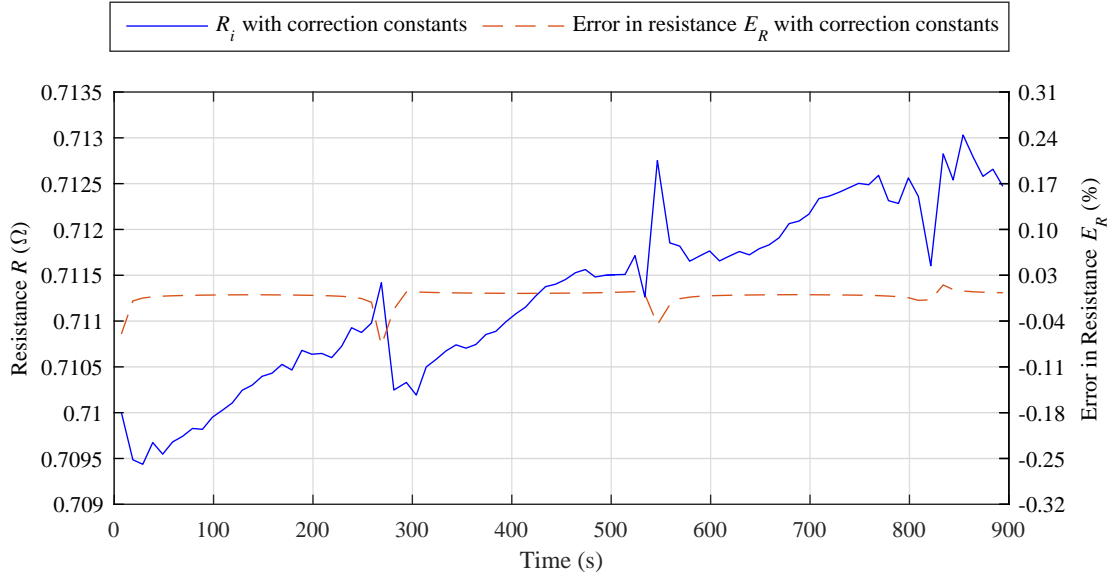


Figure 4.12: Resistance values calculated with correction constants

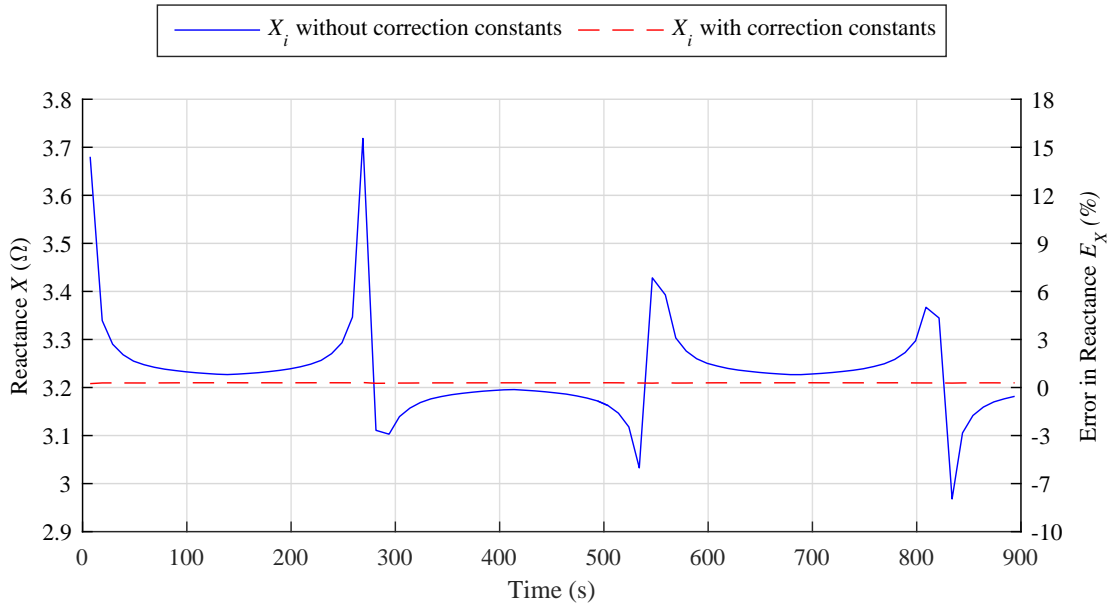


Figure 4.13: Calculated reactance values over the test period

From the graphs, it can be observed that without any error correction, resistance and reactance values vary non-linearly and periodically, with asymptotic behaviour at the times of reversal of the direction of power flow, as predicted by the observations on propagation of systematic errors in (4.16). Errors in resistance exceed $\pm 40\%$ and errors in reactance reach up to 17% , while the maximum uncertainties in the reference values are $\pm 0.6\%$ and $\pm 0.06\%$, respectively. When the identified error constants are included in the impedance calculation, errors in both parameters are reduced to below 1% .

4.3.3 Discussion of results

The results presented in the previous section have shown that constant deviations in voltage phasor measurements can cause significant errors in calculated impedance parameters and hide thermal variation of the resistance. Moreover, the new, optimization-based method identified correction constants that compensated for the systematic errors with the effect of increasing parameter estimation accuracy. The strength of the method is that it makes use of knowledge about the dynamic behaviour of line impedance; in contrast to existing approaches, time is included in the problem formulation. This additional information is used to estimate the correction constants only, and impedance is calculated more accurately in another step. The need to solve a parameter estimation problem with many unknowns (impedance parameters and correction constants) and the associated potential issue of ill-conditioning are avoided. The case study was somewhat realistic as actual phasor measurements with uncertainty were used and the size of the impedance was typical for a short line. However, overhead lines are often longer than 80 km, especially at transmission level, with significant capacitive leakage currents that require a pi-circuit representation using impedance and admittance parameters. In addition, resistance is likely to be more and the load profile less variable. Therefore, the proposed method requires further development and validation under more realistic assumptions.

4.4 Extension of the method to the pi-model for longer lines

In this section, the parameter estimation problem for a pi-circuit is modified to include systematic measurement errors. Thereafter, the new method presented in Section 4.2 for short lines is extended to the pi-circuit, which conventionally serves as a model for medium-length (up to 240 km) and long (more than 240 km) transmission lines [140].

4.4.1 Modification of the pi-circuit model

Figure 4.14 shows the circuit diagram of the pi-circuit model. Series impedance $Z \in \mathbb{C}$ and shunt admittance $Y \in \mathbb{C}$ are to be determined from measurements $V_s, I_s, V_r, I_r \in \mathbb{C}$. $Z = R + jX, Y = G + jB$, where $R, X, G, B \in \mathbb{R}_{\geq 0}, X = 2\pi fL, B = 2\pi fC, f, L, C \in \mathbb{R}_{\geq 0}$. R is the line resistance, X the reactance, G is conductance, B is susceptance, L is inductance, C is capacitance and f is the frequency.

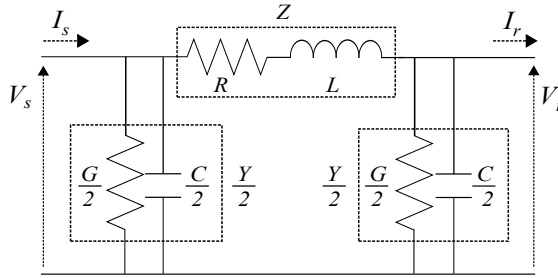


Figure 4.14: Diagram of a pi-circuit

The circuit equations are

$$V_s = (I_s - \frac{Y}{2}V_s)Z + V_r \quad (4.30)$$

$$I_s = (V_s + V_r)\frac{Y}{2} + I_r. \quad (4.31)$$

Equations (4.30) and (4.31) can be rearranged to give formulae for Z and Y :

$$Z = \frac{V_s^2 - V_r^2}{V_s I_r + V_r I_s} \quad (4.32)$$

$$Y = 2 \frac{I_s - I_r}{V_s + V_r}. \quad (4.33)$$

In the same manner as in Section 4.2.1, define $\tilde{V}_s, \tilde{V}_r, \tilde{I}_s, \tilde{I}_r \in \mathbb{C}$ as synchronized phasor measurements that have systematic errors $-a_s, -b_s, -a_r, -b_r \in \mathbb{R}$ in magnitude and $-\phi_s, -\theta_s, -\phi_r, -\theta_r \in [-\pi, \pi]$ in phase angle, respectively. Then the corrected phasors are given by

$$V_s = (1 + a_s)\tilde{V}_s \exp(j\phi_s) \quad (4.34)$$

$$I_s = (1 + b_s)\tilde{I}_s \exp(j\theta_s) \quad (4.35)$$

$$V_r = (1 + a_r)\tilde{V}_r \exp(j\phi_r) \quad (4.36)$$

$$I_r = (1 + b_r)\tilde{I}_r \exp(j\theta_r). \quad (4.37)$$

By substituting (4.34) to (4.37) into (4.32) and (4.33), the model equations for measurements with systematic errors are obtained as

$$Z = \frac{(1 + a_s)^2 \tilde{V}_s^2 \exp(j2\phi_s) - (1 + a_r)^2 \tilde{V}_r^2 \exp(j2\phi_r)}{(1 + b_r)(1 + a_s)\tilde{I}_r \tilde{V}_s \exp(j(\theta_r + \phi_s)) + (1 + b_s)(1 + a_r)\tilde{I}_s \tilde{V}_r \exp(j(\theta_s + \phi_r))} \quad (4.38)$$

$$Y = 2 \frac{(1 + b_s)\tilde{I}_s \exp(j\theta_s) - (1 + b_r)\tilde{I}_r \exp(j\theta_r)}{(1 + a_s)\tilde{V}_s \exp(j\phi_s) + (1 + a_r)\tilde{V}_r \exp(j\phi_r)}. \quad (4.39)$$

From (4.39), it can be observed that admittance Y is proportional to the difference between sending and receiving end current, thus the sensitivity to systematic errors $b_s, b_r, \theta_s, \theta_r$ is high and correction constants for voltage as well as current measurements will be estimated.

4.4.2 Explanation of the new method for the pi-circuit model

In a similar manner as in Section 4.2.3, the problem can be simplified by observing that the error in Y caused by b_s, θ_s is approximately equal and opposite to the error caused by b_r, θ_r . Therefore $b_s, b_r, \theta_s, \theta_r$ are combined into net errors b, θ in \tilde{I}_r , where $b = (b_r - b_s), \theta = (\theta_r - \theta_s)$. Equivalently, the error in Z caused by a_s, ϕ_s is approximately equal and opposite to the error caused by a_r, ϕ_r , hence, error constants a_s, a_r, ϕ_s, ϕ_r are combined into net errors a, ϕ in \tilde{V}_r , where $a = (a_r - a_s), \phi = (\phi_r - \phi_s)$. A detailed derivation of these approximations is given in Appendix B.2. The problem is thus formally stated as follows:

Given $n \in \mathbb{N}$ sets of phasor measurements $\tilde{V}_{s_i}, \tilde{I}_{s_i}, \tilde{V}_{r_i}, \tilde{I}_{r_i} \in \mathbb{C}$, each taken at time instants $t_i \in \mathbb{R}_{\geq 0}, i = 1, 2, 3, \dots, n$ over the time period $t_n - t_1$, identify optimal values of correction constants $a, \phi, b, \theta \in \mathbb{R}$ such that impedance Z_i and admittance Y_i can be calculated accurately.

$\tilde{V}_{s_i}, \tilde{I}_{s_i}, \tilde{V}_{r_i}, \tilde{I}_{r_i}, a, \phi, b, \theta$ are related by

$$Z_i = \frac{\tilde{V}_{s_i}^2 - (1+a)^2 \tilde{V}_{r_i}^2 \exp(j2\phi)}{(1+b)\tilde{I}_{r_i}\tilde{V}_{s_i} \exp(j\theta) + (1+a)\tilde{I}_{s_i}\tilde{V}_{r_i} \exp(j\phi)} \quad (4.40)$$

$$Y_i = 2 \frac{\tilde{I}_{s_i} - (1+b)\tilde{I}_{r_i} \exp(j\theta)}{\tilde{V}_{s_i} + (1+a)\tilde{V}_{r_i} \exp(j\phi)}. \quad (4.41)$$

where resistance is given by $R_i = \text{Re}(Z_i)$, reactance by $X_i = \text{Im}(Z_i)$, conductance by $G_i = \text{Re}(Y_i)$ and susceptance by $B_i = \text{Im}(Y_i)$.

Constants a, ϕ, b, θ are identified using the same principle that was introduced in Section 4.2.3. Since there are more constants and an additional model equation than for the short line model, two optimization problems will be defined. The first is based on (4.40) and exploits the higher sensitivity of Z to a and ϕ ; values for a and ϕ are found by minimizing residuals between calculated values of R, X and fitted linear functions of time. The second optimization problem is based on (4.41) and finds values for b and θ by minimizing residuals between calculated values of G, B and fitted linear functions of time.

Optimization problem 1 As in Section 4.2.3, resistance R is assumed to vary linearly over time and reactance X is assumed to have a constant value. Functions f_R, f_X, S_R, S_X are defined in the same way and the optimization problem is formulated as

$$\begin{aligned} & \underset{a, \phi}{\text{minimize}} && g_Z(a, \phi) = S_R + S_X \\ & \text{subject to} && |a| < l_a, |\phi| < l_\phi, \end{aligned} \quad (4.42)$$

and $l_a, l_\phi \in (0, 1)$ are bounding values that are chosen as the maximum expected systematic error values. On each iteration, R_i and $X_i, i = 1, 2, 3, \dots, n$, are calculated using

$$Z_i = R_i + jX_i = \frac{\tilde{V}_{s_i}^2 - (1+a)^2 \tilde{V}_{r_i}^2 \exp(j2\phi)}{\tilde{I}_{r_i}\tilde{V}_{s_i} + (1+a)\tilde{I}_{s_i}\tilde{V}_{r_i} \exp(j\phi)}, \quad (4.43)$$

where subscript i refers to measurements taken at time instant t_i . By the same justification as given in Section 4.2.3, equation (4.42) is a non-linear, constraint, convex optimization problem and optimal values a_{final}, ϕ_{final} are identified using the interior-point method [137]. The optimal values are used in the objective func-

tion of the second optimization problem, which is defined in the next paragraph.

Optimization problem 2 For the second optimization problem, define linear functions $f_G, f_B : \mathbb{R}_{\geq 0} \rightarrow \mathbb{R}$, where

$$f_G(t_i) = r_G \quad (4.44)$$

$$f_B(t_i) = r_B, \quad (4.45)$$

since conductance G and susceptance B are assumed to be constant over time. In the same way as r_X , constants $r_G, r_B \in \mathbb{R}$ are calculated as the mean of the n parameter values $G_i, B_i \in \mathbb{R}$, calculated at time instants $t_i, i = 1, \dots, n$:

$$r_G = \frac{1}{n} \sum_{i=1}^n G_i \quad (4.46)$$

$$r_B = \frac{1}{n} \sum_{i=1}^n B_i. \quad (4.47)$$

G_i, B_i are calculated using

$$Y_i = G_i + jB_i = 2 \frac{\tilde{I}_{s_i} - (1+b)\tilde{I}_{r_i} \exp(j\theta)}{\tilde{V}_{s_i} + (1+a_{final})\tilde{V}_{r_i} \exp(1 + \phi_{final})}, \quad (4.48)$$

where optimal values a_{final}, ϕ_{final} from optimization problem 1 have been included to correct voltage phasor measurements. The variation of G_i, B_i over time is measured by the sums of squared residuals S_G, S_B :

$$S_G = \sum_{i=1}^n (G_i - f_G(t_i))^2 \quad (4.49)$$

$$S_B = \sum_{i=1}^n (B_i - f_B(t_i))^2. \quad (4.50)$$

The second optimization problem is then defined as

$$\begin{aligned} & \underset{b, \theta}{\text{minimize}} && g_Y(b, \theta) = \mu(S_G + S_B) \\ & \text{subject to} && |b| < l_b, |\theta| < l_\theta, \end{aligned} \quad (4.51)$$

where $\mu \in \mathbb{R}_{\geq 0}$ is a factor to avoid bad scaling as G_i and B_i are of the order of 10^{-6} and 10^{-4} , respectively, and $l_b, l_\theta \in (0, 1)$ are bounding values that are chosen as the maximum expected systematic error values. By the same reasoning given in Section 4.2.3, equation (4.51) is a convex, non-linear constrained optimization problem that can be solved using the interior-point algorithm [137] to obtain optimal values $b_{final}, \theta_{final}$.

Optimal values $a_{final}, \phi_{final}, b_{final}, \theta_{final}$ are obtained from a moving window of n measurement sets spanning time period $t_n - t_1$ and are then used to calculate accurate values for R, X, G, B using (4.40) and (4.41). The entire process is summarized by the flow chart in Figure 4.15.

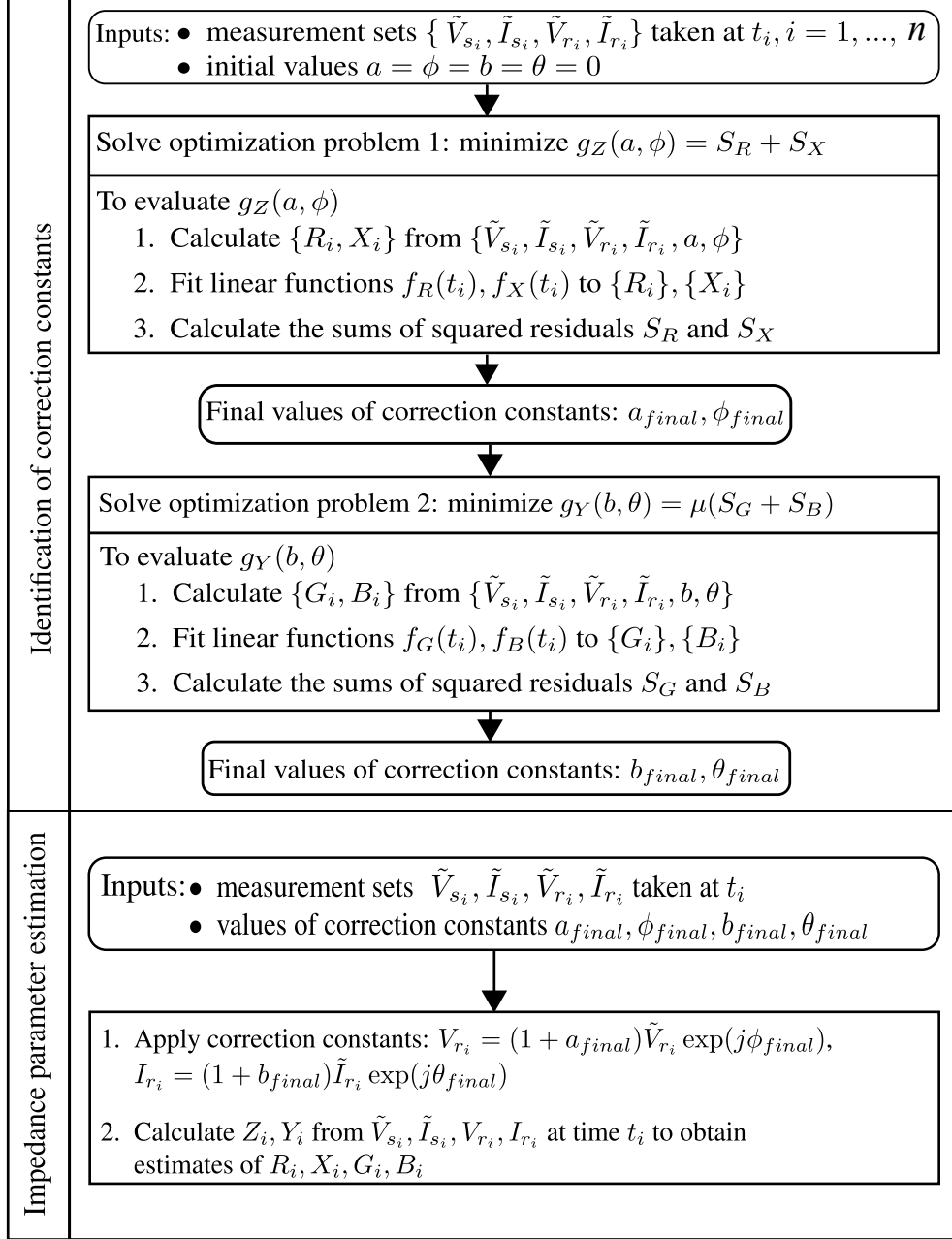


Figure 4.15: Flow chart that summarizes the steps of the proposed method for the pi-circuit model

4.5 Case study 2: medium-length and long lines

The Proposed Method (PM) presented in the last section has been applied to measurements from a simulated, medium-length transmission line. To provide a comparison, the Two-port Linear Least-squares - Single-phase (TPLL1) method as defined in Section 3.2.1.4 has also been implemented to estimate impedance parameters. This method was chosen as it achieved the highest number of acceptable values in the simulation study in 3.5. In Section 4.3, one sole case of systematic errors was studied. In this section, 10^5 cases will be considered to demonstrate the robustness of the new method.

4.5.1 Properties of the simulation

A single phase of the 400 kV, 102 km long transmission line located between substations Grendon and Staythorpe, East Midlands, England [141], was simulated in MATLAB[®] Simscape[™] Power Systems[™] software. A circuit diagram is shown in Figure 4.16.

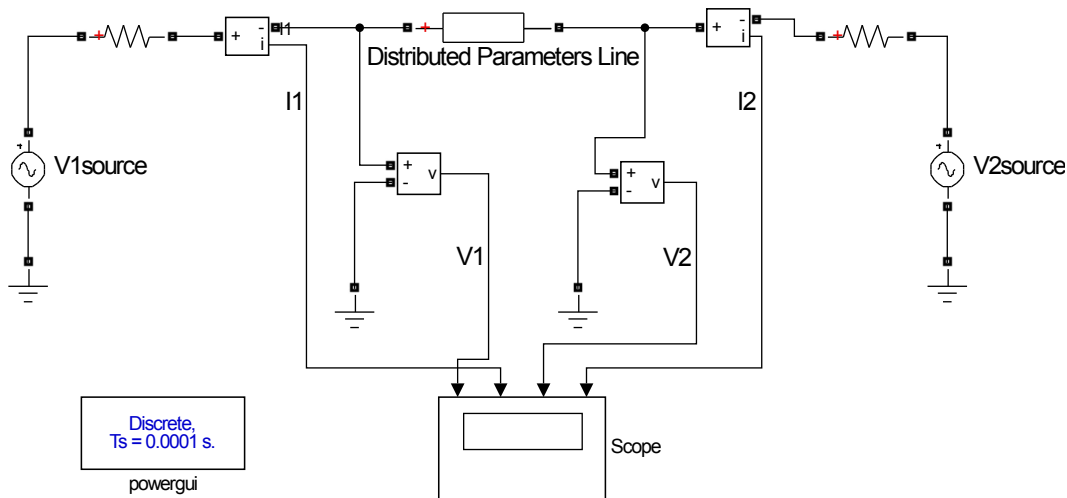


Figure 4.16: Schematic diagram of the simulation circuit

The pi-equivalent parameter values are $R_0 = 2.98 \Omega$, $X_0 = 32.3 \Omega$, $G_0 = 33.8 \text{ nS}$ and $B_0 = 3.68 \times 10^{-4} \text{ S}$ at 20°C . The resistance was set to vary sinusoidally within $\pm 4\%$ of the nominal value, which corresponds to a change in line temperature of approximately $\pm 10^\circ \text{C}$ over the period of the simulation.

The network at either end of the line was modelled by an equivalent voltage source; Figure 4.17 shows the rms magnitude of the sending and receiving end voltages. A variable load profile ranging from 15% to 100% of rated current was assumed to occur over a seven hour period; rms values of current magnitude are shown in Figure 4.18.

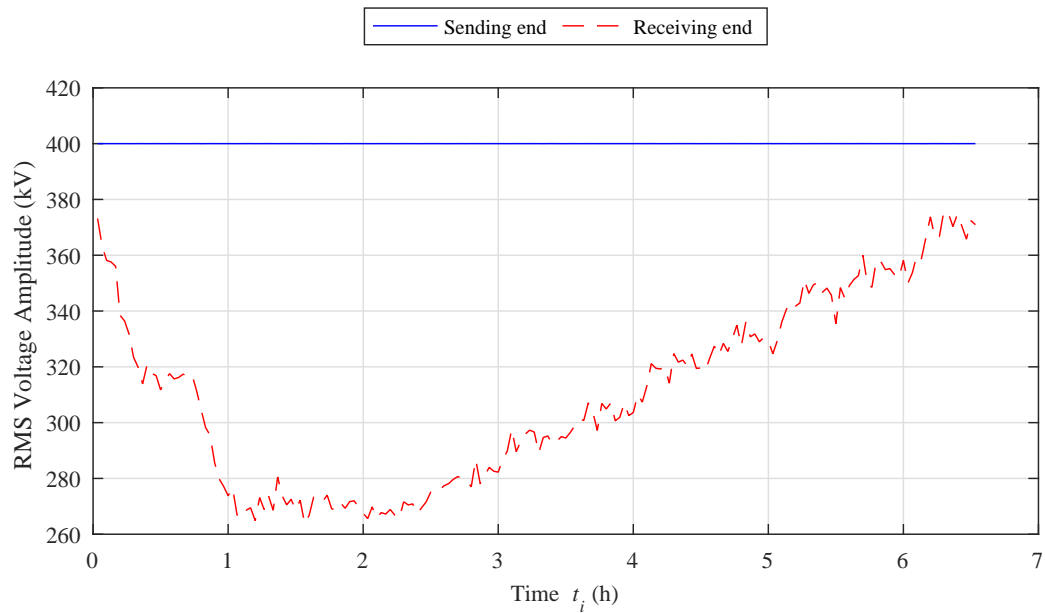


Figure 4.17: Amplitude of the sending and receiving end voltages over the period of the simulation

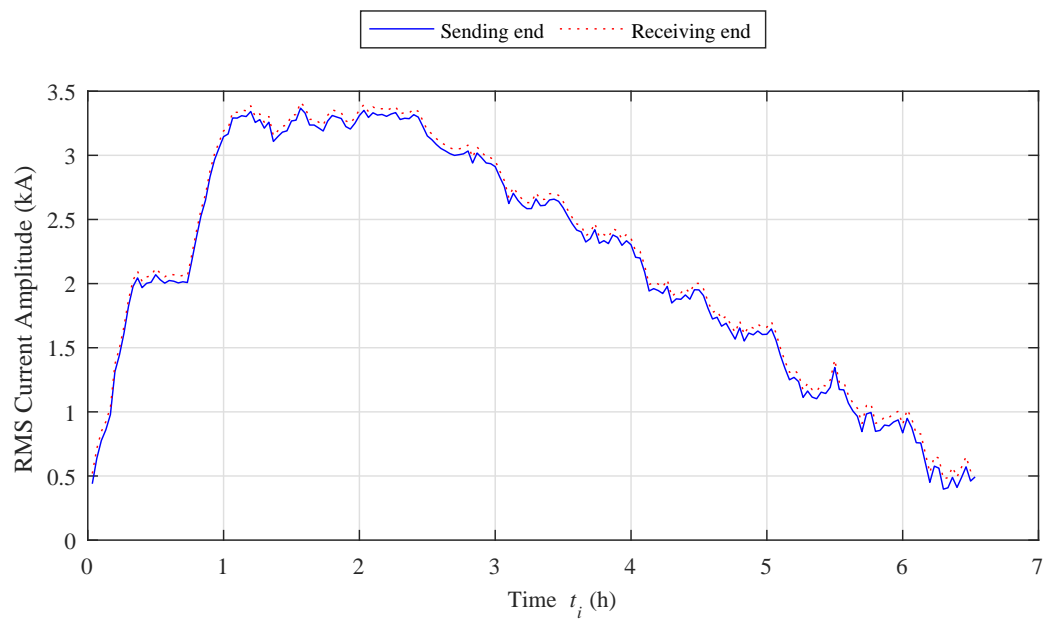


Figure 4.18: Amplitude of the sending and receiving end currents over the period of the simulation, their difference is very small compared to the individual values

Synchronized measurements of steady-state current and voltage phasors at each line end were taken at time intervals of $\Delta t = 2$ min for blocks of 10 s. In order to reflect the measurement uncertainty that is present in practice, the measurements were contaminated with Gaussian noise of mean zero and standard deviations of 0.03 % and 0.04 % in magnitudes of voltage and current, respectively, and 0.3 mrad in all phase angles. These values are typical for commercially available phasor measurement units [10].

Systematic errors in both sending and receiving end voltages and currents as modelled in (4.34) to (4.37) were applied to all synchrophasor measurements. The mean of the synchrophasors was taken over each 10 s block to generate an individual set of measurements every two minutes; in total there were 203 measurement sets. A moving window of $n = 8$ measurement points, spanning 16 min, was used to estimate the impedance and admittance parameters of the line in real-time. Thus, $203 - 8 + 1 = 196$ estimated values were computed for each of R, X, G and B .

In order to test the effectiveness of the PM and existing TPLL1 method under a range of conditions, different sets of systematic errors were applied to the measurements. In each case, the magnitude and phase errors were selected randomly from a uniform distribution in the interval $[-0.01, 0.01]$. In total, 10^5 cases were studied, giving sufficiently small confidence intervals on the relevant metrics, which will be defined in Section 4.5.2.

4.5.2 Metrics for evaluation of method performance

Two metrics are used to evaluate the accuracy of the impedance and admittance parameter estimates over the simulation period. The first is the rms error $E_{\Delta P}$ calculated over all parameter estimates; it indicates how far the estimates are from the actual values.

Let the errors in the individual parameter estimates be $\Delta P_i = P_i - P_0$. P_i refers to the parameter estimates R_i, X_i, B_i evaluated at each time instant $t_i, i = [1, \dots, 196]$ using (4.40) and (4.41) by the PM and as described in Section 3.2.1.4 by the TPLL1 method. P_0 refers to the nominal parameter values R_0, X_0, B_0 given in Section 4.5.1. Then

$$E_{\Delta P} = \frac{1}{P_0} \sqrt{\frac{1}{196} \sum_{i=1}^{196} \Delta P_i^2}. \quad (4.52)$$

The second metric is $\Sigma_{\Delta P}$, the standard deviation of the parameter errors as a fraction of the nominal values. This metric indicates the variability of the parameter error over the simulation period. $\Sigma_{\Delta P}$ is given by

$$\sigma_{\Delta P} = \frac{1}{P_0} \sqrt{\frac{1}{195} \sum_{i=1}^{196} (\Delta P_i - \mu_{\Delta P})^2}, \quad (4.53)$$

where $\mu_{\Delta P} = 1/196 \sum_{i=1}^{196} \Delta P_i$ is the mean parameter error.

The reference conductance value of 33.8 nS causes a loss of current of less than 0.1 A at 400 kV, which is 0.02% of the minimum line current of 500 A. Given a typical measurement uncertainty of 0.1%, only current losses greater than 1% become measurable and thus significant; these losses require conductance values greater than 7 μ S. It is therefore more useful to consider the absolute errors in conductance, rather than a proportion of the reference value:

$$E_{\Delta G} = \sqrt{\frac{1}{196} \sum_{i=1}^{196} \Delta G_i^2}, \Sigma_{\Delta G} = \sqrt{\frac{1}{195} \sum_{i=1}^{196} (\Delta G_i - \mu_{\Delta G})^2}, \mu_{\Delta G} = \frac{1}{196} \sum_{i=1}^{196} \Delta G_i. \quad (4.54)$$

Equations (4.52) to (4.54) were used to calculate the results presented in Section 4.5.3.

4.5.3 Analysis of parameter estimation results

The results of the case study are presented in two parts: first, one individual case with a specific set of systematic errors is considered; then the aggregated results for 10^5 cases of systematic errors are given.

4.5.3.1 Individual case

Table 4.2 lists the values of one set of systematic errors that was applied to the voltage and current phasors as well as the resulting TVE. Figure 4.19 shows the values of the correction constants that were identified from a moving window of $n = 8$ measurements by solving the two optimization problems (4.42) and (4.51) with bounds $l_a = l_\phi = l_b = l_\theta = 0.02$.

It can be observed that $a \approx -0.003 \approx a_r - a_s$ (from Table 4.2), which is consistent with the assumption that a corrects the net error, as described by (4.40) and (4.41). Similar observations can be made for ϕ, b, θ .

Table 4.2: Systematic errors in the synchrophasor measurements - individual case

	Magnitude	Phase Angle (rad)	TVE
\tilde{V}_s	$a_s = 0.0008$	$\phi_s = 0.0059$	0.60 %
\tilde{V}_r	$a_r = -0.0021$	$\phi_r = -0.0076$	0.78 %
\tilde{I}_s	$b_s = -0.0016$	$\theta_s = 0.0095$	1.02 %
\tilde{I}_r	$b_r = 0.0037$	$\theta_r = -0.0034$	0.38 %

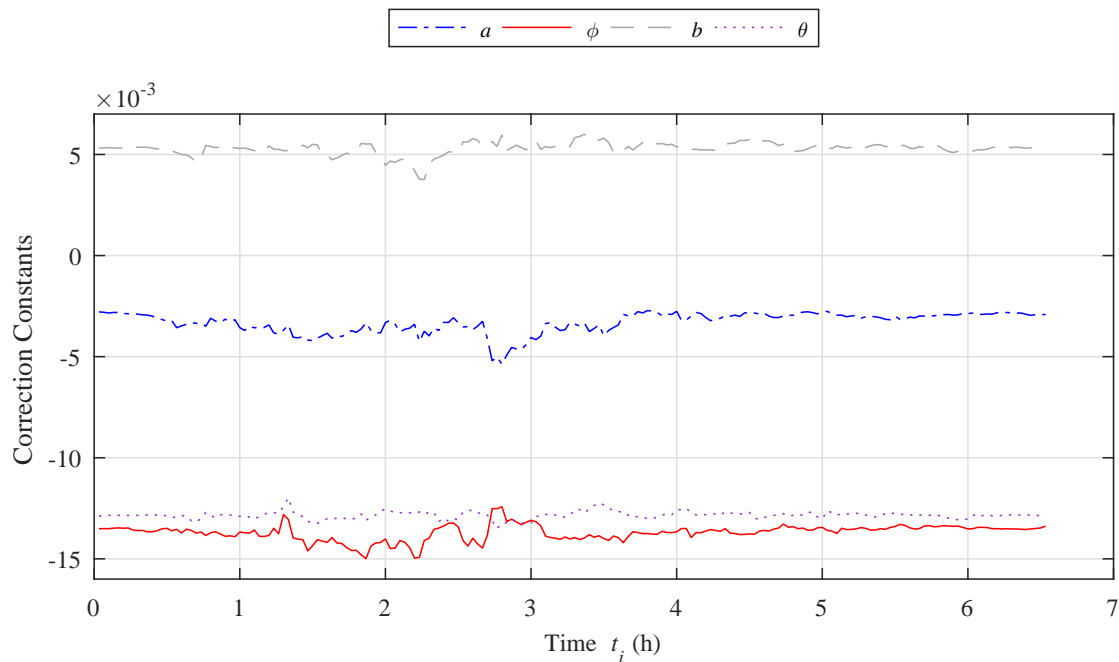


Figure 4.19: Values of the identified correction constants over time for the individual simulation case

Figures 4.20 to 4.23 show the final estimates of resistance, reactance, conductance and susceptance over the simulation period. It can be observed that the estimated values obtained by the PM are closer to the nominal values than for the TPLL1 method, and for resistance the thermal changes are tracked more accurately.

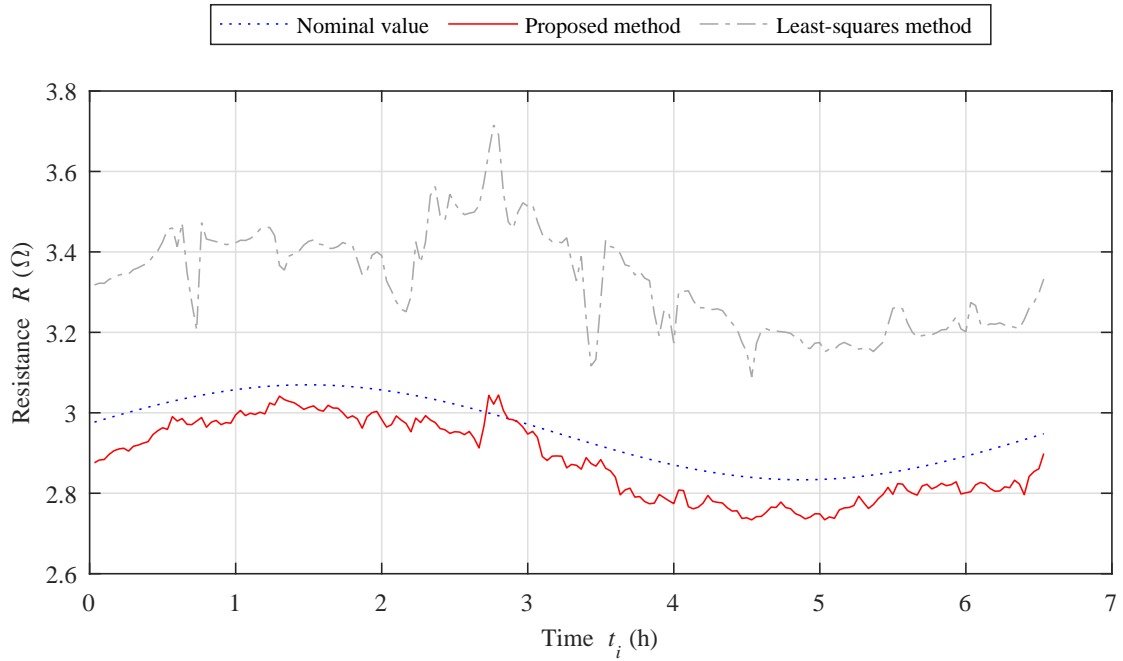


Figure 4.20: Nominal and estimated values of resistance R over time for the individual simulation case

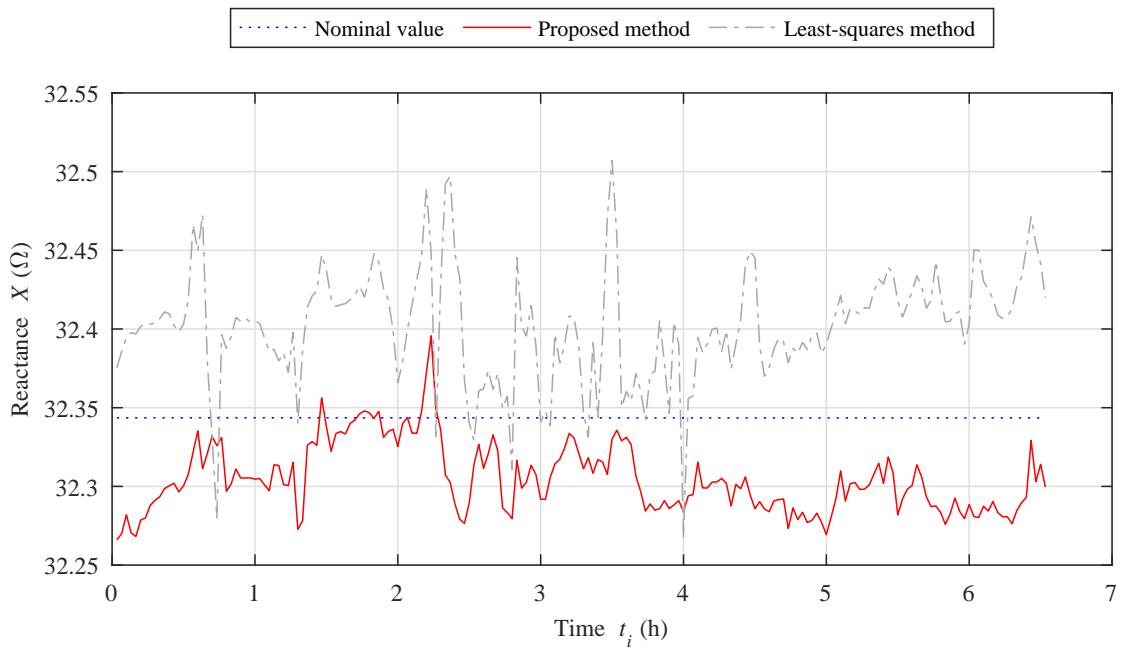


Figure 4.21: Nominal and estimated values of reactance X over time for the individual simulation case

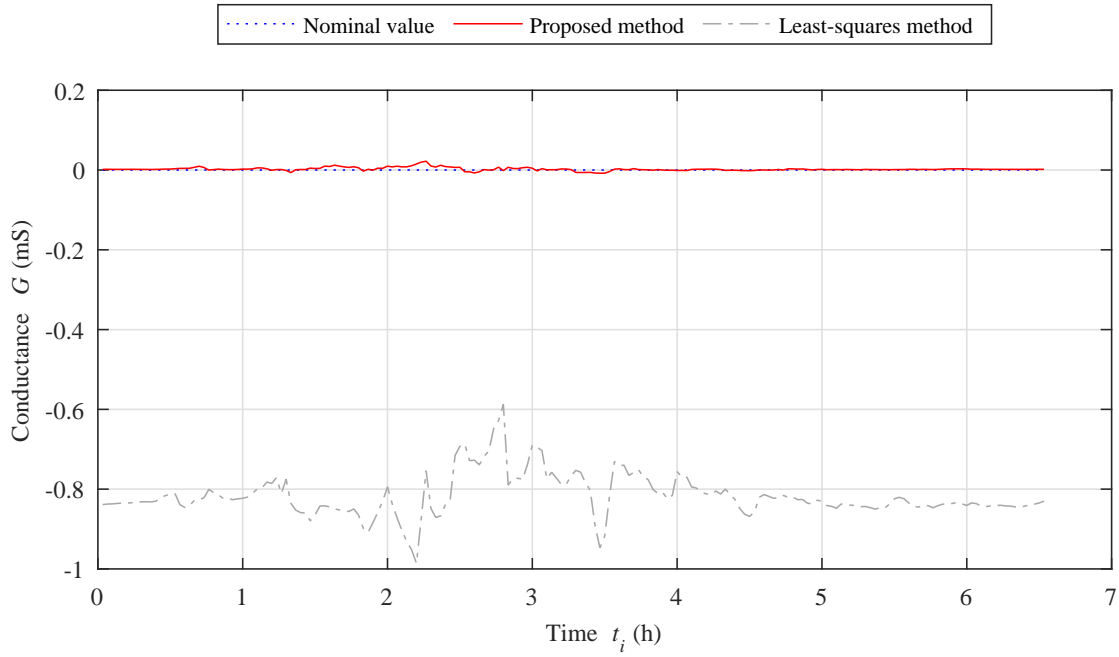


Figure 4.22: Nominal and estimated values of conductance G over time for the individual simulation case

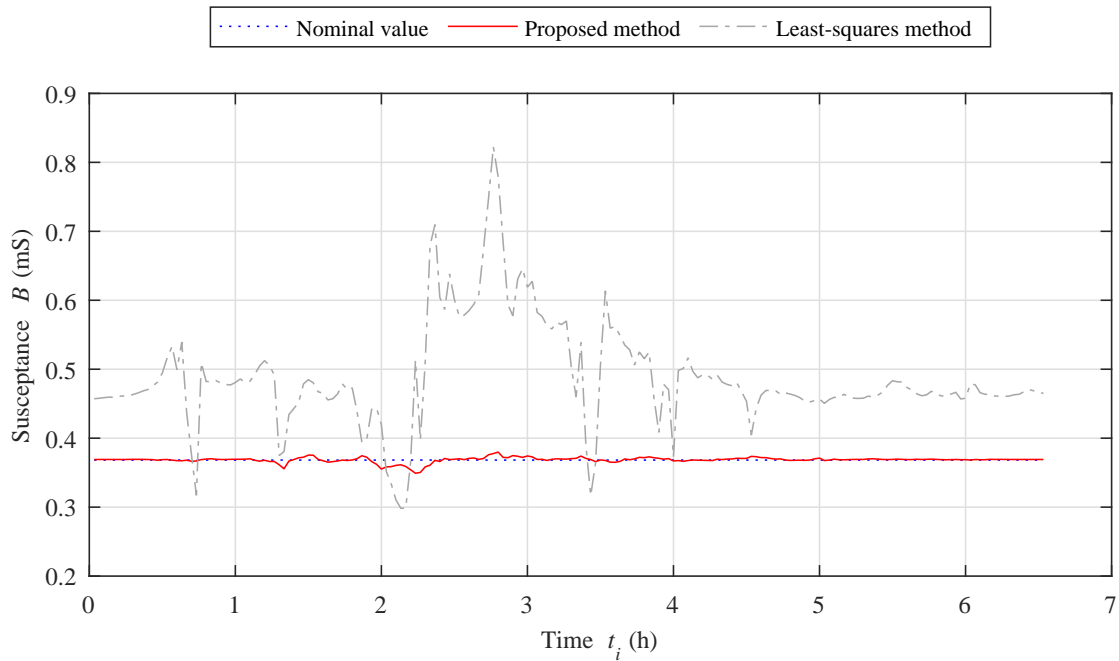


Figure 4.23: Nominal and estimated values of susceptance B over time for the individual simulation case

In Table 4.3, E_{Δ} and Σ_{Δ} as defined by (4.52) to (4.54) are given for R, X, B and G . E_{Δ} for estimated parameter values by the PM is significantly smaller than for values estimated by the TPLL1 method. Similarly, Σ_{Δ} is lower, indicating less non-thermal variability in the parameter estimates.

Table 4.3: Parameter errors for one individual case

		R	X	B	G	
E_{Δ} (%)	PM ¹	2.5	0.14	1.5	4.7	μS
	TPLL1 ²	13.1	0.21	38.5	819.0	μS
Σ_{Δ} (%)	PM ¹	0.9	0.07	1.1	4.1	μS
	TPLL1 ²	2.9	0.11	20.8	52.3	μS

¹ Proposed Method

² Two-port Linear Least-squares - Single-phase

4.5.3.2 Large number of cases

Tables 4.4 to 4.7 summarize the results from the simulation of 10^5 different cases of systematic errors. The 50th, 75th and 95th percentiles of the distributions of E_{Δ} and Σ_{Δ} as defined by (4.52) to (4.54) are listed to give an indication of the level of accuracy and consistency of the applied methods. For each percentile, the 95% confidence interval is given in brackets.

Table 4.4: Errors in resistance R for 10^5 cases

		Percentile		
		50th	75th	95th
$E_{\Delta R}$ (%)	PM ¹	6.4 ± 0.1	10.8 ± 0.1	16.9 ± 0.1
	TPLL1 ²	7.2 ± 0.0	11.6 ± 0.1	17.9 ± 0.1
$\Sigma_{\Delta R}$ (%)	PM	0.9 ± 0.0	0.9 ± 0.0	1.1 ± 0.0
	TPLL1	2.9 ± 0.0	2.9 ± 0.0	2.9 ± 0.0

¹ Proposed Method

² Two-port Linear Least-squares - Single-phase

Table 4.4 show that for resistance R , the distributions of $E_{\Delta R}$ occupy a similar range for both the PM and the TPLL1 method, with the 95th percentiles at 17% and 18%, respectively. However, the PM yields significantly lower values of $\Sigma_{\Delta R}$ at around 1%, whereas the TPLL1 method yields 2.9%. For reactance X , both methods produce lower values of $E_{\Delta X}$ and $\Sigma_{\Delta X}$, of the order of 1% and 0.1%, respectively, as shown in Table 4.5.

Table 4.5: Errors in reactance X for 10^5 cases

		Percentile		
		50th	75th	95th
$E_{\Delta X}$ (%)	PM ¹	0.58 ± 0.00	0.98 ± 0.01	1.52 ± 0.01
	TPLL1 ²	0.60 ± 0.01	1.01 ± 0.01	1.56 ± 0.01
$\Sigma_{\Delta X}$ (%)	PM	0.06 ± 0.00	0.07 ± 0.00	0.08 ± 0.00
	TPLL1	0.11 ± 0.00	0.11 ± 0.00	0.11 ± 0.00

¹ Proposed Method² Two-port Linear Least-squares - Single-phase

For conductance G and susceptance B the level of errors differs between the methods to a greater extent than for R and X .

Table 4.6: Errors in conductance G for 10^5 cases

		Percentile		
		50th	75th	95th
$E_{\Delta G}$ (μS)	PM ¹	4.7 ± 0.0	5.6 ± 0.0	7.3 ± 0.0
	TPLL1 ²	364.0 ± 3.0	617.0 ± 3.0	955.0 ± 4.0
$\Sigma_{\Delta G}$ (μS)	PM	4.1 ± 0.0	4.1 ± 0.0	4.2 ± 0.0
	TPLL1	53.1 ± 0.0	54.1 ± 0.0	55.5 ± 0.0

¹ Proposed Method² Two-port Linear Least-squares - Single-phase

Values of $E_{\Delta G}$ reach up to approximately $7 \mu\text{S}$ for the PM, but the TPLL1 method results in values of almost 1 mS . Results for $\Sigma_{\Delta G}$ are more than ten times higher for the TPLL1 method than for the PM.

Table 4.7: Errors in susceptance B for 10^5 cases

		Percentile		
		50th	75th	95th
$E_{\Delta B}$ (%)	PM	1.2 ± 0.0	1.5 ± 0.0	1.9 ± 0.0
	TPLL1	99.9 ± 0.7	168.0 ± 1.0	261.0 ± 1.0
$\Sigma_{\Delta B}$ (%)	PM	1.1 ± 0.0	1.1 ± 0.0	1.1 ± 0.0
	TPLL1	21.5 ± 0.0	21.9 ± 0.0	22.3 ± 0.0

¹ Proposed Method² Two-port Linear Least-squares - Single-phase

While the PM gives values of $E_{\Delta B}$ of 1% to 2% for susceptance, the TPLL1 method gives results for $E_{\Delta B}$ of over 100% . Values for $\Sigma_{\Delta B}$ are also an order of magnitude greater for the TPLL1 method.

4.5.4 Discussion of results

4.5.4.1 Comparison of methods

Based on the case study results presented in Section 4.5.3, the Proposed Method (PM) demonstrated equal or better performance compared to the existing Two-port Linear Least-squares - Single-phase (TPLL1) method. The TPLL1 method finds an optimal estimate for the parameters of a two-port network; these are then used to calculate impedance and admittance parameters of the pi-circuit. The advantage of this approach over calculating the pi-circuit parameters directly, is that it makes use of redundant measurements such that constant systematic errors, as modelled in (4.34) to (4.37), either cancel or only cause a constant offset in the estimated parameter values. However, the TPLL1 method also assumes constant parameters in time, and even small variations over a moving window lead to variable parameter errors. This robustness to systematic errors, yet weak accuracy for variable parameters, explains the relatively similar results in the rms errors in the resistance and reactance parameters in the case study for both methods. Therefore it may appear that the PM does not have a significant advantage. However, one of the crucial differences is that the PM has demonstrated approximately 60 % lower variability in the errors in resistance over the simulation period (standard deviation of errors of 1 % versus 3 %). The resistance is the parameter with the highest temperature sensitivity, hence, it is of interest for safety monitoring. Expanded uncertainties of 2 % and 6 % in resistance errors correspond to uncertainties of 5 °C and 15 °C in temperature error, respectively, assuming a resistance-temperature coefficient of 0.4 %. Hence, for the line under consideration, the safety margin for maximum temperature can be reduced by 10 °C when the PM is used, thus creating more transmission capacity.

4.5.4.2 Limitations of the proposed method

While the PM has demonstrated its capability to improve the accuracy of impedance parameter estimation, it does have limitations. Correction factors for systematic errors are found by minimizing residuals of constant or linear functions fitted to estimated parameter values from a given time window. For residuals to be increased by systematic errors, load variation must occur during this time window. There is an open question about how to determine the minimum level of load variation that is required for the method to be effective. At a minimum, the difference in line loading must be clearly distinguishable from random measurement noise and must therefore be at least ten times the measurement uncertainty.

Assuming a maximum TVE of 1%, a minimum level of variation of 10% is proposed. However, further work is necessary to give a comprehensive answer to this question.

The extent to which impedance and admittance parameters are constant or change linearly over time can differ between time windows. To maximize load variation, the window length can be increased, but the rate of thermal change of resistance can also change. On the one hand, it can be argued that the PM only relies upon relative changes in the residuals. As long as the residuals are increased by systematic measurement errors, it does not matter how well the variation in resistance is described by a linear function. On the other hand, it has not yet been generally proven that the identified correction constants restore the actual parameter estimates regardless of the non-linearity of resistance variation.

The PM in its current form only corrects net errors, i.e. the difference between the sending and receiving end. If the errors are equal at both line ends, the error in impedance and admittance is independent of the system state (see (4.17) and (B.20)), and residuals of fitted linear functions are not increased. In these cases, the method does not increase parameter estimation accuracy. This failure is due to the fact that the PM is designed to restore parameter variation to correct levels, but it lacks a mechanism to restore the correct absolute level of parameter values. A calibration procedure must be developed to tackle this limitation.

In presenting the PM, systematic errors were assumed to be constant, directly proportional in magnitude and additive in phase angle. The systematic errors can follow different, non-linear models. These variations can still be approximated by a linear error model. A useful extension of the PM is to test different systematic error models and select the one that achieves the most accurate impedance parameter estimates.

4.6 Conclusion

In this chapter, a novel method has been presented that can be used to accurately estimate impedance and admittance parameters of an overhead line from synchrophasor measurements with systematic errors. Building from a simple short line model, the method was extended to be applicable to the general pi-circuit, which can model medium-length and long transmission lines. An innovative feature of the method is that it takes into account the time dimension, that means the dynamic behaviour of the electrical properties of an overhead line. Through the assumption of constant or linearly changing parameters over short periods of time, correction constants for systematic errors are identified through optimization, allowing subsequent calculation of impedance parameters with increased accuracy.

The effectiveness of the proposed method was demonstrated in two case studies: initially, using measurements from a physical, laboratory-based line model and thereafter with a software-simulated transmission line. In comparison to an existing parameter estimation method, the new method has achieved 60 % lower variation in errors in resistance, which is especially useful with respect to real-time monitoring of changes in temperature.

Limitations of the proposed method have been discussed, highlighting that further work is necessary to facilitate accurate real-time monitoring of overhead line impedance parameters under a wide range of conditions. This is the objective of Chapter 5, which will build on the contributions made in this chapter. A method will be presented that is designed to correct for systematic errors even if individual windows have low levels of load variation; correction factors for measurements at both line ends are included; in addition, line temperature measurements are used to maximize the accuracy of absolute parameter values as well as of variation over time.

Chapter 5

An innovative approach to increasing the accuracy of real-time impedance parameter monitoring

5.1 Introduction

The aim of this thesis is to contribute methodology for synchrophasor-based, real-time monitoring of overhead line impedance parameters with acceptable accuracy. This objective is translated into a requirement to calculate series impedance and shunt admittance with acceptable accuracy from a set of synchronized phasor measurements of voltage and current signals taken at any given time at the two ends of an overhead line.

In Chapter 3 it was shown that systematic errors in the synchrophasor measurements can reduce the accuracy of calculated parameters to unacceptable level. To solve this problem, Chapter 4 proposed an adaptation of standard transmission line models, consisting of correction factors for the synchrophasor measurements, and a novel method for their identification. The novel method showed to be effective in two case studies, but it does have some weaknesses: correction factors are estimated for one line end only; moreover, the factors are continually updated based on a moving time window of measurements such that variation in impedance and admittance is physically consistent within each time window, but not necessarily over longer time scales; there is also no control to achieve acceptability of absolute values of impedance and admittance.

This chapter seeks to address these weaknesses by introducing a new problem formulation. As in Chapter 4, correction factors for systematic errors in synchrophasor measurements are added to the transmission line model. Furthermore, the linear resistance-temperature relationship is included since recent research has shown that handbook parameters for the resistance-temperature relationship may not describe individual systems with sufficient accuracy [130, 142]. Correction factors as well as resistance-temperature parameters are assumed constant through time, thus they can be estimated using measurements from an unlimited time span. Two novel methods will be proposed for this estimation, making use of synchrophasor as well as conductor temperature measurements. The first method will be based directly on the method proposed in Chapter 4, while the second method derives more closely from some of the existing impedance parameter estimation methods. Moreover, a procedure for selecting the optimal correction factors and resistance-temperature parameters obtained from different measurement sets is given.

The next section will outline the new methods and selection procedure in detail. Thereafter, two case studies on the overhead line that was considered in Chapter 3 will be presented; the first one in Section 5.3 compares the new methods to existing ones using synchronized measurements from a laboratory-based emulation of the overhead line; the second case study in Section 5.4 tests the new methods using actual field measurements spread over a ten-month period. Section 5.5 concludes this chapter.

5.2 Methods

To begin with, this section will introduce a new parameter estimation problem and then go on to explain two novel parameter estimation methods in detail as well as a procedure for selecting the optimal parameter estimates.

5.2.1 A different parameter estimation problem

The overhead line system model is built from the pi-circuit, which is shown in Figure 5.1, the standard model for medium-length and long transmission lines [135].

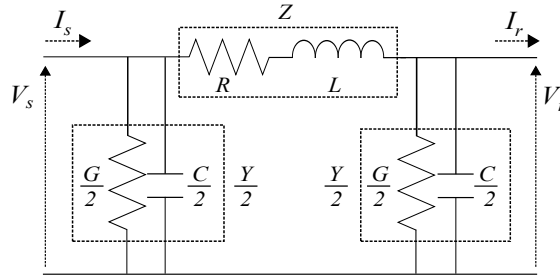


Figure 5.1: Diagram of a pi-circuit

Define the following variables:

- $V_s, I_s, V_r, I_r \in \mathbb{C}$ positive sequence voltage and current at nominal system frequency at the sending (s) and receiving (r) transmission line ends,
- $Z, Y \in \mathbb{C}$ are positive sequence series impedance and shunt admittance at fundamental system frequency, where $Z = R + jX, Y = G + jB$,
- $R \in \mathbb{R}$ resistance,
- $X \in \mathbb{R}$ reactance, $X = 2\pi fL$
- $G \in \mathbb{R}$ conductance,
- $B \in \mathbb{R}$ susceptance, $B = 2\pi fC$
- $f \in \mathbb{R}$ frequency,
- L inductance,
- C capacitance,
- $\tilde{V}_s, \tilde{I}_s, \tilde{V}_r, \tilde{I}_r \in \mathbb{C}$ synchrophasor measurements with systematic errors,
- $a_s, a_r, b_s, b_r \in \mathbb{C}$ correction factors.

The linear relationship between measurements and actual voltage and current is given by [70–73, 125]:

$$\begin{aligned} V_s &= a_s \tilde{V}_s, & I_s &= b_s \tilde{I}_s \\ V_r &= a_r \tilde{V}_r, & I_r &= b_r \tilde{I}_r. \end{aligned} \quad (5.1)$$

The electro-thermal system model consists of three equations. The first two are the pi-circuit equations with correction constants (see Section 4.4.1):

$$a_s \tilde{V}_s = (b_s \tilde{I}_s - Y/2)Z + a_r \tilde{V}_r \quad (5.2)$$

$$b_s \tilde{I}_s = (a_s \tilde{V}_s + a_r \tilde{V}_r)Y/2 + b_r \tilde{I}_r. \quad (5.3)$$

Let $T_c \in \mathbb{R}$ be measurements of conductor temperature and $R_0 \in \mathbb{R}_{\geq 0}$ be the line resistance value at a reference temperature T_0 , with resistance-temperature coefficient $\alpha \in [-1, 1]$. The third equation is the linear resistance-temperature relationship [43]:

$$R = R_0(1 + \alpha(T_c - T_0)). \quad (5.4)$$

The three equations are coupled by $R = \text{Re}(Z)$. The new parameter estimation problem is stated as follows:

Given n measurements $\tilde{V}_{s_i}, \tilde{I}_{s_i}, \tilde{V}_{r_i}, \tilde{I}_{r_i}, T_{c_i}$ taken at time instants $t_i \in \mathbb{R}_{\geq 0}, i = 1, 2, 3, \dots, n$ and a reference temperature T_0 , find values for correction constants a_s, a_r, b_s, b_r as well as resistance-temperature parameters R_0 and α .

Once a_s, a_r, b_s, b_r have been identified, values of impedance Z_i and Y_i at fixed time $t_i, i = 1, \dots, N, N \geq n$ can be calculated from the set of measurements $\tilde{V}_{s_i}, \tilde{I}_{s_i}, \tilde{V}_{r_i}, \tilde{I}_{r_i}$ by rearranging (5.2) and (5.3):

$$Z_i = R_i + jX_i = \frac{a_s \tilde{V}_{s_i}^2 - a_r \tilde{V}_{r_i}^2}{a_s \tilde{V}_{s_i} b_r \tilde{I}_{r_i} + a_r \tilde{V}_{r_i} b_s \tilde{I}_{s_i}} \quad (5.5)$$

$$Y_i = G_i + jB_i = 2 \frac{b_s \tilde{I}_{s_i} - b_r \tilde{I}_{r_i}}{a_s \tilde{V}_{s_i} + a_r \tilde{V}_{r_i}}. \quad (5.6)$$

In addition, conductor temperature can be calculated from estimates of R_0 and α by rearranging (5.4):

$$T_{c_i} = T_0 + \frac{1}{\alpha R_0}(R_i - R_0). \quad (5.7)$$

In the following paragraphs, two methods will be proposed for solving the new parameter estimation problem.

5.2.2 Estimation of correction factors and resistance-temperature parameters

Two novel approaches to estimating the unknown parameters from voltage and current measurements will be presented in this section.

5.2.2.1 New Method - Linear Time (NMLT)

The first approach is based on the novel method presented in Chapter 4, which is based on the assumption that parameter values change linearly over time or remain constant. Hence, this method is referred to as New Method - Linear Time (NMLT). The method is explained in two steps: firstly, an optimization problem for the identification of correction factors is defined and secondly, resistance-temperature parameter values are obtained by linear least-squares estimation.

Step 1: Estimation of correction factors

Suppose that measurements of voltage, current and temperature are available from $N \in \mathbb{N}$ time instants, where N is a constant. Unknown parameters will be estimated from a subset of measurements from $n \leq N$ time instants. Let $R_i = \text{Re}(Z_i)$, $X_i = \text{Im}(Z_i)$, $G_i = \text{Re}(Y_i)$, $B_i = \text{Im}(Y_i)$ be values of resistance, reactance, conductance and susceptance, respectively, calculated at time instant t_i using (5.5) and (5.6). Resistance is known to change with conductor temperature [43] and is therefore assumed to vary linearly over time, while reactance and susceptance are assumed constant as explained in Appendix A.1. Conductance depends on the conductor surface and can vary with humidity, but its overall magnitude is normally below $10 \mu\text{S}$ [143]; therefore, conductance is modelled as a constant value of zero. Hence, the following functions $f_R, f_X, f_G, f_B \in \mathbb{R} \rightarrow \mathbb{R}$ are defined for modelling R_i, X_i, G_i and B_i :

$$f_R(t_i) = q_R t_i + r_R \quad (5.8)$$

$$f_X(t_i) = r_X \quad (5.9)$$

$$f_G(t_i) = 0 \quad (5.10)$$

$$f_B(t_i) = r_B \quad (5.11)$$

Constants q_R, r_R are found through a linear least-squares fit of $R_i, i = 1, 2, 3, \dots, n$, which was explained in Section 4.2.3.

Constants r_X, r_B are calculated as the mean values of X_i, B_i , respectively:

$$r_X = \frac{1}{n} \sum_{i=1}^n X_i \quad (5.12)$$

$$r_B = \frac{1}{n} \sum_{i=1}^n B_i \quad (5.13)$$

Systematic errors in the voltage and current measurements cause the calculated values R_i, X_i, G_i, B_i to deviate from their physically expected, linear behaviour with respect to time, that means an increase in the residuals between f_R, f_X, f_G, f_B and R_i, X_i, G_i, B_i , respectively. Define $S_R \in \mathbb{R}_{\geq 0}$ as the sum of the squares of the residuals of the linear least-squares fit of (5.8), where

$$S_R = \sum_{i=1}^n (R_i - f_R(t_i))^2, \quad (5.14)$$

S_X, S_G and S_B are defined similarly in terms of X_i, f_X, B_i, f_B and G_i, f_G , respectively:

$$S_X = \sum_{i=1}^n (X_i - f_X(t_i))^2, \quad (5.15)$$

$$S_B = \sum_{i=1}^n (B_i - f_B(t_i))^2, \quad (5.16)$$

$$S_G = \sum_{i=1}^n G_i^2. \quad (5.17)$$

The objective is to find values for correction factors a_s, a_r, b_s, b_r that maximise the goodness of fit, which is achieved by minimizing S_R, S_X, S_G, S_B . Hence, the following optimization problem is defined:

$$\begin{aligned} \text{let } h \in \mathbb{R}^8, \quad h &= (|a_s|, \arg(a_s), |a_r|, \arg(a_r), |b_s|, \arg(b_s), |b_r|, \arg(b_r)), \\ \text{minimize}_h \quad g(h) &= \mu_R^2 S_R + \mu_X^2 S_X + \mu_G^2 S_G + \mu_B^2 S_B \\ \text{subject to} \quad &|a_s|, |\arg(a_s)|, |a_r|, |\arg(a_r)| < 0.1, \\ &|b_s|, |\arg(b_s)|, |b_r|, |\arg(b_r)| < 0.1, \end{aligned} \quad (5.18)$$

with initial values $a_s = a_r = b_s = b_r = 1$.

S_R, S_X, S_G, S_B are functions of h since R_i, X_i, G_i, B_i are calculated using a_s, a_r, b_s, b_r . Constants $\mu_R, \mu_X, \mu_G, \mu_B \in \mathbb{R}_{\geq 0}$ are weighting factors that can be used to adjust the relative magnitudes of the terms of $g(h)$. The choice of weighting factors has an effect on the optimized goodness of fit of f_R, f_X, f_B to R_i, X_i, B_i and the overall magnitude of G_i , that means to what extent the identified correction factors make

the calculated impedance and admittance more compliant to expected physical behaviour. For instance, if $\mu_R = \mu_X = \mu_G = \mu_B = 1$, S_R and S_X will dominate and no significant improvement occurs in S_G, S_B .

The inequality constraints arise from existing accuracy classes of instrument transformers [133, 134] and characterization of instrumentation channels [52], which imply that systematic errors in voltage and current magnitude do typically not exceed $\pm 10\%$, and errors in phase angle are less than ± 0.1 rad.

Equation (5.18) is a non-linear, constrained optimization problem. The objective function $g : \mathbb{R}_{\geq 0}^8 \rightarrow \mathbb{R}_{\geq 0}$ is a linear combination of the four independent variables S_R, S_X, S_G, S_B with positive constants $\mu_R, \mu_X, \mu_G, \mu_B$. Therefore $g(h)$ is a convex function and any local minimum of $g(h)$ is a global minimum. In this instance, the interior-point method is used to identify local minima of the non-linear, constrained optimization problem [137].

Let $\hat{a}_s, \hat{a}_r, \hat{b}_s, \hat{b}_r$ be the identified correction factors, which are used to calculate values of $Z_i = R_i + jX_i$ and $Y_i = G_i + jB_i, i = 1, 2, 3, \dots, N$ by substituting into (5.5) and (5.6). Since X, G and B are assumed constant, a single estimate can be obtained by taking the mean values

$$\bar{X} = 1/N \sum_{i=1}^N X_i, \bar{G} = 1/N \sum_{i=1}^N G_i, \bar{B} = 1/N \sum_{i=1}^N B_i. \quad (5.19)$$

Step 2: Estimation of resistance-temperature parameters

To obtain estimates for R_0 and α , express the linear resistance-temperature relationship (5.4) as

$$R_i = x_0 + x_1 T_{c_i}, \quad (5.20)$$

where $x_0, x_1 \in \mathbb{R}$ are unknown constants with $x_0 = R_0(1 - \alpha T_0), x_1 = R_0 \alpha T_0$. x_0, x_1 are identified through linear least-squares estimation from temperature measurements T_{c_i} and calculated resistance values R_i . Define vectors $\mathbf{R}, \mathbf{T} \in \mathbb{R}^N, \mathbf{x} \in \mathbb{R}^2$ where $\mathbf{R} = [R_1, R_2, \dots, R_N]^T, \mathbf{T} = [T_{c_1}, T_{c_2}, \dots, T_{c_N}]^T, \mathbf{x} = [x_0, x_1]$. The vectors are related by the N -dimensional matrix equation

$$\mathbf{R} = \mathbf{T}\mathbf{x} + \boldsymbol{\varepsilon}, \quad (5.21)$$

which is based on the theoretical model (5.20). $\boldsymbol{\varepsilon} = [\varepsilon_1, \varepsilon_2, \dots, \varepsilon_N]^T$ models the deviation between synchrophasor-based values \mathbf{R} and temperature-based values $\mathbf{T}\mathbf{x}$.

An estimate $\hat{\mathbf{x}} = [\hat{x}_0, \hat{x}_1]$ of \mathbf{x} is computed by satisfying the least-squares criterion, $\min \sum_{i=1}^n \varepsilon_i^2$:

$$\hat{\mathbf{x}} = (\mathbf{T}^T \mathbf{T})^{-1} \mathbf{T}^T \mathbf{R}. \quad (5.22)$$

Estimated values of reference resistance \hat{R}_0 and coefficient $\hat{\alpha}$ are calculated from \hat{x}_0 and \hat{x}_1 . $\hat{R}_0, \hat{\alpha}, \bar{X}, \bar{G}, \bar{B}$ and temperature measurements T_{c_i} are combined to give estimates of impedance and admittance, \hat{Z}_i, \hat{Y} :

$$\hat{Z}_i = \hat{R}_0(1 + \hat{\alpha}(T_{c_i} - T_{c_0})) + j\bar{X}, \hat{Y} = \bar{G} + j\bar{B}. \quad (5.23)$$

Conversely, temperature estimates \hat{T}_{c_i} can be obtained from calculated resistance using the resistance-temperature model:

$$\hat{T}_{c_i} = (R_i - \hat{x}_0)/\hat{x}_1. \quad (5.24)$$

\hat{Z}_i, \hat{Y} and \hat{T}_{c_i} will be used in Section 5.2.3. Next, the second novel method will be explained.

5.2.2.2 New Method - Non-linear Least-squares (NMNL)

The second approach uses non-linear least-squares estimation, similarly to some of the existing impedance parameter estimation methods [111, 125]. Hence, the method is referred to as New Method - Non-linear Least-squares (NMNL). Suppose that measurements of voltage, current and temperature are available from $N \in \mathbb{N}$ time instants, where N is a constant. Unknown parameters will be estimated from a subset of measurements from $n \leq N$ time instants. Define a vector of unknowns $\mathbf{P} \in \mathbb{R}^{13}$,

$$\mathbf{P} = [\alpha, R_0, X, G, B, \text{Re}(a_s), \text{Im}(a_s), \text{Re}(b_s), \text{Im}(b_s), \text{Re}(a_r), \text{Im}(a_r), \text{Re}(b_r), \text{Im}(b_r)].$$

Rearrange (5.2) and (5.3) to give

$$\tilde{I}_{s_i} = \frac{1}{b_s} \left((a_s \tilde{V}_{s_i} - a_r \tilde{V}_{r_i})/Z_i + a_s \tilde{V}_{s_i} Y/2 \right) \quad (5.25)$$

$$\tilde{I}_{r_i} = \frac{1}{b_r} \left((a_s \tilde{V}_{s_i} - a_r \tilde{V}_{r_i})/Z_i - a_r \tilde{V}_{r_i} Y/2 \right), \quad (5.26)$$

where subscript $i = 1, 2, 3, \dots, n$ refers to measurements taken at time t_i , $Z_i = R_0(1 + \alpha(T_{c_i} - T_0)) + jX$ and $Y = G + jB$.

Define functions $f_{1_i}, f_{2_i}, f_{3_i}, f_{4_i} : \mathbb{R}^{13} \rightarrow \mathbb{R}$,

$$f_{1_i} = \operatorname{Re} \left(\frac{1}{\tilde{b}_s} ((\tilde{V}_{s_i} - \tilde{V}_{r_i})/Z_i + \tilde{V}_{s_i} Y/2) \right) \quad (5.27)$$

$$f_{2_i} = \operatorname{Im} \left(\frac{1}{\tilde{b}_s} ((\tilde{V}_{s_i} - \tilde{V}_{r_i})/Z_i + \tilde{V}_{s_i} Y/2) \right) \quad (5.28)$$

$$f_{3_i} = \operatorname{Re} \left(\frac{1}{\tilde{b}_r} ((\tilde{V}_{s_i} - \tilde{V}_{r_i})/Z_i - \tilde{V}_{r_i} Y/2) \right) \quad (5.29)$$

$$f_{4_i} = \operatorname{Im} \left(\frac{1}{\tilde{b}_r} ((\tilde{V}_{s_i} - \tilde{V}_{r_i})/Z_i - \tilde{V}_{r_i} Y/2) \right). \quad (5.30)$$

Note that $f_{1_i}, f_{2_i}, f_{3_i}, f_{4_i}$ are functions of the elements of \mathbf{P} by the definition of Z_i and Y . Combine $f_{1_i}, f_{2_i}, f_{3_i}, f_{4_i}$ into a vector of functions $\mathbf{F} \in \mathbb{R}^{4n}$, $\mathbf{F} = [f_{1_i}, f_{2_i}, f_{3_i}, f_{4_i}]$. Furthermore, define the measurement vector $\mathbf{M} \in \mathbb{R}^{4n}$, $\mathbf{M} = [\operatorname{Re}(\tilde{I}_{s_i}), \operatorname{Im}(\tilde{I}_{s_i}), \operatorname{Re}(\tilde{I}_{r_i}), \operatorname{Im}(\tilde{I}_{r_i})]$. The estimation model is given by the vector equation

$$\mathbf{M} = \mathbf{F}(\mathbf{P}) + \boldsymbol{\varepsilon}, \quad (5.31)$$

where $\boldsymbol{\varepsilon} \in \mathbb{R}^{4n}$ models measurement uncertainty. To find an optimal estimate of \mathbf{P} , minimize the $J \in \mathbb{R}$, which is defined according to the least-squares criterion,

$$J = [\mathbf{M} - \mathbf{F}(\mathbf{P})]^T [\mathbf{M} - \mathbf{F}(\mathbf{P})]. \quad (5.32)$$

The optimal estimate

$\hat{\mathbf{P}} = [\hat{\alpha}, \hat{R}_0, \hat{X}, \hat{G}, \hat{B}, \operatorname{Re}(\hat{a}_s), \operatorname{Im}(\hat{a}_s), \operatorname{Re}(\hat{b}_s), \operatorname{Im}(\hat{b}_s), \operatorname{Re}(\hat{a}_r), \operatorname{Im}(\hat{a}_r), \operatorname{Re}(\hat{b}_r), \operatorname{Im}(\hat{b}_r)]$ can be computed using an iterative algorithm such as a trust-region method [144]. Estimates for impedance and admittance are given by

$$\hat{Z}_i = \hat{R}_0(1 + \hat{\alpha}(T_{c_i} - T_0)) + j\hat{X}, \hat{Y} = \hat{G} + j\hat{B}. \quad (5.33)$$

Estimated correction factors $\hat{a}_s, \hat{b}_s, \hat{a}_r, \hat{b}_r$ are used in (5.5) to calculate resistance estimates \hat{R}_i , from which temperature estimates can be obtained:

$$\hat{T}_{c_i} = T_0 + \frac{1}{\hat{\alpha}\hat{R}_0}(\hat{R}_i - \hat{R}_0). \quad (5.34)$$

\hat{Z}_i, \hat{Y} and \hat{T}_{c_i} will be used in the next subsection to select optimal estimates of correction factors and resistance-temperature parameters.

5.2.3 Selection of optimal parameter estimates

Both methods introduced in Section 5.2.2 make use of n sets of measurements $\tilde{V}_{s_i}, \tilde{I}_{s_i}, \tilde{V}_{r_i}, \tilde{I}_{r_i}, T_{c_i}$ taken at times $t_i, i = 1, 2, 3, \dots, n$ to obtain values for correction factors a_s, a_r, b_s, b_r , and resistance-temperature parameters R_0, α . Estimated parameter values vary with the choice of measurement set, depending on load variation over the time window and the level and distribution of measurement noise. For this reason, it is proposed to estimate parameters from a range of measurement sets and to select the best results according to an optimality criterion.

Let $\Lambda \in \mathbb{N}$ be the number of subsets selected according to steps detailed in Appendix C.1 and \hat{Z}_{i_λ} and $\hat{Y}_\lambda, \lambda = 1, 2, 3, \dots, \Lambda$ the impedance parameter estimates obtained from each subset by the methods proposed in Section 5.2.2. To assess the accuracy of impedance parameter values, residuals $S_{V_\lambda}, S_{I_\lambda}$ of calculated receiving end voltage and current $\hat{V}_{r_i}, \hat{I}_{r_i}$ are evaluated. $\hat{V}_{r_i}, \hat{I}_{r_i}$ are calculated by rearranging (5.2) and (5.3):

$$\hat{V}_{r_i} = (1 + \hat{Y}_\lambda \hat{Z}_{i_\lambda} / 2)(a_{s_\lambda} \tilde{V}_{s_i}) - \hat{Z}_\lambda (b_{s_\lambda} \tilde{I}_{s_i}) \quad (5.35)$$

$$\hat{I}_{r_i} = (1 + \hat{Y}_\lambda \hat{Z}_{i_\lambda} / 2)(b_{s_\lambda} \tilde{I}_{s_i}) - (\hat{Y}_\lambda + \hat{Y}_\lambda^2 \hat{Z}_{i_\lambda})(a_{s_\lambda} \tilde{V}_{s_i}). \quad (5.36)$$

$S_{V_\lambda}, S_{I_\lambda} \in \mathbb{R}_{\geq 0}$ are the rms of the voltage and current residuals, respectively, given by:

$$S_{V_\lambda} = \sqrt{\frac{1}{N} \sum_{i=1}^N |\hat{V}_{r_i} - a_{r_\lambda} \tilde{V}_{r_i}|^2} \quad (5.37)$$

$$S_{I_\lambda} = \sqrt{\frac{1}{N} \sum_{i=1}^N |\hat{I}_{r_i} - b_{r_\lambda} \tilde{I}_{r_i}|^2}. \quad (5.38)$$

In addition, the rms of the temperature residuals S_{T_λ} is evaluated using temperature estimates \hat{T}_{c_i} and temperature measurements T_{c_i} . $S_{T_\lambda} \in \mathbb{R}_{\geq 0}$ is given by

$$S_{T_\lambda} = \sqrt{\frac{1}{N} \sum_{i=1}^N [\hat{T}_{c_i} - T_{c_i}]^2}. \quad (5.39)$$

$S_{V_\lambda}, S_{I_\lambda}, S_{T_\lambda}$ are combined to give a single quantity $S_{VIT_\lambda} : \mathbb{R}^3 \rightarrow \mathbb{R}_{\geq 0}$,

$$S_{VIT_\lambda}(S_{V_\lambda}, S_{I_\lambda}, S_{T_\lambda}) = S_{V_\lambda} S_{I_\lambda} S_{T_\lambda}. \quad (5.40)$$

Once S_{VIT_λ} has been evaluated for all Λ measurement sets, the optimal set of correction factors and resistance-temperature parameters is that with the minimum value of S_{VIT_λ} . The selected correction factors can then be used to calculate Z_i, Y_i and T_{c_i} from a set of synchrophasor measurements taken at any given time t_i .

5.3 Case study 1: physical simulation of three-phase measurements

This section presents the first of two case studies that will demonstrate the effectiveness of the novel methodology proposed in Section 5.2. The transmission line that was considered in Chapter 3 is also the subject of both case studies in this chapter. Details of the properties of the 330-kV, 521-km overhead line are therefore referred to Section 3.4.1. Measurements from the same 24-hour period were used. In the same manner as in Section 3.5.1, voltage measurements, theoretically calculated impedance parameters and conductor temperature were combined into a software simulation that provides ideal measurements from a line with known parameters.

5.3.1 Laboratory-based measurements

Values of voltage and current at the line ends were taken from the software simulation and used as input files for two physical waveform generators. The voltage and current signals were played out simultaneously, then captured by two power quality instruments that report time-tagged phasors at the fundamental frequency. A diagram of the experimental setup is shown in Figure 5.2. The waveform generators have a stated accuracy of $\pm 0.02\%$ in magnitude and $\pm 0.005^\circ$ in phase angle [145], while the power quality instruments have a stated accuracy of 0.1% [67]. The GPS antennae provide UTC to within $1\ \mu\text{s}$ to both the waveform generators and the power quality instruments.

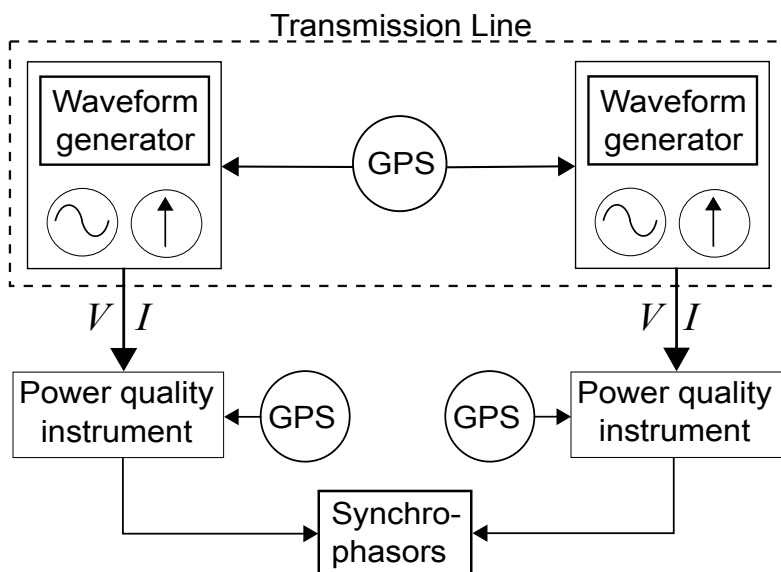


Figure 5.2: Experimental setup for laboratory-based synchrophasor measurements

By physically measuring the voltage and current signals, a realistic level of uncertainty due to the measurement units and time-tagging is introduced. Systematic errors in magnitudes and phase angles due to the remaining instrumentation channel were added to the reported phasors. Based on the accuracy classes of instrument transformers and characterization of instrumentation channels [52, 133, 134], errors in voltage and current magnitude were assumed to be up to $\pm 4\%$ and $\pm 6\%$, respectively, and errors in phase angle up to ± 0.04 rad and ± 0.07 rad for voltage and current, respectively. 100 cases of randomly selected systematic errors were applied to the phasor measurements.

5.3.2 Analysis of parameter estimation results

The phasor measurements from the 24-hour period gave $\Lambda = 34,924$ subsets that were chosen as detailed in Appendix C.1. From each subset of measurements, values of correction factors a_s, b_s, a_r, b_r were obtained by NMLT by solving optimization problem (5.18), and resistance temperature parameters R_0, α were determined using (5.20) to (5.22) assuming a value of $T_0 = 20^\circ\text{C}$; the non-linear least-squares problem defined by (5.27) to (5.32) was solved for each subset of measurements to identify $a_s, b_s, a_r, b_r, R_0, \alpha$ by NMNL. The optimal estimates from all subsets were chosen as described by (5.35) to (5.40) and then used to calculate impedance and admittance for the entire set of measurements using (5.5) to (5.7). For comparison, impedance parameters were also estimated by the selection of existing methods from Section 3.2. For the existing methods, a moving window spanning one hour of measurements was used in each estimation. The estimated values of positive sequence resistance were used to estimate average conductor temperature according to the linear-resistance temperature relationship (5.4), assuming a handbook value for α [17] and the theoretically calculated reference value for R_0 .

Firstly, the results for one individual case of systematic errors will be considered in detail, followed by a comparison of the effectiveness of new and existing methods across 100 cases. The accuracy of the impedance parameter estimation results will be assessed using the rms and standard deviation of the parameter errors as defined in Section 4.5.2. In the same manner as for conductance, the metrics $E_{\Delta T_c}$ and $\Sigma_{\Delta T_c}$ for temperature are calculated as absolute values rather than percentages (see equation (4.54)).

5.3.2.1 Individual case

Table 5.1 lists the systematic errors in magnitude and phase angle of voltage and current that have been applied in one individual case, together with the correction factors identified by the proposed methods NMLT and NMNL. It can be recognized that the corrections for V_s, V_r, I_s, I_r individually differ substantially from the systematic error; for example, the magnitude error in V_s is 0.79%, but the correction factors identified by the NMLT and NMNL methods are -0.0058% and 1.2% , respectively. However, the 'net' correction, i.e. the difference between receiving and sending end values for each quantity matches the 'net' systematic errors more closely.

Table 5.1: Systematic errors and corrections for one individual case

		V_s	V_r	Net ¹	I_s	I_r	Net ¹
Magnitude (%)	Systematic error	0.79	1.1	-0.31	-0.64	2.1	-2.7
	NMLT	-0.0058	-0.29	0.28	5.6	2.7	2.9
	NMNL	1.2	0.88	0.29	1.5	-1.2	2.7
Phase angle (mrad)	Systematic error	-5.9	28	-34	2.7	2.8	-0.10
	NMLT	12	-22	34	6.7	6.0	0.70
	NMNL	14	-20	34	2.2	1.9	0.35

¹ Difference between sending and receiving end values

Identified values of resistance-temperature parameters R_0 and α are 15.9Ω and 0.0039 , respectively, by NMLT and 15.6Ω and 0.0041 by NMNL, compared to reference values of 16.2Ω and 0.0039 .

Figure 5.3 shows values of positive sequence resistance R estimated by the two new methods and single-phase methods SM1, TLS1, NLOE1, TPLL1 as well as the nominal values that were put into the software simulation. It can be observed that the parameter values estimated by the proposed methods agree more closely with the nominal values than the selected existing methods. In contrast, the existing methods give parameter estimates with greater and more variable deviations. Similar observations can be made from graphs of estimated reactance, conductance and susceptance, which can be found in Appendix C.2.1.

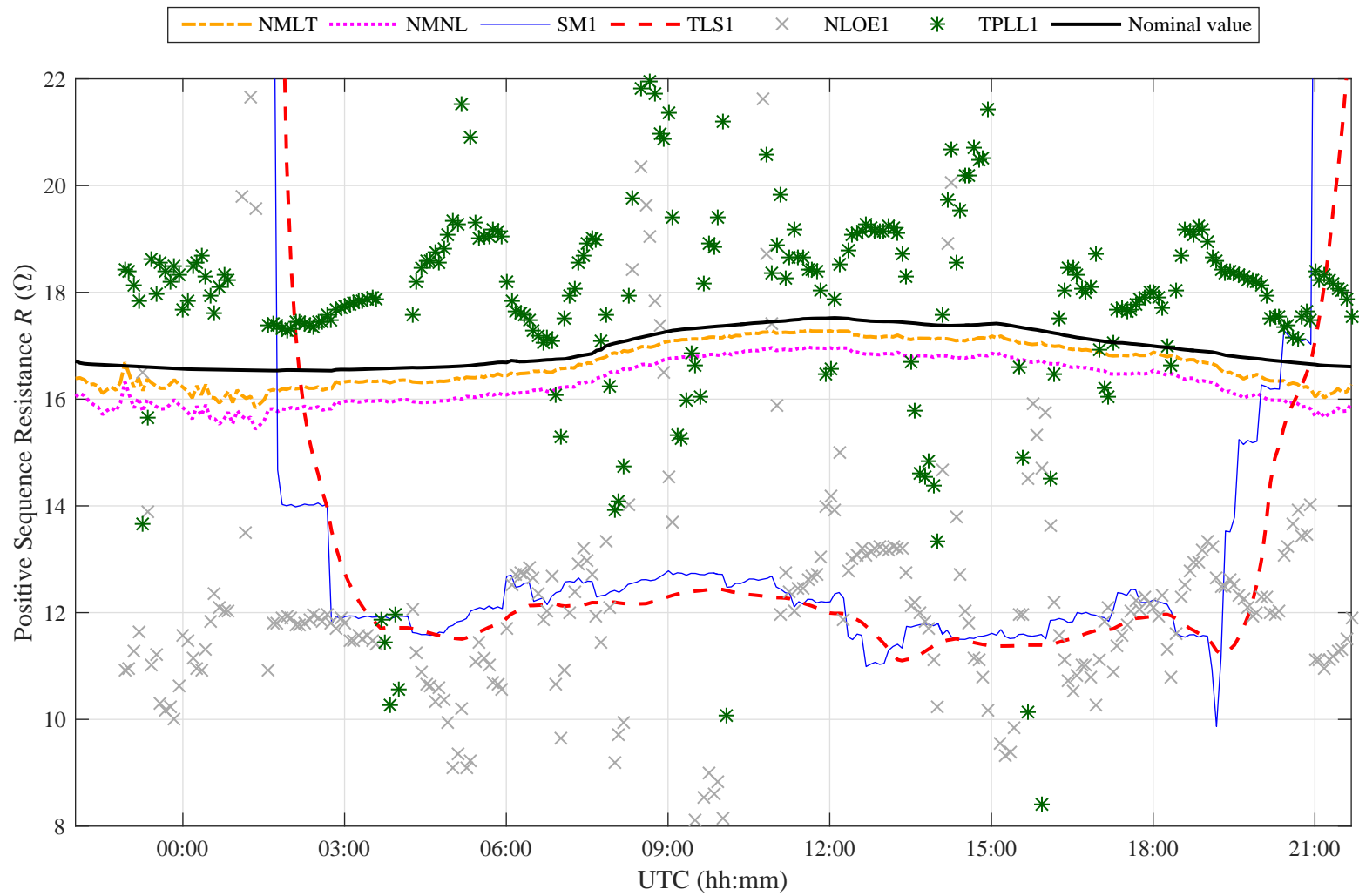


Figure 5.3: Nominal and estimated values of resistance R over time for the individual case

The observations from the graphs are confirmed by the values in Table 5.2, which lists the rms of errors in estimated impedance parameter and temperature values. While the rms error in resistance $E_{\Delta R}$ takes values of 1.8% and 3.8% for NMLT and NMNL, respectively, the existing methods give at least 16% and reach beyond 100%. For reactance, $E_{\Delta X}$ is lowest for estimates by NMNL at 1.1%, followed by 4.0% by NMLT; the existing methods give at least double these values, ranging from 10% to 134%. Some of the existing methods give lower values of rms error for susceptance $E_{\Delta B}$: SM1, TLS1, LLS3 and NLCO3 give 0.8%, while the new methods NMLT and NMNL resulted in 4.1% and 1.2%, respectively. With regards to estimates of conductance, the new method NMLT has an rms error $E_{\Delta G}$ of 3.9 μS , which is the same as three of the existing methods (TLS1, LLS3, NLCO3), which assume a constant value of zero for conductance. Both new methods give a value of 1.1 $^{\circ}\text{C}$ for $E_{\Delta T_c}$, while the existing methods have much larger errors ranging from 45 $^{\circ}\text{C}$ to over 1000 $^{\circ}\text{C}$.

Table 5.2: Rms of parameter errors for one individual case

	$E_{\Delta R}$ (%)	$E_{\Delta X}$ (%)	$E_{\Delta B}$ (%)	$E_{\Delta G}$ (μS)	$E_{\Delta T_c}$ ($^{\circ}\text{C}$)
NMLT	1.8	4.0	4.1	3.9	1.1
NMNL	3.8	1.1	1.2	6.2	1.1
SM1	103	29	0.8	31	271
TLS1	82	25	0.8	4	217
NLOE1	36	10	6.7	428	97
TPLL1	31	10	12.4	496	83
LLS3	170	16	0.8	4	447
NLLC3	3346	134	6.0e+05	4.9e+06	8764
NLCO3	16	10	1.4	4	45
TPLL3	404	85	236.7	1726	1079

Table 5.3 lists the standard deviation of errors Σ_{Δ} in estimated impedance and admittance parameters as well as temperature. The values of $\Sigma_{\Delta R}$ are 0.64% and 0.75% for NMLT and NMNL, respectively, but above 10% for the selected existing methods; hence, the new methods give more consistent resistance estimates, with lower error variability. Equivalent observations can be made for values of $\Sigma_{\Delta X}$. The difference in $\Sigma_{\Delta B}$ between new and existing methods is not as stark: NMLT and NMNL give a value of 0.2% and the SM1, TLS1, LLS3 and NLCO3 give greater standard deviations of error in susceptance, but all below 1%. For conductance, $\Sigma_{\Delta G}$ is two orders of magnitude smaller for the new methods than for the existing methods, except for TLS1, LLS3, NLCO3, which assume a constant value of zero. Errors in temperature estimates also have lower variability when the new methods

are used, which is indicated by values of $\Sigma_{\Delta T_c}$ of 1.1 °C compared to the existing methods, which give values ranging from 33 °C to over 1000 °C.

Table 5.3: Standard deviation of parameter errors for one individual case

	$\Sigma_{\Delta R}$ (%)	$\Sigma_{\Delta X}$ (%)	$\Sigma_{\Delta B}$ (%)	$\Sigma_{\Delta G}$ (μS)	$\Sigma_{\Delta T_c}$ (°C)
NMLT	0.64	0.19	0.22	0.22	1.1
NMNL	0.75	0.19	0.21	0.19	1.1
SM1	102	29	0.5	21	269
TLS1	82	25	0.4	0	217
NLOE1	26	10	6.6	353	71
TPLL1	30	9	11.9	453	81
LLS3	168	16	0.4	0	441
NLLC3	3346	99.6	6.0e+05	4.9e+06	8763
NLCO3	12	9	0.8	0	33
TPLL3	175	15	83.5	1726	463

5.3.2.2 All cases

The results given in the previous paragraphs were for one individual case of systematic measurement errors. Tables 5.4 and 5.5 show the 95th percentiles of the rms and standard deviation of the errors in estimated impedance parameter and temperature values for 100 cases of systematic errors. 95 % confidence intervals are given in square brackets next to the values; their width can be reduced by considering a larger number of cases. In this instance, 100 cases give confidence intervals that are of a smaller or the same order of magnitude as the percentile values, which allows for comparison of the methods.

The 95th percentile of rms errors in estimated resistance and temperature is significantly lower when the newly proposed methods are used compared to the eight existing methods. While the value for $E_{\Delta R}$ is below 10 % for both NMLT and NMNL, the other methods give values ranging from 30 % to over 400 %. Similarly for temperature, NMLT and NMNL achieve a 95th percentile of 1.1 °C and 1.2 °C for $E_{\Delta T_c}$, respectively, whereas the existing methods give at least 84 °C. For reactance, three of the existing methods (NLOE1, TPLL1, NLCO3) achieve 95th percentiles of $E_{\Delta X}$ as low as 10 % and 11 %, however, the new method NMLT has lower errors at 8.4 % and NMNL even yields 3.1 %. For susceptance, the SM1, TLS1, and LLS3 methods give slightly lower 95th percentiles of $E_{\Delta B}$ of about 7.5 % than NMLT at 8.4 %, but still double the value of NMNL at 3.1 %. The same three existing methods assume a constant value of zero for conductance, giving a value of 4 μS for $E_{\Delta G}$, which is the same as NMLT.

Table 5.4: 95th percentiles of the rms of parameter errors for 100 cases,
95 % confidence bounds are given in brackets

	$E_{\Delta R}$ (%)	$E_{\Delta X}$ (%)	$E_{\Delta B}$ (%)	$E_{\Delta G}$ (μS)	$E_{\Delta T_c}$ ($^{\circ}\text{C}$)
NMLT	5.4[4.8,6.0]	7.7[7.2,8.6]	8.4[7.8,9.3]	4.0[4.0,4.1]	1.1[1.1,1.1]
NMNL	7.0[6.0,7.7]	3.2[2.5,4.2]	3.1[2.5,4.1]	6.3[6.3,6.4]	1.2[1.2,1.2]
SM1	430[330,480]	31[27,38]	7.5[6.3,8.1]	120[94,130]	1100[860,1200]
TLS1	370[280,410]	27[23,32]	7.6[6.4,8.2]	4[4,4]	960[740,1100]
NLOE1	58[53,62]	11[11,11]	27.0[23.0,33.0]	590[540,650]	160[140,170]
TPLL1	65[57,73]	11[11,12]	29.0[26.0,34.0]	680[660,750]	170[150,200]
LLS3	420[350,500]	37[29,43]	7.5[6.4,8.2]	4[4,4]	1100[920,1300]
NLLC3	3700[1400,6000]	210[160,870]	4.7e+06[3.6e+06,6.6e+06]	6.5e+07[5.2e+07,1.2e+08]	1.0e+04[3.7e+03,1.6e+04]
NLCO3	31[25,36]	10[9,11]	5.1[4.6,6.0]	4[4,4]	84[69,96]
TPLL3	450[440,460]	92[91,93]	300.0[290.0,310.0]	2700[2300,3200]	1200[1200,1200]

In contrast, the other existing methods give values greater than $100\ \mu\text{S}$, which would account for a current loss along the line of the order of $33\ \text{kA}$.

Table 5.5 shows the 95th percentiles of the standard deviation of the errors in estimated impedance parameter and temperature values for 100 cases of systematic errors. It can be seen that the error variability is lower for the new methods NMLT and NMNL than for the existing methods. More specifically, the values are below 1% for resistance, reactance and susceptance when the new methods are used, but at least 15%, 7% and 2%, respectively, for the existing methods. Similarly, for conductance, the 95th percentile of $\Sigma_{\Delta G}$ is at $0.3\ \mu\text{S}$ for new methods, but reaches beyond $1\ \text{mS}$ for some of the existing methods. For temperature estimates, the new methods give values below $1.5\ ^\circ\text{C}$, while the existing methods give values at least ten times larger.

Table 5.5: 95th percentiles of the standard deviation of parameter errors for 100 cases, 95 % confidence bounds are given in brackets

	$\Sigma_{\Delta R}$ (%)	$\Sigma_{\Delta X}$ (%)	$\Sigma_{\Delta B}$ (%)	$\Sigma_{\Delta G}$ (μS)	$\Sigma_{\Delta T_c}$ ($^{\circ}\text{C}$)
NMLT	0.7[0.7,0.7]	0.2[0.2,0.2]	0.23[0.22,0.23]	0.3[0.3,0.3]	1.1[1.1,1.2]
NMNL	0.8[0.8,0.8]	0.2[0.2,0.2]	0.22[0.22,0.22]	0.3[0.3,0.4]	1.2[1.2,1.2]
SM1	430[330,470]	31[27,38]	3.0[2.6,3.3]	42[37,48]	1100[870,1200]
TLS1	370[280,410]	27[23,32]	2.9[2.5,3.1]	0[0,0]	960[740,1100]
NLOE1	30[29,31]	10[10,11]	9.3[8.6,10.0]	440[430,440]	82[78,83]
TPLL1	32[32,33]	10[10,10]	16.0[15.0,17.0]	550[540,550]	86[85,87]
LLS3	420[340,500]	36[28,43]	2.8[2.5,3.1]	0[0,0]	1100[900,1300]
NLLC3	3700[1400,6000]	190[140,870]	5e+06[4e+06,7e+06]	7e+07[5e+07,1e+08]	1e+04[4e+03,2e+04]
NLCO3	15[14,16]	7[6,9]	2.1[1.9,2.6]	0[0,0]	41[37,43]
TPLL3	210[200,210]	19[18,20]	210.0[200.0,240.0]	2700[2300,3200]	560[530,570]

5.3.3 Discussion of results

The results of the case study show that the parameter identification methods that have been proposed in Section 5.2 can be used to calculate values of overhead line impedance and admittance as well as temperature with higher accuracy than a selection of eight existing methods. For a variety of cases of systematic errors, estimates of resistance, reactance and susceptance within 10% of known values were achieved. The superior performance of the new methods is attributed to various factors.

In contrast to all but one of the existing methods (NLLC3), the new methods include systematic measurement errors in the estimation model. Moreover, instead of treating resistance as a constant parameter, resistance-temperature variation is taken into account, such that longer measurement periods can be utilized to estimate correction factors, reference resistance and resistance-temperature coefficient. Finally, a range of possible measurement sets are considered and the best results are chosen based on data validation. On the other hand, the existing methods treat resistance as a quasi-constant quantity, which limits the time span and thus operational states of the measurements that are utilized in real-time parameter estimation. Especially the three-phase methods are thus prone to badly conditioned problem formulations, resulting in high error sensitivity in the estimation process.

Since the two new methods estimate and validate model parameters from a large number of measurement subsets, there is an initial computational burden. However, once correction factors and resistance-temperature parameters are identified, the real-time calculation of impedance parameters has the same computational cost as the SM1 method, which is lower than most other existing methods that are based on linear or non-linear estimation theory. While both new methods, NMLT and NMNL, have performed better in this case study than the selection of existing methods and achieved the same accuracy for estimated temperature, they have some differences. Errors in resistance and conductance as given by NMLT occupy lower ranges than those given by NMNL, but the opposite is true for reactance and susceptance. However, the level of variation in parameter estimation accuracy is the same.

In this case study, transmission line measurements have been emulated using laboratory-based apparatus, providing a partially realistic, and controllable scenario. The effectiveness of the new methods when field measurements from an actual overhead line system are used will be investigated in the next section.

5.4 Case study 2: field measurements

In the last section, the newly proposed methods have been used to estimate line impedance parameter and temperature values with greater accuracy than a selection of existing methods. The utilized synchrophasor measurements were taken from a laboratory-based, emulated transmission line and contaminated with systematic errors.

In this case study, the novel and existing methods will be tested on actual field measurements from the same line that was considered in Sections 3.4 and 5.3. Up to this point, only measurements from one 22-hour period have been used. For comparison, results for the same measurements will be presented in detail in this section. Moreover, the correction factors and resistance-temperature parameters identified from measurements from this time period have been used to calculate line impedance parameters and temperature in real-time for nine other 22-hour periods spread over ten months, which will also be presented. Furthermore, results from a cross validation will be given, whereby all ten 22-hour periods have been used to estimate correction factors and resistance-temperature parameters that were then used to calculate real-time impedance, admittance and temperature values for all ten 22-hour periods. The ten 22-hour periods will be referred to as Days 1 to 10; Day 8 refers to the 22-hour period that was considered in Chapter 3 and Section 5.3.

Figure 5.4 shows the level of active power for each 22-hour period, averaged between the sending and receiving ends; the graph illustrates the differences in overall level of power flow and daily load variation. In addition to synchrophasor measurements, the new methods require values of average conductor temperature as inputs. Since this field measurement campaign did not include such measurements, conductor temperature has been calculated from known conductor properties, weather data and line current measurements as described in Section 3.4.1.2 and Appendix A.3. The resulting temperature profiles are shown in Figure 5.5. The daily variation of 15 °C to 20 °C is similar for all 22-hour periods, however, the overall temperature levels differ due to seasonal levels of ambient temperature, solar radiation and line current.

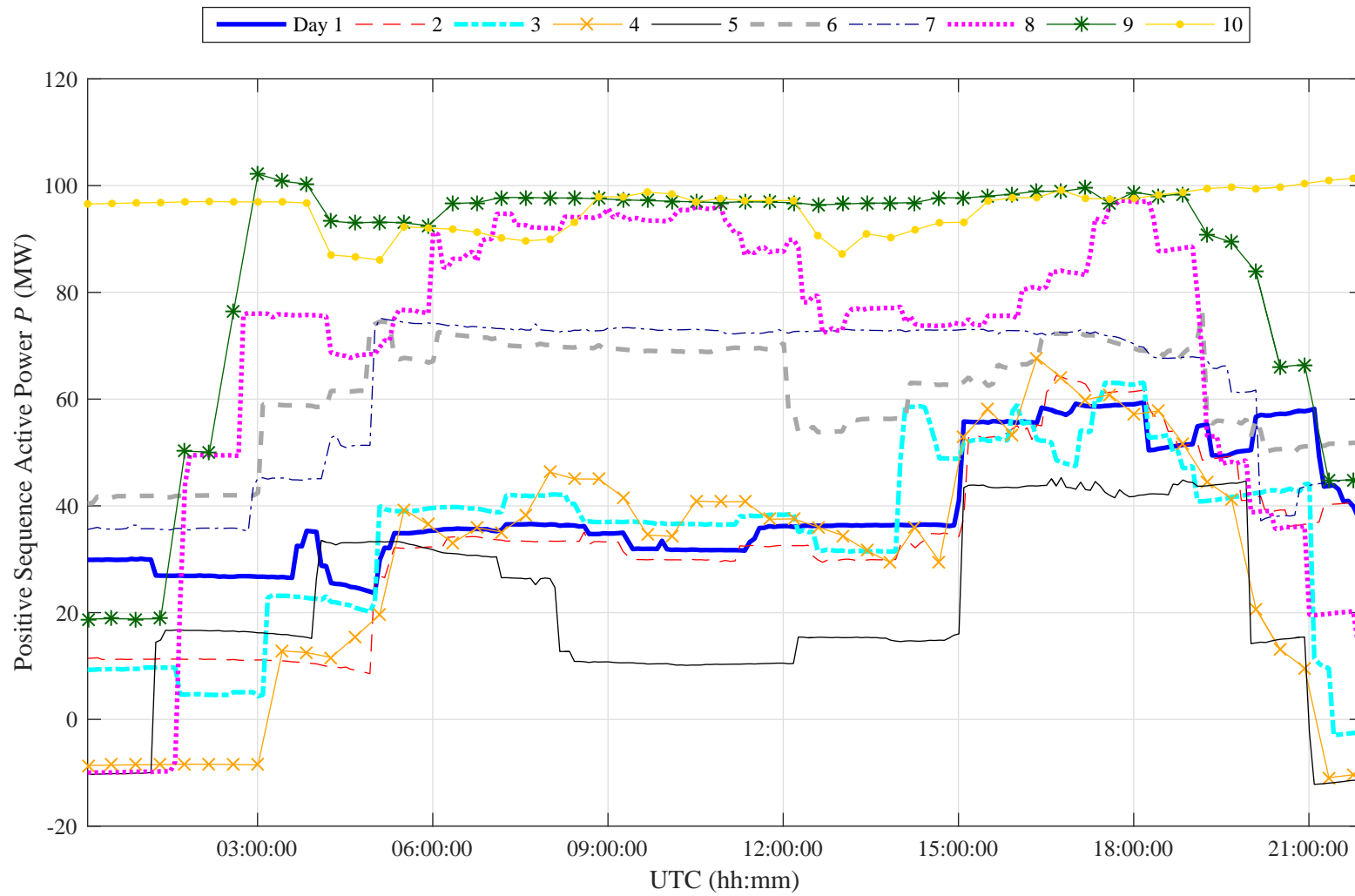


Figure 5.4: Mean values of sending and receiving end active power for ten 22-hour periods

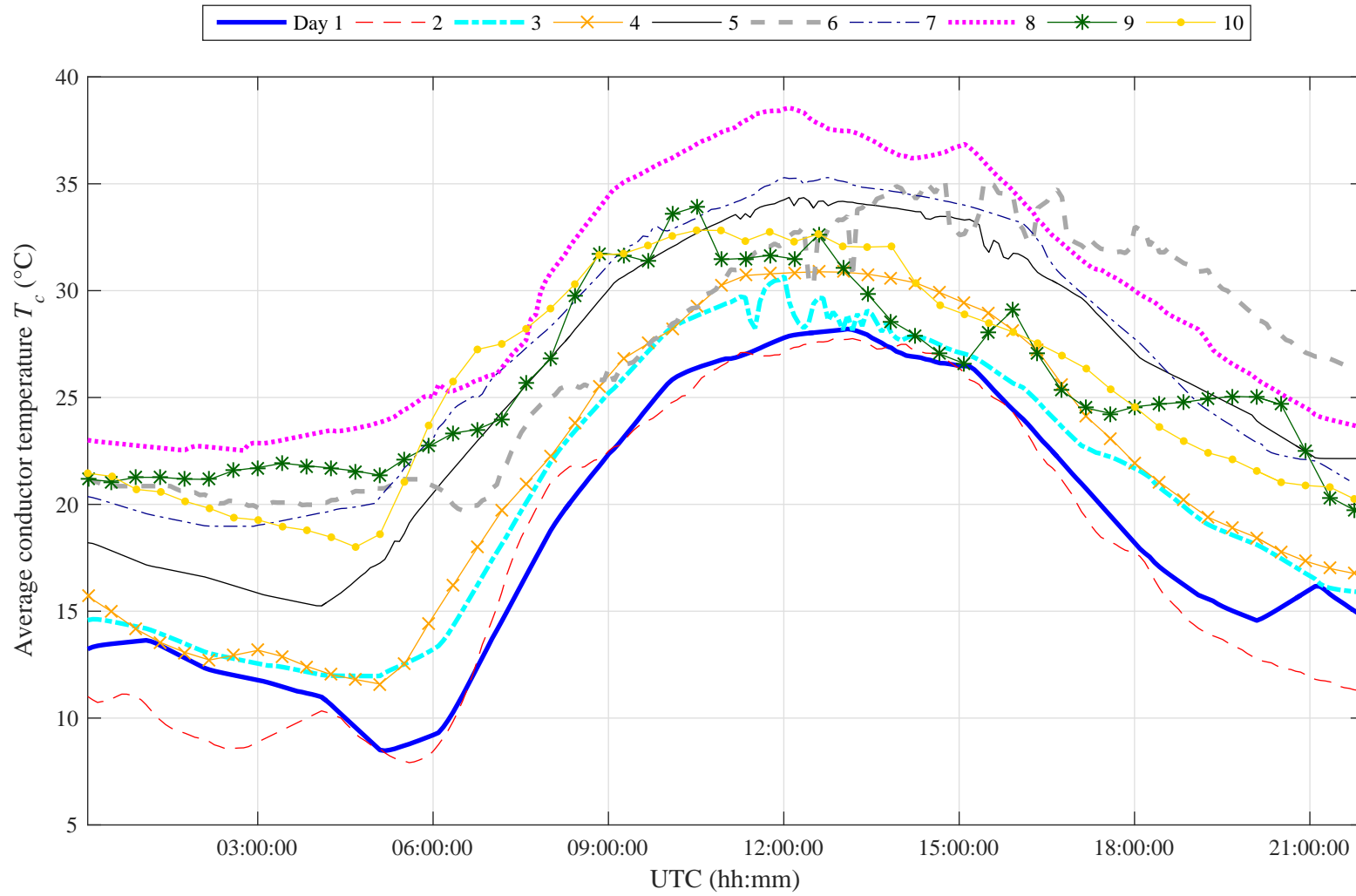


Figure 5.5: Calculated average conductor temperature for ten 22-hour periods

5.4.1 Analysis of parameter estimation results

The accuracy of calculated impedance and admittance will be assessed by the acceptability criteria defined in Section 3.3, a summary of which is given in Table 5.6.

Table 5.6: Limits for acceptable parameter estimates

	Median of estimated parameter values over a given time period	Interdecile Range (IDR) of estimated parameter values over a given time period
Resistance	within $\pm 50\%$ of the theoretical value	less than maximum of $\{0.8\%$ of theoretical reference value, 150% of theoretical range $\}$
Reactance		less than 5% of the theoretical parameter value
Susceptance		
Conductance	within $\pm 10\%$ of (minimum line current/nominal phase voltage)	less than 10% of (minimum line current/nominal phase voltage)

5.4.1.1 Results for Day 8

The following results have been obtained by estimating correction factors for synchrophasor measurements (a_s, a_r, b_s, b_r) as well as reference resistance R_0 at $T_c = 20^\circ\text{C}$ and resistance-temperature coefficient α as described in Section 5.2.2 using measurements from Day 8 and then calculating impedance parameters and temperature using (5.5) to (5.7). Table 5.7 shows the identified values of the correction factors for both methods NMLT and NMNL. As for the first case study, the two methods give differing values for the correction factors of V_s, V_r, I_s, I_r , but the net error values match more closely.

Table 5.7: Values of identified correction factors for Day 8

		V_s	V_r	Net ¹	I_s	I_r	Net ¹
Magnitude (%)	NMLT	-3.8	-2.8	-0.95	-3.7	7.6	-11
	NMNL	5.6	6.7	-1.05	-9.9	0.49	-10
Phase angle (mrad)	NMLT	41	47	-5.5	-30	-55	26
	NMNL	33	39	-5.6	-43	-68	25

¹ Difference between sending and receiving end values

Figure 5.6 shows the resistance estimates for Day 8 obtained in this way, as well as resistance estimates obtained by the single-phase methods as presented in Section 3.2.1. It can be observed that the new methods NMLT and NMNL give values between $10\ \Omega$ to $20\ \Omega$, forming smooth curves over the entire time period, while the single-phase methods result in values occupying the range $0\ \Omega$ to $60\ \Omega$. Graphs of reactance, conductance and susceptance estimates can be found in Appendix C.3.1.

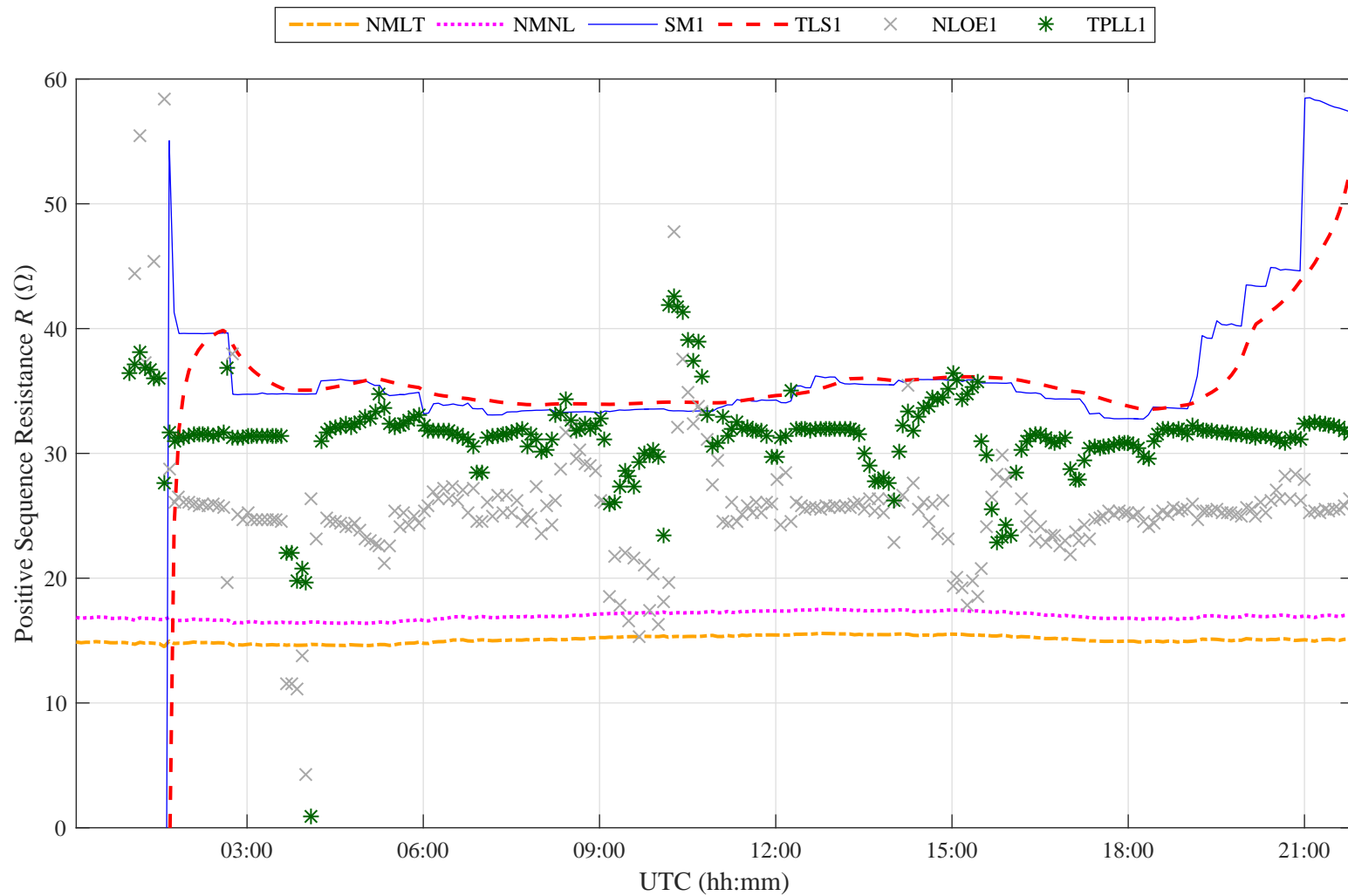


Figure 5.6: Estimated values of resistance R over time for Day 8, by the new methods and existing single-phase methods

Identified values of resistance-temperature parameters R_0 and α are $14.6\ \Omega$ and 0.0037 , respectively, by NMLT and $16.4\ \Omega$ and 0.0032 by NMNL, compared to reference values of $16.2\ \Omega$ and 0.0039 . Figure 5.7 shows the estimated temperature values, including the nominal, i.e. the theoretically calculated values. The estimates from the new methods fall within $0\ ^\circ\text{C}$ to $50\ ^\circ\text{C}$ and follow the curve described by the theoretical values. The existing single-phase methods, on the other hand, mainly give estimates between $150\ ^\circ\text{C}$ and $400\ ^\circ\text{C}$, which is outside the normal operating range of typical Aluminium Conductor Steel Reinforced (ACSR) conductors [146].

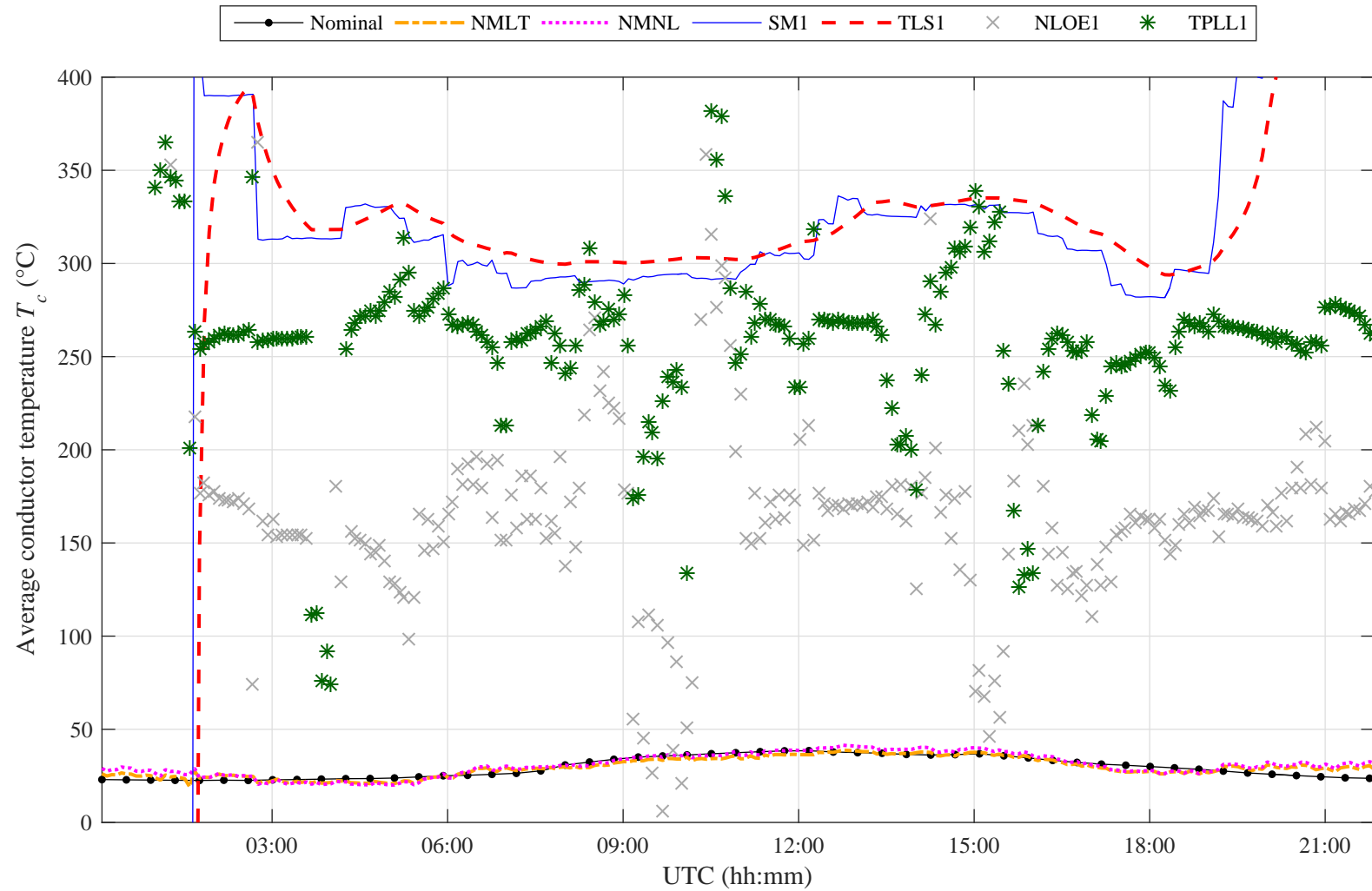


Figure 5.7: Estimated values of conductor temperature T_c over time for Day 8, by the new methods and existing single-phase methods

Table 5.8 lists the acceptability of estimated impedance parameters for Day 8, according to the criteria in Table 3.4. The two novel methods, NMLT and NMNL, give acceptable values for estimated resistance, reactance, conductance and susceptance and are thus the only methods that have an overall score of 8. The highest scoring existing methods, TLS1 and LLS3, lag behind with a score of 6 because of unacceptable values of median and IDR of estimated resistance over the time period. Numerical values of median and IDR for each parameter are given in the Appendix in Table C.1.

Table 5.8: Acceptability of estimated impedance and admittance parameters for Day 8, numerical values are given in Table C.1

	Resistance		Reactance		Conductance		Susceptance		Score ³
	M ¹	IDR ²	M	IDR	M	IDR	M	IDR	
NMLT	✓	✓	✓	✓	✓	✓	✓	✓	8
NMNL	✓	✓	✓	✓	✓	✓	✓	✓	8
SM1	✗	✗	✓	✓	✓	✗	✓	✓	5
TLS1	✗	✗	✓	✓	✓	✓	✓	✓	6
NLOE1	✗	✗	✓	✗	✗	✗	✓	✗	2
TPLL1	✗	✗	✓	✗	✗	✗	✓	✗	2
LLS3	✗	✗	✓	✓	✓	✓	✓	✓	6
NLLC3	✗	✗	✗	✗	✗	✗	✗	✗	0
NLCO3	✓	✗	✓	✗	✓	✓	✓	✗	5
TPLL3	✗	✗	✓	✗	✗	✗	✓	✗	2

¹ Median

² Interdecile Range

³ Number of acceptable values (maximum 8)

Table 5.9 gives the rms error $E_{\Delta T_c}$ and standard deviation of errors $\Sigma_{\Delta T_c}$ in estimated temperature for Day 8. NMLT and NMNL both give a value of 2.4 °C for $E_{\Delta T_c}$, while the existing methods reach values between 85 °C and 1200 °C. Similarly, $\Sigma_{\Delta T_c}$ is 3 °C for the new methods, but at least ten times as large for the existing ones.

Table 5.9: Rms error $E_{\Delta T_c}$ and standard deviation of errors $\Sigma_{\Delta T_c}$ in estimated temperature for Day 8

	NMLT	NMNL	SM1	TLS1	NLOE1	TPLL1	LLS3	NLLC3	NLCO3	TPLL3
$E_{\Delta T_c}$ (°C)	2.4	3.1	374	331	195	239	344	518	85	1181
$\Sigma_{\Delta T_c}$ (°C)	2.4	2.9	293	198	125	77	200	464	37	512

The values for correction factors a_s, a_r, b_s, b_r and resistance-temperature parameters R_0, α that were identified by NMLT and NMNL from Day 8 measurements were used to calculate impedance parameters and temperature estimates not only for Day 8, but all ten 22-hour periods, Days 1 to 10. For comparison, values were also calculated using the selection of eight existing methods. Table 5.10 lists the number of days out of ten, for which each method resulted in acceptable values for median and IDR of resistance, reactance, conductance and susceptance. The rightmost column lists the sum of the scores in each row, hence, the maximum total score is 80. All numerical values are given in the Appendix, Table C.2. In Table 5.10, it can be observed that the new method NMLT gives acceptable values for median and IDR of reactance, conductance and susceptance on all ten days; NMNL follows closely, only failing on one day for the IDR of reactance. Both new methods achieve acceptable values for the IDR of resistance estimates on seven days, which is 30% below the ideal score of ten, but still more than twice the maximum score achieved by existing methods.

Table 5.10: Estimation day 8 - number of days with acceptable estimated values of Median (M) and Interdecile Range (IDR) of each parameter, and the total number of acceptable values over ten days, numerical values are given in Table C.2.

	Resistance		Reactance		Conductance		Susceptance		Total (max 80)
	M	IDR	M	IDR	M	IDR	M	IDR	
NMLT	●	●	●	●	●	●	●	●	77
NMNL	●	●	●	●	●	●	●	●	76
SM1	●	●	●	●	●	●	●	●	44
TLS1	●	●	●	●	●	●	●	●	59
NLOE1	●	●	●	●	●	●	●	●	21
TPLL1	●	●	●	●	●	●	●	●	23
LLS3	●	●	●	●	●	●	●	●	55
NLLC3	●	●	●	●	●	●	●	●	2
NLCO3	●	●	●	●	●	●	●	●	69
TPLL3	●	●	●	●	●	●	●	●	14

Legend:

0 1 2 3 4 5 6 7 8 9 10

● ● ● ● ● ● ● ● ● ● ●

Table 5.11 shows values of rms and standard deviation of temperature estimates for Days 1 to 10 obtained by the new and existing methods, numerical values are given in the Appendix, Table C.3. Table 5.11 illustrates that errors in estimated conductor temperature across the ten days are lower and less variable if the new methods NMLT and NMNL are employed, compared to the use of the eight existing methods. In fact, both rms error $E_{\Delta T_c}$ and standard deviation of error $\Sigma_{\Delta T_c}$ are less than 20 °C on six days for NMLT, which does not apply for any of the existing methods on any one day.

Table 5.11: Estimation day 8 - rms error $E_{\Delta T_c}$ and standard deviation of error $\Sigma_{\Delta T_c}$ of estimated temperature values, numerical values are given in Tables C.3 and C.4

Day	1	2	3	4	5	6	7	8	9	10
NMLT	●◆	●◆	●◆	●◆	●◆	●◆	●◆	●◆	●◆	●◆
NMNL	●◆	●◆	●◆	●◆	●◆	●◆	●◆	●◆	●◆	●◆
SM1	●◆	●◆	●◆	●◆	●◆	●◆	●◆	●◆	●◆	●◆
TLS1	●◆	●◆	●◆	●◆	●◆	●◆	●◆	●◆	●◆	●◆
NLOE1	●◆	●◆	●◆	●◆	●◆	●◆	●◆	●◆	●◆	●◆
TPLL1	●◆	●◆	●◆	●◆	●◆	●◆	●◆	●◆	●◆	●◆
LLS3	●◆	●◆	●◆	●◆	●◆	●◆	●◆	●◆	●◆	●◆
NLLC3	●◆	●◆	●◆	●◆	●◆	●◆	●◆	●◆	●◆	●◆
NLCO3	●◆	●◆	●◆	●◆	●◆	●◆	●◆	●◆	●◆	●◆
TPLL3	●◆	●◆	●◆	●◆	●◆	●◆	●◆	●◆	●◆	●◆

Legend:
Value in °C ≤ 20 ≤ 40 ≤ 60 ≤ 80 ≤ 100 ≤ 250 ≤ 500 ≤ 750 ≤ 1000 > 1000
 $E_{\Delta T_c}$ ● ◆
 $\Sigma_{\Delta T_c}$ ◆ ◆

5.4.1.2 Cross validation

In addition to Day 8, synchrophasor measurements from the other nine 22-hour periods have also been used to identify values for correction factors a_s, a_r, b_s, b_r and resistance-temperature parameters R_0, α by the new methods, NMLT and NMNL. To validate the correction factors and resistance-temperature parameters for each estimation day, they have been used to estimate impedance parameters and temperature for Days 1 to 10. Tables 5.12 and 5.13 show the number of days with acceptable values of impedance parameters for each estimation day for NMLT and NMNL, respectively. Tables C.5 and C.6 in the Appendix list the numerical scores.

From Table 5.12 it can be seen that values of median resistance, reactance, conductance as well as IDR of conductance and susceptance are acceptable for all ten days regardless of which measurement period was used for estimation of $a_s, a_r, b_s, b_r, R_0, \alpha$. The IDR of resistance is always acceptable for at least half of the validation days, with scores ranging from five to eight; scores for existing methods are between zero and three as shown in Table 5.10. For the median of susceptance, acceptability has fallen to two out of ten days for estimation day 6. The reason is that the median for the remaining eight days is 2.38 mS, which exceeds the theoretical line susceptance by 52 %, whereas the acceptable range is defined as ± 50 %.

Table 5.12: Number of days with acceptable estimated values of Median (M) and Interdecile Range (IDR), when correction factors and resistance-temperature parameters are estimated from Days 1 to 10 by NMLT, numerical values are given in Table C.5

Estimation day	Resistance		Reactance		Conductance		Susceptance		Total (max 80)
	M	IDR	M	IDR	M	IDR	M	IDR	
1	●	●	●	●	●	●	●	●	71
2	●	●	●	●	●	●	●	●	74
3	●	●	●	●	●	●	●	●	78
4	●	●	●	●	●	●	●	●	77
5	●	●	●	●	●	●	●	●	78
6	●	●	●	●	●	●	●	●	69
7	●	●	●	●	●	●	●	●	77
8	●	●	●	●	●	●	●	●	77
9	●	●	●	●	●	●	●	●	75
10	●	●	●	●	●	●	●	●	74

Legend:

0 1 2 3 4 5 6 7 8 9 10

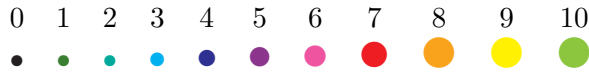
● ● ● ● ● ● ● ● ● ● ●

In contrast, if NMNL is used, median values for all impedance parameters are acceptable on all days, irrespective of the estimation day as can be seen in Table 5.13. The same is true for the IDR of calculated conductance and susceptance. In the same manner as for NMLT, the IDR of resistance estimates is unacceptable for a number of days. In fact, the score is five out of ten for estimation days 1, 7 and 10 and only on estimation day 6 does the score reach eight acceptable days.

Table 5.13: Number of days with acceptable estimated values of Median (M) and Interdecile Range (IDR), when correction factors and resistance-temperature parameters are estimated from Days 1 to 10 by NMNL, numerical values are given in Table C.6

Estimation day	Resistance		Reactance		Conductance		Susceptance		Total (max 80)
	M	IDR	M	IDR	M	IDR	M	IDR	
1	●	●	●	●	●	●	●	●	71
2	●	●	●	●	●	●	●	●	77
3	●	●	●	●	●	●	●	●	77
4	●	●	●	●	●	●	●	●	77
5	●	●	●	●	●	●	●	●	76
6	●	●	●	●	●	●	●	●	78
7	●	●	●	●	●	●	●	●	75
8	●	●	●	●	●	●	●	●	76
9	●	●	●	●	●	●	●	●	75
10	●	●	●	●	●	●	●	●	74

Legend:



Tables 5.14 and 5.15 illustrate the size of the rms and standard deviation of errors in temperature estimates obtained from the cross validation of methods NMLT and NMNL, respectively. Numerical values are given in the Appendix in Tables C.7 to C.10. Both Tables 5.14 and 5.15 show that $E_{\Delta T_c}$ and $\Sigma_{\Delta T_c}$ are less than or equal to 20°C for the majority of validations; in particular, estimation days 6 to 10 give low errors on all validation days, except for Day 2, when rms errors reach 50°C and 54°C for NMLT and NMNL, respectively. Day 2 is also the weakest estimation day, giving rms errors above 20°C on eight out of ten validation days. The days on which both $E_{\Delta T_c}$ and $\Sigma_{\Delta T_c}$ are below 20°C are the same for the two methods NMLT and NMNL. However, on some other days, NMNL has been less effective than NMLT: on validation day 1, NMNL resulted in rms errors up to 105°C whereas the maximum rms error for NMLT is 68°C and on validation day 8, NMNL gives rms errors up to 60°C whereas the maximum rms error for NMLT is 48°C .

Table 5.14: Cross validation of NMLT - each column gives the rms error $E_{\Delta T_c}$ and standard deviation of errors $\Sigma_{\Delta T_c}$ in calculated temperature, numerical values are given in Tables C.7 and C.8

		Validation day									
		1	2	3	4	5	6	7	8	9	10
Estimation day	1	●◆	●◆	●◆	●◆	●◆	●◆	●◆	●◆	●◆	●◆
	2	●◆	●◆	●◆	●◆	●◆	●◆	●◆	●◆	●◆	●◆
	3	●◆	●◆	●◆	●◆	●◆	●◆	●◆	●◆	●◆	●◆
	4	●◆	●◆	●◆	●◆	●◆	●◆	●◆	●◆	●◆	●◆
	5	●◆	●◆	●◆	●◆	●◆	●◆	●◆	●◆	●◆	●◆
	6	●◆	●◆	●◆	●◆	●◆	●◆	●◆	●◆	●◆	●◆
	7	●◆	●◆	●◆	●◆	●◆	●◆	●◆	●◆	●◆	●◆
	8	●◆	●◆	●◆	●◆	●◆	●◆	●◆	●◆	●◆	●◆
	9	●◆	●◆	●◆	●◆	●◆	●◆	●◆	●◆	●◆	●◆
	10	●◆	●◆	●◆	●◆	●◆	●◆	●◆	●◆	●◆	●◆

Legend:
 Value in °C ≤ 20 ≤ 40 ≤ 60 ≤ 80
 $E_{\Delta T_c}$ ● ● ● ● ●
 $\Sigma_{\Delta T_c}$ ◆ ◆ ◆ ◆ ◆

Table 5.15: NMNL - each column gives the rms and standard deviation of errors in calculated temperature, numerical values are given in Tables C.9 and C.10

		Validation day									
		1	2	3	4	5	6	7	8	9	10
Estimation day	1	●◆	●◆	●◆	●◆	●◆	●◆	●◆	●◆	●◆	●◆
	2	●◆	●◆	●◆	●◆	●◆	●◆	●◆	●◆	●◆	●◆
	3	●◆	●◆	●◆	●◆	●◆	●◆	●◆	●◆	●◆	●◆
	4	●◆	●◆	●◆	●◆	●◆	●◆	●◆	●◆	●◆	●◆
	5	●◆	●◆	●◆	●◆	●◆	●◆	●◆	●◆	●◆	●◆
	6	●◆	●◆	●◆	●◆	●◆	●◆	●◆	●◆	●◆	●◆
	7	●◆	●◆	●◆	●◆	●◆	●◆	●◆	●◆	●◆	●◆
	8	●◆	●◆	●◆	●◆	●◆	●◆	●◆	●◆	●◆	●◆
	9	●◆	●◆	●◆	●◆	●◆	●◆	●◆	●◆	●◆	●◆
	10	●◆	●◆	●◆	●◆	●◆	●◆	●◆	●◆	●◆	●◆

Legend:
 Value in °C ≤ 20 ≤ 40 ≤ 60 ≤ 80 ≤ 100 ≤ 250
 $E_{\Delta T_c}$ ● ● ● ● ● ● ●
 $\Sigma_{\Delta T_c}$ ◆ ◆ ◆ ◆ ◆ ◆ ◆

5.4.2 Discussion of results

The case study results presented in this section clearly show that for the field measurements of the overhead line under consideration, the novel methods are more effective than the selection of eight existing methods. Especially the acceptability of estimated resistance and conductor temperature with respect to theoretically calculated values has been increased. Further, it has been demonstrated that one day of measurements suffices for the new methods to identify correction factors for systematic errors as well as parameters of the resistance-temperature relationship that can be used to calculate impedance parameter estimates with acceptable accuracy, in particular from independent measurements from other time periods.

A fundamental difference between the newly proposed methods and existing ones is that measurement correction factors as well as thermal variability of resistance are taken into account in the system model. Moreover, these parts of the model are assumed to be unknown, and only by their identification is it possible to establish a measurement model that can be used in real-time calculations. The identified model is validated using conductor temperature measurements, creating a means to assess the reliability of real-time parameter estimation results, which is necessary for practical implementation purposes.

Out of the two proposed methods, NMLT has shown slightly stronger performance in this case study than NMNL, and may thus be the preferred method. However, NMNL has the benefit of easier implementation as this method consists of only one non-linear least-squares problem, whose solution simultaneously yields estimates of correction factors and resistance-temperature parameters. NMNL on the other hand, requires the solution of two sub-problems, the first being a non-linear constraint optimization problem to identify correction factors, and the second a linear least-squares fit to obtain estimated values of resistance-temperature parameters.

Both methods require temperature measurements as initial inputs, but subsequent real-time overhead line monitoring is entirely based on synchrophasor measurements of voltage and current. This case study provided a semi-simulated scenario since synchrophasor measurements from the field were used, but weather data, line current and calculated conductor properties were used to calculate a realistic temperature profile. The next step towards further validation of the new methods is a case study based on direct conductor temperature measurements. Furthermore, validation on other overhead lines with different lengths and load profiles is desirable, since the results from this case study cannot necessarily be generalized to other systems.

5.5 Conclusion

In this chapter, a modified problem formulation for parameter estimation of overhead line systems has been presented. Instead of focusing on direct estimation of impedance parameters, two novel methods for estimation of correction factors and resistance-temperature parameters as well as a procedure for selecting optimal parameter values from different measurement sets of voltage, current and conductor temperature have been proposed. The identified correction factors and resistance-temperature parameters serve as a refinement to the overhead line electro-thermal model, such that series impedance and shunt admittance can be monitored in real-time using simple closed-form calculations. Of the two proposed methods, one uses traditional non-linear least-squares estimation while the other method consists of an optimization procedure that minimizes variability of impedance and admittance over time.

In two case studies, one fully and another semi-simulated, both methods have shown superior performance in comparison to existing synchrophasor-based impedance parameter estimation methods, especially with regards to providing an acceptable level of accuracy for calculated resistance and temperature values. The optimization-based method was slightly more accurate than the method based on non-linear least-squares estimation, especially when applied to field measurements.

For practical applications in power networks, the proposed methods can be utilized to determine correction factors and resistance-temperature parameters that can then be stored in databases of network management systems and thus support applications such as state estimation, protection, fault location, dynamic thermal line rating and safety monitoring. An initial measurement campaign for collecting synchrophasor and line temperature data is necessary, but all or at least some of the instrumentation does not have to be installed permanently.

Chapter 6

Conclusion

This chapter concludes this thesis. Section 6.1 gives a summary of how the contributions address the problem statement and discusses their relevance with respect to wider developments in power systems research and Section 6.2 provides an overview of future research directions.

6.1 Summary and discussion of contributions to knowledge

The central problem of this thesis was the identification of overhead line impedance parameters from synchronized phasor measurements of voltage and current such that average conductor temperature can be tracked. The motivation for investigation of this problem arises primarily from the importance of line impedance parameter values to a range of power system monitoring and control applications. These applications underpin the reliable and safe operation of electricity networks, as was described in the introduction to this thesis in Chapter 1, Section 1.1. A detailed problem statement was also given in the first chapter in Section 1.2, along with the summarizing illustration shown in Figure 6.1.

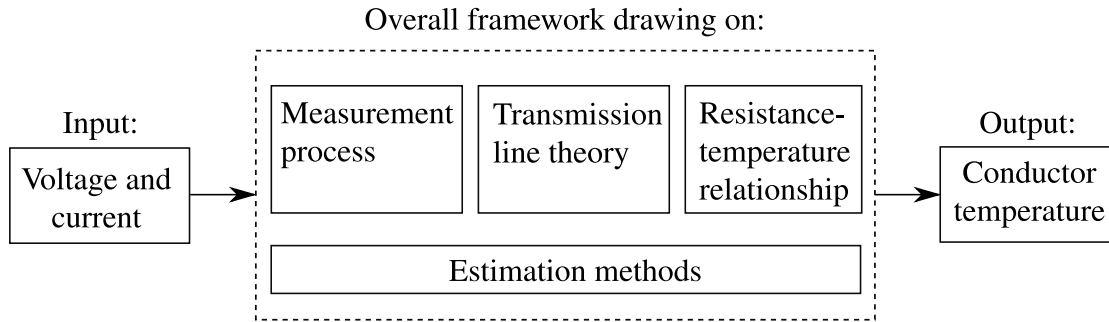


Figure 6.1: Illustration of the problem addressed in this thesis

To begin with, a literature review was presented in Chapter 2, examining previous work related to overhead line impedance parameter identification. Existing methods were analysed in terms of their assumptions about the synchrophasor measurement process, transmission line theory and parameter estimation. It was found that there is a lack of methods designed to identify line impedance parameters in real-time with an accuracy that is sufficient to track changes in average conductor temperature under practical, real-world field conditions such as random and systematic measurement errors. The need to understand specific strengths and weaknesses of existing methods was recognised to provide a basis for development of new methodology.

This need was met in Chapter 3 of this thesis. Two main findings resulted from a comparative assessment based on synchrophasor measurement data from an actual overhead line:

1. Out of eight methods that were found in the literature review in Chapter 2, with differing assumptions about measurement and overhead line modelling as well as numerical estimation, none was able to identify impedance parameters consistently with acceptable accuracy for the line under consideration.
2. Systematic errors in the phasor measurements as well as poor conditioning of the parameter estimation problems are practical obstacles to accurate tracking of overhead line impedance and average conductor temperature.

Thus, a concrete problem formulation of practical relevance emerged from Chapter 3: how can impedance parameters be monitored accurately using synchrophasor measurements with unknown systematic errors? This question became the subject of Chapter 4, which contributed a novel method for the identification of measurement correction factors, enabling increased accuracy of real-time impedance parameter calculation. The novelty of the method is distinguished by its utiliza-

tion of information about the dynamic behaviour of overhead line impedance and admittance; specifically, time-variance of series resistance and time-invariance of series reactance and shunt parameters. The effectiveness of the innovative method was demonstrated in two case studies, the first involving a laboratory-based short line model and the second a software simulation of a medium-length line. The results show that the proposed method can reduce the variability in impedance parameter estimates compared to an existing method.

The contribution of Chapter 5 centres around achieving reliability in impedance-based conductor temperature estimation as well as robustness in the identification of correction factors and impedance parameters. The parameters of the resistance-temperature relationship for the overhead line are assumed to be unknown and identified from measured data, instead of assuming fixed values found in handbooks. The conditioning of the estimation problem is improved by making use of conductor temperature measurements. Two estimation methods were proposed to obtain values for correction factors and resistance-temperature parameters, in addition to an algorithm for finding optimal results from different measurement sets. The effectiveness of this innovative approach was demonstrated in two case studies; one on a laboratory-based, emulated overhead line and the second study validated the novel methods on field data spanning a ten-month period. The case study results show that the novel methods can increase the accuracy of estimated impedance parameters and temperature values by at least one order of magnitude compared to previously proposed methods.

The development and effectiveness of the novel methods presented in this thesis have shown that a fundamental shift in assumptions has the potential to greatly advance power network modelling. Conventionally, fixed model structures were assumed for overhead lines and other network components; some parameter values were even assumed to be known based on theoretical calculations and general material properties. The improvements in synchrophasor-based overhead line impedance monitoring in this thesis were achieved by questioning these modelling assumptions, importantly by including additional model parameters. The demonstrated strengths of this approach should initiate a move towards more adaptive network modelling, taking into account the individual and dynamic characteristics of each power system component and associated data collection instrumentation.

The wide-spread development of WAMPAC systems means that synchrophasor measurements are becoming available at an increasing number of nodes in power systems, hence, wide-area adaptive and dynamic system identification is becoming a practical possibility.

The creation of more accurate and dynamic network models is not only an application of WAMPAC systems, but supplements a range of other operational activities that are facilitated or enhanced by synchrophasor measurements. Operational planning, real-time state estimation, protection as well as fault analysis and prevention are some of the tasks that are critical to security of electricity supply and which benefit from increased system visibility and situational awareness.

To summarize, in this thesis, practical limitations of existing work on overhead line impedance parameter identification were revealed and addressed with novel contributions. Building on the contributions in this thesis, directions for further research are outlined in the next section.

6.2 Future work

In this thesis, novel contributions have been made to increase the accuracy of synchrophasor-based overhead line impedance parameter monitoring. In this final section, attention is brought to potential areas for further research.

Comparison with other novel methods The calibration of synchrophasor measurements within the context of overhead line impedance parameter monitoring is an imminent challenge that is attracting the attention of many researchers. During the final stages of writing this thesis, Pisani *et al.* have presented an adaptive sensing framework for overhead line conductor monitoring using synchrophasor measurements [147], including a preliminary calibration process using line temperature measurements. Since synchrophasor-based overhead line impedance monitoring is an ongoing area of research, further publications of different novel methods are expected in the near future. Therefore, an interesting piece of future work will be a comparative study that investigates the estimation accuracy and sensitivity to various non-ideal conditions of the methods proposed in this thesis, Pisani *et al.*'s work and further relevant publications. Based on such a comparison, the strongest aspects of each method can be combined to further generalize and advance the reliability of synchrophasor-based overhead line impedance monitoring.

Detection and modelling of systematic measurement errors The novel methods contributed in this thesis have focussed on addressing the problem of monitoring line impedance parameters using synchrophasor measurements with systematic errors. A useful topic for further research is the automated detection of systematic measurement errors; an effective detection mechanism can facilitate a more customized selection of impedance parameter estimation methods. Potential approaches include residual analysis, or as recently proposed by Khandeparkar *et al.*, analysing the bias of calculated shunt conductance values [148].

Another specific point for further investigation is the model of the systematic errors; in this thesis, a constant, multiplicative complex factor was assumed that linearly scales amplitudes and is additive to phase angles. However, the systematic errors can be non-linear and vary significantly over time or along the measurement range of the instruments. By developing an adaptive error model, for instance using genetic algorithms, compensation of systematic errors can be generalized to further increase impedance parameter estimation accuracy.

More efficiency in selection of measurements Estimated measurement correction factors and resistance-temperature parameters depend on the selection of measurements which differ due to uncertainty as well as variation in operating conditions. In this thesis an enumerative algorithm for selection of the best parameter estimates from different measurement sets was given. There is an incentive to increase numerical efficiency through a more systematic selection algorithm.

Time sensitivity of measurement campaign In this thesis, novel methods have been proposed to improve the accuracy of real-time line impedance monitoring through estimation of measurement correction factors and resistance-temperature parameters. A further aspect of investigation is the optimal timing and length of the initial required measurement campaign including conductor temperature measurements. The need to save time and minimize costs has to be balanced against the requirement to validate estimated parameter values under diverse environmental and system operating conditions. Hence, determination of the sensitivity of parameter values to time and length of the measurement campaign is an important area for future work.

Untransposed lines The focus of this thesis is on real-time monitoring of positive sequence impedance parameters, assuming a transposed line with geometrical symmetry. For untransposed lines, the sequence components do not decouple, which means the single-phase equivalent model is an approximate representation. It would be of interest to apply and adapt the newly proposed methods to three-phase transmission line models to obtain self and mutual impedance parameters as well as calibration factors for the individual phases. Measurement of unbalanced conditions, including faults, can help to reduce ill-conditioning of the parameter estimation problems.

Application in medium and low voltage networks The novel methodology was applied mostly on high voltage overhead transmission lines. However, network constraints can also occur in low voltage distribution networks, especially due to increases in embedded generation. Therefore, a possible area for future work is extension of the proposed methods to measurements from medium and low voltage distribution lines, which are often underground cables. Another consequence of embedded generation of solar and wind power are higher levels of harmonics in distribution networks, which are considered to be a power quality problem that can reduce the lifetime of transformers and other network assets. Knowledge of

harmonic impedance is required for network modelling and design of harmonic filters. The proposed methodology can be adapted to increase accuracy of harmonic impedance determination.

References

- [1] U.S. Energy Information Administration. (2016). International Energy Outlook 2016 - Report Number DOE/EIA-0484(2016), [Online]. Available: <https://www.eia.gov/outlooks/archive/ieo16/electricity.php> (visited on 27/08/2017).
- [2] A. G. Phadke, “Synchronized phasor measurements in power systems,” *IEEE Computer Applications in Power*, vol. 6, no. 2, pp. 10–15, Apr. 1993.
- [3] S. Chakrabarti, E. Kyriakides, Tianshu Bi, Deyu Cai and V. Terzija, “Measurements get together,” *IEEE Power and Energy Magazine*, vol. 7, no. 1, pp. 41–49, Jan. 2009.
- [4] P. Wall, P. Dattaray, Z. Jin, P. Mohapatra, J. Yu, D. Wilson, K. Hay, S. Clark, M. Osborne, P. M. Ashton, V. Terzija and P. M. Ashton, “Deployment and demonstration of wide area monitoring system in power system of Great Britain,” *Journal of Modern Power Systems and Clean Energy*, vol. 4, no. 3, pp. 506–518, 2016.
- [5] V. Terzija, M. Osborne, P. Wall and D. Cai, “Roadmap for the deployment of WAMPAC in the future GB power system,” *IET Generation, Transmission & Distribution*, vol. 10, no. 7, pp. 1553–1562, May 2016.
- [6] V. Terzija, G. Valverde, Deyu Cai, P. Regulski, V. Madani, J. Fitch, S. Skok, M. M. Begovic and A. Phadke, “Wide-Area monitoring, protection, and control of future electric power networks,” *Proceedings of the IEEE*, vol. 99, no. 1, pp. 80–93, Jan. 2011.
- [7] A. Abur and A. G. Exposito, *Power System State Estimation: Theory and Implementation*. Boca Raton, FL: CRC Press, Taylor & Francis Group, 2004.
- [8] *IEEE Guide for Determining Fault Location on AC Transmission and Distribution Lines*. IEEE Std C37.114, 2014.

- [9] R. Schulze, P. Schegner and R. Zivanovic, "Parameter identification of unsymmetrical transmission lines using fault records obtained from protective relays," *IEEE Transactions on Power Delivery*, vol. 26, no. 2, pp. 1265–1272, Apr. 2011.
- [10] Arbiter Systems, *Model 1133a Power Sentinel GPS-synchronized Power Quality Revenue Standard Operation Manual*, Paso Robles, CA, 2013.
- [11] Y. Cong, P. Regulski, P. Wall, M. Osborne and V. Terzija, "On the use of dynamic thermal-line ratings for improving operational tripping schemes," *IEEE Transactions on Power Delivery*, vol. 31, no. 4, pp. 1891–1900, Aug. 2016.
- [12] D. Ritzmann, J. Rens, P. S. Wright, W. Holderbaum and B. Potter, "A novel approach to noninvasive measurement of overhead line impedance parameters," *IEEE Transactions on Instrumentation and Measurement*, vol. 66, no. 6, pp. 1155–1163, Jun. 2017.
- [13] D. Ritzmann, P. S. Wright, W. Holderbaum and B. Potter, "A method for accurate transmission line impedance parameter estimation," *IEEE Transactions on Instrumentation and Measurement*, vol. 65, no. 10, pp. 2204–2213, Oct. 2016.
- [14] D. Ritzmann, W. Holderbaum, B. Potter and P. Wright, "Improving the accuracy of synchrophasor-based overhead line impedance measurement," in *2015 IEEE International Workshop on Applied Measurements for Power Systems (AMPS)*, IEEE, Sep. 2015, pp. 132–137.
- [15] D. Ritzmann, P. S. Wright, W. Holderbaum and B. Potter, "Application and analysis of synchrophasor-based online impedance measurement methods," in *23rd International Conference on Electricity Distribution (CIRED)*, Lyon, 2015.
- [16] B. M. Weedy, B. J. Cory, N. Jenkins, J. B. Ekanayake and G. Strbac, *Electric Power Systems*, 5th ed., Chichester: John Wiley & Sons, 2012.
- [17] L. Kirkpatrick, *Aluminum Electrical Conductor Handbook*, 3rd ed., Aluminum Association, 1989.
- [18] T. Gönen, *Electrical Power Transmission System Engineering: Analysis and Design*, 3rd ed., Boca Raton, FL: CRC Press, 2014.
- [19] W. Thomson, "On the Theory of the Electric Telegraph," *American Journal of Physics*, vol. 7, pp. 382–399, 1855.

- [20] O. Heaviside, “Electromagnetic Induction and its Propagation,” in *Electrical Papers Volume I*, London: Macmillan, 1892, pp. 429–560.
- [21] J. L. R. d. Alembert, “Recherches sur la courbe que forme une corde tendue mise en vibration,” in *Memoires de l’Academie royale des sciences et belles lettres. Classe de mathematique. Année 1747*, Berlin: Haude, 1749, pp. 214–219.
- [22] L. J. B. Bergeron, *Du Coup de Bélier en Hydraulique - Au Coup de Foudre en Electricité*. Paris: Dunod, 1950.
- [23] H. W. Dommel, “Digital computer solution of electromagnetic transients in single- and multiphase networks,” *IEEE Transactions on Power Apparatus and Systems*, vol. PAS-88, no. 4, pp. 388–399, 1969.
- [24] T. Sekine, K. Kobayashi and S. Yokokawa, “Transient analysis of lossy nonuniform transmission line using the finite difference time domain method,” *Electronics and Communications in Japan (Part III: Fundamental Electronic Science)*, vol. 85, no. 8, pp. 1–10, Aug. 2002.
- [25] C. R. Paul, “A brief history of work in transmission lines for EMC applications,” *IEEE Transactions on Electromagnetic Compatibility*, vol. 49, no. 2, pp. 237–252, May 2007.
- [26] K. S. Kunz and R. J. Luebbers, *The Finite Difference Time Domain Method for Electromagnetics*. CRC Press, 1993.
- [27] O. Heaviside, *Electromagnetic Theory Volume I*. London: The Electrician, 1893.
- [28] F. Breisig, *Theoretische Telegraphie: Eine Anwendung der Maxwellschen Elektrodynamik auf Vorgänge in Leitungen und Schaltungen*. Braunschweig: Druck und Verlag von Friedrich Vieweg & Sohn, 1924.
- [29] F. Strecker and R. Feldtkeller, *Grundlagen der Theorie des allgemeinen Vierpols: Mitteilg aus d. Patentabt. u. d. Zentrallaboratorium d. Wernerwerkes d. Siemens u. Halske A.-G.* Berlin: Siemens u. Halske A.-G., 1929.
- [30] A. E. Kennelly, *The Application Of Hyperbolic Functions To Electrical Engineering Problems*, 2nd ed., New York, NY: Mcgraw-Hill Book Company, 1916, p. 28.
- [31] L. Wedepohl, “Application of matrix methods to the solution of travelling-wave phenomena in polyphase systems,” *Proceedings of the Institution of Electrical Engineers*, vol. 110, no. 12, pp. 2200–2212, 1963.

- [32] D. E. Hedman, "Propagation on overhead transmission lines I - Theory of modal analysis," *IEEE Transactions on Power Apparatus and Systems*, vol. 84, no. 3, pp. 200–205, Mar. 1965.
- [33] C. L. Fortescue, "Method of symmetrical co-ordinates applied to the solution of polyphase networks," *Proceedings of the American Institute of Electrical Engineers*, vol. 37, no. 6, pp. 629–716, Jun. 1918.
- [34] E. Clarke, *Circuit Analysis of A-C Power Systems Volume I: Symmetrical and Related Components*. New York, NY: John Wiley & Sons, 1943.
- [35] H. V. Nguyen, H. W. Dommel and J. R. Marti, "Modelling of single-phase nonuniform transmission lines in electromagnetic transient simulations," *IEEE Transactions on Power Delivery*, vol. 12, no. 2, pp. 916–921, Apr. 1997.
- [36] A. Semlyen, "Some frequency domain aspects of wave propagation on nonuniform lines," *IEEE Transactions on Power Delivery*, vol. 18, no. 1, pp. 315–322, Jan. 2003.
- [37] V. Cecchi, A. S. Leger, K. Miu and C. O. Nwankpa, "Incorporating temperature variations into transmission-line models," *IEEE Transactions on Power Delivery*, vol. 26, no. 4, pp. 2189–2196, 2011.
- [38] J. R. Marti, H. W. Dommel, L. Marti and V. Brandwajn, "Approximate transformation matrices for unbalanced transmission lines," in *9th Power System Computation Conference*, London, 1987, pp. 416–422.
- [39] F. Castellanos, J. Martí and F. Marcano, "Phase-domain multiphase transmission line models," *International Journal of Electrical Power & Energy Systems*, vol. 19, no. 4, pp. 241–248, May 1997.
- [40] J. Brandao Faria and J. Hildemaro Briceno, "On the modal analysis of asymmetrical three-phase transmission lines using standard transformation matrices," *IEEE Transactions on Power Delivery*, vol. 12, no. 4, pp. 1760–1765, 1997.
- [41] A. Prado, S. Kurokawa, J. P. Filho and L. F. Bovolato, "Step by step analyses of Clarke's matrix correction procedure for untransposed three-phase transmission line cases," in *IEEE PES General Meeting*, IEEE, Jul. 2010, pp. 1–9.
- [42] CIGRE Working Group 22.12, "The thermal behavior of overhead conductors," Tech. Rep., 2002.

- [43] *IEEE Standard for Calculating the Current-Temperature Relationship of Bare Overhead Conductors*. IEEE Standard 738-2012, 2013.
- [44] H. B. Dwight, “Sag calculations for transmission lines,” *Transactions of the American Institute of Electrical Engineers*, vol. XLV, pp. 796–805, Jan. 1926.
- [45] D. O. Ehrenburg, “Transmission line catenary calculations,” *Transactions of the American Institute of Electrical Engineers*, vol. 54, no. 7, pp. 719–728, Jul. 1935.
- [46] J. R. Carson, “Wave propagation in overhead wires with ground return,” *Bell System Technical Journal*, vol. 5, no. 4, pp. 539–554, Oct. 1926.
- [47] H. W. Dommel, “Overhead line parameters from handbook formulas and computer programs,” *IEEE Transactions on Power Apparatus and Systems*, vol. PAS-104, no. 2, pp. 366–372, Feb. 1985.
- [48] —, *Electromagnetic Transients Program Theory Book*. Portland, OR: Bonneville Power Administration, 1987.
- [49] A. Russell, *A Treatise on the Theory of Alternating Currents Volume I*. Cambridge: University Press, 1904, pp. 99–102.
- [50] G. Kron, *Tensor Analysis of Networks*. New York, NY: John Wiley & Sons, 1939.
- [51] M. Hesse, “Electromagnetic and electrostatic transmission-line parameters by digital computer,” *IEEE Transactions on Power Apparatus and Systems*, vol. 82, no. 66, pp. 282–291, Jun. 1963.
- [52] *IEEE Guide for Synchronization, Calibration, Testing, and Installation of Phasor Measurement Units (PMUs) for Power System Protection and Control*. IEEE Standard C37.242, 2013.
- [53] A. G. Phadke, “Synchronized phasor measurements - a historical overview,” in *IEEE/PES Transmission and Distribution Conference and Exhibition*, IEEE, 2002, pp. 476–479.
- [54] A. G. Phadke and J. S. Thorp, *Synchronized Phasor Measurements and Their Applications*, ser. Power Electronics and Power Systems. Boston, MA: Springer US, 2008.
- [55] P. Castello, P. Ferrari, A. Flammini, C. Muscas and S. Rinaldi, “A New IED with PMU functionalities for electrical substations,” *IEEE Transactions on Instrumentation and Measurement*, vol. 62, no. 12, pp. 3209–3217, Dec. 2013.

- [56] *IEEE Standard for Synchrophasor Measurements for Power Systems*. IEEE Standard C37.118.1, 2011.
- [57] J. De La Ree, V. A. Centeno, J. S. Thorp and A. G. Phadke, “Synchronized phasor measurement applications in power systems,” *IEEE Transactions on Smart Grid*, vol. 1, no. 1, pp. 20–27, Jun. 2010.
- [58] A. G. Phadke, J. S. Thorp and M. G. Adamiak, “A new measurement technique for tracking voltage phasors, local system frequency, and rate of change of frequency,” *IEEE Power Engineering Review*, vol. PER-3, no. 5, pp. 23–23, May 1983.
- [59] J.-Z. Yang and C.-W. Liu, “A precise calculation of power system frequency and phasor,” *IEEE Transactions on Power Delivery*, vol. 15, no. 2, pp. 494–499, Apr. 2000.
- [60] P. Zhang, H. Xue, R. Yang and J. Zhang, “Shifting window average method for phasor measurement at offnominal frequencies,” *IEEE Transactions on Power Delivery*, vol. 29, no. 3, pp. 1063–1073, 2014.
- [61] M. Wang and Y. Sun, “A practical method to improve phasor and power measurement accuracy of DFT algorithm,” *IEEE Transactions on Power Delivery*, vol. 21, no. 3, pp. 1054–1062, 2006.
- [62] R. K. Mai, Z. Y. He, L. Fu, B. Kirby and Z. Q. Bo, “A dynamic synchrophasor estimation algorithm for online application,” *IEEE Transactions on Power Delivery*, vol. 25, no. 2, pp. 570–578, Apr. 2010.
- [63] H. C. Wood, N. G. Johnson and M. S. Sachdev, “Kalman filtering applied to power system measurements relaying,” *IEEE Transactions on Power Apparatus and Systems*, vol. PAS-104, no. 12, pp. 3565–3573, Dec. 1985.
- [64] V. V. Terzija, M. B. Djuric and B. D. Kovacevic, “Voltage phasor and local system frequency estimation using newton type algorithm,” *IEEE Transactions on Power Delivery*, vol. 9, no. 3, pp. 1368–1374, Jul. 1994.
- [65] J. A. de la O Serna, “Synchrophasor estimation using Prony’s method,” *IEEE Transactions on Instrumentation and Measurement*, vol. 62, no. 8, pp. 2119–2128, Aug. 2013.
- [66] G. Barchi, D. Macii and D. Petri, “Synchrophasor estimators accuracy: A comparative analysis,” *IEEE Transactions on Instrumentation and Measurement*, vol. 62, no. 5, pp. 963–973, May 2013.
- [67] CT LAB, *Impedo DUO Power Quality Recorder User Manual*, Stellenbosch, South Africa, 2015.

- [68] North American SynchroPhasor Initiative (NASPI), “Synchrophasor measurement accuracy characterization,” Performance & Standards Task Team, Tech. Rep., 2007.
- [69] A. P. S. Meliopoulos and G. J. Cokkinides, “Visualization and animation of instrumentation channel effects on DFR data accuracy,” in *Proceedings of the 2002 Georgia Tech Fault and Disturbance Analysis Conference*, Atlanta, Georgia, 2002, pp. 1–7.
- [70] Q. Zhang, V. Vittal, G. T. Heydt, N. Logic and S. Sturgill, “The integrated calibration of synchronized phasor measurement data in power transmission systems,” *IEEE Transactions on Power Delivery*, vol. 26, no. 4, pp. 2573–2581, Oct. 2011.
- [71] D. Shi, D. J. Tylavsky and N. Logic, “An adaptive method for detection and correction of errors in PMU measurements,” *IEEE Transactions on Smart Grid*, vol. 3, no. 4, pp. 1575–1583, Dec. 2012.
- [72] M. Zhou, V. A. Centeno, J. S. Thorp and A. G. Phadke, “Calibrating instrument transformers with phasor measurements,” *Electric Power Components and Systems*, vol. 40, no. 14, pp. 1605–1620, Oct. 2012.
- [73] A. Pal, P. Chatterjee, J. S. Thorp and V. A. Centeno, “Online calibration of voltage transformers using synchrophasor measurements,” *IEEE Transactions on Power Delivery*, vol. 31, no. 1, pp. 370–380, Feb. 2016.
- [74] L. Ljung, *System Identification: Theory for the User*, 2nd ed., Upper Saddle River, NJ: Prentice-Hall, 1997.
- [75] P. Eykhoff, *System Identification: Parameter and State Estimation*, 1st ed., Chichester: John Wiley & Sons, 1974.
- [76] R. Fisher, “On an absolute criterion for fitting frequency curves,” *Messenger of Mathematics*, vol. 41, no. 1, pp. 155–160, 1912.
- [77] A. C. Aitken, “IV. On least squares and linear combination of observations,” *Proceedings of the Royal Society of Edinburgh*, vol. 55, pp. 42–48, Sep. 1936.
- [78] S. M. Stigler, “Gauss and the invention of least squares,” *The Annals of Statistics*, vol. 9, no. 3, pp. 465–474, May 1981.
- [79] G. H. Golub and C. F. van Loan, “An analysis of the total least squares problem,” *SIAM Journal on Numerical Analysis*, vol. 17, no. 6, pp. 883–893, Dec. 1980.
- [80] R. L. Plackett, “Some theorems in least squares,” *Biometrika*, vol. 37, no. 1-2, pp. 149–57, Jun. 1950.

- [81] B. Farhang-Boroujeny, *Adaptive Filters*. Chichester: John Wiley & Sons, Apr. 2013.
- [82] B. Widrow and M. E. Hoff, "Adaptive switching circuits," in *1960 IRE WESCON Convention Record*, Los Angeles, CA, 1960, pp. 96–104.
- [83] R. E. Kalman, "A new approach to linear filtering and prediction problems," *Journal of Basic Engineering*, vol. 82, no. 1, pp. 35–45, Mar. 1960.
- [84] R. E. Kalman and R. S. Bucy, "New results in linear filtering and prediction theory," *Journal of Basic Engineering*, vol. 83, no. 1, pp. 95–108, Mar. 1961.
- [85] F. Schweppe and J. Wildes, "Power system static-state estimation, Part I: Exact model," *IEEE Transactions on Power Apparatus and Systems*, vol. PAS-89, no. 1, pp. 120–125, Jan. 1970.
- [86] F. Schweppe and D. Rom, "Power system static-state estimation, Part II: Approximate model," *IEEE Transactions on Power Apparatus and Systems*, vol. PAS-89, no. 1, pp. 125–130, Jan. 1970.
- [87] F. Schweppe, "Power system static-state estimation, Part III: Implementation," *IEEE Transactions on Power Apparatus and Systems*, vol. PAS-89, no. 1, pp. 130–135, Jan. 1970.
- [88] T. Stuart and C. Herczet, "A sensitivity analysis of weighted least squares state estimation for power systems," *IEEE Transactions on Power Apparatus and Systems*, vol. PAS-92, no. 5, pp. 1696–1701, Sep. 1973.
- [89] A. S. Debs, "Estimation of steady-state power system model parameters," *IEEE Transactions on Power Apparatus and Systems*, vol. PAS-93, no. 5, pp. 1260–1268, Sep. 1974.
- [90] P. Zarco and A. G. Exposito, "Power system parameter estimation: A survey," *IEEE Transactions on Power Systems*, vol. 15, no. 1, pp. 216–222, Feb. 2000.
- [91] W.-H. E. Liu, F. F. Wu and S.-M. Lun, "Estimation of parameter errors from measurement residuals in state estimation," *IEEE Transactions on Power Systems*, vol. 7, no. 1, pp. 81–89, Feb. 1992.
- [92] W.-H. E. Liu and S.-L. Lim, "Parameter error identification and estimation in power system state estimation," *IEEE Transactions on Power Systems*, vol. 10, no. 1, pp. 200–209, Feb. 1995.
- [93] O. Alsac, N. Vempati, B. Stott and A. Monticelli, "Generalized state estimation," *IEEE Transactions on Power Systems*, vol. 13, no. 3, pp. 1069–1075, Aug. 1998.

- [94] S. Arafeh and R. Schinzinger, “Estimation algorithms for large-scale power systems,” *IEEE Transactions on Power Apparatus and Systems*, vol. PAS-98, no. 6, pp. 1968–1977, Nov. 1979.
- [95] I. W. Slutsker, S. Mokhtari and K. a. Clements, “Real time recursive parameter estimation in energy management systems,” *IEEE Transactions on Power Systems*, vol. 11, no. 3, pp. 1393–1399, Aug. 1996.
- [96] A. Abel Augusto, J. C. Stacchini de Souza and M. Brown Do Coutto Filho, “Correction of power grid parameters using genetic algorithms,” in *2015 18th International Conference on Intelligent System Application to Power Systems (ISAP)*, IEEE, Sep. 2015, pp. 1–6.
- [97] S. Zhou, L. Zhang, Y. Zhang, Y. Xu, G. Lin, B. Li, L. Li and C. Gong, “A new approach to branch parameter estimation of power grid based on PMU,” in *2011 Asia-Pacific Power and Energy Engineering Conference*, IEEE, Mar. 2011, pp. 1–5.
- [98] X. Bian, X. R. Li, H. Chen, D. Gan and J. Qiu, “Joint estimation of state and parameter with synchrophasors - Part II: Parameter tracking,” *IEEE Transactions on Power Systems*, vol. 26, no. 3, pp. 1209–1220, Aug. 2011.
- [99] L. Philippot and J.-C. Maun, “An application of synchronous phasor measurement to the estimation of the parameters of an overhead transmission line,” in *Fault Disturbance Analysis & Precise Measurements in Power Systems*, Arlington, VA, 1995.
- [100] H. Koglin and M. Schmidt, “Estimation of transmission line parameters by evaluating fault data records,” in *12th Power System Computation Conference*, Dresden, 1996, pp. 135–141.
- [101] R. Schulze and P. Schegner, “Parameter identification of unsymmetrical transmission lines,” in *2009 IEEE Bucharest PowerTech*, IEEE, Jun. 2009, pp. 1–7.
- [102] M. Kato, T. Hisakado, H. Takani, H. Umezaki and K. Sekiguchi, “A method of measuring three phase transmission line parameters for relay settings,” in *2009 Transmission & Distribution Conference & Exposition: Asia and Pacific*, IEEE, Oct. 2009, pp. 1–4.
- [103] Z. Hu and Y. Chen, “New method of live line measuring the inductance parameters of transmission lines based on GPS technology,” *IEEE Transactions on Power Delivery*, vol. 23, no. 3, pp. 1288–1295, Jul. 2008.

- [104] *IEEE Standard for SCADA and Automation Systems*. IEEE Std C37.1, 2008.
- [105] Y. Wang, W. Xu and J. Shen, “Online tracking of transmission-line parameters using SCADA data,” *IEEE Transactions on Power Delivery*, vol. 31, no. 2, pp. 674–682, Apr. 2016.
- [106] K. Levenberg, “A method for the solution of certain non-linear problems in least squares,” *Quarterly of Applied Mathematics*, vol. 2, no. 2, pp. 164–168, Jul. 1944.
- [107] D. W. Marquardt, “An algorithm for least-squares estimation of nonlinear parameters,” *Journal of the Society for Industrial and Applied Mathematics*, vol. 11, no. 2, pp. 431–441, Jun. 1963.
- [108] S. S. Mousavi-Seyedi, F. Aminifar and S. Afsharnia, “Parameter estimation of multiterminal transmission lines using joint PMU and SCADA data,” *IEEE Transactions on Power Delivery*, vol. 30, no. 3, pp. 1077–1085, Jun. 2015.
- [109] G. Sivanagaraju, S. Chakrabarti and S. Srivastava, “Uncertainty in transmission line parameters: Estimation and impact on line current differential protection,” *IEEE Transactions on Instrumentation and Measurement*, vol. 63, no. 6, pp. 1496–1504, Jun. 2014.
- [110] J.-a. Jiang, J.-z. Yang, Y.-h. Lin, C.-w. Liu and J.-c. Ma, “An adaptive PMU based fault detection/location technique for transmission lines. I. Theory and algorithms,” *IEEE Transactions on Power Delivery*, vol. 15, no. 2, pp. 486–493, Apr. 2000.
- [111] Y. Du and Y. Liao, “On-line estimation of transmission line parameters, temperature and sag using PMU measurements,” *Electric Power Systems Research*, vol. 93, pp. 39–45, Dec. 2012.
- [112] Y. Liao and M. Kezunovic, “Online optimal transmission line parameter estimation for relaying applications,” *IEEE Transactions on Power Delivery*, vol. 24, no. 1, pp. 96–102, Jan. 2009.
- [113] R. E. Wilson, G. A. Zevenbergen, D. L. Mah and A. J. Murphy, “Calculation of transmission line parameters from synchronized measurements,” *Electric Machines & Power Systems*, vol. 27, no. 12, pp. 1269–1278, Nov. 1999.

- [114] D. Shi, D. J. Tylavsky, N. Logic and K. M. Koellner, "Identification of short transmission-line parameters from synchrophasor measurements," in *40th North American Power Symposium*, IEEE, Sep. 2008, pp. 1–8.
- [115] L. Shengfang, F. Chunju, Y. Weiyong, C. Huarong and K. K. Li, "A new phase measurement unit (PMU) based fault location algorithm for double circuit lines," in *Eighth IEE International Conference on Developments in Power System Protection*, Amsterdam, Netherlands: IEE, 2004, pp. 188–191.
- [116] T. Bi, J. Chen, J. Wu and Q. Yang, "Synchronized phasor based on-line parameter identification of overhead transmission line," in *2008 Third International Conference on Electric Utility Deregulation and Restructuring and Power Technologies*, IEEE, Apr. 2008, pp. 1657–1662.
- [117] R. Rubesa, V. Kirincic and S. Skok, "Transmission line positive sequence impedance estimation based on multiple scans of phasor measurements," in *2014 IEEE International Energy Conference (ENERGYCON)*, IEEE, May 2014, pp. 644–651.
- [118] L. Ding, T. Bi and D. Zhang, "Transmission line parameters identification based on moving-window TLS and PMU data," in *2011 International Conference on Advanced Power System Automation and Protection (APAP)*, IEEE, Oct. 2011, pp. 2187–2191.
- [119] K. Dasgupta and S. A. Soman, "Line parameter estimation using phasor measurements by the total least squares approach," in *2013 IEEE Power & Energy Society General Meeting*, IEEE, 2013, pp. 1–5.
- [120] P. Hering and E. Janecek, "A technique for simultaneous parameter identification and measurement calibration for overhead transmission lines," in *Proceedings of the 3rd European Conference of Control (ECC '12)*, O. Arslan and S. Oprisan, Eds., Paris: WSEAS Press, 2012, pp. 75–80.
- [121] P. Hering, P. Janecek and E. Janecek, "On-line ampacity monitoring from phasor measurements," in *Preprints of the 19th World Congress The International Federation of Automatic Control*, Cape Town, 2014, pp. 3164–3169.
- [122] A. M. Dan and D. Raisz, "Estimation of transmission line parameters using wide-area measurement method," in *2011 IEEE Trondheim PowerTech*, IEEE, Jun. 2011, pp. 1–6.

- [123] G. A. Asti, S. Kurokawa, E. C. M. Costa and J. Pissolato, “Real-time estimation of transmission line impedance based on modal analysis theory,” in *2011 IEEE Power and Energy Society General Meeting*, IEEE, Jul. 2011, pp. 1–7.
- [124] C. Mishra, V. A. Centeno and A. Pal, “Kalman-filter based recursive regression for three-phase line parameter estimation using synchrophasor measurements,” in *2015 IEEE Power & Energy Society General Meeting*, IEEE, Jul. 2015, pp. 1–5.
- [125] Z. Wu, L. T. Zora and A. G. Phadke, “Simultaneous transmission line parameter and PMU measurement calibration,” in *2015 IEEE Power & Energy Society General Meeting*, IEEE, Jul. 2015, pp. 1–5.
- [126] H. Zhou, X. Zhao, D. Shi, H. Zhao and C. Jing, “Calculating sequence impedances of transmission line using PMU measurements,” in *2015 IEEE Power & Energy Society General Meeting*, IEEE, Jul. 2015, pp. 1–5.
- [127] D. Shi, D. J. Tylavsky, K. M. Koellner, N. Logic and D. E. Wheeler, “Transmission line parameter identification using PMU measurements,” *European Transactions on Electrical Power*, vol. 21, no. 4, pp. 1574–1588, May 2011.
- [128] B. S. Lowe, “A new method of determining the transmission line parameters of an untransposed line using synchrophasor measurements,” M.S. thesis, Virginia Polytechnic Institute and State University, 2015.
- [129] C. Borda, A. Olarte and H. Diaz, “PMU-based line and transformer parameter estimation,” in *2009 IEEE/PES Power Systems Conference and Exposition*, IEEE, Mar. 2009, pp. 1–8.
- [130] G. M. Giannuzzi, C. Pisani, A. Vaccaro and D. Villacci, “Overhead transmission lines dynamic line rating estimation in WAMS environments,” in *2015 International Conference on Clean Electrical Power (ICCEP)*, IEEE, Jun. 2015, pp. 165–169.
- [131] R. Puffer, M. Schmale, B. Rusek, C. Neumann and M. Scheufen, “Area-wide dynamic line ratings based on weather measurements,” in *CIGRE Session 2012 B2-106*, Paris: Cigre, 2012, pp. 1–10.
- [132] A. Arroyo, P. Castro, R. Martinez, M. Manana, A. Madrazo, R. Lecuna and A. Gonzalez, “Comparison between IEEE and CIGRE thermal behaviour standards and measured temperature on a 132-kV overhead power line,” *Energies*, vol. 8, no. 12, pp. 13 660–13 671, Dec. 2015.

- [133] *IEC Standard for Instrument Transformers - Part 3: Additional Requirements for Inductive Voltage Transformers*. IEC 61869-3:2011, 2012.
- [134] *IEC Standard for Instrument Transformers - Part 2: Additional Requirements for Current Transformers*. IEC 61869-2:2012, 2012.
- [135] A. E. Kennelly, "Artificial lines for continuous currents in the steady state," *Proceedings of the American Academy of Arts and Sciences*, vol. 44, no. 4, pp. 97–130, 1908.
- [136] J. J. Grainger and W. D. Stevenson, *Power System Analysis*. McGraw-Hill, 1994.
- [137] R. H. Byrd, M. E. Hribar and J. Nocedal, "An interior point algorithm for large-scale nonlinear programming," *SIAM Journal on Optimization*, vol. 9, no. 4, pp. 877–900, Jan. 1999.
- [138] P. S. Wright and P. Clarkson, "Development of an ethernet-enabled digitizer for on-site AC measurements," *IEEE Transactions on Instrumentation and Measurement*, vol. 60, no. 7, pp. 2229–2234, Jul. 2011.
- [139] Joint Committee for Guides in Metrology (JCGM), *Evaluation of Measurement Data: Guide to the Expression of Uncertainty in Measurement (GUM)*, 2008.
- [140] J. Zaborszky and J. W. Rittenhouse, *Electric Power Transmission: the Power System in the Steady State*. New York, NY: The Ronald Press Company, 1954.
- [141] National Grid. (2014). Electricity Ten Year Statement 2014 Appendix B - System Data, [Online]. Available: <http://www2.nationalgrid.com/UK/Industry-information/Future-of-Energy/Electricity-ten-year-statement/ETYS-Archive/> (visited on 23/03/2017).
- [142] E. M. Carlini, C. Pisani, A. Vaccaro and D. Villacci, "Dynamic line rating monitoring in WAMS: Challenges and practical solutions," in *2015 IEEE 1st International Forum on Research and Technologies for Society and Industry Leveraging a better tomorrow (RTSI)*, IEEE, Sep. 2015, pp. 359–364.
- [143] A. Fernandes, W. Neves, E. Costa and M. Cavalcanti, "Transmission line shunt conductance from measurements," *IEEE Transactions on Power Delivery*, vol. 19, no. 2, pp. 722–728, Apr. 2004.

- [144] T. F. Coleman and Y. Li, “An interior trust region approach for nonlinear minimization subject to bounds,” *SIAM Journal on Optimization*, vol. 6, no. 2, pp. 418–445, 1996.
- [145] Omicron. (2017). CMC 256plus Technical Data, [Online]. Available: https://www.omicronenergy.com/fileadmin/user_upload/pdf/literature/CMC-256plus-Technical-Data-ENU.pdf (visited on 23/01/2017).
- [146] EPRI, *Increased Power Flow Guidebook: Increasing Power Flow in Transmission and Substation Circuits*. Palo Alto, CA, 2005.
- [147] C. Pisani, A. Vaccaro and D. Villacci, “Conceptualization and experimental deployment of an adaptive synchronized sensing system for power line thermal monitoring,” *IEEE Transactions on Industrial Informatics*, vol. 12, no. 6, pp. 2158–2165, Dec. 2016.
- [148] K. V. Khandeparkar, S. A. Soman and G. Gajjar, “Detection and correction of systematic errors in instrument transformers along with line parameter estimation using PMU data,” *IEEE Transactions on Power Systems*, vol. PP, no. 99, pp. 1–10, 2016.
- [149] National Climatic Data Center - US Department of Commerce. (2016). NNDC Climate Data Online, [Online]. Available: <http://www7.ncdc.noaa.gov/CDO/cdopoemain.cmd?datasetabbv=DS3505&countryabbv=&georegionabbv=&resolution=40> (visited on 01/05/2016).
- [150] Weather Underground. (2016). Historical Weather, [Online]. Available: <https://www.wunderground.com/history/> (visited on 24/06/2016).

Appendices

Appendix A

Chapter 3

A.1 Sensitivity of series inductance and shunt capacitance to conductor temperature

A.1.1 Series inductance

Carson's formulae for the self and mutual impedance of conductors with ground return are considered to assess the sensitivity of positive sequence inductance to conductor height above ground [46]. Define the following variables,

- $Z_{s_i} \in \mathbb{C}$ per unit length self impedance of the i th conductor with ground return
- $Z_{m_{ik}} \in \mathbb{C}$ per unit length mutual impedance between the i th and k th conductors with ground return
- $g_i \in \mathbb{R}_{\geq 0}$ geometric mean radius of i th conductor
- $h_i \in \mathbb{R}_{\geq 0}$ height of i th conductor
- $R_i \in \mathbb{R}_{\geq 0}$ AC resistance of i th conductor
- $d_{ik} \in \mathbb{R}_{\geq 0}$ distance between the i th and k th conductors
- $D_{ik} \in \mathbb{R}_{\geq 0}$ distance between the i th conductor and image of k th conductors
- $f \in \mathbb{R}_{\geq 0}$ frequency, $\omega = 2\pi f$ - angular frequency
- $\mu \in \mathbb{R}_{\geq 0}$ permeability of the conductor
- $I_g \in \mathbb{C}$ infinite integral that models the effect of earth resistivity

The geometrical quantities are illustrated in Figure A.1.

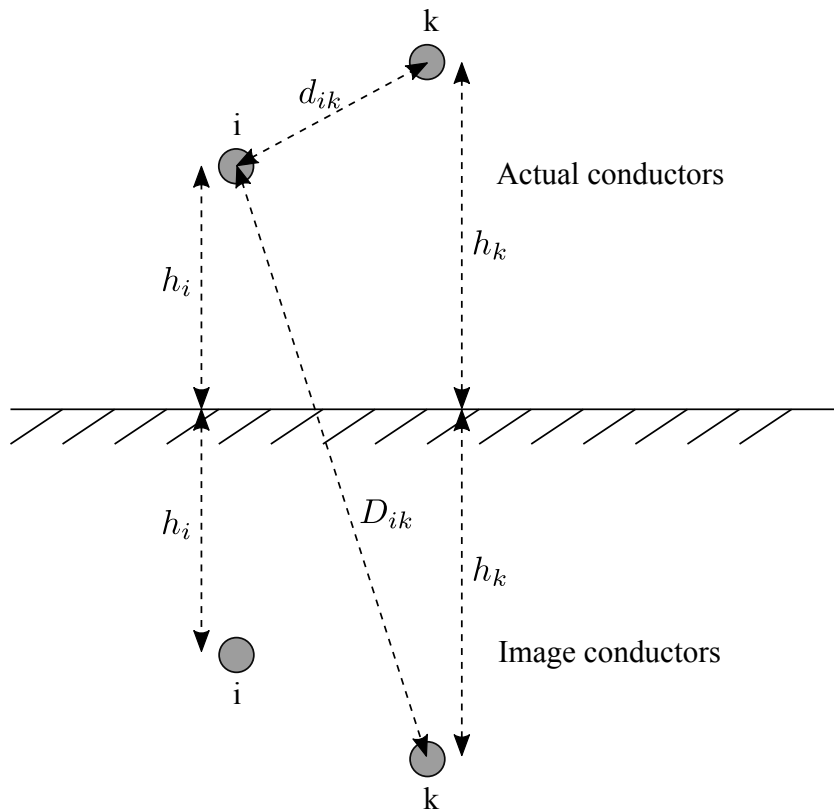


Figure A.1: Schematic diagram of the geometrical configuration of two actual conductors and their images

Self and mutual impedance are given by

$$Z_{s_i} = R_i + j \frac{\omega \mu}{2\pi} \ln(2h_i/g_i) + 4\omega I_g \quad (\text{A.1})$$

$$Z_{m_{ik}} = j \frac{\omega \mu}{2\pi} \ln(D_{ik}/d_{ik}) + 4\omega I_g. \quad (\text{A.2})$$

Consider the positive sequence inductance L , given by

$$L = \frac{\mu}{2\pi} \ln(2h_i/g_i) - \frac{\mu}{2\pi} \ln(D_{ik}/d_{ik}) \quad (\text{A.3})$$

$$= \frac{\mu}{2\pi} \ln\left(\frac{2h_i}{g_i} \frac{d_{ik}}{D_{ik}}\right). \quad (\text{A.4})$$

By making the approximation $D_{ik} \approx 2h_i$, the expression for L becomes

$$L \approx \frac{\mu}{2\pi} \ln\left(\frac{2h_i}{g_i} \frac{d_{ik}}{2h_i}\right) = \frac{\mu}{2\pi} \ln\left(\frac{d_{ik}}{g_i}\right). \quad (\text{A.5})$$

Hence, the positive sequence inductance is approximately independent of the conductor height, and has low sensitivity to changes in sag caused by changes in conductor temperature.

A.1.2 Shunt capacitance

Shunt capacitance is calculated by considering the potential of a conductor due to its own charge and that of other transmission line conductors [34, 49]. Define

- n number of conductors above ground
- $q_i \in \mathbb{C}$ charge per unit length of i th conductor, $i = 1, 2, 3, \dots, n$
- $d_{ii} \in \mathbb{R}_{\geq 0}$ radius of i th conductor
- $d_{ik} \in \mathbb{R}_{\geq 0}$ distance between the i th and k th conductor, $i \neq k$
- $D_{ii} \in \mathbb{R}_{\geq 0}$ distance between the i th conductor and its image
- $D_{ik} \in \mathbb{R}_{\geq 0}$ distance between the i th conductor and image of k th conductors, $i \neq k$
- $\epsilon \in \mathbb{R}_{\geq 0}$ permittivity of the medium
- $V_i \in \mathbb{C}$ voltage of i th conductor to ground

By derivation from Gauss's law for electric fields, V_i is given by [34]:

$$V_i = \frac{1}{2\pi\epsilon} \sum_{k=1}^n q_k \ln \left(\frac{D_{ik}}{d_{ik}} \right) \quad (\text{A.6})$$

Define the following matrices:

$\mathbf{P} \in \mathbb{C}^{n \times n}$ - potential coefficient matrix with elements

$$p_{ij} = \frac{1}{2\pi\epsilon} \ln \left(\frac{D_{ik}}{d_{ik}} \right). \quad (\text{A.7})$$

$\mathbf{V} \in \mathbb{C}^n$ - voltage vector, $\mathbf{V} = [V_1 \ V_2 \ V_3 \ \dots \ V_n]^T$,

$\mathbf{Q} \in \mathbb{C}^n$ - charge vector, $\mathbf{Q} = [q_1 \ q_2 \ q_3 \ \dots \ q_n]^T$

Based on (2.37), the voltages for n conductors can be summarized by the matrix equation

$$\mathbf{V} = \mathbf{P}\mathbf{Q}. \quad (\text{A.8})$$

Capacitance is defined as the ratio of charge to voltage, $C = q/V$. Given matrices \mathbf{Q} and \mathbf{V} , let \mathbf{C} be the matrix of capacitance coefficients (also known as Maxwell's coefficients [34]), where

$$\mathbf{C} = \mathbf{Q}\mathbf{V}^{-1} = \mathbf{P}^{-1}. \quad (\text{A.9})$$

For a transposed line with geometrical phase symmetry, the positive sequence components P_1 and C_1 of \mathbf{P} and \mathbf{C} , respectively, have a direct inverse relationship:

$$C_1 = 1/P_1. \quad (\text{A.10})$$

Now, P_1 is given by

$$P_1 = p_{ii} - p_{ik} = \frac{1}{2\pi\epsilon} \ln \left(\frac{D_{ii}}{d_{ii}} \right) - \frac{1}{2\pi\epsilon} \ln \left(\frac{D_{ik}}{d_{ik}} \right) \quad (\text{A.11})$$

$$= \frac{1}{2\pi\epsilon} \ln \left(\frac{D_{ii} d_{ik}}{d_{ii} D_{ik}} \right). \quad (\text{A.12})$$

By making the approximation $D_{ik} \approx D_{ii}$, P_1 becomes

$$P_1 \approx \frac{1}{2\pi\epsilon} \ln \left(\frac{d_{ik}}{d_{ii}} \right). \quad (\text{A.13})$$

Thus, P_1 is approximately independent of conductor height, which means that positive sequence shunt capacitance has low sensitivity to thermally induced changes in sag.

A.2 Preservation of positive sequence through the delta-star conversion

Let $V_a, V_b, V_c \in \mathbb{C}$ be phase voltage of a three-phase transmission line as shown in Figure A.2, which may or may not be balanced, where balance is defined as $|V_a| = |V_b| = |V_c|$ and $\angle V_a - \angle V_b = \angle V_b - \angle V_c = \angle V_c - \angle V_a = 2\pi/3$.

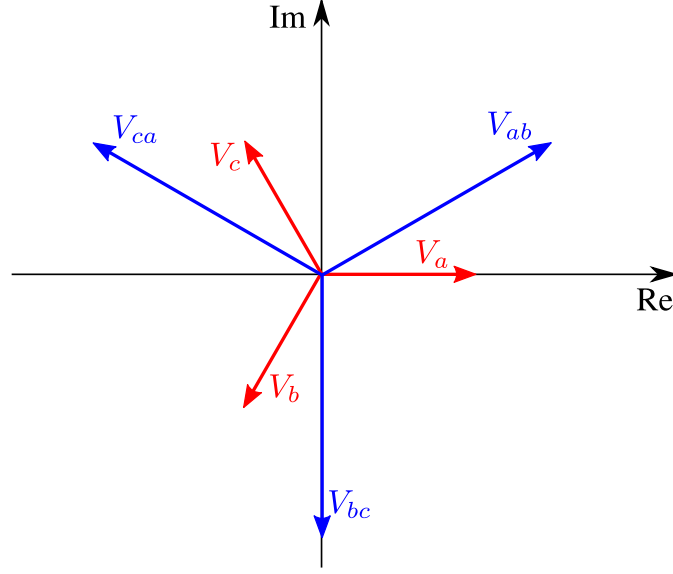


Figure A.2: Phasor diagram of star and delta voltages

Let $a = \exp(j2\pi/3)$. The positive sequence voltage V_1 is defined as

$$V_1 = \frac{1}{3} (V_a + aV_b + a^2V_c). \quad (\text{A.14})$$

Define the line-to-line (delta) voltages as $V_{ab} = V_a - V_b$, $V_{bc} = V_b - V_c$, $V_{ca} = V_c - V_a$. The positive sequence of the delta voltages is given by

$$V_{1\Delta} = \frac{1}{3} (V_{ab} + aV_{bc} + a^2V_{ca}). \quad (\text{A.15})$$

Now, convert $V_{1\Delta}$ to a positive sequence star voltage V_{1*} ; define $b = \sqrt{3} \exp(j\pi/6)$, then

$$V_{1*} = V_{1\Delta}/b \quad (\text{A.16})$$

$$= \frac{1}{3b} (V_{ab} + aV_{bc} + a^2V_{ca}) \quad (\text{A.17})$$

$$= \frac{1}{3} \left(\frac{1-a^2}{b} V_a + \frac{a-1}{b} V_b + \frac{a^2-a}{b} V_c \right). \quad (\text{A.18})$$

But

$$\frac{1-a^2}{b} = 1, \quad \frac{a^2-a}{b} = a^2, \quad \frac{a-1}{b} = a. \quad (\text{A.19})$$

Hence,

$$V_{1*} = \frac{1}{3} (V_a + a^2 V_b + a V_c) = V_1. \quad (\text{A.20})$$

Thus, the positive sequence of the phase voltages V_1 can be retrieved from measurements of delta voltages V_{ac}, V_{ba}, V_{cb} only, regardless of the level of unbalance.

A.3 Calculation of average conductor temperature

The calculation of average conductor temperature from ambient weather conditions is based on the IEEE Standard 738-2012 for Calculating the Current-Temperature Relationship of Bare Overhead Conductors [43]. The non-steady state heat balance equation is used to calculate the change in temperature at regular time intervals to reflect changes in weather conditions and line current.

Define the following variables:

$T_c \in \mathbb{R}$	Average conductor temperature in $^{\circ}\text{C}$
$t \in \mathbb{R}_{\geq 0}$	Time in s
$m \in \mathbb{R}_{\geq 0}$	Mass of conductor in kg
$C_p \in \mathbb{R}_{\geq 0}$	Heat capacity of conductor in $\text{J } ^{\circ}\text{C}^{-1}$
$R(T_c) \in \mathbb{R}_{\geq 0}$	AC resistance at temperature T_c in $\Omega \text{ m}^{-1}$
$ I \in \mathbb{R}_{\geq 0}$	Magnitude of conductor current in A
$q_s \in \mathbb{R}_{\geq 0}$	Solar heat gain rate in W m^{-1}
$q_c \in \mathbb{R}_{\geq 0}$	Convection heat loss rate in W m^{-1}
$q_r \in \mathbb{R}_{\geq 0}$	Radiation heat loss rate in W m^{-1}
$\Delta t \in \mathbb{R}_{\geq 0}$	Time step in s

The non-steady state heat balance equation is [43]:

$$\frac{dT_c}{dt} = \frac{1}{mC_p} (R(T_c)I^2 + q_s - q_c - q_r). \quad (\text{A.21})$$

T_c is a continuous variable that is discretized for the purpose of iterative calculation with respect to time t [43]. Let subscript i denote quantity values from time t_i . By a first order Taylor approximation, the temperature $T_{c_{i+1}}$ at t_{i+1} is given by:

$$T_{c_{i+1}} = T_{c_i} + \left. \frac{dT_c}{dt} \right|_{t=t_i} (t_{i+1} - t_i) \quad (\text{A.22})$$

Let $\Delta t = t_{i+1} - t_i$, then

$$T_{c_{i+1}} = T_{c_i} + \left. \frac{dT_c}{dt} \right|_{t=t_i} \Delta t = \frac{\Delta t}{mC_p} (R(T_{c_i})I_i^2 + q_{s_i} - q_{c_i} - q_{r_i}). \quad (\text{A.23})$$

The conductor type is Zebra ACSR (Aluminium Conductor Steel Reinforced), hence, the material is non-homogeneous. Define

$m_a \in \mathbb{R}_{\geq 0}$	Per unit length mass of the aluminium strands in kg m^{-1}
$C_a \in \mathbb{R}_{\geq 0}$	Specific heat capacity of aluminium in $\text{J kg}^{-1} ^{\circ}\text{C}^{-1}$

$m_s \in \mathbb{R}_{\geq 0}$ Per unit length mass of the steel core in kg m^{-1}
 $C_s \in \mathbb{R}_{\geq 0}$ Specific heat capacity of steel in $\text{J kg}^{-1} \text{ }^\circ\text{C}^{-1}$.

The heat capacity C_p is thus a linear combination of the heat capacities of aluminium and steel [43]:

$$C_p = m_a C_a + m_s C_s. \quad (\text{A.24})$$

Define $\alpha \in [-1, 1]$ as the resistance-temperature coefficient with unit $^\circ\text{C}^{-1}$. The resistance depends linearly on the conductor temperature:

$$R(T_{c_i}) = R(20)(1 + \alpha(T_{c_i} - 20)). \quad (\text{A.25})$$

The conductor current is taken to be the mean of sending and receiving end current magnitudes and divided by 2, the number of conductors per bundle:

$$I_i = (|I_{s_i}| + |I_{r_i}|)/4. \quad (\text{A.26})$$

To calculate the rate of solar heat gain q_s , define the following variables:

$\alpha_s \in [0.23, 0.91]$ Solar absorptivity, no dimensions
 $Q_{se} \in \mathbb{R}_{\geq 0}$ Total solar and sky radiated heat intensity corrected for elevation in W m^{-2}
 $Q_s \in \mathbb{R}_{\geq 0}$ Total solar and sky radiated heat intensity in W m^{-2}
 $K_{solar} \in \mathbb{R}_{\geq 0}$ Solar altitude correction factor, no dimensions
 $\theta \in \mathbb{R}$ Effective angle of incidence of the sun's rays in $^\circ$
 $A \in \mathbb{R}$ Projected area of conductor in m^2 linear m
 $H_c \in [0, 90]$ Altitude of sun in $^\circ$
 $Z_c \in \mathbb{R}$ Azimuth of sun in $^\circ$
 $Z_l \in \mathbb{R}$ Azimuth of line in $^\circ$
 $L \in \mathbb{R}$ Degrees of latitude in $^\circ$
 $\delta \in [-23.45, 23.45]$ Solar declination in $^\circ$
 $\omega \in \mathbb{R}$ Hour angle relative to noon in $^\circ$
 $X \in \mathbb{R}$ Solar azimuth variable, no dimensions
 $N \in \mathbb{N}$ Day of the year in, no dimensions.

At t_i , q_s is calculated as [43]:

$$q_{s_i} = \alpha_s Q_{se_i} \sin(\theta) A, \quad (\text{A.27})$$

where

$$Q_{se_i} = K_{solar} Q_{s_i} \quad (\text{A.28})$$

$$\theta = \arccos(\cos(H_c) \cos(Z_c - Z_l)) \quad (\text{A.29})$$

$$H_c = \arcsin(\cos(L) \cos(\delta) \cos(\omega) + \sin(L) \sin(\delta)) \quad (\text{A.30})$$

$$Z_c = C + \arctan(X) \quad (\text{A.31})$$

$$X = \sin(\omega) / (\sin(L) \cos(\omega) - \cos(L) \tan(\delta)) \quad (\text{A.32})$$

$$\delta = 23.46 \sin\left(\frac{360}{365}(284 + N)\right). \quad (\text{A.33})$$

The solar azimuth $C \in \{0, 180, 360\}$ is a function of the hour angle ω and solar azimuth variable X [43]. Further, define

$D \in \mathbb{R}$	Conductor diameter in m
$T_a \in \mathbb{R}$	Ambient temperature in °C
$\rho \in \mathbb{R}$	Density of air in kg m^{-3}
$v_w \in \mathbb{R}$	Wind speed in m s^{-1}
$\mu_f \in \mathbb{R}$	Absolute viscosity of air in $\text{kg m}^{-1} \text{s}^{-1}$
$k_f \in \mathbb{R}$	Thermal conductivity of air at temperature T_{film} in $\text{W m}^{-1} \text{°C}^{-1}$
$K_{angle} \in \mathbb{R}$	Wind direction factor, no dimensions
$H_e \in \mathbb{R}$	Elevation of conductor above sea level in m
$\phi \in \mathbb{R}$	Angle between wind and axis of conductor in °.

Convection heat loss q_{c_i} is taken as $\max\{q_{cn_i}, q_{c1_i}, q_{c2_i}\}$, the maximum value of calculated natural convection q_{cn_i} , convective heat loss at low wind speeds q_{c1_i} and high wind speeds q_{c2_i} , which are calculated by [43]:

$$q_{cn_i} = 3.645 \rho_f^{0.5} D^{0.75} (T_{c_i} - T_{a_i}) \quad (\text{A.34})$$

$$q_{c1_i} = (1.01 + 0.0372 \left(\frac{D \rho_f v_w}{\mu_f}\right)^{0.52}) k_f K_{angle} (T_{c_i} - T_{a_i}) \quad (\text{A.35})$$

$$q_{c2_i} = 0.0119 \left(\frac{D \rho_f v_w}{\mu_f}\right)^{0.6} k_f K_{angle} (T_{c_i} - T_{a_i}), \quad (\text{A.36})$$

where

$$\rho_f = \frac{1.293 - 1.525 \times 10^{-4} H_e + 6.379 \times 10^{-9} H_e^2}{1 + 0.00367 T_{film}} \quad (\text{A.37})$$

$$\mu_f = \frac{1.458 \times 10^{-6} (T_{film} + 273)^{1.5}}{T_{film} + 383.4} \quad (\text{A.38})$$

$$k_f = 2.424 \times 10^{-2} + 7.477 \times 10^{-5} T_{film} - 4.407 \times 10^{-9} T_{film}^2 \quad (\text{A.39})$$

$$K_{angle} = 1.194 - \cos(\phi) + 0.194 \cos(2\phi) + 0.368 \sin(2\phi) \quad (\text{A.40})$$

$$T_{film} = (T_{c_i} - T_{a_i})/2. \quad (\text{A.41})$$

The radiation heat loss rate is computed as [43]

$$q_{r_i} = 0.138D\varepsilon \left[\left(\frac{T_{c_i} + 273}{100} \right)^4 - \left(\frac{T_{a_i} + 273}{100} \right)^4 \right]. \quad (\text{A.42})$$

Measurements of ambient temperature, wind speed as well as solar radiation were used as input data for the calculations over the 24-hour period [149, 150]. Since the nearest weather stations are 200 km from the line ends, the wind speed values may not be reflective of the conditions close to the line. Therefore the values from both locations were averaged and a constant value was assumed throughout the day; the wind direction was assumed to be $\phi = 90^\circ$, i.e. perpendicular to the line. Table A.1 lists the remaining input quantity values.

Table A.1: List of fixed input quantity values

Variable	Value	Explanation
$R(20)$	$6.74 \times 10^{-5} \Omega \text{ m}^{-1}$	Zebra conductor property
Δt	60 s	Time steps at which impedance is calculated
m_a	1.288 kg m^{-1}	Zebra conductor property
C_a	$476 \text{ J kg}^{-1} \text{ }^\circ\text{C}^{-1}$	Material property
m_s	0.4836 kg m^{-1}	Zebra conductor property
C_s	$955 \text{ J kg}^{-1} \text{ }^\circ\text{C}^{-1}$	Material property
α	$0.0039 \text{ }^\circ\text{C}^{-1}$	Material property
α_s	0.5	Standard value for ACSR conductors
A	0.028 62 m	Equal to conductor diameter
Z_l	180°	Line runs in a north-south direction
L	-19.4°	Location of line in Namibia
N	73	14 March
D	0.028 62 m	Zebra conductor diameter
H_e	0	Line has no elevation
ε	0.5	Standard value for ACSR conductors

Figure A.3 shows the calculated rates of convection, solar heat gain, radiation and Joule heating over the 24-hour period.

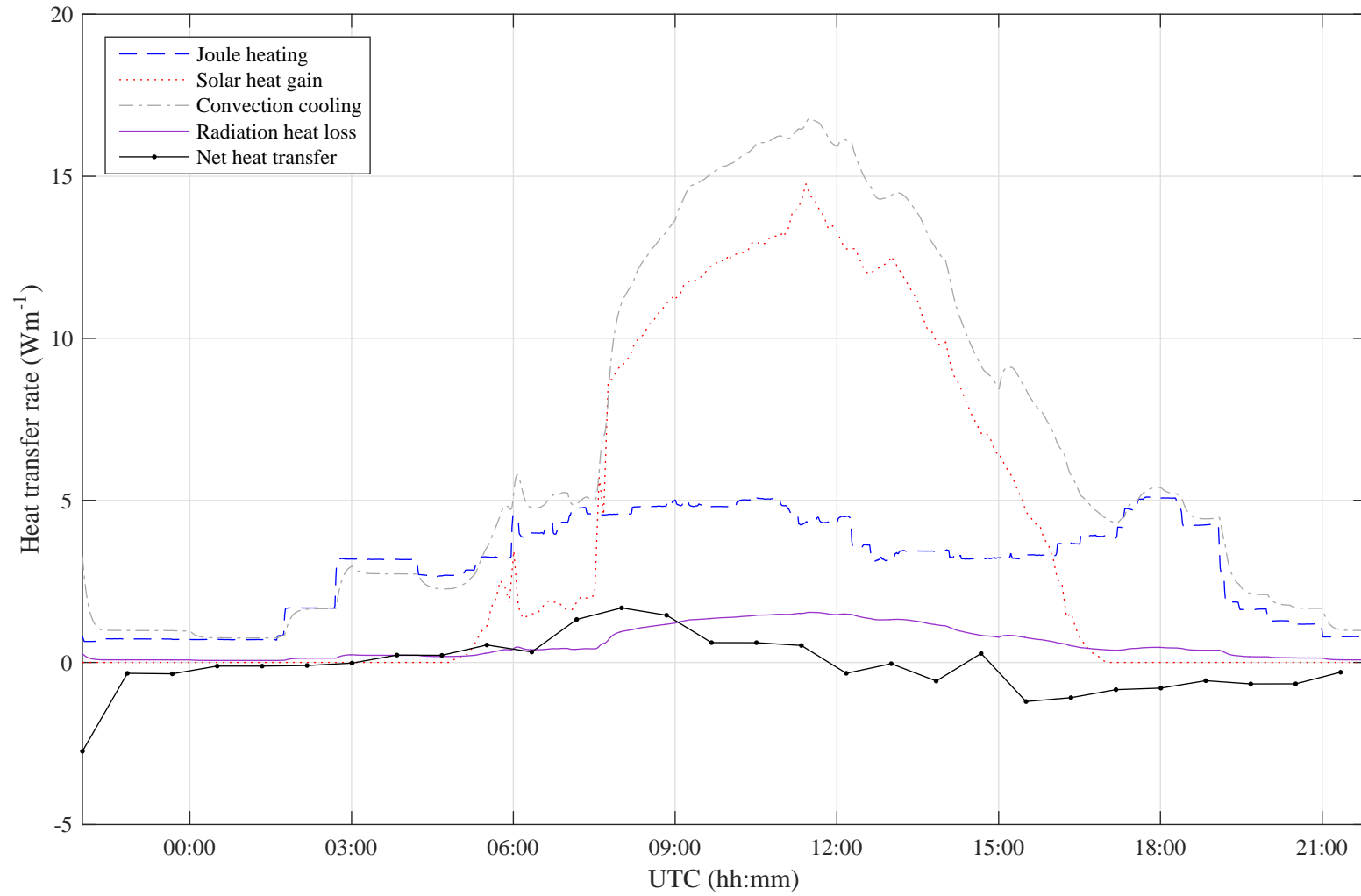


Figure A.3: Heat transfer rates as calculated from the heat balance equation

A.4 Field measurement results

Table A.2 lists the Median (M) and Interdecile Range (IDR) of the estimated values for resistance R , reactance X , conductance G and susceptance B .

Table A.2: Results for field measurements, 22-hour period, as presented in Tables 3.6, 3.7, 3.8, 3.9 and 3.10

	R (Ω)		X (Ω)		G (mS)		B (mS)	
	M	IDR	M	IDR	M	IDR	M	IDR
SM1	34.7	8.1	148	3	0.06	0.24	2.07	0.04
TLS1	35.1	5.8	148	3	0.00	0.00	2.07	0.03
NLOE1	25.5	7.7	140	20	-0.26	0.73	2.30	0.17
TPLL1	31.6	4.7	157	28	-0.10	0.45	1.85	0.37
LLS3	34.7	11.7	145	7	0.00	0.00	2.07	0.03
NLLC3	0.3	40.6	0	45	5.71	4276.89	9.57	4613.57
NLCO3	22.7	5.2	155	11	0.00	0.00	1.66	0.10
TPLL3	90.8	53.6	118	66	-1.06	7.84	0.24	6.92

A.5 Simulation measurement results

Tables A.3 to A.8 list the Median (M) and Interdecile Range (IDR) of the estimated values for resistance R , reactance X , conductance G and susceptance B , for each of the six simulated scenarios described in Section 3.5.2.

Table A.3: Results for the Ideal Scenario, as presented in Table 3.13

	R (Ω)		X (Ω)		G (mS)		B (mS)	
	M	IDR	M	IDR	M	IDR	M	IDR
SM1	16.0	0.0	189	0	0.01	0.00	1.57	0.00
TLS1	16.1	0.0	189	0	0.00	0.00	1.57	0.00
NLOE1	16.0	0.0	189	0	0.01	0.00	1.57	0.00
TPLL1	16.0	0.0	189	0	0.01	0.00	1.57	0.00
LLS3	16.0	0.2	188	0	0.00	0.00	1.57	0.00
NLLC3	16.0	0.0	189	0	0.01	0.00	1.57	0.00
NLCO3	16.0	0.3	188	2	0.00	0.00	1.57	0.00
TPLL3	16.0	0.0	189	0	0.01	0.00	1.57	0.00

Table A.4: Results for the Delta-star Scenario, as presented in Table 3.14

	R (Ω)		X (Ω)		G (mS)		B (mS)	
	M	IDR	M	IDR	M	IDR	M	IDR
SM1	16.0	0.0	189	0	0.01	0.00	1.57	0.00
TLS1	16.1	0.0	189	0	0.00	0.00	1.57	0.00
NLOE1	16.0	0.0	189	0	0.01	0.00	1.57	0.00
TPLL1	16.0	0.0	189	0	0.01	0.00	1.57	0.00
LLS3	16.0	2.8	188	4	0.00	0.00	1.57	0.00
NLLC3	2.2	236.4	1	229	9.11	55 163.48	17.99	62 575.80
NLCO3	16.1	0.4	188	1	0.00	0.00	1.57	0.00
TPLL3	93.7	0.0	134	0	-0.68	0.00	1.18	0.00

Table A.5: Results for the Variation Scenario, as presented in Table 3.15

	R (Ω)		X (Ω)		G (mS)		B (mS)	
	M	IDR	M	IDR	M	IDR	M	IDR
SM1	16.6	0.9	189	0	0.01	0.00	1.57	0.00
TLS1	16.8	0.9	189	0	0.00	0.00	1.57	0.00
NLOE1	16.6	2.8	189	1	0.01	0.03	1.57	0.06
TPLL1	16.6	2.0	189	1	0.01	0.02	1.57	0.04
LLS3	16.7	1.1	188	1	0.00	0.00	1.57	0.00
NLLC3	15.8	139.7	184	228	0.01	18.12	1.58	15.51
NLCO3	16.7	0.8	188	2	0.00	0.00	1.57	0.00
TPLL3	16.6	1.5	188	1	0.01	0.04	1.57	0.03

Table A.6: Results for the Uncertainty Scenario, as presented in Table 3.16

	R (Ω)		X (Ω)		G (mS)		B (mS)	
	M	IDR	M	IDR	M	IDR	M	IDR
SM1	16.0	0.0	192	0	0.01	0.00	1.57	0.00
TLS1	16.0	0.0	192	0	0.00	0.00	1.57	0.00
NLOE1	16.0	0.5	192	1	0.01	0.01	1.57	0.01
TPLL1	16.0	0.1	192	0	0.01	0.00	1.57	0.00
LLS3	16.0	0.2	191	0	0.00	0.00	1.57	0.00
NLLC3	12.1	34.1	195	29	-0.07	2.46	1.95	2.27
NLCO3	69.0	2.6	285	23	0.00	0.00	1.47	0.03
TPLL3	15.7	15.1	184	21	-0.01	0.99	1.76	0.94

Table A.7: Results for the Systematic Error Scenario, as presented in Table 3.17

	R (Ω)		X (Ω)		G (mS)		B (mS)	
	M	IDR	M	IDR	M	IDR	M	IDR
SM1	25.1	122.6	164	201	0.02	0.01	1.56	0.08
TLS1	25.2	101.0	164	174	0.00	0.00	1.56	0.08
NLOE1	6.3	0.0	182	0	0.44	0.00	1.94	0.00
TPLL1	19.4	0.0	184	0	-0.37	0.00	1.28	0.00
LLS3	21.1	20.3	170	21	0.00	0.00	1.56	0.08
NLLC3	14.0	0.0	187	0	0.02	0.00	1.59	0.00
NLCO3	68.9	2.0	283	22	0.00	0.00	1.47	0.02
TPLL3	19.4	0.0	184	0	-0.37	0.00	1.28	0.00

Table A.8: Results for the Realistic Scenario, as presented in Table 3.18

	R (Ω)		X (Ω)		G (mS)		B (mS)	
	M	IDR	M	IDR	M	IDR	M	IDR
SM1	25.6	115.4	164	202	0.02	0.01	1.56	0.08
TLS1	25.9	100.5	164	173	0.00	0.00	1.56	0.08
NLOE1	6.9	3.1	182	2	0.44	0.03	1.94	0.05
TPLL1	19.9	2.1	184	1	-0.37	0.02	1.28	0.04
LLS3	21.5	76.2	163	52	0.00	0.00	1.56	0.08
NLLC3	102.9	145.6	196	139	-1.72	10.21	2.43	9.38
NLCO3	23.7	8.8	163	46	0.00	0.00	1.58	0.15
TPLL3	90.0	19.5	127	13	-0.97	0.98	0.82	0.88

Appendix B

Chapter 4

B.1 Estimating the uncertainty in the calculated impedance of a copper coil

The uncertainty in the resistance and reactance values that were calculated from the synchrophasor measurements was estimated in line with the Guide to the Expression of Uncertainties in Measurement [139]. Recall that impedance $Z_i \in \mathbb{R}$ is calculated using

$$Z_i = R_i + jX_i = \frac{V_{s_i} - V_{r_i}}{I_i} = \frac{|V_{s_i}| \exp(j\theta_{s_i}) - |V_{r_i}| \exp(j\theta_{r_i})}{|I_i| \exp(j\theta_{I_i})}, \quad (\text{B.1})$$

where $V_{s_i}, V_{r_i}, I \in \mathbb{C}$, $\theta_{s_i}, \theta_{r_i}, \theta_{I_i} \in \mathbb{R}$ are mean values of measurements from a 10 s interval. θ_{r_i} and θ_{I_i} are measured relative to θ_{s_i} , hence $\theta_{s_i} = 0$. Subscript i refers to time instants $t_i = i\Delta t$, where $\Delta t = 10$ s. A summary of components that contribute to uncertainty in R_i and X_i is given in Table B.1.

Table B.1: Components of uncertainty calculation for resistance

Type	Symbol	Source of uncertainty	Absolute expanded uncertainty	Probability Distribution	Sensitivity coefficient
A	u_{R_i}	Repeatability from statistical calculation		Normal	
B	$u_{ V_s }$	Uncertainty in amplitude	66 ppm	Normal	$\frac{\partial R_i}{\partial V_{s_i} }$
	$u_{ V_r }$	measurement of digitizer channels	66 ppm	Normal	$\frac{\partial R_i}{\partial V_{r_i} }$
	$u_{ I }$		32 ppm	Normal	$\frac{\partial R_i}{\partial I_i }$
B	u_{θ_r}	Uncertainty in phase angle measurement of digitizer channels relative to channel	2 μ rad	Normal	$\frac{\partial R}{\partial \theta_{r_i}}$
	u_{θ_I}	measuring V_{s_i}	62 μ rad	Normal	$\frac{\partial R_i}{\partial \theta_{I_i}}$
B	$u_{ V_i }$	Correlation between digitizer channels			
	u_{θ_i}				

Type A uncertainty u_{R_i} is calculated as the standard deviation of the mean of 100 values R_k obtained at times $t_k = k\Delta t$, $\Delta t = 0.1$ s, $k = 1, 2, 3, \dots, 100$ from phasor measurements over each 10 second interval:

$$\mu(R_k) = \frac{1}{100} \sum_{k=1}^{100} R_k \quad (\text{B.2})$$

$$s(R_k) = \sqrt{\frac{1}{100-1} \sum_{k=1}^{100} (R_k - \mu(R_k))^2} \quad (\text{B.3})$$

$$u(R_i) = \frac{s(R_k)}{\sqrt{100}} \quad (\text{B.4})$$

Uncertainties $u_{|V_{s_i}|} = |V_{s_i}|u_{|V_s|}$, $u_{|V_{r_i}|} = |V_{r_i}|u_{|V_r|}$, $u_{|I_i|} = |I_i|u_{|I|}$, u_{θ_r} , u_{θ_I} are of Type B and obtained from calibration of the digitizer instrument, current transformer and resistive burden.

The terms in $u_{|V_i|}$ and u_{θ_i} reflect correlation between input quantities and are computed as

$$u_{|V_i|}^2 = 2u_{|V_{s_i}|} \frac{\partial R}{\partial |V_{s_i}|} u_{|V_{r_i}|} \frac{\partial R}{\partial |V_{r_i}|} \quad (\text{B.5})$$

$$u_{\theta_i}^2 = 2u_{\theta_r} \frac{\partial R}{\partial \theta_{r_i}} u_{\theta_I} \frac{\partial R}{\partial \theta_{I_i}}. \quad (\text{B.6})$$

All partial derivatives are evaluated at V_{s_i}, V_{r_i}, I_i , which are mean values over 10 s intervals:

$$V_{s_i} = \frac{1}{100} \sum_{j=1}^{100} V_{s_j}, V_{r_i} = \frac{1}{100} \sum_{j=1}^{100} V_{r_j}, I_i = \frac{1}{100} \sum_{j=1}^{100} I_j. \quad (\text{B.7})$$

For each calculated resistance value R_i , the combined standard uncertainty U_{R_i} has been calculated according to the law of propagation of uncertainty:

$$U_{R_i} = \left(u_{R_i}^2 + u_{|V_{s_i}|}^2 \frac{\partial R_i}{\partial |V_{s_i}|}^2 + u_{|V_{r_i}|}^2 \frac{\partial R_i}{\partial |V_{r_i}|}^2 + u_{|I_i|}^2 \frac{\partial R_i}{\partial |I_i|}^2 + u_{\theta_r}^2 \frac{\partial R_i}{\partial \theta_{r_i}}^2 + u_{\theta_I}^2 \frac{\partial R_i}{\partial \theta_{I_i}}^2 + u_{|V_i|}^2 + u_{\theta_i}^2 \right)^{\frac{1}{2}}. \quad (\text{B.8})$$

The degrees of freedom for the Type B uncertainty components are assumed to be infinite, while the degree of freedom for the Type A uncertainty is 99, giving a number greater than 100 effective degrees of freedom and a coverage factor of 2. The combined standard uncertainty is assumed to be the standard deviation of a normal probability distribution around the measured value; the expanded uncertainty is obtained by multiplying with the coverage factor for a 95 % coverage probability. The same procedure was used to obtain the uncertainty in reactance values X_i .

B.2 Derivation of net error

In order to show that the net systematic errors between sending and receiving ends are a good approximation, the partial derivatives of Z and Y with respect to V_s, V_r, I_s, I_r are required. These will be derived in Section B.2.1 and the error approximation is considered in Section B.2.2.

B.2.1 Partial derivatives of Z and Y

Let $V_s, I_s, V_r, I_r \in \mathbb{C}, \Omega = \mathbb{C}^4 \setminus \{V_s I_r + V_r I_s = 0\}, \Gamma = \mathbb{C}^4 \setminus \{V_s + V_r = 0\}$. Define complex functions $Z : \Omega \rightarrow \mathbb{C}, Y : \Gamma \rightarrow \mathbb{C}$, where

$$Z = (V_s^2 - V_r^2)/(V_s I_r + V_r I_s) \quad (\text{B.9})$$

$$Y = 2(I_s - I_r)(V_s + V_r). \quad (\text{B.10})$$

Rewrite Z as $Z = h_1/h_2$ and Y as $Y = h_3/h_4$, where $h_1 : \mathbb{C}^2 \rightarrow \mathbb{C}, h_2 : \Omega \rightarrow \mathbb{C}, h_3 : \mathbb{C}^2 \rightarrow \mathbb{C}, h_4 : \mathbb{C}^2 \setminus \{V_s + V_r = 0\} \rightarrow \mathbb{C}$,

$$h_1(V_s, V_r) = V_s^2 - V_r^2, \quad h_2(V_s, I_r, V_r, I_s) = V_s I_r + V_r I_s \quad (\text{B.11})$$

$$h_3(I_s, I_r) = 2(I_s - I_r), \quad h_4(V_s, V_r) = V_s + V_r. \quad (\text{B.12})$$

Since h_1, h_2, h_3, h_4 are complex polynomials, Z and Y are rational functions. By the differentiability of complex polynomials and the quotient rule, Z and Y are differentiable at all points in Ω and Γ , respectively. The partial derivatives of Z with respect to V_s and V_r are

$$\frac{\partial Z}{\partial V_s} = \frac{2V_s}{V_s I_r + V_r I_s} - \frac{(V_s^2 - V_r^2)I_r}{(V_s I_r + V_r I_s)^2} \quad (\text{B.13})$$

$$\frac{\partial Z}{\partial V_r} = \frac{-2V_r}{V_s I_r + V_r I_s} - \frac{(V_s^2 - V_r^2)I_s}{(V_s I_r + V_r I_s)^2}. \quad (\text{B.14})$$

The partial derivatives of Y with respect to I_s and I_r are

$$\frac{\partial Y}{\partial I_s} = \frac{2}{V_s + V_r} \quad (\text{B.15})$$

$$\frac{\partial Y}{\partial I_r} = -\frac{2}{V_s + V_r}. \quad (\text{B.16})$$

B.2.2 Net error approximation

To a first order linear approximation, the change in Z caused by changes in V_s and V_r is given by

$$\delta Z = \frac{\partial Z}{\partial V_s} \delta V_s + \frac{\partial Z}{\partial V_r} \delta V_r \quad (\text{B.17})$$

$$= \frac{2(V_s \delta V_s - V_r \delta V_r)}{V_s I_r + V_r I_s} - \frac{(V_s^2 - V_r^2)(I_r \delta V_s + I_s \delta V_r)}{(V_s I_r + V_r I_s)^2}. \quad (\text{B.18})$$

Let the relative change in Z be

$$\Delta Z = \frac{\delta Z}{Z} = \frac{2(V_s \delta V_s - V_r \delta V_r)}{V_s^2 - V_r^2} - \frac{I_r \delta V_s + I_s \delta V_r}{V_s I_r + V_r I_s}. \quad (\text{B.19})$$

Suppose errors are modelled at both line ends by $\delta V_s = (a_s + j\phi_s)\tilde{V}_s$ and $\delta V_r = (a_r + j\phi_r)\tilde{V}_r$. Then the relative change around \tilde{V}_s, \tilde{V}_r is

$$\Delta Z_{exact} = \frac{2((a_s + j\phi_s)\tilde{V}_s^2 - (a_r + j\phi_r)\tilde{V}_r^2)}{\tilde{V}_s^2 - \tilde{V}_r^2}, \quad (\text{B.20})$$

where only the first, dominant term is considered. Now suppose all errors are modelled to be in \tilde{V}_r , such that $\delta V_s = 0, \delta V_r = (a + j\phi)\tilde{V}_r$ where $a = a_r - a_s, \phi = \phi_r - \phi_s$. Then the relative error becomes

$$\Delta Z_{app} = \frac{-2(a_r - a_s + j\phi_r - j\phi_s)\tilde{V}_r^2}{\tilde{V}_s^2 - \tilde{V}_r^2}. \quad (\text{B.21})$$

The difference between the exact and approximate relative error is

$$\Delta Z_{exact} - \Delta Z_{app} = \frac{2(a_s + j\phi_s)(\tilde{V}_s^2 - \tilde{V}_r^2)}{\tilde{V}_s^2 - \tilde{V}_r^2} = 2(a_s + j\phi_s). \quad (\text{B.22})$$

Hence, by modelling all error to be in \tilde{V}_r , an approximation of $2(a_s + j\phi_s)$ is made in the relative error of the impedance, which is constant and of a lower order than the overall error ΔZ_{exact} . Using an equivalent expression for ΔY , a similar argument can be produced for modelling all errors in current in \tilde{I}_r .

Appendix C

Chapter 5

C.1 Selection of measurement subsets

Suppose there are $N \in \mathbb{N}$ available sets of synchrophasor measurements $V_{s_i}, I_{s_i}, V_{r_i}, I_{r_i}, i = 1, 2, 3, \dots, N$, then one can choose

$$\Gamma = 1 + (N - 1) + (N - 2) + \dots + N = \sum_{m=0}^{N-1} N - m$$

distinct subsets of consecutive measurements of sizes $n = 1$ to $n = N$. Some subsets are excluded because of their size and lack of variation of operational states. In order to ensure enough variation within the subsets, only those with a minimum range of current magnitudes are chosen. Given Γ possible subsets, exclude those for which

$$n < p \tag{C.1}$$

$$|\max |I_{s_i}| - \min |I_{s_i}|| < \frac{\eta}{n} \sum_{i=1}^n |I_{s_i}|, \tag{C.2}$$

where $p \in \mathbb{N}$ is the minimum number of required measurement sets and $\eta \in \mathbb{R}_{\geq 0}$ is a factor that is chosen at least one order of magnitude larger than the measurement uncertainties. For instance, if the measurement uncertainty in I_s is less than 1%, $\eta = 10\%$. Let the number of subsets that satisfy criteria (C.1) and (C.2) be $\Psi \in \mathbb{N}$, hence, the number of remaining subsets is $\Lambda = \Gamma - \Psi$. Measurement correction factors and resistance-temperature parameters are estimated for each of the Λ subsets by the new methods NMLT and NMNL as described in Section 5.2. The subset that gives the best estimated values is identified according to the optimality criterion defined in Section 5.2.3.

C.2 Case study 1 results

C.2.1 Individual case

Figures C.1, C.2 and C.3 show estimated values of positive sequence reactance, conductance and susceptance for one individual case of the case study in Section 5.3.2.1. Results for the two new methods NMLT and NMNL as well as for the selection of existing single-phase methods are shown.

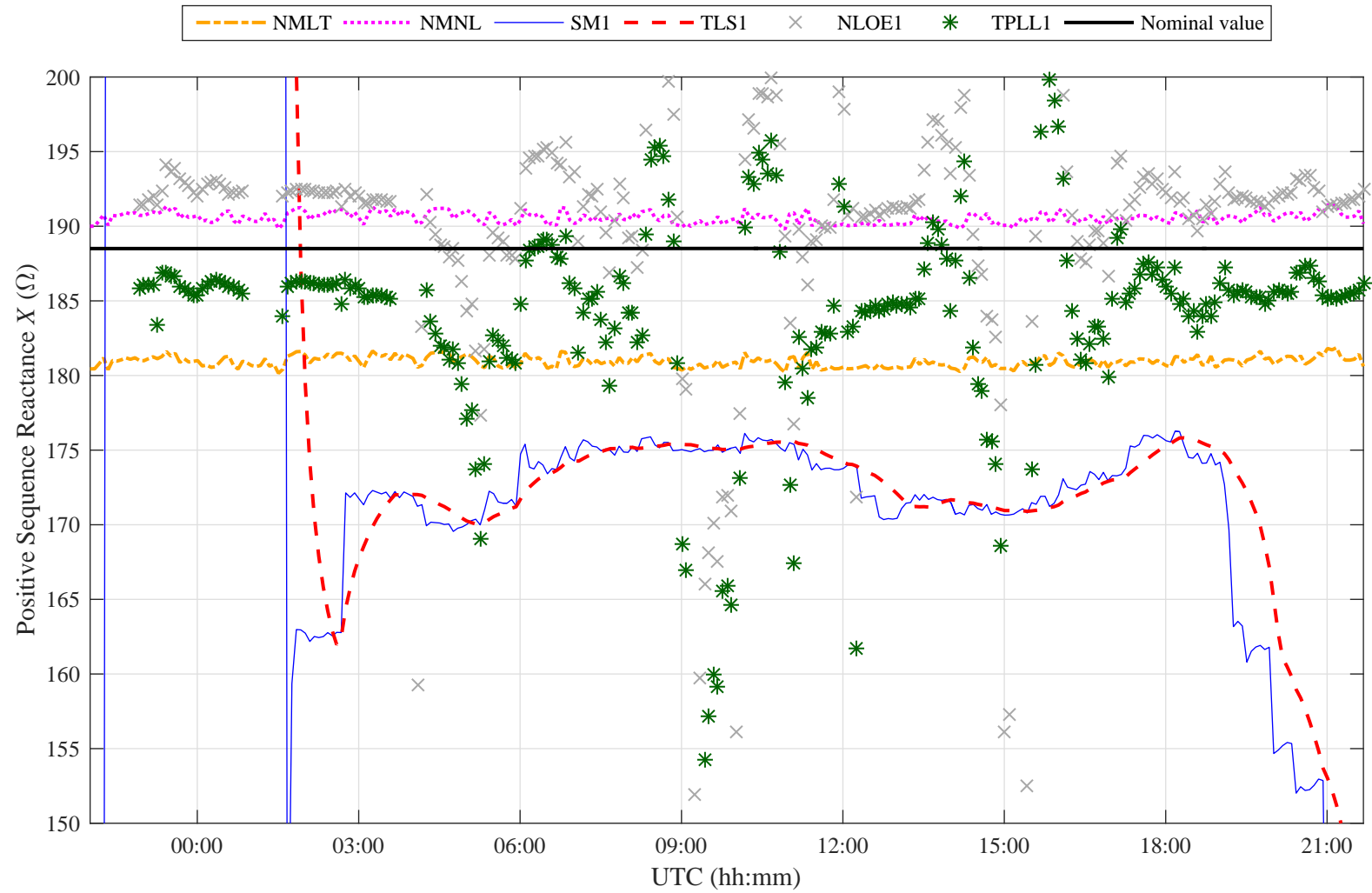


Figure C.1: Nominal and estimated values of reactance X over time for the individual case

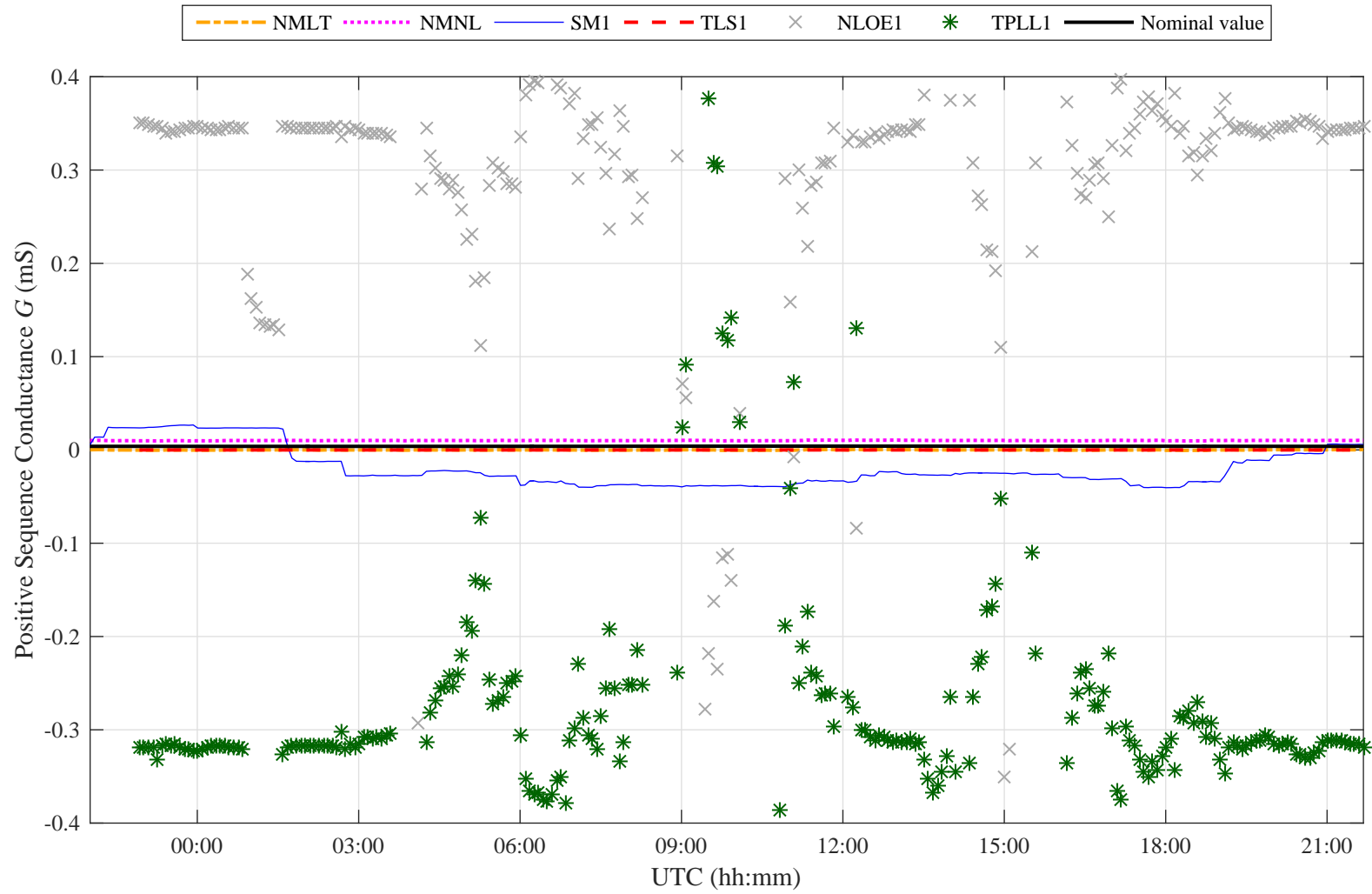


Figure C.2: Nominal and estimated values of conductance G over time for the individual case

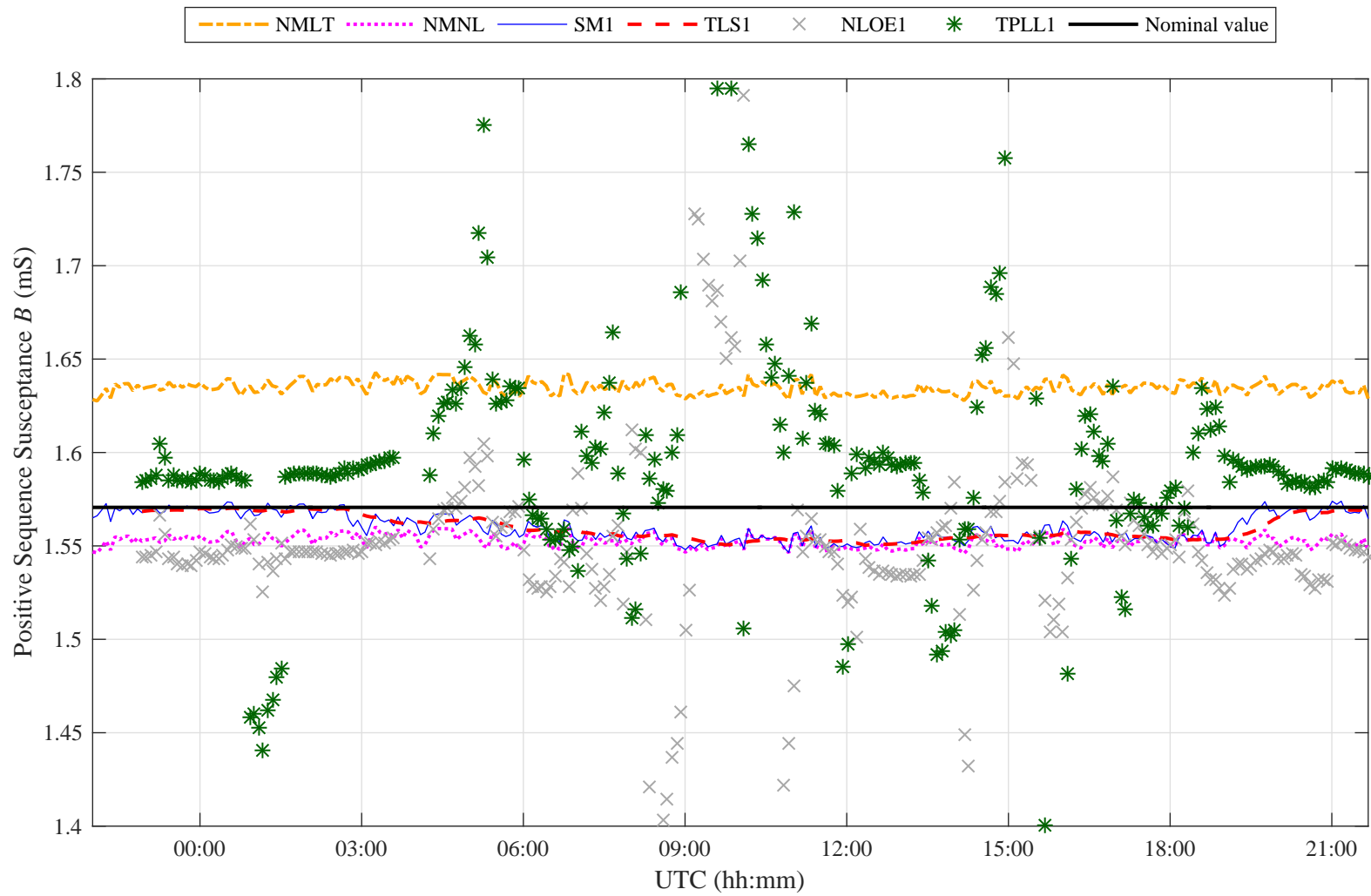


Figure C.3: Nominal and estimated values of susceptance B over time for the individual case

C.3 Case study 2 results

C.3.1 Day 8

Figures C.4 to C.6 show values of positive sequence reactance, conductance and susceptance estimated by the new methods NMLT and NMNL as well as by the existing single-phase methods using measurements from Day 8, as presented in Section 5.4.1.1.

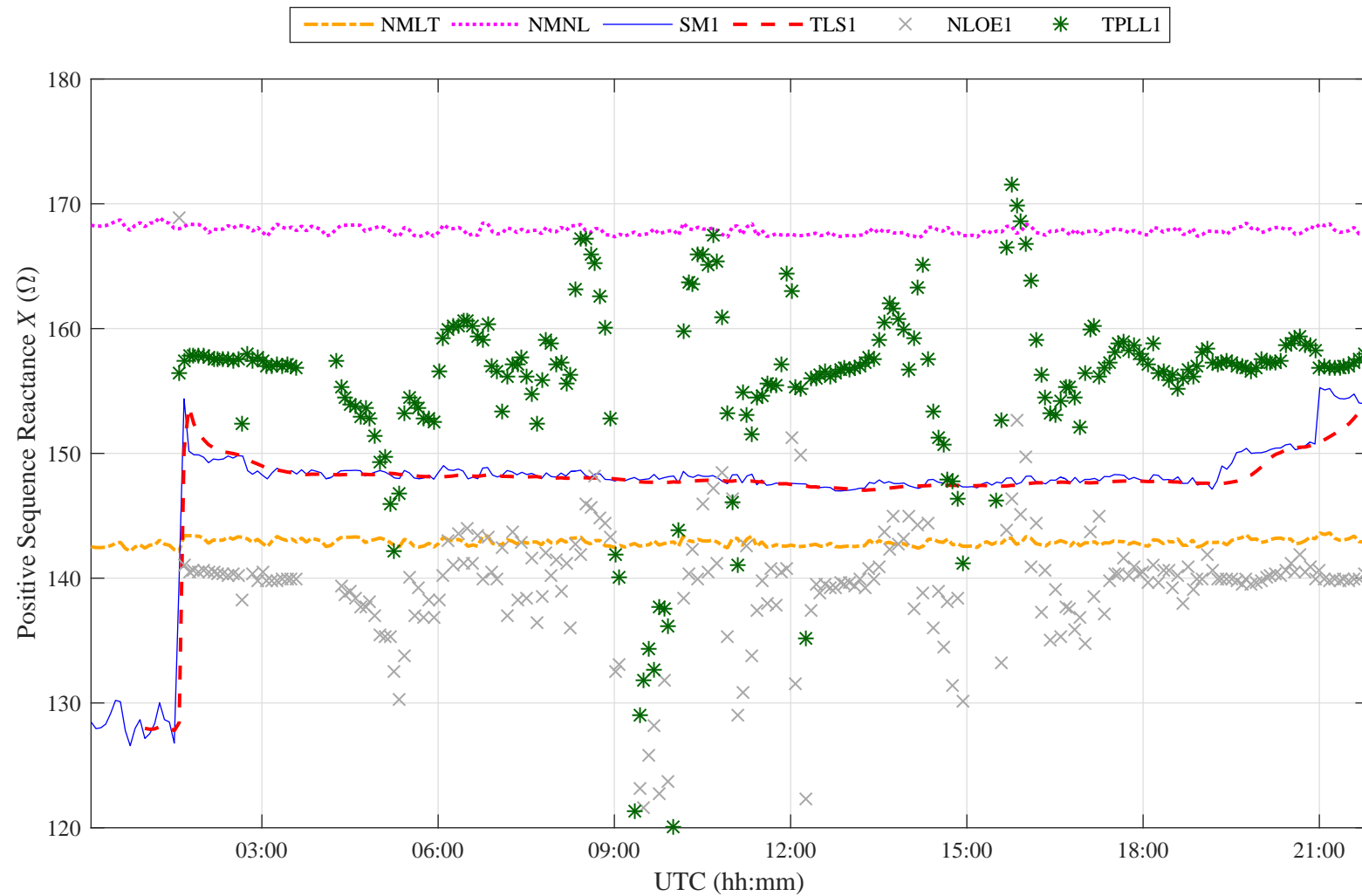


Figure C.4: Estimated values of reactance X over time for Day 8, by the new methods and existing single-phase methods

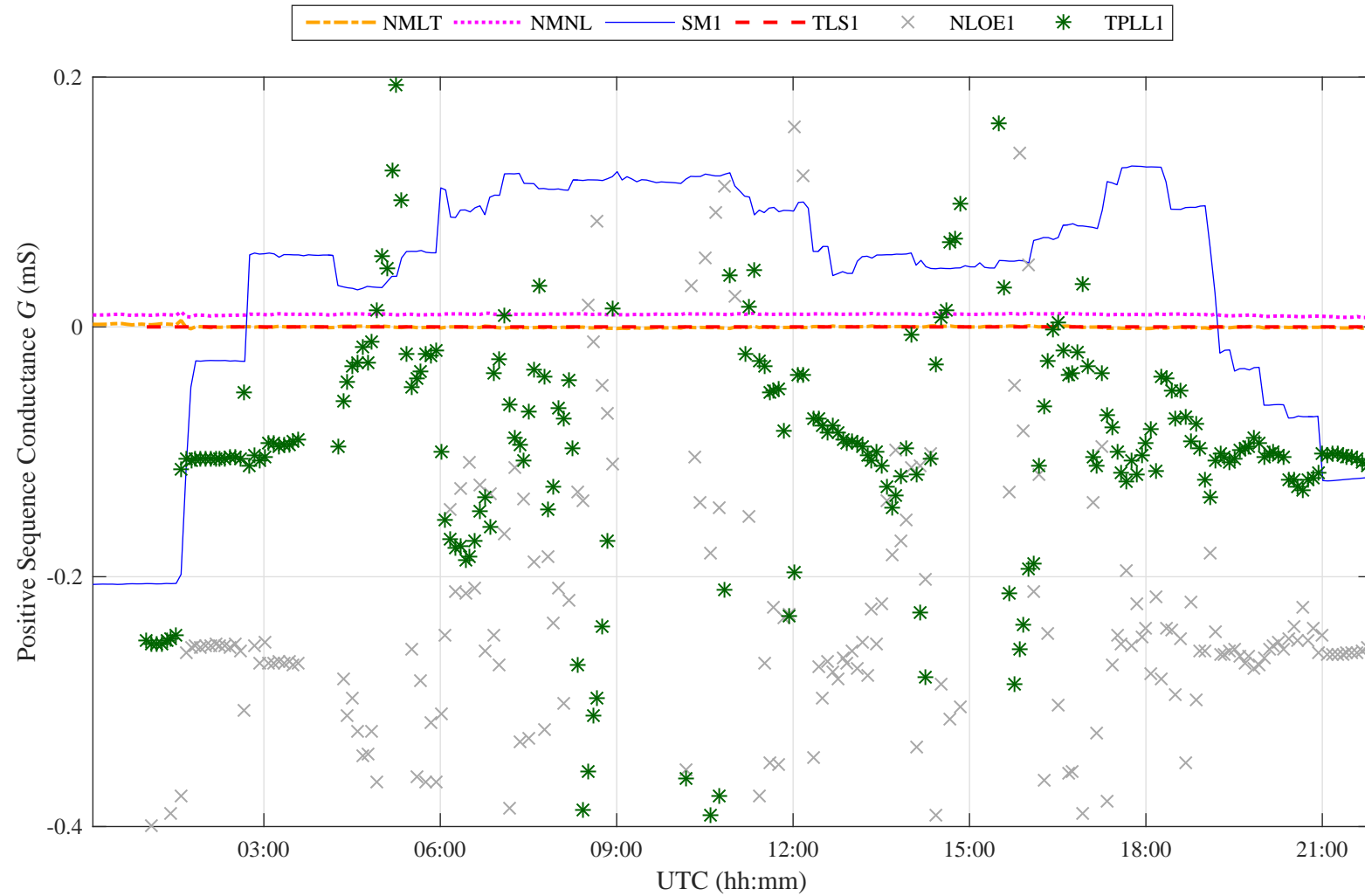


Figure C.5: Estimated values of conductance G over time for Day 8, by the new methods and existing single-phase methods

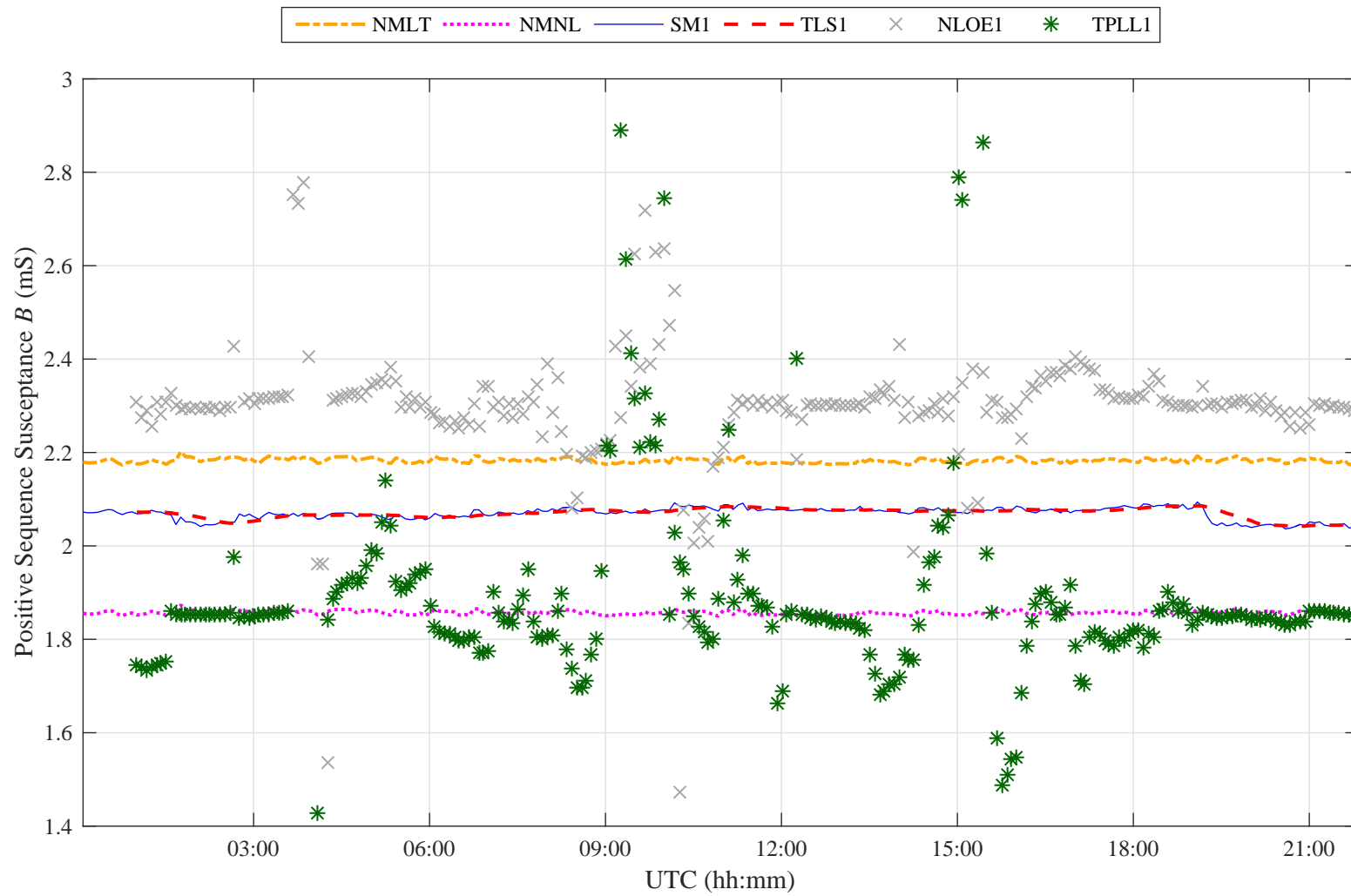


Figure C.6: Estimated values of susceptance B over time for Day 8, by the new methods and existing single-phase methods

Tables C.1 to C.4 give numerical values for the acceptability scores and errors in temperature estimates for Day 8, as presented in Section 5.4.1.1.

Table C.1: Values of Median (M) and Interdecile Range (IDR) for impedance and admittance parameters for Day 8, as presented in Table 5.8

	R (Ω)		X (Ω)		G (mS)		B (mS)	
	M	IDR	M	IDR	M	IDR	M	IDR
NMLT	15.1	0.8	143	1	0.00	0.00	2.18	0.01
NMNL	16.9	0.9	168	1	0.01	0.00	1.86	0.01
SM1	34.7	7.9	148	3	0.06	0.24	2.07	0.04
TLS1	35.1	5.7	148	3	0.00	0.00	2.07	0.03
NLOE1	25.4	7.6	140	20	-0.26	0.85	2.30	0.17
TPLL1	31.6	6.3	157	30	-0.09	0.66	1.85	0.46
LLS3	34.7	11.5	145	7	0.00	0.00	2.07	0.03
NLLC3	-0.1	33.1	1	39	-10.56	28 151.71	77.63	20 818.92
NLCO3	22.7	3.5	154	10	0.00	0.00	1.64	0.10
TPLL3	89.6	77.2	121	87	-0.79	7.82	0.97	11.02

Table C.2: Estimation day 8 - number of days with acceptable estimated values of Median (M) and Interdecile Range (IDR) of each parameter, and the total number of acceptable values over ten days, as presented in Table 5.10

	Resistance		Reactance		Conductance		Susceptance		Total (max 80)
	M	IDR	M	IDR	M	IDR	M	IDR	
NMLT	10	7	10	10	10	10	10	10	77
NMNL	10	7	10	9	10	10	10	10	76
SM1	0	0	10	8	5	1	10	10	44
TLS1	0	1	10	8	10	10	10	10	59
NLOE1	0	0	10	0	0	0	10	1	21
TPLL1	0	0	10	0	3	0	9	1	23
LLS3	0	0	10	5	10	10	10	10	55
NLLC3	0	0	0	0	0	0	2	0	2
NLCO3	10	3	10	9	10	10	10	7	69
TPLL3	0	0	8	0	0	0	6	0	14

Table C.3: Estimation day 8 - rms error $E_{\Delta T_c}$ of estimated temperature values in °C, as presented in Table 5.11

Day	1	2	3	4	5	6	7	8	9	10
NMLT	19	45	48	33	38	5.4	3.5	2.4	4	3.9
NMNL	26	50	60	40	44	6.5	3.8	3.1	5	5.1
SM1	464	687	818	608	715	331	337	374	314	257
TLS1	457	657	675	543	662	328	332	331	299	266
NLOE1	408	411	263	294	379	239	270	195	944	834
TPLL1	398	324	271	256	266	360	297	239	443	615
LLS3	496	901	1700	704	981	360	357	344	295	243
NLLC3	2020	1082	675	690	726	416	548	518	470	446
NLCO3	54	53	50	56	44	76	78	85	95	99
TPLL3	4395	1285	979	1145	1345	851	860	1181	1112	1612

Table C.4: Estimation day 8 - standard deviation of error $\Sigma_{\Delta T_c}$ of estimated temperature values in °C, as presented in Table 5.11

Day	1	2	3	4	5	6	7	8	9	10
NMLT	15	5	44	32	32	5.0	3.0	2.4	3	3.1
NMNL	19	5	56	39	38	5.9	3.0	2.9	4	4.2
SM1	66	273	594	545	466	34	57	293	103	6
TLS1	61	250	384	440	298	29	49	198	72	4
NLOE1	365	411	232	200	355	188	233	125	898	786
TPLL1	386	247	201	119	231	299	214	77	444	602
LLS3	94	456	1413	509	496	60	94	200	92	9
NLLC3	2016	1053	629	663	658	334	482	464	380	353
NLCO3	14	13	16	45	29	21	20	37	19	14
TPLL3	3997	388	455	331	335	433	320	512	542	1420

C.3.2 Cross validation

Tables C.5 to C.10 give numerical values for the acceptability scores and errors in temperature estimates for Days 1 to 10, as presented in Section 5.4.1.2.

Table C.5: Number of days with acceptable estimated values of Median (M) and Interdecile Range (IDR), when correction factors and resistance-temperature parameters are estimated from Days 1 to 10 by NMLT as presented in Table 5.12

Estimation day	Resistance		Reactance		Conductance		Susceptance		Total (max 80)
	M	IDR	M	IDR	M	IDR	M	IDR	
1	10	6	10	6	10	10	9	10	71
2	10	7	10	10	10	10	7	10	74
3	10	8	10	10	10	10	10	10	78
4	10	7	10	10	10	10	10	10	77
5	10	8	10	10	10	10	10	10	78
6	10	7	10	10	10	10	2	10	69
7	10	8	10	9	10	10	10	10	77
8	10	7	10	10	10	10	10	10	77
9	10	6	10	9	10	10	10	10	75
10	10	5	10	9	10	10	10	10	74

Table C.6: Number of days with acceptable estimated values of Median (M) and Interdecile Range (IDR), when correction factors and resistance-temperature parameters are estimated from Days 1 to 10 by NMNL, as presented in Table 5.13

Estimation day	Resistance		Reactance		Conductance		Susceptance		Total (max 80)
	M	IDR	M	IDR	M	IDR	M	IDR	
1	10	5	10	6	10	10	10	10	71
2	10	7	10	10	10	10	10	10	77
3	10	7	10	10	10	10	10	10	77
4	10	7	10	10	10	10	10	10	77
5	10	6	10	10	10	10	10	10	76
6	10	8	10	10	10	10	10	10	78
7	10	5	10	10	10	10	10	10	75
8	10	7	10	9	10	10	10	10	76
9	10	6	10	9	10	10	10	10	75
10	10	5	10	9	10	10	10	10	74

Table C.7: Cross validation of NMLT - rms error $E_{\Delta T_c}$ of estimated temperature values in °C, as presented in Table 5.14

		Validation day									
		1	2	3	4	5	6	7	8	9	10
Estimation day	1	4	50	25	35	17	9	19	19	13	10
	2	29	2	23	26	15	25	25	45	30	38
	3	68	31	2	9	7	17	13	48	21	27
	4	39	33	4	2	5	11	12	33	13	15
	5	32	28	11	12	2	13	8	38	13	34
	6	7	35	8	10	8	4	4	5	4	8
	7	7	35	7	9	7	3	1	4	2	8
	8	14	37	13	18	13	5	17	2	9	6
	9	11	39	13	17	10	3	3	4	2	8
	10	7	39	10	12	8	3	2	4	2	2

Table C.8: NMLT - standard deviation of error $\Sigma_{\Delta T_c}$ of estimated temperature values in °C, as presented in Table 5.14

		Validation day									
		1	2	3	4	5	6	7	8	9	10
Estimation day	1	4	14	15	20	9	7	14	15	11	10
	2	15	2	5	9	5	3	11	5	4	6
	3	67	20	2	9	7	14	12	44	18	24
	4	38	16	4	2	5	10	9	32	10	9
	5	32	19	9	10	2	10	8	32	10	21
	6	4	5	5	6	4	4	4	5	4	4
	7	5	2	2	2	3	3	1	3	2	5
	8	12	6	11	16	11	5	17	2	9	6
	9	10	3	5	7	4	2	3	3	2	7
	10	3	3	2	4	2	2	2	3	2	2

Table C.9: Cross validation of NMNL - rms error $E_{\Delta T_c}$ of estimated temperature values in °C, as presented in Table 5.15

		Validation day									
		1	2	3	4	5	6	7	8	9	10
Estimation day	1	5	54	32	34	17	18	21	26	15	12
	2	46	2	26	27	14	23	25	50	30	38
	3	105	33	2	10	9	8	13	60	22	29
	4	62	36	5	2	6	8	14	40	13	15
	5	52	30	13	13	2	6	8	44	14	35
	6	5	37	9	9	8	4	5	6	5	8
	7	5	37	8	8	8	2	1	4	3	7
	8	19	39	15	18	13	13	19	3	10	7
	9	14	42	14	16	11	5	5	5	2	9
	10	5	41	11	12	8	3	2	5	2	2

Table C.10: Cross validation of NMNL - standard deviation of error $\Sigma_{\Delta T_c}$ of estimated temperature values in °C, as presented in Table 5.15

		Validation day									
		1	2	3	4	5	6	7	8	9	10
Estimation day	1	5	16	18	20	9	12	15	19	12	12
	2	21	2	7	9	5	7	13	5	4	5
	3	102	20	2	10	8	6	13	56	19	27
	4	62	18	5	2	6	5	11	39	10	9
	5	51	21	12	11	2	3	7	38	11	21
	6	4	5	5	6	4	4	5	6	4	4
	7	5	3	2	2	3	2	1	3	2	5
	8	18	6	13	16	11	13	19	3	9	7
	9	14	3	6	8	4	3	5	4	2	8
	10	2	3	3	4	2	2	2	4	2	2